Radial Velocities of Faint Galaxies from Objective Prism Spectra

John Alan Cooke

Doctor of Philosophy
University of Edinburgh
1980

This thesis has been composed by me, and consists entirely of my own work, except where specifically indicated in the text.

1980 August 29.

Radial velocities of faint galaxies from objective prism spectra.

Contents

Radial velocities of faint galaxies from objective prism spectra

Abstract

Since Hubble's discovery of the correlation between galaxy radial velocity and distance, velocities of galaxies have been obtained using slit spectra to establish the value of the Hubble constant. More recently, with the acceptance of a general Hubble flow, velocities have also been used to examine the distribution of galaxies in space. Velocities within clusters of galaxies have also been used to establish cluster velocity dispersions, and hence virial masses. Large numbers of galaxy velocities obtained over a small area of sky to a faint limiting magnitude would help to construct a clearer picture of the medium scale (supercluster-sized) structure of the Universe.

In this thesis the basis for a method of obtaining radial velocities of faint galaxies from their objective prism spectra is described. Measurement techniques, both manual and computer-based, using digitised data from several measuring machines, are discussed. The parameters able to affect the velocity measurement are examined, and checks are made to compare velocities obtained from objective prism spectra with velocities of the same objects obtained from slit spectra. The method is shown to be easily applied to measurements of individual known galaxies, but quite difficult to apply to large numbers of objects using computer techniques. In particular the signal to noise ratio in galaxy spectra has a very important effect on automated velocity measurements.

The application of the method to clusters of galaxies is demonstrated, and preliminary results presented for several Abell clusters. The application of the method to the general field is discussed, and the problems encountered with this application described. It is concluded that the technique described has great potential for both the study of clusters of galaxies, and if certain measurement problems can be overcome, for the study of the distribution of galaxies in large volumes of space.

Acknowledgments

The work described in this thesis could not have been undertaken without the co-operation, guidance, and encouragement of a number of people. The project as a whole was instigated by Professor V.C. Reddish, to whom I am also grateful for the hospitality of the Department of Astronomy. Not only the Department, in fact, but also of the Royal Observatory, Edinburgh; our existence in the same buildings has ensured almost daily contact between myself as a user of the National facilities (UKSTU, COSMOS) and members of the teams providing those facilities.

Firstly, though, I wish to thank my supervisors, David Emerson and Kashi Nandy, for their time and effort on my behalf. I have benefitted greatly from discussions with them about the project over the years, and look forward to continuing this collaboration.

The UK Schmidt Telescope Unit are to be thanked for providing the 'bread and butter' in the form of very high quality photographs; though of course we always want more, and better!

A large amount of COSMOS data has been provided for me, mainly measured under the careful hand of Graham Smith. I am very grateful for the efforts of the COSMOS team, especially when faced with a user complaining about data quality -again- in the early days.

I also wish to thank Professor D.W.N Stibbs and members of the University Observatory, St. Andrews, for help with measurements made at St. Andrews.

I am grateful to the Panel for the Allocation of Telescope Time for time which has enabled preliminary checks of velocities to be carried out, and to the Science Research Council for computer time (at Atlas, Rutherford and ROE). For the first 2¾ years of this work I was supported by a Science Research Council Research Studentship.

To name names, I have had many helpful discussions with the following people in particular during the course of this work: Ralph Martin, Harvey MacGillivray, Phil Williams (COSMOS); Russell Cannon, Tim Hawarden, Liz Sim, Keith Tritton (UKSTU); Mike Hawkins and Malcolm Smith. Over the latter half of the period, Dennis Kelly has suffered more than most through sharing an office with

me, but has provided stimulating discussion. I am grateful to all my fellow research students (too numerous to note) who help to make Edinburgh such an interesting place to work in, but especially to Iain Coulson and Mark Bailey who were in Edinburgh for the first three years.

Thanks also go to my parents who have not been the least in exhorting me to 'get it finished'!

Finally, I wish to thank Kim Chambers for typing this thesis.

Acknowledgments for specific assistance in this work are given in the text of the thesis.

1. Introduction

Radial velocities of galaxies have in the past been obtained from slit spectrograms. Most early velocities were obtained for work on the redshift-distance relation (e.g. Humason, Mayall and Sandage, 1956, henceforth referred to as HMS), or, within clusters of galaxies, for determining cluster velocity dispersions (e.g. Holmberg, 1961.). More recently, with the acceptance of a general Hubble flow, velocities have been used to define distances and hence the distribution of galaxies in space (e.g. Tifft and Gregory, 1976; Tarenghi et al, 1979). However as we reach out to fainter objects it becomes more difficult to secure spectra, because considerable quantities of large telescope time are required. The National Geographic sky survey in the northern hemisphere showed that very large numbers of faint galaxies could be photographed using a large Schmidt telescope. In the southern hemisphere, we now have the U.K. 1.2m Schmidt telescope which has been equipped with a thin objective prism; a prism with three times the dispersion is under construction. The thin prism allows us to examine the low dispersion spectra of large numbers of faint galaxies.

It is only in recent years that objective prism spectra of galaxies have been examined in detail, in the Byurakan (Markaryan et al , 1967-73) and Cerro Tololo (Smith 1975) surveys, both of which are primarily concerned with emission-line galaxies. At low spectral resolution absorption lines in particular become difficult to detect in objective prism spectra, due to the smearing of the spectrum produced by the galaxy luminosity profile in the direction of dispersion; and the resulting spectra have a resolution similar to that produced using scanning spectrographs to measure galaxy energy distributions.

The measurement of radial velocities from objective prism spectra has in the past been confined to stars with measurable lines, from photographs taken with dispersions of the order of 100 Å mm^{-1}. The extension of these techniques to galaxies, at much lower dispersions, is the object of the present study, the goal being to obtain radial velocities of large numbers of faint galaxies from sky limited objective prism photographs. The work is part of a larger project to

study the spectra of faint galaxies on objective prism photographs taken with the UK Schmidt telescope (UKST), a project begun by Professor V.C. Reddish, Dr. K. Nandy and Dr. D. Emerson. This thesis is concerned with the techniques successfully used to obtain velocities of faint galaxies, and with some preliminary applications of the method.

A survey of work previously done relating to the present study is given in chapter 2. This covers objective prism work (both on stars and galaxies), the spectra of galaxies, and previous work on obtaining velocities of galaxies.

Chapter 3 covers the material and techniques used in the present work. Section 3.1 gives details of the photographic material available, with some remarks on the effects of the photographic process. Section 3.2 lists the machines used; both measuring machines, used to extract information from the photographs, and computing machines, used to analyse data, in particular the large quantities of data produced by the COSMOS measuring machine(Stobie et al, 1979). In sections 3.3 and 3.4 the methods used for obtaining velocities, both by manual measurement of microdensitometer tracings of the spectra, and by automatic computer analysis of COSMOS machine data, are described. The manual method is particularly simple to apply, and should be of use to many workers wanting to obtain quickly an approximate velocity for, say, a cluster of galaxies. The automatic techniques are more complex, and great care has to be taken over the quality of the data used with them. Section 3.5 describes the tests and calibration that have been applied throughout the work, and procedures which should be undertaken for any new set of measurements to ensure consistency.

Chapter 4 covers applications of the method, in particular to clusters of galaxies; this appears to be the area where the method holds the most immediate promise with the opportunity of quickly obtained results, but section 4.2 looks at the more common case of a general field on a photograph, which should provide the more significant results. Finally in section 4.3 the conclusions that may be drawn from

this work are summarised, along with some speculation as to the lines along which this work is likely to proceed in future.

The timescale of this work has been dictated by many events. It was initially started in October 1975; at that stage the COSMOS machine was available, but only objective prism plates from the Curtis Schmidt telescope at Cerro Tololo could be used for initial tests, through a generous loan by Dr. M.G.Smith. The first UKST objective prism photographs became available in July 1976, although early deep plates at high galatic latitude were few in number. The basis of the technique was well established in early 1977, and continuous effort was made to establish software capable of producing accurate velocities, software to extract and display spectra from COSMOS data having previously been developed. A major computing machine change occured in March 1978. Work done between that date and the present includes the majority of the work on clusters of galaxies.

2. Previous related work.

2.1 Objective prism work.

The objective prism as a tool for astronomical research has its origin in the beginning of spectroscopy itself. Fraunhofer used an objective prism for visual observation of the lines in stellar spectra, and later Secchi (1869) examined stellar spectra visually and classified them. A catalogue of visually classified spectra of over 4000 stars between -1° and $+20^{\circ}$ declination was later produced by Vogel (1883), using Secchi's classification scheme.

Objective prism work was considerably changed with the introduction of photography, which allowed the observation of very large numbers of stars. The Henry Draper Memorial provided the facilities for such work to be done, resulting in the Henry Draper catalogue (1918-36). The first objective prism photograph was taken in May 1885, and the classification of the spectra of about 222,000 stars from over 2000 photographs took about four years. These photographs each covered a field five degrees square, using dispersions ranging from about 10 $\mathring{A}\ mm^{-1}$ to about 45 $\mathring{A}\ mm^{-1}$. The possibility of obtaining radial velocities from the objective prism spectra was mentioned by Pickering (1891a) in a description of the work of the Henry Draper Memorial.

A review of early work done in the field of objective prism radial velocities was given by Millman (1931); there had by that time been several attempts to obtain stellar radial velocities by different methods. The main methods being considered were:

(i) the use of an absorption standard, ideally an absorbing screen which would produce a sharp calibration line in the spectrum; knowing the dispersion curve of the prism, the wavelengths of lines observed in the spectrum could be found

(ii) the 'reversion' method, whereby two exposures would be taken with dispersions in opposite directions on the one photograph, the two spectra of each star arranged to be parallel and adjacent to each

other. Any wavelength shift works in opposite directions in the two spectra, and the separation between the two positions of each spectral line can be measured. With this system, only the relative radial velocities of the measured stars can be deduced; a standard velocity would be needed to provide an absolute calibration.

(iii) the length of spectrum method. Due to the differential dispersion of a prism with wavelength, the spectrum shortens with increased radial velocity; measurement of the amount by which the spectrum shortens can be used to obtain the radial velocity.

The advantages and disadvantages of each method were later discussed by Fehrenbach (1947 a,b). Bok and McCuskey (1937) and Cherry (1937) made a serious attempt to obtain radial velocities using the absorption method, and obtained velocities of over 200 stars. They aimed for an accuracy of better than $\pm$ 10 kms^{-1} using a dispersion of 95 Å mm^{-1} at $H\gamma$, and estimated that their probable errors were about this value; after analysing their data, Fehrenbach (1947a) claimed that they were actually slightly worse. Bok and McCuskey attempted to correct for changes in dispersion across the field, but noted that the change of dispersion with position differed from night to night; thus plates were obtained at the beginning and end of each night's observations to check the dispersion, and used in the reduction. Even though their velocities agreed quite well with velocities from slit spectra, it seems that the disadvantages of the detailed checks needed in reduction outweighed the advantages of obtaining many velocities from one plate.

The reversion method was again put forward by Fehrenbach (1944) but with a modification; he replaced the single prism by a normal-field direct vision prism, that consisted of three components, with front and back faces parallel and normal to the optical axis of the telescope; this design of prism removes many of the field distortions introduced by a single prism, and removes the need for a reduction procedure as detailed as that of Bok and McCuskey. Fehrenbach later (1947 a,b) discussed at length the various methods of obtaining radial velocities. He concluded that the absorption standard, Neodymium Chloride, was not good enough because (a) the absorption maximum varies with concentration and temperature, (b) the absorption

feature itself is too wide, and (c) the asymmetry of the feature makes measurement difficult. In fact the variations in wavelength with temperature and concentration are small, causing a change of about 3 kms^{-1} in the measured velocity for a $10^{o}C$ change in temperature. However these effects combined with the asymmetry of the feature, with solutions giving enough absorption to provide a visible calibration on the photograph (Fehrenbach measured a change in apparent position of the feature of over 4 Å over a large concentration range) could easily introduce errors of several tens of kilometers per second. The length of spectrum method he also rejected, because, he claimed, variations in spectrum length due to variations in the prism properties (e.g. with temperature) are about 1000 times larger than the variations due to radial velocities; in addition, the ends of a spectrum are difficult to define exactly. Fehrenbach also discussed the difficulties in the reversion method as it had been used, in particular the great difficulties caused by the change in dispersion across the plate.

The problems of obtaining radial velocities from objective prism spectra were discussed at the same time by Treanor (1948). He came to much the same conclusions as Fehrenbach, and also suggested the use of a direct vision prism, calibrated using a direct image formed on the photograph at the same time as the dispersed image, instead of using the reversion method. He did not reject the length of spectrum method outright as did Fehrenbach; in fact the change in spectrum length, if defined by two lines at opposite ends of the spectrum (e.g. $H\alpha$ and $H\delta$), is only a few times less sensitive than the absolute wavelength shift of the lines, using a prism with a large change in dispersion over the wavelength range used. Treanor discussed temperature effects in some detail, but omitted the effect of temperature on the neodymium absorption standard in his discussion of that method. The errors he calculated are of the order 15–20 kms^{-1} per ^{o}C for all methods, due entirely to changes in the prism glass properties.

Comstock (1906) had suggested the use of two direct vision prisms, with opposite dispersions, in front of the objective; this would distort the field less than a single prism. Fehrenbach took

this a stage further in introducing his normal-field prism which removed the field distortions; it had another particular advantage in that the dispersion variations were symmetric, so that an image at any position on the plate would have the same dispersion for the two orientations of the prism. In the third paper of the series (Fehrenbach 1948) he presented the first results obtained with the normal-field prism. In a later series of papers (Fehrenbach 1955 a,b; Duflot and Fehrenbach 1955 a,b; Barbier and Fehrenbach 1955) the method of measurement and reduction were described in more detail; the best velocities obtained, from 4 measurements, have internal errors of about $\pm$ 2 kms^{-1}. Fehrenbach's prism gave a dispersion of about 80 $\mathring{A}\ mm^{-1}$ between $H\gamma$ and $H\delta$; this result implies measurement accuracy, on the photograph, to better than $\pm$ 1 μm. Schalén (1954) also used Fehrenbach's technique, with a prism giving a dispersion of 113 $\mathring{A}\ mm^{-1}$ between $H\gamma$ and $H\delta$; the mean error obtained, for measurements of two to four photographs, was about 6 kms^{-1}.

Fehrenbach (1966) considered a Schmidt telescope to be inferior to a refractor for obtaining radial velocities, because of light loss in the Schmidt due to the central obscuration, and also due to loss of resolution away from the optimum wavelength of the corrector plate. However a great advantage of the Schmidt was indicated by Stock and Osborn (1972, 1973); the field distortions are of a different form to those produced in a telescope with a flat focal plane, and can be corrected for much more easily. The method used by Stock and Osborn is similar to the 'reversion' method; the difference being that two separate photographs with dispersions in opposite directions are taken. The x and y positions of spectral features in the spectra obtained are then measured on both photographs. For concentric projection of the sky onto a Schmidt plate, the co-ordinate difference for a given spectral line in the direction of dispersion is given by

$$\Delta y_i = a_{oo} + a_{10}x_i + a_{01}y_i + a_{22}(x_i^2 + y_i^2)$$

neglecting higher order terms, where x_i and y_i are the average co-ordinates of feature 'i' from both plates, and Δy_i the

difference between the two y measurements (in the direction of the dispersion). They determined the coefficients a_{oo}, a_{10} and a_{01} by a least squares method; a_{22} is an instrumental constant which has to be determined independently. Any different between the observed Δy_i and that obtained from the equation is interpreted as a radial velocity.

Stock and Osborn applied the method to more than 50 stars using the Curtis Schmidt telescope at Cerro Tololo and a 4^o prism, giving a dispersion of about 240 $\mathring{A}\ mm^{-1}$ at $H\gamma$. They found an average mean error of about $\pm$ 20 kms^{-1} for each programme star, comparing its velocity to 10 comparison stars. The error here, as with Fehrenbach's measurements, also corresponds to a measurement accuracy of about $\pm$ 1 μm, which must be maintained over the area on the photograph containing the comparison stars. This may be rather more difficult than in Fehrenbach's method of measuring the two adjacent spectra, but measurement accuracies of better than 1 μm should be possible with a good spectrocomparator (Abt and Smith, 1969).

Objective prism plates can be calibrated in intensity by various means, and thus used for spectrophotometry. For example, Lindblad (1922) used spectrophotometric methods to determine stellar luminosities. He calibrated his photographs by using a series of different exposures on the same plate, thus knowing (if atmospheric conditions remained constant!) the relative magnitudes of the various exposures, and hence, by comparing the exposures of different stars, the relative magnitudes of the stars on the photograph. Lindblad also defined an effective colour index for each star, measuring the relative intensities on either side of an intensity drop in the spectrum. (His actual definition was of log E, E being the ratio of exposures t_1, t_2 needed to make the intensity on one side of a given wavelength in t_1 equal to that on the other side in exposure t_2). This enabled him to plot a colour-magnitude diagram, on which he put stars from different groups reduced to absolute magnitude by using known parallaxes. These stars all fell on approximately the same curve, and Lindblad suggested that this colour-magnitude diagram could be used to determine

absolute magnitude of stars (over the limited spectral range B8 to A3) by measuring the colour index. Later a different method of calibration was used (Lindblad and Stenquist, 1934); a diffraction grating constructed of parallel wires was placed perpendicular to the direction of dispersion and in front of the prism, thus producing higher-order spectra on either side of the zero-order prism spectrum. Knowing the 'grating constant', the reduction in magnitudes of the secondary images could easily be calculated. This 'crossed prism and grating' technique was also used by Nandy in his studies of interstellar reddening (Nandy 1964-1968) and by numerous workers from Uppsala, following Lindblad and Stenquist (e.g. Schalén 1952). Samson (1969) also used this technique to calibrate his photographs used for the determination of coarse metal-abudance parameters. This type of calibration method, using secondary images at a known reduction in magnitude from primary images is ideal for objective prism work, as only the brighter images will have visible secondaries, the secondaries of the fainter images being too faint to register on the photograph. A similar method, producing secondaries about five magnitudes fainter than the primaries, was described by Pickering (1891 b).

Nandy and Smriglio (1970-76) used yet another method for the calibration of their plates; they calibrated direct photographs and applied this calibration to the objective prism photographs, taken to study the distribution of carbon and M stars.

A review of objective prism work with particular reference to surveys was given by Stephenson (1966); much survey work has been done since the Henry Draper catalogue, particularly using dispersions of around 300-600 $\mathring{A}\ mm^{-1}$ (at about Hγ). Bidelman (1964) noted that much was to be gained in classification using higher dispersions and cited Fenrenbach's work (at 80 and 110 $\mathring{A}\ mm^{-1}$), the Vatican observatory (80 $\mathring{A}\ mm^{-1}$, Treanor 1969) and the Curtis Schmidt at Michigan (108 $\mathring{A}\ mm^{-1}$). Since the removal of the latter telescope to the Cerro Tololo Inter-American Observatory (CTIO), the re-classification of HD stars has begun, using photographs taken at this dispersion (Houk and Cowley 1975). Bidelman (1972) has noted several other recent surveys of particular regions.

A recent publication of particular interest in the case of stellar classification is the Bonn Spectral Atlas (Seitter 1970, 1973, 1975). This gives examples of sequences of spectral types from objective prism spectra, at dispersions of 240 Å mm^{-1} (vol. I) and 645 and 1280 Å mm^{-1} (vol. II). The spectra at this lowest dispersion are of interest as the dispersion is not too dissimilar to that used by Markaryan (1967) at Byurakan, 2500 Å mm^{-1} at Hβ, and the new thin prism at Cerro Tololo (Blanco 1974), 1360 Å mm^{-1} at Hγ, both being used in the study of galaxies.

The surveys have often been used to isolate classes of objects, and occasionally have been made specifically for such 'discovery' purposes; for example, Minkowski's use of a Mount Wilson objective prism survey by Miller to discover new Hα emission nebulae (Minkowski, 1946). Much use has been made of the Schmidt telescope at the Warner and Swasey observatory (Nassau, 1945) for identification of particular types of objects; for example OB stars (Nassau and Morgan, 1950), carbon stars (Nassau and Blanco, 1954 a; McCarthy, 1960) and M stars (Nassau and Blanco, 1954 b).

Very low dispersions were shown to be useful for the segregation of classes of objects, in particular reddened O and B stars, by Morgan, Meinel and Johnson (1954), who used the rather extreme dispersion of about 30,000 Å mm^{-1}! This necessitated the use of very careful photographic techniques as the spectra obtained, using a Schmidt camera of 8 inches focal length, were only about 100 to 200 μm long. However the authors concluded that, with care, a 70-80 per cent success rate could be achieved in a search for early B stars; the great advantage being that this system would allow much fainter objects to be discovered than had been possible before. This is one of the most important reasons for using a low dispersion; the sky background is the same for an objective prism photograph as for a direct photograph, so in order not to lose too many of the fainter objects visible on a direct photograph, the prism photograph must be at low dispersion.

Schulte (1956) made further experiments at low dispersion using a 6.5 inch prism on the Yerkes 24-inch f/4 reflector at a dispersion of about 10,000 Å mm^{-1} at Hβ. He concluded that instruments used

for extremely low dispersion work need not give exceptionally small stellar images, as long as the ratio of length to width of the spectra produced was at least 10. In practice, the width would be governed primarily by the seeing rather than the telescope optics for a fairly normal Schmidt telescope.

Philip and Sanduleak (1966) explored Schulte's suggestions adopting a slightly different approach; having no thin prism to hand, they crossed two prisms at almost 180° to obtain very low-dispersion curved spectra, giving a dispersion from 3000 Å mm^{-1} at the blue end to about 20,000 Å mm^{-1} in the infrared. They used these spectra for a rough visual classification of stars from the intensity distributions within the spectra, down to about the 15th magnitude, but found that their plates were not suitable for detecting with certainty reddened early-type stars.

Philip and Sanduleak also investigated the images of galaxies appearing on their photographs; due to the concentration of light in the nucleus, they found galaxies showing semi-stellar spectra, and found it possible to identify very red and very blue systems. They noted that the vast majority of systems show an intermediate G-type spectrum. This work brings us to the field most relevant to the present study.

Some objective prism spectra of galaxies were studied by Vandekerkhove (1963, 1965) who was attempting to correlate the slope of the galaxy continua with redshift; this work is discussed in section 2.3. Much more extensive work was begun by Markaryan; after some early work on the colours and colour distributions within galaxies, Markaryan et al (1967-73) began to publish lists of 'galaxies with an ultraviolet continuum' found on objective prism photographs taken with the Schmidt telescope at Byurakan. Using a $1^{\circ}.5$ prism giving a dispersion of 1800 Å mm^{-1} at $H\gamma$, he noted that very sharp and intense lines could be detected in stellar spectra, and unbroadened spectra of objects down to 17 m could be obtained, using the Kodak IIa-F emulsion. Markaryan's 'ultraviolet continuum' objects have continua in the ultraviolet of similar strength to those observed in O and B stars (Markaryan and Lipovetskii, 1971).

Markaryan had the choice of using other dispersions, either 900 Å mm^{-1} or 280 Å mm^{-1}, but chose the lower value for several reasons: (i) the desire to investigate very faint objects; (ii) to reduce the overlapping of images and (iii) because of a photographic feature which eased identification of the objects; early type stellar spectra were divided by the 'green gap' in the sensitivity of the photographic emlusion into two roughly equal parts in intensity, thus facilitating the detection of the ultraviolet continuum in faint stars and galaxies. Markaryan has thus brought a feature of stellar objective prism work, that of isolating a class of objects, into the field of galaxy investigations, and his lists have been used extensively for further work on these interesting objects. The sample appears to contain a variety of types of object, including Seyfert galaxies and QSO's, confirmed by obtaining larger-dispersion slit spectra of the Markaryan objects.

Markaryan's success in the northern hemisphere has prompted a southern hemisphere survey at CTIO (Smith 1975). In his paper Smith describes the survey and its applications.

The prism used for the CTIO survey was described by Blanco (1974), and has a dispersion of 1360 Å mm^{-1} at H γ . Again, the photographs are being used for the isolation of classes of objects, in this case emission-line galaxies and QSO's. The survey is at a higher dispersion than Markaryan's but reaches a fainter limiting magnitude (blue magnitude 18) due to the use of sensitised (Nitrogen baked) Kodak IIIa-J photographic plates instead of the IIa-F plates used by Markaryan; this has advantages in that the IIIa-J emulsion cutoff is at about 5400 Å, thus limiting exposure due to the λ5577 and λ6300 night sky lines, whereas the IIa-F emulsion used by Markaryan is sensitive to about 7000 Å. Other advantages are the finer grain and increased contrast of IIIa-J. A disadvantage noted by Smith is the reduced spectral range, thus reducing the redshift range over which Lyman α can be detected in high redshift quasars, and also causing the loss of Hα .

The survey is performed by two observers, searching by eye 'with a view to isolating the maximum number of objects in a period of about 1 hour per plate per observer', and checks for completeness

are also performed. Smith found that galaxy identification is positive, although checks for galactic planetary nebulae occasionally need to be made. He gave no details about the appearance of the images on the photographs, other than the fact that stellar images are 'hard' on direct photographs, and this seems to have some bearing on the separation of galaxy and star images on the objective prism photographs.

Smith discussed applications to quasars, Seyferts, large-scale instabilities in galaxies, evolution of the emission-line phenomena in sharp-lined galaxies, and the study of outlying H II regions in galaxies. He found that all his QSO candidates were in fact new radio-quiet QSO's, and those showing more than one emission line on the objective prism photograph could have the lines tentatively identified, and a rough redshift estimated by reference to the green cutoff of the IIIa-J emulsion. Extension of QSO identifications to higher reshifts is being attempted by the use of red emulsions, to detect Ly α shifted beyond the IIIa-J cutoff.

Seyferts are being isolated directly from the objective prism plates by the detection of a forbidden Neon line with some success. Isolation of objects with peculiar features is also achieved from the emission-line sample by further analysis using the 4m reflector at CTIO for direct photography and to obtain spectra.

The first note on results from the UK 1.2m Schmidt telescope (UKST) (Bolton et al, 1977) indicated that work similar to that at CTIO could be done to fainter magnitude limits (Bolton et al estimated that 60 minute unfiltered and untrailed photographs on hypersensitised Kodak IIIa-J emulsion reach beyond 20th magnitude); in particular, a large sample of optically selected QSO's was isolated. Smith (1978) has described his extension to the CTIO work on quasars using the U.K. Schmidt telescope. His discussion is primarily concerned with the spectra of quasars, but he also discusses objective prism work ('slitless spectroscopy') as a technique for their discovery. He also mentions a problem of surveys of this type, that of non-uniformity, citing Savage's

(1978) remarks on incompleteness, particularly that due to selection of objects using ultraviolet excess alone: the selection criterion for Markaryan's survey.

The usefulness of a low dispersion objective prism in the study of faint galaxies, particularly in the isolation of specific classes of 'unusual' objects, can clearly be seen; however little work on 'normal' galaxies comparable to the early stellar work has yet been undertaken, perhaps because of the magnitude of the task. Philip and Sanduleak (1970) followed up their early stellar work using crossed prisms (described above) with a study of galaxy spectra in clusters; the technique allowed them to allocate colour indices to the spectra. Results were given for the Coma and Virgo clusters, and also the Hercules cluster and clusters Abell 2197 and 2199 (Philip, 1970).

Galaxy objective prism spectra are dominated by the distribution of luminosity in the galaxy, which in both spirals and ellipticals is clearly peaked towards the centre (Van Houten, 1961), more so in spirals than ellipticals, giving the general appearance of a diffuse stellar spectrum, which in the case of spirals is sharper and surrounded by a diffuse region. As, in the case of objective prism photographs, the image being dispersed is a star or galaxy, instead of (as in a slit spectrum) the image of a narrow slit, the spectral resolution is determined by the size and light distribution of the object. This puts a restriction on the range of galaxies for which the spectra can be measured, or even used for classification purposes, and a more detailed discussion of this problem is given in section 3.1.

Vanderkerkhove (1963) gives photographs which show the general appearance of large bright galaxies in objective prism photographs. Bolton et al (1977) presented photographs from a UKST objective prism plate, but gave only two photographs of quasar spectra, and none of 'normal' galaxy spectra; photographs of the appearance of stellar spectra are given in a more recent paper by Krug et al (1980).

A technique related to objective prism work which should be mentioned for completeness is the use of a transmission grating-prism

combination ("grism") used near the focal plane at prime focus of a telescope to obtain photographs with both zero order images and first order (blazed) spectra of objects (e.g. Hoag, 1976; Hoag and Smith, 1977). This technique can be used to extend objective prism surveys to fainter magnitudes over limited areas by utilising the light-gathering power of large telescopes.

2.2 Energy distribution and colours of galaxies.

The intrinsic colour, or to be more precise, the intrinsic spectral energy distribution, and the distribution of colour within galaxies, is important in any consideration of the appearance of galaxy spectra on objective prism photographs. As early as 1916 Seares (1916) noted that the nuclei of several galaxies were 'stronger in yellow light than in blue', from photographic plates taken using filters and different emulsions to restrict the wavelength range. For galaxies smaller than the dispersed (stellar) image, the overall appearance on an objective prism photograph is determined principally by the energy distribution (in the direction of dispersion) and the luminosity and colour distributions perpendicular to the direction of dispersion. Additionally the image is smeared in the direction of dispersion by the luminosity distribution in that direction.

Generally the brightest part of a galaxy spectrum will be in the centre, because of the concentration of light in the nucleus. This concentration also means that the highest spectral resolution will be at the centre of the spectrum, and this will be the part of the spectrum of interest in any measurement, for example using a microdensitometer. Thus the colours of the central regions of galaxies will be of interest in the present study, although for the fainter and more distant galaxy images with a smaller overall size, much more of the galaxy, and hence perhaps a slightly different energy distribution, would be sampled by a given aperture in a measuring machine.

In the study of galaxy luminosities photoelectric photometry has played a prominent part. Whitford (1936) published magnitudes of 11 bright galaxies, and this was followed with a paper by Stebbins and Whitford (1937) which contained magnitudes of 165 galaxies and colours for 112 of these, all determined photoelectrically. Later work (Stebbins and Whitford, 1948) giving observations in six colours, originated the arguments about the 'Stebbins-Whitford effect', which is discussed below. A brief summary of photoelectric work to 1964 is given by Holmberg (1975).

Stebbins and Whitford (1952) noted some correlation between colour and Hubble type, in that Sc galaxies were measured as being about 0.4m bluer than E to Sb galaxies; they found both 'red'

and 'blue' irregular galaxies. They used apertures of 11 arcsec for colour measurements and 24 arcsec for magnitudes (Stebbins and Whitford, 1948), recognising that these apertures were rather small, but choosing them to avoid field stars, and to give a better galaxy signal to sky background ratio. The detailed problems of galaxy photometry are not a concern of the present study; however the effect of aperture size on measured colour is important, and the fairly constant colour of galaxy types E to Sb using a small aperture is relevant to the objective prism plate appearance of these galaxies. This 'colour-aperture' relation is given by de Vaucouleurs (1961) for galaxies of different morphological type, in a paper giving colours of 148 bright galaxies in the standard U,B,V system. De Vaucouleurs corrected his colour measurements for inclination of the galaxies and plotted them as a function of a standard ratio: the observational aperture divided by the 'face-on' diameter, A/D_o. For E to Sb galaxies, the 'central' colour tended to the values (B-V) = 1.0, (U-B) = 0.6; Sbc and Sc to (B-V) = 0.8, (U-B) = 0.3. The outer regions of these galaxies were all bluer, from 0.1m in B-V for E and S0 galaxies, to 0.3m for type Sc. The Magellanic irregular types were observed to be more blue in the centre; although observations for types Scd to Im were rather more scattered than those of the earlier types. De Vaucouleurs (1972) later gave data for a much larger sample, 461 galaxies, together with a more detailed analysis of effects on observed colours. He found that he could express colour effects as simple mathematical functions of Hubble type T (from T = -5 (type E) through 0 (type S0/Sa) to 10 (type Im)). However some of these functions contain discontinuities, one of which de Vaucouleurs suspects may vanish in an analysis of an even larger data sample!

Using de Vaucouleurs' data, and his colour aperture relation, the colour-type relation for the nuclear regions of galaxies can be calculated, at least approximately; these relations are given in fig. 2.2.1 , for the (B-V) colours, where $X = \log (A/D_o)$. Even with the disappearance of the discontinuity between T = -1 and T = 0, there would be some change in colour from T = -5 (type E)

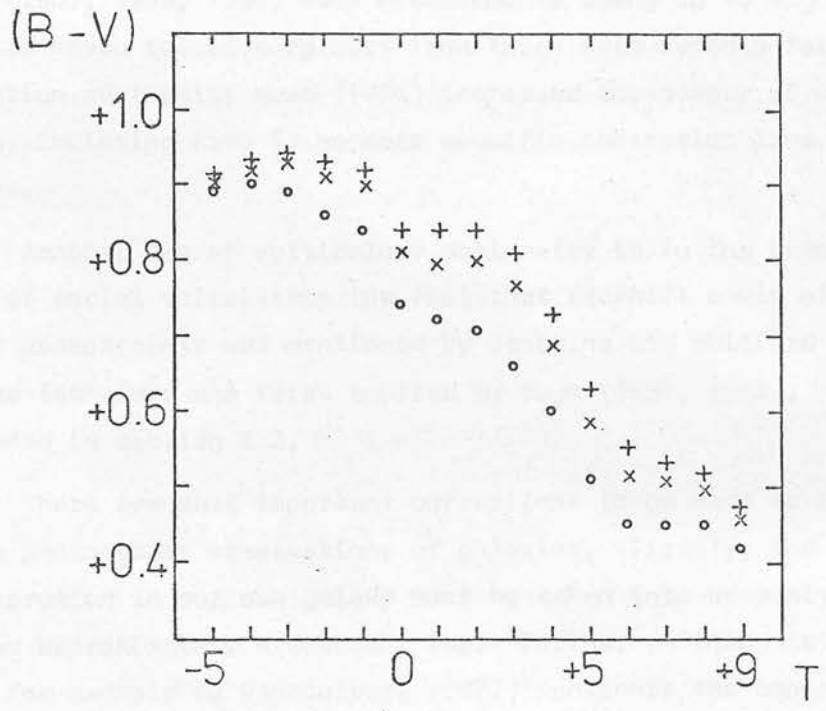

Fig. 2.2.1

Colour - type relation for the nuclear regions of galaxies, from de Vaucouleurs' data.

o X = 0

× X = -0.7

\+ X = -1.0 (extrapolation)

to T = 3 (type Sb) but it is rather less for the central regions (crosses) than for the whole galaxy (circles).

De Vaucouleurs' data is presented in the three colours of the U,B,V system, and he gave reduction formulae to the (B-V) colours for other workers' results, which were often in only two colours. However many workers have used multicolour photometry, from Stebbins and Whitford's six colours (1948) onwards, mainly to provide data for the synthesis of galaxy stellar populations, which is one use of multicolour photometry; Stebbins and Whitford had given an example of a synthesis of the observed colours of an Sb galaxy. Tifft (1961, 1963, 1969) made measurements using up to eight filters, and used seven relative colours from these measurements for stellar population synthesis; Wood (1966) increased the number of colours to twelve, including five to measure specific absorption line indices.

Another use of multicolour photometry is in the determination of radial velocities; the fact that redshift would affect colour measurements was mentioned by Stebbins and Whitford (1937), but the technique was first applied by Baum (1957, 1962). This is discussed in section 2.3.

There are some important corrections to be made to multicolour photometric observations of galaxies. Firstly, the effect of absorption in our own galaxy must be taken into account; this follows approximately a cosecant law. Further refinements may be made, for example de Vaucouleurs (1972) considers the amounts of absorption at the two galatic poles to be slightly different. Secondly, the effect of absorption in the galaxy under study can be considered, and again de Vaucouleurs (1961, 1972) has made a fairly detailed analysis of this effect, reducing measurements to the values that would be obtained for a 'face-on' galaxy. A third effect is that due to redshift, known as the 'K-correction'. For a redshifted galaxy, different parts of the energy distribution fall in the wavelength bands being observed as compared with a zero-redshift galaxy. The colours required are those that would be obtained in the rest-frame of the observed galaxy, and so corrections, which depend on the energy distribution of the observed galaxy,

have to be applied to the observed colours. These corrections are called 'K-corrections'.

Stebbins and Whitford (1948) realised that to compute such corrections, the complete energy curve (at rest wavelengths) of a galaxy of the same colour is required; the difference in observed colours at different redshifts (the K-corrections) can then be computed, knowing the response curves of the detectors. However even after application of the K-corrections, Stebbins and Whitford were left with a colour reddening that increased with redshift; this became known as the 'Stebbins-Whitford effect', and led to much work being done to obtain accurate K-corrections.

Whitford (1975) has given a comprehensive review of measurements of galaxy energy distributions to 1973. Measurements of energy distributions have been made using multicolour photometry, examples of which have been given above, and in more detail using scanning spectrometers. In these 'scanners' the dispersed light from an object is scanned using a photometer behind an exit aperture in the plane of the spectrum, the spectrum generally being scanned by rotation of the grating, although in the first primitive scanner an objective prism was placed in front of a telescope with a photometer, and the telescope moved in declination to trail the stellar spectrum over the photometer aperture (Stock, 1956).

Code (1959) made scanner observations of an elliptical galaxy (M32) to investigate the Stebbins-Whitford effect; he found the energy distribution to be rather different from the smoothed energy curves that had previously been used, and using his curve of M32 to calculate the K-corrections found that the excess reddening of the Stebbins-Whitford effect was reduced to 20 per cent of the value obtained by Stebbins and Whitford. De Vaucouleurs (1948, cited in Whitford, 1975) had suggested that the sharp drop in the energy distribution of the galaxies near 4000 Å could have been responsible for the Stebbins-Whitford effect, the filters used having had inadequate resolution to indicate the presence of this feature. Oke's (1962) measurements seemed to indicate that the Stebbins-Whitford effect did exist, but Whitford

(1962) pointed out that Oke's results did not agree with those of Code. Oke and Sandage (1968) made further scanner observations of giant elliptical galaxies, and demonstrated the absence of a Stebbins-Whitford effect to the 3 per cent level, using their spectral energy distributions; subsequently only small changes have been made to the K-corrections for giant elliptical galaxies (e.g. Schild and Oke, 1971).

Scanner observations have generally been made to obtain more accurate K-corrections, this being important in any cosmological tests involving magnitudes, and much of this work has centred on the energy curves of elliptical, and in particular, giant elliptical galaxies (Oke and Sandage, 1968; Whitford, 1971; Schild and Oke, 1971; Oke, 1971) although other stellar systems, for example globular clusters, have also been observed (van den Bergh and Henry, 1962; Schild, 1972). The measurements have not been without problems; the determination of all these absolute energy curves depends on the absolute flux calibration for Vega (α Lyr). Oke (1964) used an absolute calibration for α Lyr based on a model atmosphere which fitted well with data available at that time; the star was subsequently recalibrated (Oke and Schild, 1970) using terrestrial standards, and this affected subsequent scanner observations of galaxies. The α Lyr standard has continued in use (e.g. Oke and Schwarzchild, 1975).

The use of scanner observations of galaxies has not been confined to K-corrections; they have been used for the determination of redshifts (discussed in section 2.3), and to provide fairly detailed information for stellar population synthesis; for example, Spinrad and Taylor's work at a resolution of 16 Å (Spinrad and Taylor, 1971). Recent work has been possible on very faint objects by the introduction of faster systems, for example the multichannel spectrometer on the Hale 5m telescope (Oke 1969) enabling simultaneous observations to be made with 18 channels, and more recently the image-dissector scanner system of Robinson and Wampler (1972), using a computer-controlled scan of an image-tube screen to provide 2048 channels, and the Image Photon Counting System (Boksenberg 1972). This type of system enables the sky background to be subtracted

from the spectrum easily, as in standard photoelectric photometry.

As noted above, most of the work on energy distributions of galaxies has been on elliptical galaxies. However Wells (1973) observed energy distributions of 13 galaxies from type E2 to types Im and IO, using a scanner, at a resolution of about 50 Å. Wells used the revised calibration of α Lyr by Oke and Schild (1970) with slight corrections for instrumental differences. He grouped his observations into 4 sections: E and SO, Sa and Sb, Sbc, Sdm and Im; then obtained K-corrections for each of these groups, out to a redshift of $\sim$ 0.3, for B and V colours. Wells' corrections for galaxy types that had previously determined K-corrections agreed well with the earlier values, except in cases where adopted extrapolations of energy curves could have been different. He suggested that the OAO-2 ultraviolet photometry of galaxies could be used to provide improved extrapolations, and this suggestion was taken up by Pence (1976). Pence constructed energy distributions of 5 groups of galaxies: E-SO, Sab, Sbc, Scd, Sdm-Im, from the work of Wells; Oke and Sandage (1968); and OAO-2 ultraviolet observations. In several cases he had to use interpolations between types, and the extrapolations of Wells into the red for spiral galaxies; however most uncertainty comes from the OAO-2 data, which Pence notes to be based on a preliminary analysis, and could be 'significantly revised in the future'. Pence did attempt to synthesise a better curve for the E-SO galaxy type in the ultraviolet, using an observation of such a galaxy at high redshift, and OAO-2 stellar observations.

The energy distributions given by Wells and Pence are useful when considering the appearance of low-dispersion objective prism spectra of faint galaxies. In particular, the metallic-line blanketing continuum drop at $\lambda \sim$ 4000 Å is shown well for galaxies of type E-SO, and this feature still appears fairly strongly for type Sa and Sb galaxies. These measurements were made with $A/D_o \sim 1$, thus tracings through the nuclear regions of objective prism spectra of Sa/b galaxies should more closely resemble the energy distributions of E-SO galaxies. This 4000 Å feature, henceforth referred to as such, has however reduced in size to the level of

other features in the spectrum at that resolution for Sbc galaxies, and for Sdm and Im galaxies, emission lines dominate the spectrum. The usefulness of these features for the determination of radial velocities is discussed in section 2.3.

Galaxies of type E to Sb can thus be expected to exhibit the main features of E-S0 type intensity distributions in their nuclear spetra, or in other terms, to have late-type spectra. At very high redshifts ($z \gtrsim 0.4$) the 4000 Å feature is redshifted out of the range of the IIIa-J emulsion, and the energy distribution from the ultraviolet is shifted into the IIIa-J spectral range. There are no prominent features in this range in Pence's distributions, almost certainly due to lack of resolution in the OAO-2 observations; any features present would have to be determined by reference to spectra of high-redshift objects obtained using large telescopes.

At extremely high radial velocities ($z \rightarrow 1.0$), the sharp rise in intensity in the ultraviolet of the spectra of spiral galaxies would appear in the IIIa-J passband, but these objects would probably be too faint to appear on low dispersion objective prism photographs. If they did appear it would be as very blue objects.

Morton et al (1977) noted the problems of identification of satisfactory features in the spectra of very high redshift galaxies. They suggested the use of features observed in stellar spectra using the Copernicus satellite.

More recently with the advent of the IUE satellite, it is likely that medium resolution ultraviolet spectra of galaxies will become available, such as those given by Johnson (1979) for the nuclei of M31 and M32. These cover a wavelength range of 1100 Å to 3400 Å at resolutions better than 10 Å. Further work along these lines is needed to ascertain the ultraviolet spectra for galaxies of different types.

2.3 Radial velocities of galaxies.

The increase in redshift with distance is a fact now taken almost completely for granted; yet it came as something totally new to astronomers making early measurements of radial velocities. Interest in such measurements was principally in the determination of the solar motion in our galaxy, then considered to be an enormous system comparable in mass to the Coma-Virgo cloud of galaxies (Shapley, 1929). Slipher obtained the first radial velocities of galaxies, the first one being M31 (Slipher, 1914), and these were examined by Strömberg (1925) in an investigation to determine the solar motion; he attempted to correlate radial velocity with distance (obtained by assuming the same brightness for all galaxies) and also direction, and from the limited data available concluded that the only correlation that could be accepted for the galaxies was between velocity and galactic latitude. It was left to Hubble (1929) to use distances estimated by more accurate means to find the correlation between velocity and distance, out to a velocity of +1090 kms^{-1} and a distance estimated at that time to be 2 Mpc. The Hubble constant, H_o, was estimated to be about 500 kms^{-1} Mpc^{-1}, the exact value depending on the grouping of the data. Radial velocity work from these beginnings up to about 1971 is discussed by Sandage (1975a) who also discusses the cosmological ideas and implications of redshifts.

Here it would be useful to discuss the terms 'radial velocity' and 'redshift'. What is actually measured is the displacement in wavelength, $\Delta\lambda$, of spectral lines, or the energy distribution; for a given object $\Delta\lambda/\lambda_o = z$ is constant for all wavelengths, where λ_o is the rest wavelength of the measured line, and z is the redshift. In stellar work in our own galaxy, the radial velocity is, fairly accurately, cz (c being the velocity of light) as the velocities involved are very small; Hubble and Humason (1931) applied this to galaxies, and calculated the 'apparent velocity' cz. This expression has continued in use as the convention for velocities, although it is not, strictly speaking, a velocity. The terms 'redshift' and 'radial velocity'

are, however, used rather loosely in the literature and this carries over into this thesis. The reshift z is generally quoted for the higher velocity objects, rather than the radial velocity, cz.

From 1929 to the present date much work has been done in obtaining velocities of fainter and more distant objects. Hubble and Humason (1931) extended the redshift-distance relation to nearly 20,000 kms^{-1} at over 30 Mpc, with H_o = 560 kms^{-1} Mpc^{-1}; the uncertainty in this value, including possible systematic errors in the magnitudes, was said to be'definitely less than 20 per cent'. However Humason, Mayall and Sandage (1956)(HMS), in their huge work on 'Redshifts and magnitudes of extragalatic nebulae', reduced H_o to 180 kms^{-1} Mpc^{-1},'probably uncertain by 20 per cent'. Their total sample was of over 800 galaxies, as compared to Hubble and Humason's (1931) sample of about 90 galaxies, half of these being from Hubble's (1929) original sample; the change in H_o was caused partly by a change in the distance scale, and partly by the discovery that some of the objects in galaxies identified by Hubble as stars are in fact HII regions.

Further revision of the distance scale led Sandage (1958) to suggest that H_o could range between 50 and 100 kms^{-1} Mpc^{-1} with a very large uncertainty, and in fact the values found to the present have been over this range, for example $H_o = 56.9 \pm 3.4$ kms^{-1} Mpc^{-1} (Sandage and Tammann 1975b) and $H_o = 75 \pm 5$ kms^{-1} Mpc^{-1} (de Vaucouleurs 1976); it is notable that recent workers in this field are even more optimistic than their predecessors when quoting errors in H_o!

The highest redshift in HMS is that of a galaxy in the Hydra cluster, with a velocity of 61,241 kms^{-1} (z = 0.204); subsequently Baum (1958), using a different technique, measured the velocities of two clusters near the plate limit of the National Geographic sky survey, the clusters having z = 0.29 and 0.35. Objects measured at higher redshift have been radio sources, identified from positions in radio source catalogues, beginning with Minkowski's determination of the redshift of 3C295 in 1960 (Minkowski, 1960) at z = 0.461, from the identification of only one emission line on two

plates of 4.5 and 9 hours exposure at a dispersion of 700 Å mm^{-1}. This remained the highest published redshift until the advent of new image intensification techniques; in 1975 Spinrad et al (1975) published the redshift of 3C411, $z = 0.469$, obtained using the Robinson-Wampler image dissector scanner (IDS). Further redshifts of radio sources out to that of 3C318, $z = 0.752$, have been obtained using the same technique (Spinrad and Smith, 1976), using two emission lines seen after a total of 11.6 hours integration. Kron, Spinrad and King (1977) have observed a galaxy in a very faint and rather blue cluster of galaxies seen on a deep plate taken with the 4m telescope at Kitt Peak, and claim a possible redshift of $z = 0.947$; this is however based on very weak features in a very noisy spectrum, and they themselves considered other possible redshifts for this object.

A recent review of radio source identifications and redshifts is given by Spinrad (1976), who cites earlier reviews of similar work. Redshifts are still obtained, of course, for galaxies that are not necessarily radio sources, especially for cluster galaxies (e.g. Faber and Dressler, 1977). A 'Catalogue of galaxies having radial velocities' was given by Fredrick and Gutsch (1974); unfortunately not complete to 1971, as Sandage (1975a) claims: many objects from HMS are not included, probably because objects from HMS with velocities greater than 15,000 kms^{-1} would not have appeared in the 'Reference catalogue of bright galaxies' (de Vaucouleurs and de Vaucouleurs, 1964 (BGC)), which was one of the sources used by Fredrick and Gutsch. The revised BGC (RBGC) (de Vaucouleurs et al, 1976) also does not contain <u>all</u> objects with measured velocities greater than 15,000 kms^{-1}. There have been several further compilations of radial velocities (e.g. Sandage, 1978; Kelton, 1980; Eastmond and Abell, 1978; Rubin et al, 1976; Kirshner et al, 1978) which however are all of bright galaxies, with the exception of the data provided by Kirshner et al which extend to $m_B \sim 15.5$.

In addition to the work of Spinrad et al, present groups actively producing radial velocities of faint galaxies include Sandage et al (e.g. Sandage, Kristian and Westphal, 1976) and Gunn and Oke (1975); however even with image tube systems work of

this nature can only proceed slowly; only a very small percentage of even moderately faint galaxies have their redshifts determined.

The low surface brightness of galaxies has always made the determination of radial velocities difficult, as compared to stars. With each improvement in technique, long exposures or integration times have been considered worthwhile to obtain velocities of objects as distant as possible (e.g. Slipher, 1914; Minkowshi, 1960; Spinrad and Smith, 1976). Such problems with slit spectra, where redshifts are obtained from absorption and emission lines, or, quite often for the faintest objects, emission lines only, have caused astronomers to look for different techniques. Essentially two other techniques have been used to determine redshifts; firstly, by the measurement of galaxy colours; secondly, by fitting a standard energy distribution to that of the observed galaxy.

The first technique was applied by Baum (1957, 1962) although he used it in a way that more closely resembles the second technique! Baum obtained multicolour photometry of galaxies in clusters, over a very wide wavelength range (using filters centered on wavelengths from 3730 $\mathring{A}$ to 9875 $\mathring{A}$). He then plotted these colours as a very low resolution energy distribution, and fitted to the observed curves the mean energy distribution of six elliptical galaxies in the Virgo cluster, by shifting the standard curve to the red, thus obtaining the redshift; Baum's errors in z were about $\pm$ 0.03.

Oke and Sandage (1968), investigating K-corrections for giant elliptical galaxies, gave a plot of observed B-V colours against redshift, which is well correlated over the range $0 < z < 0.2$; this effect was later discussed in more detail by Sandage (1973b), who looked at plots of (B-V), (V-R) and (B-R) against redshift. He concluded that redshifts of giant elliptical galaxies to an accuracy of about $\pm$ 0.01 in z could be obtained from the measurement of colours alone; and to cover the range $0 < z \lesssim 0.9$ only 4 filters would be needed. His error is estimated from the dispersion of the colour-redshift plot; of course this only applies to giant elliptical galaxies,

or galaxies with exactly the same intrinsic colours as giant ellipticals. There is a correlation between the absolute magnitudes and colours of galaxies; this was noted by de Vaucouleurs (1961). The higher redshifts could be affected by colour evolution of galaxies; Sandage suggested that this could be looked for by comparing the observed colour-velocity relation with that predicted for a standard giant elliptical energy distribution.

The second method of determining radial velocities, by fitting spectral energy distributions, was first used by Oke (1971). Scanner observations of galaxies, again giant ellipticals in clusters, were correlated with the energy distribution, suitably redshifted, obtained by Schild and Oke (1971), shifting the standard distribution until the best fit was obtained. Oke also quotes the error as $\pm$ 0.01 in z; and again, the procedure can only be used for galaxies with the same energy distribution as the standard galaxy. This method does require long integration times; with Oke's original equipment, 3C295 (observed by Minkowski (1960)) required a total of 8 hours observing time.

Another investigation related to this second method was that of Vanderkerkhove, who compared the gradient of the galaxy continuum observed at a fixed wavelength, from microdensitometer tracings of galaxy spectra on objective prism photographs, with published redshifts of galaxies (Vanderkerkhove, 1963). He later noted, however (Vanderkerkhove, 1965) that for galaxies in the Virgo cluster, the dispersion of velocity at a given gradient was very large, and that the effect of velocity on gradient was very small, the main cause of the dispersion being due to variation in composition of the galaxies observed. Vanderkerkhove obtained only a poor correlation between gradient and colour index, parameters which should be reasonably well correlated; a possible explanation is that he neglected the smoothing effect of the galaxy luminosity profile on the spectrum, an effect which would vary considerably from an E galaxy to an Sc galaxy.

These methods have some relevance to the determination of radial velocities of galaxies from an objective prism plate. Vanderkerkhove calibrated his photographs to construct the energy

distribution, and this could be done for the UKST photographs. With some form of wavelength calibration either relative colours could then be obtained, which seems a little wasteful of the information content on the plate, or the whole energy distribution could be fitted to a standard. Again, however, this standard would have to possess the same intrinsic energy distribution as the galaxy being observed, which puts severe limitations on the technique. Easily identifiable features in the galaxy spectra would ease these problems considerably. Such a feature is that at 4000 Å mentioned in section 2.2. If this feature could be identified unambiguously, it would be ideal to enable redshifts to be provided directly, instead of indirectly (by causing a colour change as it passes through a filter bandpass), since it is a very large feature and is prominent even in low dispersion objective prism spectra. The only difficulty is that there are other changes in slope and breaks in galaxy energy distributions (Wells 1973, Pence 1976) and care would need to be taken in order that other features distorted by the emulsion's response were not mistaken for the 4000 Å feature. Ideally all the features present in these energy distributions would be used to obtain redshifts from low dispersion spectra.

The vast majority of radial velocities of galaxies obtained to the present have been of galaxies with velocities less than about 15000kms^{-1} (z= 0.05). Even though incomplete and out of date, the catalogue of Fredrick and Gutsch (1974) shows the general trend; fig 2.3.1 is a histogram of the numbers of redshifts in that catalogue, binned into 1000 kms^{-1} intervals. This shows the general picture at the commencement of the present work; between that date and the present the diagram has been filled in somewhat, mainly below about 15,000 kms^{-1}. The subsidiary peak around 6000 kms^{-1} is caused by velocities in the Coma cluster of galaxies. This histogram gives a general picture of the relative numbers of redshifts obtained at different velocities, and contains a total of about 2600 galaxies. A complete histogram to 1971 would go out to z = 0.461 for 3C295 and contain other high redshifts, but in tens rather than hundreds.

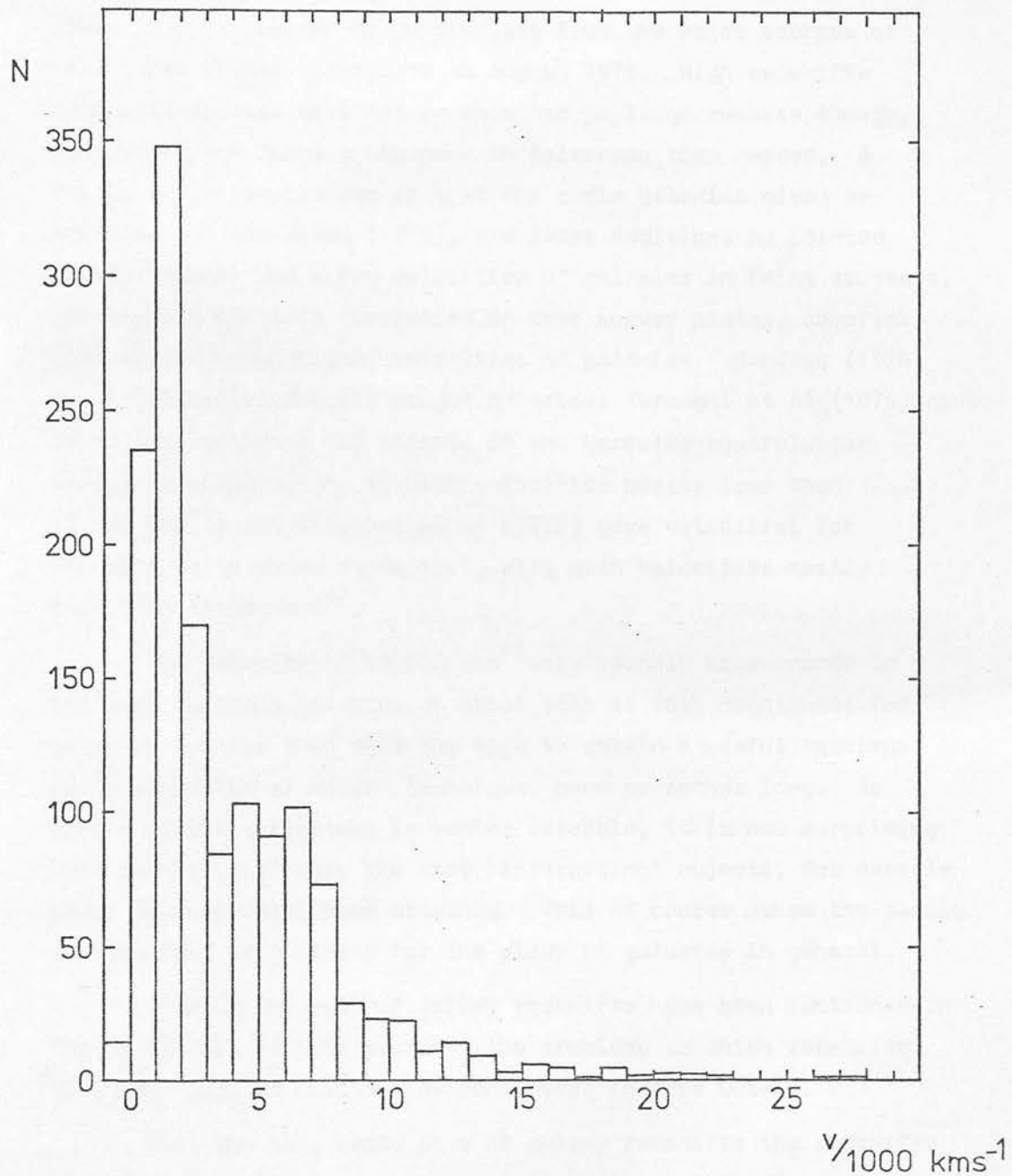

Fig. 2.3.1

Histogram of redshifts in the Fredrick and Gutsch (1974) catalogue.

A more recent sample is that in the RBGC, which contains 2502 radial velocities less than about 16,000 kms^{-1}. The authors state that this catalogue is not complete. Gisler and Friel (1979) give an index to spectra of 2004 northern hemisphere galaxies; these, too, mostly have velocities less than 15,000 kms^{-1}. Their list is claimed to be complete from the major sources of velocities in the literature to August 1978. High redshifts from slit spectra will not be obtained in large numbers though, because of the large investment in telescope time needed. A fairly large compilation is that for radio galaxies given by Kristian and Minkowski (1975), and later additions by Spinrad (1976); these, and a few velocities of galaxies in faint clusters, for example clusters discovered on deep survey plates, comprise most of the known higher velocities of galaxies. Sandage (1978) gives velocities for 719 bright galaxies; Tarenghi et al (1979) give velocities of about 150 objects in the Hercules supercluster field, to about $m_B \sim 16$ with velocities mostly less than 15,000 kms^{-1}; and Kirshner et al (1978) gave velocities for 164 objects to about $m_B \sim 15.5$, also with velocities mostly less than 15,000 kms^{-1}.

The velocity of 15,000 kms^{-1} very roughly corresponds to the more luminous galaxies at about 15th or 16th magnitude; for galaxies fainter than this the time to obtain a useful spectrum using conventional modern techniques becomes rather long. As time on large telescopes is rather valuable, it is not surprising that redshifts of only the more 'interesting' objects, for example radio sources, have been obtained. This of course makes the sample of redshifts very biased for the study of galaxies in general.

Some of the uses of galaxy redshifts have been mentioned in the first part of this section; the problems to which redshifts have been applied will now be considered in more detail.

From the very early days of galaxy redshifts the redshift-distance or redshift-magnitude relation (the Hubble diagram) has been used in cosmological investigations. Details of the progress of the Hubble diagram have been given in the first part of this section, and we turn now to the use of the Hubble diagram

and redshifts as indicators of the large-scale structure of the universe.

Sandage has written extensively on this subject, both in reviews (e.g. Sandage, 1961; Sandage, 1975a) and in a series of papers on the redshift-distance relation (Sandage 1972 a-c; 1973 a-d; 1975 b) and the Hubble constant (Sandage and Tammann 1974 a-d; 1975 a,b; 1976). In an early review (Sandage 1961) he showed how the Hubble diagram is expected to change for different values of the deceleration parameter, q_o; current estimates of the value of q_o cover the range -1 to 1 (Gunn and Oke, 1975; Sandage and Tammann, 1975 b; Hawkins and Martin, 1977) but there is little difference in the Hubble diagram for $q_o = -1$ and $q_o = +1$ out to $m_B \sim 19$, the range of q_o at this magnitude corresponding to a factor of 1.2 in velocity. To obtain a better estimate of q_o from the Hubble diagram, it must be extended to fainter magnitudes; this is the intention of Sandage, Kristian and Westphal (1976, also Kristian, Sandage and Westphal 1978). The deceleration parameter can be obtained directly from the shape of the Hubble diagram, but the determination of H_o itself depends on the absolute magnitude (and hence distance) scale. This is a great problem itself, though not a part of the present study, and is the principal concern of the papers by Sandage and those of Sandage and Tammann. This field of study is not without some controversy; de Vaucouleurs (1977) has criticised the distances used by Sandage and Tammann for Cepheids and HII regions (paper I) and their calibration of galaxy luminosity classes (paper IV). Another consideration in this type of work is the fact that possible evolutionary corrections may be needed to the parameters used to determine the Hubble diagram.

The Hubble diagram can also be used to test the isotropy of the universe, by looking at the redshift-distance relation in different directions; de Vaucouleurs (1976) considered this problem locally (insofar as the local supercluster, the cloud of galaxies centered on the Virgo cluster, can be considered 'local') and concluded that there is anisotropy between the local supercluster centre and anticentre. This he attributed to a rotation-expansion model of the local supercluster. On a larger scale Sandage,

Tammann and Hardy (1972) attempted to put limits on perturbations from a linear redshift-magnitude relation from first-ranked cluster galaxies, and on large-scale inhomogeneity; from both their cluster data, and from galaxy counts, they concluded that there is no significant departure from large scale homogeneity. This discussion continues. Recently, de Vaucouleurs and Bollinger (1979) presented results showing variations in the Hubble constant from $\sim$75 to $\sim$110 kms^{-1} Mpc^{-1}. Tammann et al (1979, 1980) and Sandage et al (1979) see no evidence for a deviation from an isotropic velocity field. Rubin et al (1976b) also considered that an isotropic velocity field is more likely than the anisotropic case. There is clearly still a lack of concensus on this matter.

High dispersion spectra of resolved galaxies can be used to obtain radial velocities at locations within the galaxies, and hence deduce the internal motions of the galaxies. A large number of papers, mainly dealing with individual galaxies and performing similar analyses for each, have been published by Burbidge et al; an example, that on the velocity field in NGC 6181 is by Burbidge, Burbidge and Prendergast (1965). The main use of the galaxy rotation curves produced from such observations is in the determination of galaxy masses; the theory behind this is described by Burbidge and Burbidge (1975). This type of work is not of relevance to objective prism techniques, and is mentioned here only as an example of another use of galaxy radial velocities.

In addition to using the redshifts of particular (for example, first ranked) cluster galaxies in the Hubble diagram, redshifts of cluster galaxies are also used in the determination of cluster velocity dispersions. (A recent compilation is given by Yahil and Vidal (1977), who include clusters having redshifts of at least ten member galaxies; unlike the compilation of Solinger and Tucker (1972) which has the dispersion of the Centaurus cluster calculated from the velocities of three galaxies!) Cluster velocity dispersions can be used to obtain the virial mass (Schwarzchild, 1954), a dynamical mass which combined

with cluster luminosities has been used to estimate the mass to light ratio of clusters. There is also some evidence that velocity dispersion is correlated with X-ray source luminosity, for those X-ray sources located within clusters (e.g. Dawe et al, 1977). A problem allied to cluster dispersions is that of cluster membership; any galaxy appearing in a cluster field but having a widely discrepant velocity from the other cluster members is generally excluded as a foreground or background object. The ability to discriminate between cluster and field galaxies is useful when attempting to determine the total extent of a cluster.

One interesting application of large numbers of redshifts in a small region of sky has been described by Tifft and Gregory (1976), who compiled a list of all the redshifts obtained in the vicinity of the Coma cluster of galaxies. The sample was complete to a limiting $m_p = 15.7$ to a 3^o radius from the cluster, and to $m_p = 14.9$ out to a 6^o radius. For the foreground galaxies they found that the entire sample fell into three groups, with the exception of one galaxy; the areas between the groups being totally devoid of galaxies. Tifft and Gregory give charts of the galaxy locations on the sky for various redshift ranges, corresponding to 'slices' through the region; the distribution of the groups involved can be clearly seen. They point out that much additional work is needed to refine the picture of the Coma cluster (their sample consisted of over 300 galaxies) by obtaining more galaxy velocities. Similarly, Tarenghi et al (1979) have, more recently, performed a similar study on galaxies in the Hercules supercluster, showing the distribution of galaxies in depth with a 'cone' diagram of declination and redshift. This work is summarised neatly by Chincarini and Rood (1980).

This application could be extended to much larger volumes of space if large samples of redshifts could be obtained for fainter galaxies; it is not really necessary to have an accuracy so great as to be able to measure directly cluster velocity

dispersions; the ability to resolve one cluster from another is all that is required. This approach over sufficiently large volumes of space could also give more information on the superclustering of galaxies, i.e. clouds of galaxies from about 6 to 30 Mpc in diameter (Shane, 1975) consisting of several galaxy clusters. The exact distribution of galaxies in depth is certainly not well known; both Tifft and Gregory, and Tarenghi et al, remarked on the 'voids' between clusters in which there appear to be no galaxies. With the reported 'shell' of galaxies at $\sim$ 10,000 kms^{-1} (Kirshner et al, 1979), and the 'pancake' models of Doroshkevich and Shandarin (1978) for the formation of clusters of galaxies, it is clearly still of great interest to resolve the the structure of the universe on the scale of superclusters. Details of this application are discussed in section 4.2.

3. Establishing the technique.

3.1 Photographic material

The objective prism spectra used in this work are all on photographs. In this section the source plate material itself is summarised, and the appearance of objective prism spectra on the photographic emulsion described, in conjunction with a discussion of the intensity calibration problems, all of which ought to be understood before setting out to interpret the images. The prism dispersion curve is also presented, as this relates directly to the spectra observed on the photographs. Finally, essential details of the UK Schmidt telescope are given.

(a) Source material

In late 1975, when this work was started, no objective prism photographs had been taken with the UK Schmidt telescope. Several trial photographs of fields containing galaxies had been taken using a prism on the Edinburgh Schmidt telescope, but nothing useful showed on these plates because the only galaxies bright enough to be photographed against the bright sky background are so large that spectral information is smeared out by the galaxy luminosity profiles. The earliest material available containing good spectra of galaxies came from the Curtis Schmidt telescope at the Cerro Tololo Interamerican Observatory (CTIO), consisting of photographs taken by Smith (1975) for the morphological classification of spectra of galaxies. This was essentially an emission-line object survey. These plates are taken on nitrogen-baked Kodak IIIa J emulsion; no intensity calibration is given. The plates are about 8 inches square, with a plate scale of 97 arcsec mm^{-1}. The plates initially available are listed in table 3.1.1; most of the initial work was undertaken in an area two degrees square on plate 17732. The results of this preliminary work on redshift determination are given in Cooke et al (1977) and described in section 3.3.

The first prism run on the UK Schmidt telescope occured in July 1976, and one of the areas selected by the UK Schmidt telescope unit (UKSTU) for the first few objective prism photographs, UKSTU survey area 345, was chosen for the preliminary measurements.

Table 3.1.1

Plate material from the CTIO survey loaned by Dr. M.G. Smith

Plate no.	α	δ	exposure min	emulsion	filter	type
18482	11 00	-4^{o}	80	IIIa-J	--	Prism
19138	11 00	-4^{o}	45	IIa-O	GG385	Direct
17725	12 00	$-8^{o}.5$	80	IIIa-J	--	P
19139	12 00	$-8^{o}.5$	45	IIa-O	GG385	D
18483	12 20	-13^{o}	80	IIIa-J	--	P
19140	12 20	-13^{o}	45	IIa-O	GG385	D
17732	12 40	-4^{o}	80	IIIa-J	--	P
19141	12 40	-4^{o}	45	IIa-O	GG385	D
18097	13 20	-4^{o}	80	IIIa-J	--	P
19151	13 20	-4^{o}	45	IIa-O	GG385	D
19152	13 20	-4^{o}	3	IIa-O	--	D
18105	14 00	$-8^{o}.5$	80	IIIa-J	--	P
19143	14 00	$-8^{o}.5$	45	IIa-O	GG385	D

IIIa-J plates are nitrogen baked.

Several prism runs have occurred since that time,and a list of plates used directly in this work is given in table 3.1.2. This list also inclues direct (taken without the prism) plates of the prism plate areas. The plates were all hypersensitised (Sim, 1977; Sim et al, 1976). In the table are also given the exposure time, UKSTU estimated seeing size, and plate batch number, as these factors are useful when determining the quality of the plates. The UKSTU plates are about 14 inches square, with a plate scale of 67 arcsec mm^{-1}; the unvignetted area of the plates is the central circle about 4 degrees across.

Initially the area of sky chosen for this work, area 345, was selected because of the availability of a fairly good plate (UJ2461P) from the first prism run, covering an area at high galactic latitude(to avoid problems of crowding due to stellar spectra). Once a fair amount of work had been carried out on this area it was considered better to have more plates of that area, for repeat work, rather than to start on a completely new area. This has proved not to be a particularly good choice; area 345 is lacking in rich clusters of galaxies suitably placed, and in a suitable magnitude range, to provide plentiful sources of galaxies for which the velocities can be obtained (section 4.1). The repeat plates of survey area 345 are, however, of great use for tests of repeatability (section 3.5) and for a comparison of photographs taken under different conditions.

(b) Appearance of the spectra

The spectra on these objective prism plates are very small. On the UKSTU plates, with a plate scale of 67 arcsec mm^{-1} and a dispersion of 2400 Å mm^{-1} at 4300 Å, the spectra are a little under a millimetre long on IIIa-J emulsion, and may be as narrow as 25-30 microns for an untrailed stellar image on a plate taken in very good seeing. (The CTIO spectra are about twice as long, with a dispersion of about 1200 Å mm^{-1} at H γ .) At this scale, one arcsecond (the typical seeing disc) corresponds to about 14.5 microns on the plate, or about 30 Å at 4300 Å. To the eye, spectral features can be confused with plate effects for unwidened spectra; features are much better seen in widened spectra (plate 3.1.1). (The terms

Table 3.1.2

Plate material from the UKSTU. The plates were initially taken for various workers; full details can be found in the UKSTU plate catalogue.

Plate	area	α	δ	exposure min	emulsion batch	grade	seeing arcsec	comments
UJ2616P	SGP	00 53.0	-28 03	60	1I5	AF	3	
UJ3682P	SGP	..	..	70	2C7	A	1	
UJ4543P	475	01 06.0	-25 00	60	188	B	2	
UJ4117P	789	12 30.0	-05 00	20	2I6	A	2	
UJ2451P	141	19 00.0	-60 00	2	2H5	A	2	widened
UJ2620P	HTM	22 14.0	-35 40	75	3C6	BI	2	
J1665	345	22 32.0	-40 00	38	3C5	C	2	
UJ2461P	345	..	..	60	1I5	A	2	
J2599	345	..	..	60	1I5	BP2	2	
UJ3092P	345	..	..	60	2I6	BIF	1	peculiar fog
UJ4530P	345	..	..	40	188	A	2	widened 100μm
UJ4539P	345	..	..	40	188	A	1	
UJ4563P	345	..	..	40	188	B	2	prism 0°
UJ4551P	DE	23 52.0	-10 41	40	188	A	2	

codes:
- UJ unfiltered IIIa-J
- J IIIa-J, 'J' filter
- P objective prism; all prism 180° except 4563
- HTM MacGillivray, field N1
- DE A2670 field

grades:
- A,B,C overall grade
- I large images
- P processing fault
- F fogging

Details of grading procedures are to be found in Cannon,R.D., Hawarden,T.G., Sim,M.E., Tritton,S.B., 1978 Occasional Reports of the ROE no. 4.

Plate	F star	K star	Elliptical galaxy	Spiral galaxy
UJ2461P 2" seeing 60m exposure	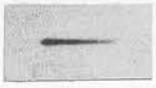			
UJ4539P 1" seeing 40m exposure				
UJ4530P 2" seeing 40m exposure				

Plate 3.1.1

Appearance of spectra on UKSTU plates

broadened, widened and trailed are used synonymously here.) Unfortunately widened plates do not penetrate deep enough for extragalactic work, but they have little advantage there in any case as the resolution is limited by a convolution of the seeing disc with the galaxy luminosity profile, rather than the seeing disc alone. Plate 3.1.1 gives a comparison of spectra from different objective prism photographs, for early and late type stars and elliptical and spiral galaxies. The sharp 'head' end of the spectrum corresponds to the sharp emulsion cutoff at the long wavelength end for the IIIa-J emulsion; the tailing off into plate background is a combination of low intrinsic UV emission in the objects and the earth's atmospheric absorption.

Several features are apparent from these photographs of spectra. Firstly, the effect of seeing is very noticeable, particularly on the stellar spectra. The improved visibility of features in the widened stellar spectra is also clear. Secondly, the spiral and elliptical galaxy types are quite distinct; the elliptical galaxy has a smoothly diffuse light distribution, whereas the distribution for the spiral can be seen to be more sharply peaked in the centre. In fact both of these galaxies are rather large for redshift determination; they were chosen to show this difference clearly. The distinction between spirals and ellipticals is rather less pronounced for smaller, fainter galaxies, owing to the seeing contribution becoming more important. The effect of widening on galaxy spectra is also clearly seen; it provides no benefit for our purposes.

(c) The prism dispersion curve

The appearance of the spectra is quite strongly affected by the prism dispersion curve; for a prism the dispersion decreases markedly to longer wavelengths. This has the effect of 'piling up' light towards the red end (actually green, for IIIa-J!) of the spectrum, in addition to any concentration of light in the red intrinsic to the source (e.g. for late-type stars). This causes the quite distinctive dense 'head' to the objective prism spectra.

To calculate wavelengths of features within the spectrum, a wavelength reference point is needed, along with the dispersion

curve of the prism, to relate position along the spectrum to wavelength. The wavelength reference is dealt with in section 3.3; the dispersion curve is discussed here. This work has been published (Nandy et al, 1977); the dispersion curve was obtained by the author.

The procedure was to obtain a set of wavelength reference points from spectra of stars. A short exposure widened plate (UJ2451P) was used, to enable a number of early-type stars to be measured. Nearby B stars were in fact overexposed, but the hydrogen lines were found to be resolved in A stars, and a number of features noted in the spectra of F,G, and K stars. These features were identified by reference to lists of lines detected in the low resolution scanner spectra of Faÿ, Stein and Warren (1974), and in many cases consist of blends, for which the mean wavelength was used. The scans of Faÿ, Stein and Warren were particularly convenient for these identifications, as the resolution (about 30 Å) matches that of a UKSTU prism photograph with a resolution of 1 arcsecond, for a star at 4000 Å. Examples of the spectra traced from the plate using a Joyce-Loebl microdensitometer are given in fig. 3.1.1 with spectral features identified; these examples show the features used to establish the dispersion curve.

Measurements of 35 individual lines from a total of nine stars were used to obtain the dispersion curve. The sets of lines from each star were superimposed by eye to give the best fit to a smooth curve on a plot of wavelength against distance. All the points were then used to fit the Hartmann dispersion formula

$$x = x_0 - a/(\lambda - \lambda_0)^{1.2}$$

$$\text{or} \quad \lambda = \lambda_0 + (a/(x_0 - x))^{(1/1.2)}$$

which gave, for the 35 lines used,

$$x_0 = 1036.95$$
$$\lambda_0 = 1313.41$$
$$a = 15591900$$

for x in microns, λ in Ångstroms. For the data used, the rms scatter was 14 Å in λ, 6 μm in x. A list of lines used, with mean wavelengths and positions, is given in table 3.1.3; this table and the coefficients above are normalised to $x = 0$ at 4340 Å. Over

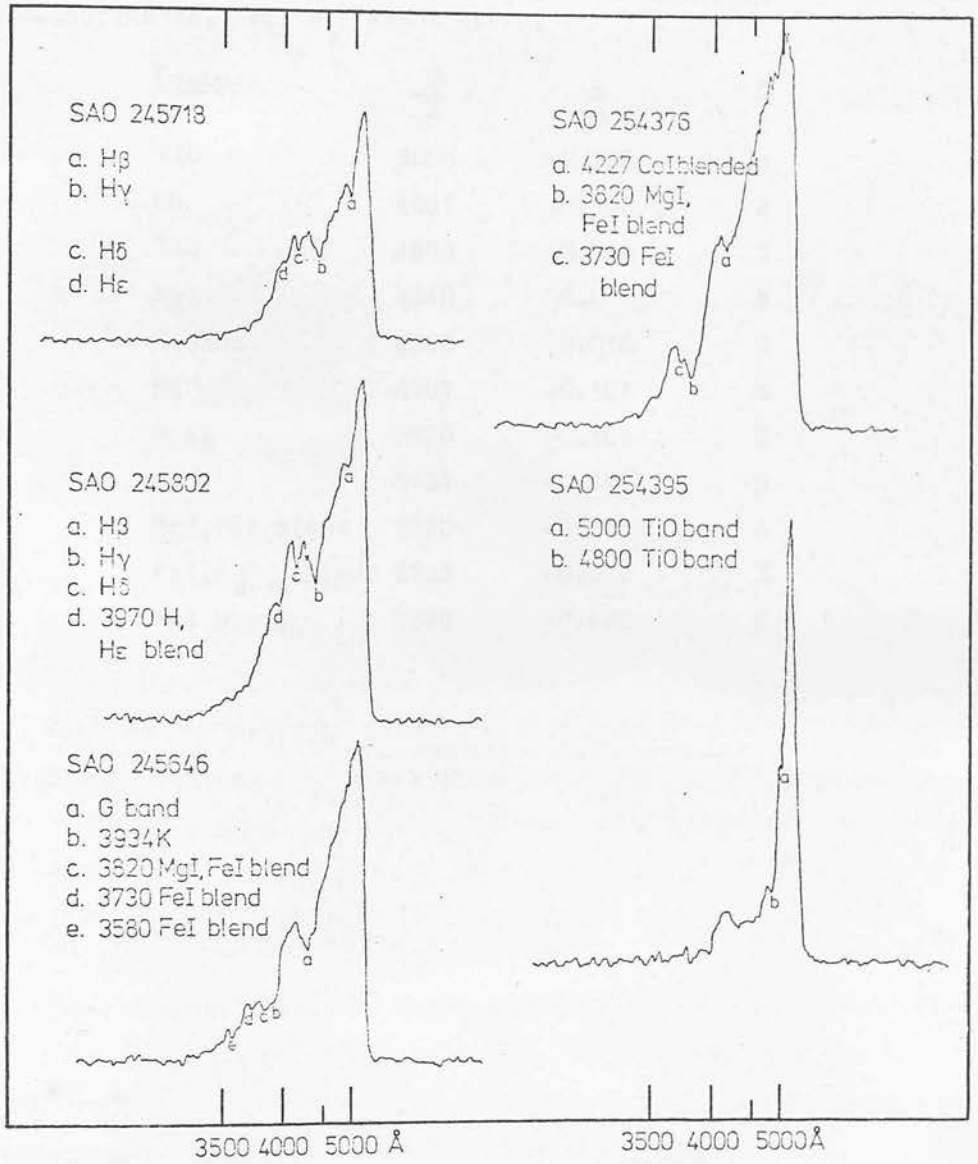

Fig. 3.1.1

Examples of stellar spectra traced from plate UJ2451P. Spectral types are given from the SAO catalogue. The ordinate is density, but the scale is not constant from star to star.

Table 3.1.3

Data from nine stars on plate UJ2451P used to obtain the prism dispersion curve (fig. 3.1.2). λ - wavelength in Å; x - distance in mm from Hγ ; n - number of measurements, from different stars.

Feature	$\frac{\lambda}{\text{Å}}$	$\frac{x}{\text{mm}}$	n
TiO	5000	+0.228	1
Hβ	4861	+0.180	4
TiO	4800	+0.168	1
Hγ	4340	0.0	5
G band	4300	-0.016	3
Hδ	4101	-0.106	5
H,Hϵ	3970	-0.184	2
K	3934	-0.196	5
MgI,FeI blend	3820	-0.254	4
FeI,H_{11-14} blend	3730	-0.322	3
FeI blend	3580	-0.422	2

the range of measurements the fitted curve agrees very well with the manufacturer's predicted curve, the deviation throughout being less than the 14 Å rms scatter. The dispersion curve is given in fig. 3.1.2, with the measured lines indicated. Also marked on the dispersion curve is the position of the cutoff of the IIIa-J emulsion, defined as the half-maximum density point; this position was obtained from the mean of cutoff positions indicated by fitting all the sets of lines to a smooth curve. The value obtained for the cutoff is 5380 ± 30 Å, for a set of objects with maximum density of the brightest objects in the set being 1.2 above sky level.

The dispersion curve is given by the manufacturer calculated for different positions across the plate. The predicted variations of the dispersion curve across the plate are small, and all well within the 14 Å rms scatter obtained from the measurements above.

(d) Intensity conversion

In an objective prism spectrum, each point in the spectrum consists of blackened plate emulsion; the blackening being caused by a combination of light at a single wavelength from the object whose spectrum we are considering, and light from all wavelengths from the sky background. The combination of these sources and the resultant effect on plate blackening is a complicated problem; some comments on this were set out by Emerson (1979) and used by Clowes et al (1980). The problem is also discussed by Clowes (1980). These effects are highly relevant to the use of the objective prism photographs for spectrophotometry, but need not be considered, apart from noting the fact that they are present, for the purpose of obtaining radial velocities.

Some form of intensity conversion is, however, useful. The photographic plate's H-D curve (Farnell, 1966) distorts the light intensity record when measured, for example, with a microdensitometer. Plate density is not, generally, linearly related to light exposure.

Machines producing output in both density form (the Joyce-Loebl microdensitometer) and transmission form (COSMOS) have been used within this project. It has proved necessary from time to time to compare data from one machine with that from another; the ideal way to do this is to convert both sets of data to intensity terms,

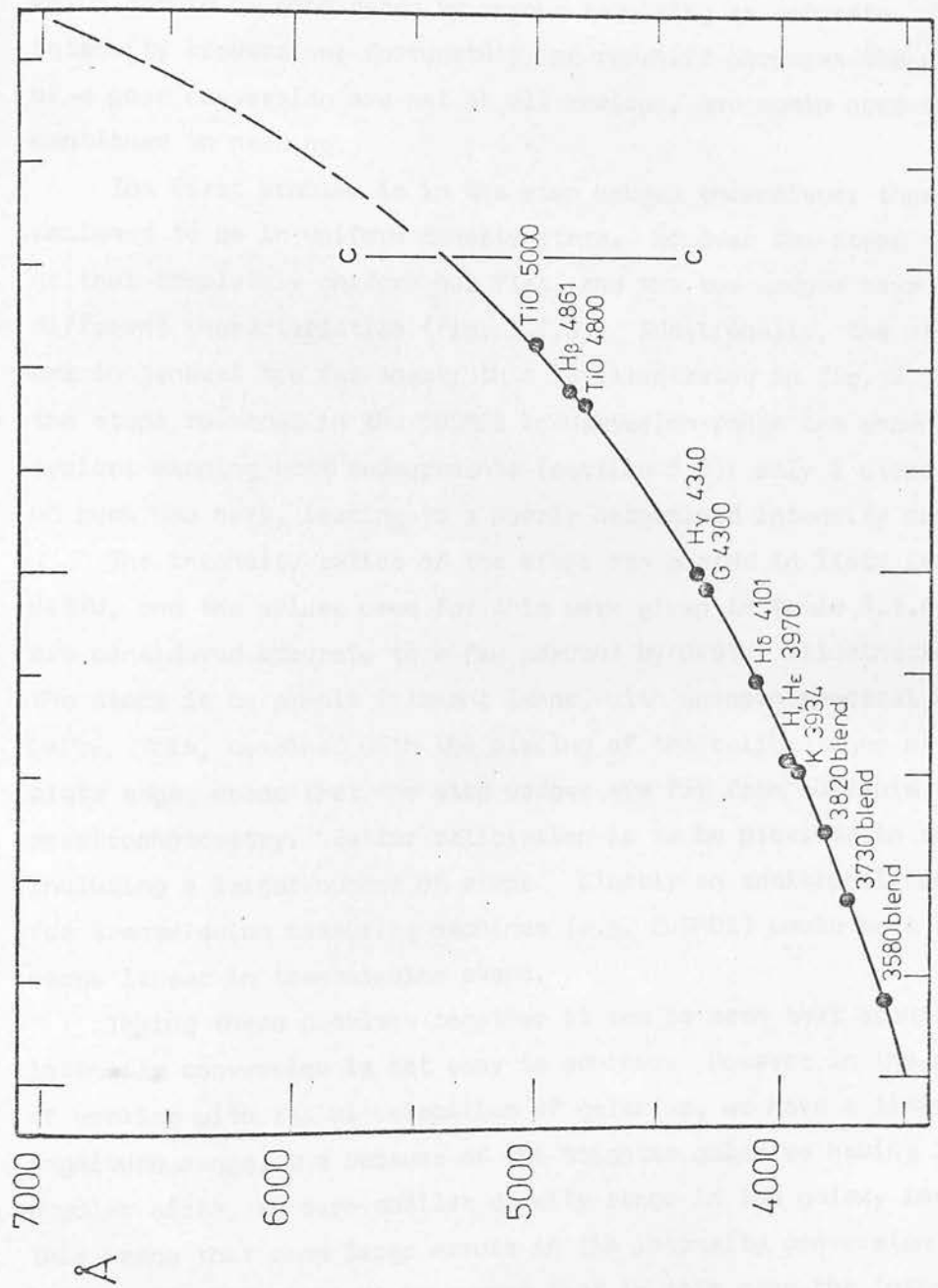

Fig. 3.1.2

Dispersion curve for the UKSTU thin prism. The cutoff position for the IIIa-J emulsion is marked 'c'.

which can then be directly compared. This procedure would appear to be simple, as 'step wedges' (areas of density steps) are photographically recorded on the edges of almost all UKSTU plates. Pickup (1979) used the step wedges to provide an intensity conversion for surface photometry, assuming that the step wedges provide an adequate calibration. There are certainly problems, though, which should be considered by anyone requiring an accurate intensity conversion; fortunately for redshift purposes the problems of a poor conversion are not at all serious, and again need only be mentioned in passing.

The first problem is in the step wedges themselves; these were designed to be in uniform density steps. However the steps are neither completely uniform nor flat, and the two wedges have different characteristics (fig. 3.1.3). Additionally, the steps are in general too far apart; this is illustrated in fig. 3.1.4, where the steps recorded in the COSMOS transmission range are shown, for typical mapping mode measurements (section 3.4); only 3 steps are of much use here, leading to a poorly determined intensity conversion.

The intensity ratios of the steps are quoted in lists issued by UKSTU, and the values used for this work given in table 3.1.4; they are considered accurate to a few percent by UKSTU. Illumination of the steps is by simple filament lamps, with unknown spectral emissivity. This, combined with the placing of the calibrations at the plate edge, means that the step wedges are far from suitable for spectrophotometry. Better calibration is to be provided in future, including a larger number of steps. Clearly an additional bonus for transmission measuring machines (e.g. COSMOS) would be a step wedge linear in transmission steps.

Taking these problems together it can be seen that accurate intensity conversion is not easy to achieve. However in the case of working with radial velocities of galaxies, we have a limited magnitude range, and because of the brighter galaxies having larger angular sizes, an even smaller density range in the galaxy images. This means that even large errors in the intensity conversion have little effect. It might be argued that in this case the intensity conversion serves little useful purpose. The use is limited, but

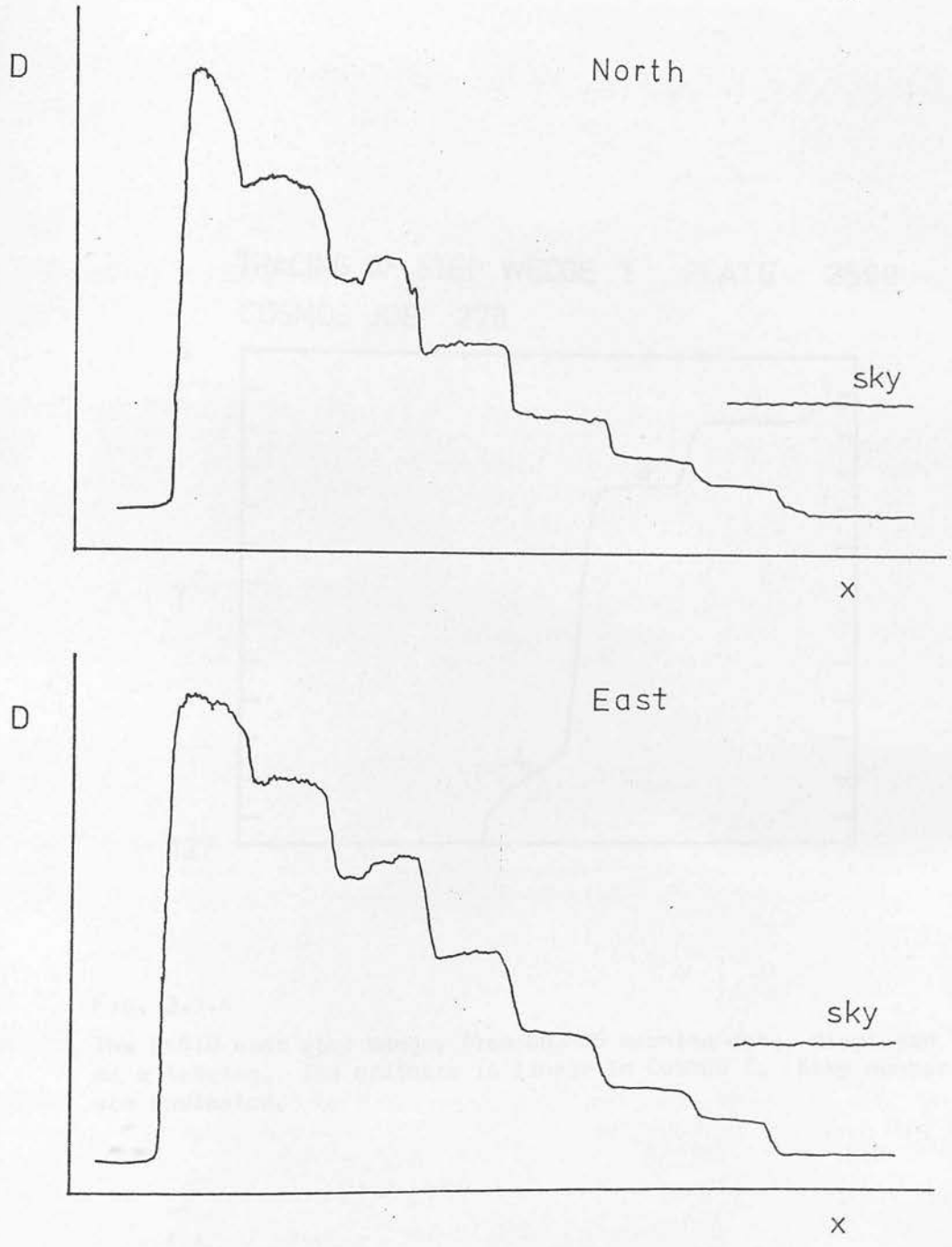

Fig. 3.1.3

Tracings of the UKSTU step wedges in use to 1980, made using a Joyce-Loebl microdensitometer. The ordinate is density. Sky background level is shown.

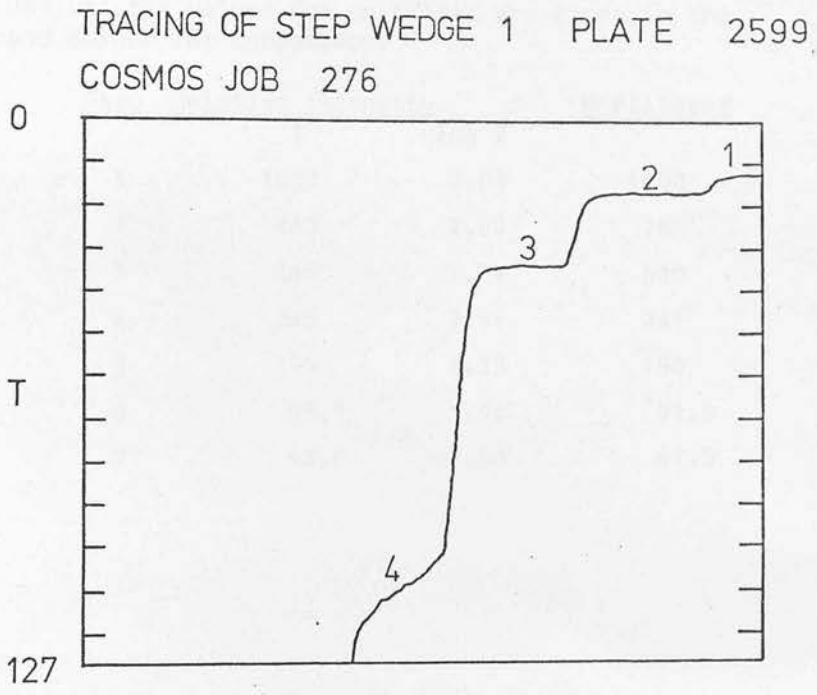

Fig. 3.1.4

The UKSTU east step wedge, from COSMOS machine data, displayed as a tracing. The ordinate is linear in COSMOS T. Step numbers are indicated.

Table 3.1.4

Relative intensities adopted for the UKSTU east step wedge. The north wedge is not used due to its poor step profiles. Values for the B filter are given as these were issued first by the UKSTU; the values for no filter are given in the right-hand column for comparison.

Step	Relative intensity		Unfiltered
	I	log I	
1	1000	3.00	1000
2	763	2.88	763
3	546	2.74	536
4	345	2.54	341
5	195	2.29	190
6	95.1	1.98	91.8
7	42.8	1.63	41.5

it does help comparison of spectra measured on different machines by adjusting the 'shape' of the spectrum (as seen in an intensity tracing) to intensity terms. It can also be used to provide some form of approximate magnitude calibration. All the software for spectrum handling has been set up with the intention of handling either normalised or un-normalised intensity converted spectra, rather than spectra still in raw data form (density or COSMOS T).

(e) The UK Schmidt telescope/objective prism combination.

The UK Schmidt telescope optics give very good image quality over the whole field, and this quality is well exploited with the low dispersion prism used for the present work.

The prism has a diameter of 1.26m, with an apex angle of 44'; it is made of Schott BK7 glass and has a high ultraviolet transmission. When initially tested it was in conjunction with the first corrector plate of the UK Schmidt telescope, which gave good images for $\lambda > 4000$ Å but not in the ultraviolet. Subsequently (plate 3149 onwards) an achromatic corrector plate has been used, giving better ultraviolet spectra.

3.2 Machines for data analysis.

The raw data in this project consist of the photographic plate material described in section 3.1. A large part of the project is concerned with the extraction of information from these photographs, and interpreting this information to produce astronomically significant results. During this process several machines have been used; both measuring machines, and large computers to process data from some of the measuring machines. In this section these machines and their associated problems are described.

3.2.1 Measuring machines.

(a) The Edinburgh Joyce-Loebl microdensitometers.

Several separate Joyce-Loebl microdensitometers exist in Edinburgh, one belonging to the University Department of Astronomy, and the others belonging to the Royal Observatory, Edinburgh. The most general use of these machines has been to provide tracings of objective prism spectra directly, using the ratio arm, density wedge, and recording pen on paper; calibration checks on parameters affected by the ratio arm and density wedge are described in section 3.5. Two of the machines were provided with a digitisation system consisting of a lead-screw table drive, rather than ratio arm drive, with recording of wedge position (hence density reading) on paper tape. This setup was rather out-of-date and slow, using a slow tape punch, and also often in need of maintenance. During the period of this work a new digitisation system was developed, using a PET minicomputer to control acquisition of data (Kelly et al, 1980a); this system has been used to transfer digitised spectra on to the large mainframe computers.

The chief advantages of the Edinburgh microdensitometers are their availability, and their use for measuring the spectra of individual objects fairly quickly almost anywhere on a plate. The disadvantage of these machines is that they are relatively slow if large numbers of objects need to be measured; typically 15 - 20 spectra can be measured in an hour, taking care over focusing and slit adjustment. The repeatability and accuracy of these machines is fairly good; checks were carried out to be sure of consistency, and these are described in section 3.5.

Modifications have had to be made to the plate support systems to handle the 14 inch square UKST plates. The initial modified plate holder consisted of a large aluminium sheet with a hole fixed over the microdensitometer specimen table. This system was not well balanced and suffered mechanical feedback problems: vibration of the plate support caused plate movement in the focal plane, causing pen movement at the density wedge, which, fed back through the microdensitometer structure, reinforced the plate support movement; the system oscillated quite freely! This problem persisted even with extensive damping of the plate support. A solution was found in a much simpler support system, consisting of two felt-covered rails attached to the specimen table. Mechanical feedback is greatly reduced, and in fact a slightly larger area of the plate can be measured.

Another effect that can happen with the Joyce-Loebl microdensitometers occurs when measuring dense spectra with a small sampling slit. In this situation few photons are available to be detected in the feedback system, and the servo loop output becomes noisy, causing the recording pen to vibrate. This is a rare occurence and has not caused any real problems.

(b) The St. Andrews Joyce-Loebl microdensitometer.

This machine merits mention although it was only used for one set of measurements relevant to this work. The system is described by Davenhall et al (1979).

The reason for its use was the existence of a problem on the Edinburgh machines. The original plate supports described above prevented measurements of quite a wide ($\sim$2cm) central strip on the plates, as the Edinburgh machines are only capable of making tracings along one axis. However the St. Andrews machine, based on a Joyce-Loebl 'isodensitracer' model of the microdensitometer can be scanned in x and y directions, thus only a small square in the centre of the plate is inaccessible. This remaining square is inaccessible because the overhang of the optical path through the specimen table is a few millimetres less than half the width of a UKST plate! Additionally, the plate supports on the St. Andrews machine allowed the plate to be traced closer to the centre line.

Thus when measurements of a cluster (Abell 2670 - section 4.1) were needed in the strip inaccessible to the Edinburgh machines, time on the St. Andrews machine was sought.

The machine is computer controlled and is driven in both x and y directions by leadscrews. Otherwise it is essentially similar to the Edinburgh machines. Data produced on this machine was recorded on magnetic tape and returned to Edinburgh for analysis. The machine is no faster than the Edinburgh machines for measuring individual objects; each object needs to be set up by hand and the method of obtaining density via a moving wedge is unchanged.

(c) The COSMOS machine

The COSMOS automatic plate-measuring machine has been described elsewhere in some detail (Pratt et al. 1975, Pratt 1977, Stobie et al 1979) but it is precisely because of these separate descriptions that some comment is needed here. The work done has involved the use of data measured by the COSMOS machine over a period in which the machine specification has changed somewhat; indeed, several references to early forms of COSMOS data are now completely out-of-date, because of recent changes involving software image analysis (Stobie et al, 1979; also COSMOS newsletter).

Only essential details need to be described here. The photographic plate is mounted in a holder which can be driven slowly in x and y. These motions define an area of the plate which is scanned by a flying spot on the face of a precision cathode ray tube (CRT). The spot is imaged on to the plate, and the amount of light transmitted measured with a photomultiplier. For the measurement mode most commonly used in this work, mapping mode (MM), the plate is positioned in X then driven slowly in Y, with a line sweep on the CRT to give a raster scan up a strip of the plate. The X position is then changed and the adjacent strip scanned. The scan is considered as a grid 128 pixels wide, each line containing a row of pixels. The scan size, hence pixel size, can be adjusted for a pixel size of 8μm, 16μm or 32μm; the value of transmission for each pixel is digitised on a scale 0 to 127, which can be scaled with a gain control to match a range of grey levels on the plate.

With the present system (mid 1980) the data produced can then be analysed off-line to produce image parameters, or used directly to provide 'picture' information about the images; this is the form used for analysis of spectra. However a system used on COSMOS in the past, and mentioned later in this thesis, is the coarse measurement (CM) mode. This was a system which produced image parameters on-line as the measurement was in progress, the image parameters being X and Y centroids, X and Y extents, area in pixels, and minimum transmission (T min). The present system with off-line analysis produces these and other parameters, including ellipicity parameters, intensity weighted parameters and background intensity. For a complete discussion see Stobie et al (1979).

Details of the form and use of the data are presented in section 3.4; suffice it to say here that considerable areas on objective prism plates have been measured on the COSMOS machine, especially in the early stages of great optimism about the use of the data. Subsequent doubts about the performance of the system mean that few of the results from these data are presented in the present work. From the experience gained, however, it should be possible in the future to extract more useful results from not only new COSMOS data, but also from the body of data already measured.

3.2.2 Off-line computers.

A series of 'mainframe' computers has been used through this work, out of necessity rather than choice. The bulk of data processing has been restricted to two large machines run by the Science Research Council's (SRC) central computing facility, but other work has been done on in-house machines at the Royal Observatory, Edinburgh, and also on a small Commodore PET minicomputer.

(a) Central computing

Large machines run by the SRC had to be used because initially COSMOS data could not be processed quickly in-house; all COSMOS data tapes were transported down to the then Atlas computer laboratories for initial reduction and then user interpretation on the ICL 1906A computer. All the initial software was written for this machine, in FORTRAN, making use of as few as possible of the machine-dependent features of the 1906A. Programs for reducing mapping mode data to spectra, and the automatic redshift program (section 3.4) were initially written and tested on this machine. This situation unfortunately did not last; the SRC decided to close down 1906A operations and transfer

users to the Rutherford Laboratories' (RL) IBM 360/195 machine in spring 1978.

This move caused many problems, firstly in transporting software from one machine to another and making it operational (for example, the word length on the two machines is different). Secondly problems occured in the use of the RL system: turnround for the type of job using COSMOS data on magnetic tape is poor, and the 'online' system for file creation, editing and job submission, called 'ELECTRIC', was from the start slow and clumsy from the users' point of view, although some improvements have been made since 1978. The research programme as a whole would have moved somewhat faster if this transfer to the RL 360/195 had not been necessary.

(b) 'In-house' computing

The University of Edinburgh has its own central computing service, but the Department of Astronomy tends to make more use of the in-house facilities at the ROE for projects that are essentially collaborative between the Department and the ROE. For the present work, the in-house machine initially available, an Elliott 4130, was used almost exclusively for backup work to the project (e.g. dispersion curve fitting, finding chart co-ordinates) except in one instance where its interactive programming capacity proved essential. This was to perform a series of tests on the automatic redshift program, and showed one valuable aspect of interactive programming. Recently this rather old computer has been replaced by a much more powerful machine, a GEC 4082. It is hoped to transfer eventually all analysis programs to this machine, which has online facilities greatly superior to those provided on the RL mainframe, and gives a better service to users. It will still be possible to use the mainframe facilities, such as the FR80 plotting machine, by submission of jobs to the RL 360/195 via SRC's computer network, to which the GEC 4082 is attached. Some future work on interactive graphics is also likely to be done on the Edinburgh node of the SRC's new 'Starlink' network for astronomical image processing.

Some minor programming has been done on a Commodore PET minicomputer bought specifically for controlling the acquisition of

data from a Joyce-Loebl microdensitometer (section 3.2.1 (a)). This system is described elsewhere (Kelly et al, 1980a).

(c) Languages.

A range of computer languages has been used through this project. Though often scorned, FORTRAN has been used for most high-level programming because it is both commonly used by astronomers and also is relatively easy to transport from one machine to another. ALGOL was used once in a situation completely unsuited to FORTRAN. The interpretive language BASIC is used on the PET minicomputer. Assembler language programs have been needed (and written) in IBM 360 assembler and 4130 assembler, in situations mainly concerned with magnetic tape format translation. Machine code for the 6502 microprocessor has been written for the PET, to improve on the speed of BASIC for data transfer.

3.3 Radial velocities - manual measurement

Our prime requirements for radial velocity measurement, given a set of galaxy spectra, are a wavelength standard in the observer's rest frame,and a wavelength standard in the galaxy rest frame. Much of this section is concerned with a discussion of these two standards.

3.3.1 Velocities from CTIO plates

As noted in section 3.1 the first plates available for the study of objective prism spectra of galaxies were taken at the CTIO. An area on plate 17732 (table 3.1.1) was searched by eye to identify galaxies, the spectra of which were then traced using a Joyce-Loebl microdensitometer. A rest wavelength standard was defined by the cutoff of the IIIa-J emulsion, measured by fitting stars with well-defined spectral features to the published dispersion curve (Blanco 1974). For standard features in the galaxy spectra both the 4000 Å feature (section 2.2) and a small dip at rest wavelength approximately 4200 Å were used; it was concluded that the 4200 Å feature was a better indicator for faint galaxies as the 4000 Å feature became low in density and more difficult to define. This work has been published, and is described in detail by Cooke et al (1977).

What is important from this preliminary work is that wavelength standards had been found that appeared to give satisfactory results; the exact redshifts obtained are not important here. The next step was to adapt this technique to the spectra on UK Schmidt photographs.

3.3.2 The approach for UKSTU plates

The wavelength standards outlined above are attractive because of their simplicity, which makes them easy to use by hand, and also readily adaptable to automated processing. The difference between the CTIO work and the work on UKSTU plates is that only the 4000 Å feature has been used as a standard in galaxy spectra; the spectral resolution of the UKSTU plates is less than that of the CTIO plates and an actual dip at 4200 Å (rest wavelength) is rarely seen.

However a break in slope of the continuum does occur at about this wavelength, which has value in helping to correctly identify the 4000 Å feature.

Other methods of obtaining a rest wavelength standard which need to be investigated in future work are that of Stock and Osborn (1973) discussed in section 2.1, and a somewhat similar method providing a wavelength standard by co-ordinate transformation from a direct plate to the prism plate. Both these methods increase processing complexity, and are more suited to automated systems than to simple manual measurements.

The basic procedure for redshift determination is very simple: positions of the emulsion cutoff and the 4000 Å feature are determined and their separation measured; by reference to the prism dispersion curve (section 3.1 (c)) this gives the wavelength of the 4000 Å feature in the galaxy spectrum, and hence the galaxy redshift. This can be simply applied to any suitable prism-emulsion combination, and it is hoped to test the method with the new higher-dispersion UKSTU prism and an emulsion with a response into the red, which would enable the 4000 Å feature to be followed to higher redshifts.

3.3.3 Position definition.

It is clearly necessary to have some positive definition of the positions of the wavelength standards, as both consist of a fairly steep variation in intensity spanning a small wavelength range. The indicator first used on manual measurements was mid-point in density (fig. 3.3.1).

For the cutoff, this point is the mid-point between sky background and spectrum maximum; for the 4000 Å feature, it is the mid-point between top and bottom of the steep slope. Strictly, mid-point in intensity, not density, should be used; this makes the position independent of magnitude effects and effects due to the size of the object producing the spectrum. A large object will have features which are not sharp, but whose mid-points in intensity are unchanged in position (fig. 3.3.2) providing that the size of the object does not become comparable to the length of the spectrum.

In practice the difference between mid-points in density and

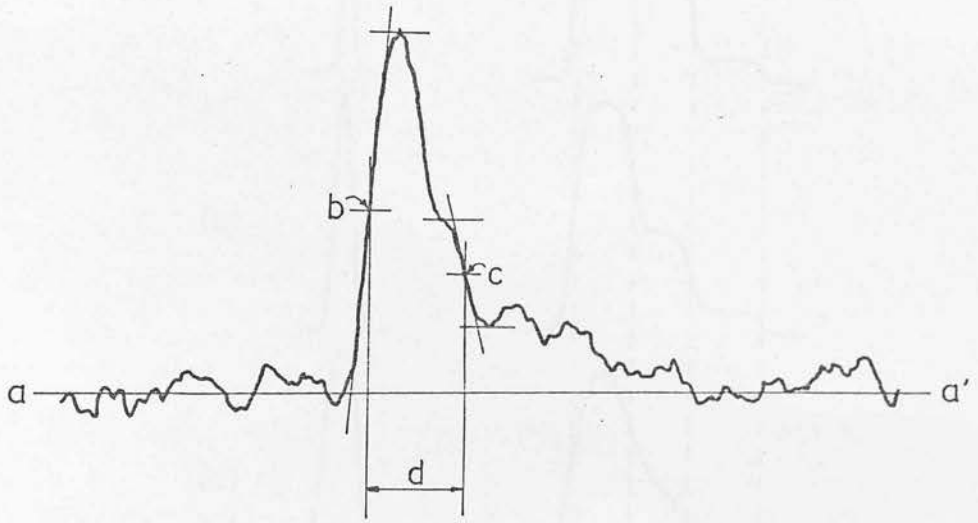

Fig. 3.3.1

Positions of the cutoff and 4000 Å feature defined by the mid-point in density. The spectrum is of a galaxy.

a – a' : sky background
b : mid-point in density of emulsion cutoff
c : mid-point in density of the 4000 Å feature
d : the cutoff to 4000 Å feature separation

Wavelength increases to the left.

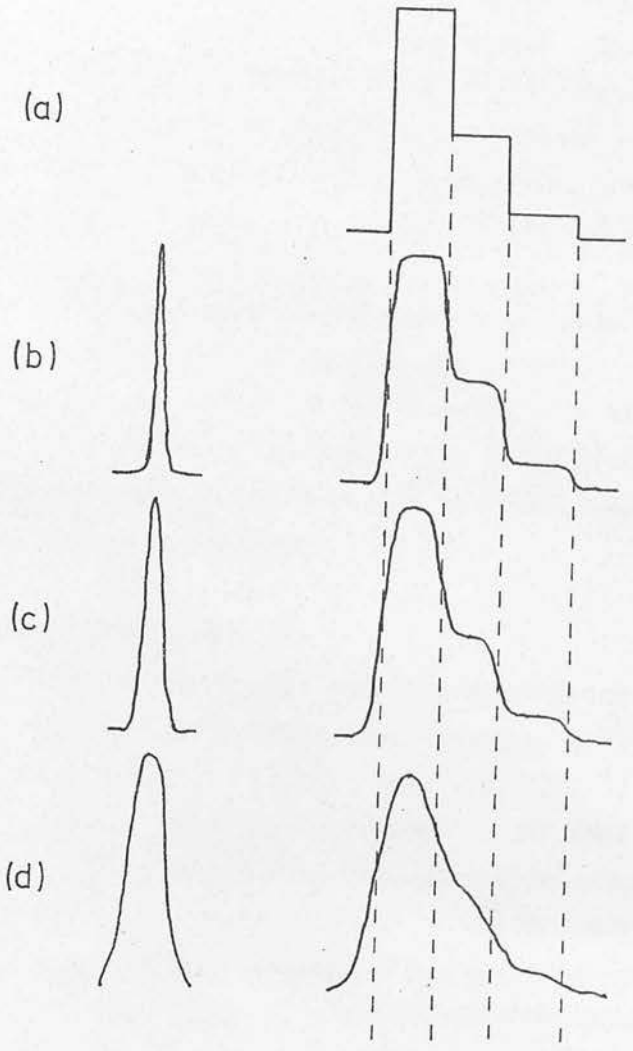

Fig. 3.3.2

Convolutions of various image profiles with a schematic 'sharp' spectrum (a). (b) to (d) show the effect on the objective prism spectrum of progressively broader luminosity profiles of the object having a slit spectrum as (a). It will be noted that the mid-points of features do not change position until the luminosity profile is broad enough to make the features very diffuse.

intensity is very small for the objects and magnitude range under study. An estimate of this quantity can be made from a plot of intensity against density for a typical plate (fig. 3.3.3); the correction in terms of peak density of the object above sky can be seen in the inset to the figure. Knowing this correction and the slope of the feature to be corrected (in density units per Ångstrom) the corrections, for stars and most galaxies, are: zero, for densities less than 1.2 above sky; increasing to 40 Å at a density of 1.8 above sky.

This has the implication that manual spectrum tracings made using a microdensitometer are quite adequate for redshift measurement from direct measurement of the tracings. It also means that checks that need to be performed over large areas using relatively few objects (section 3.5) can also be made using manual measurements on the microdensitometer.

3.3.4 The emulsion sensitivity cutoff

For the Eastman Kodak IIIa-J emulsion, the sensitivity cutoff (in the green) is fairly sharp (Eastman Kodak Company, 1973); a drop in sensitivity of a factor 10 occurs over about 270 Å, that is about 60μm on the plate at the cutoff wavelength. The fact that this sharp cutoff is not greatly affected by hypersensitised measurements is shown by measurements by Emerson (1979 b) of the emulsion response and also by simple inspection of tracings of the objective prism spectra. For the use of the emulsion cutoff as a wavelength standard, the fact that its position is constant both across any given plate, and, ideally, from one plate to another needs to be established. The checks made to establish this standard are described in section 3.5. The cutoff wavelength adopted is that obtained from the dispersion curve measurements (section 3.1 (c)): 5380 ± 30 Å.

3.3.5 The 4000 Å continuum break

This spectral feature has been noted in the literature survey (section 2.2); it is best shown in a paper by Pence (1976). It is a strong feature and an important contributor to the elliptical galaxy B and V K-corrections over the redshift range 0 to 0.5. The origin of the 4000 Å feature is shown clearly in the spectral scans

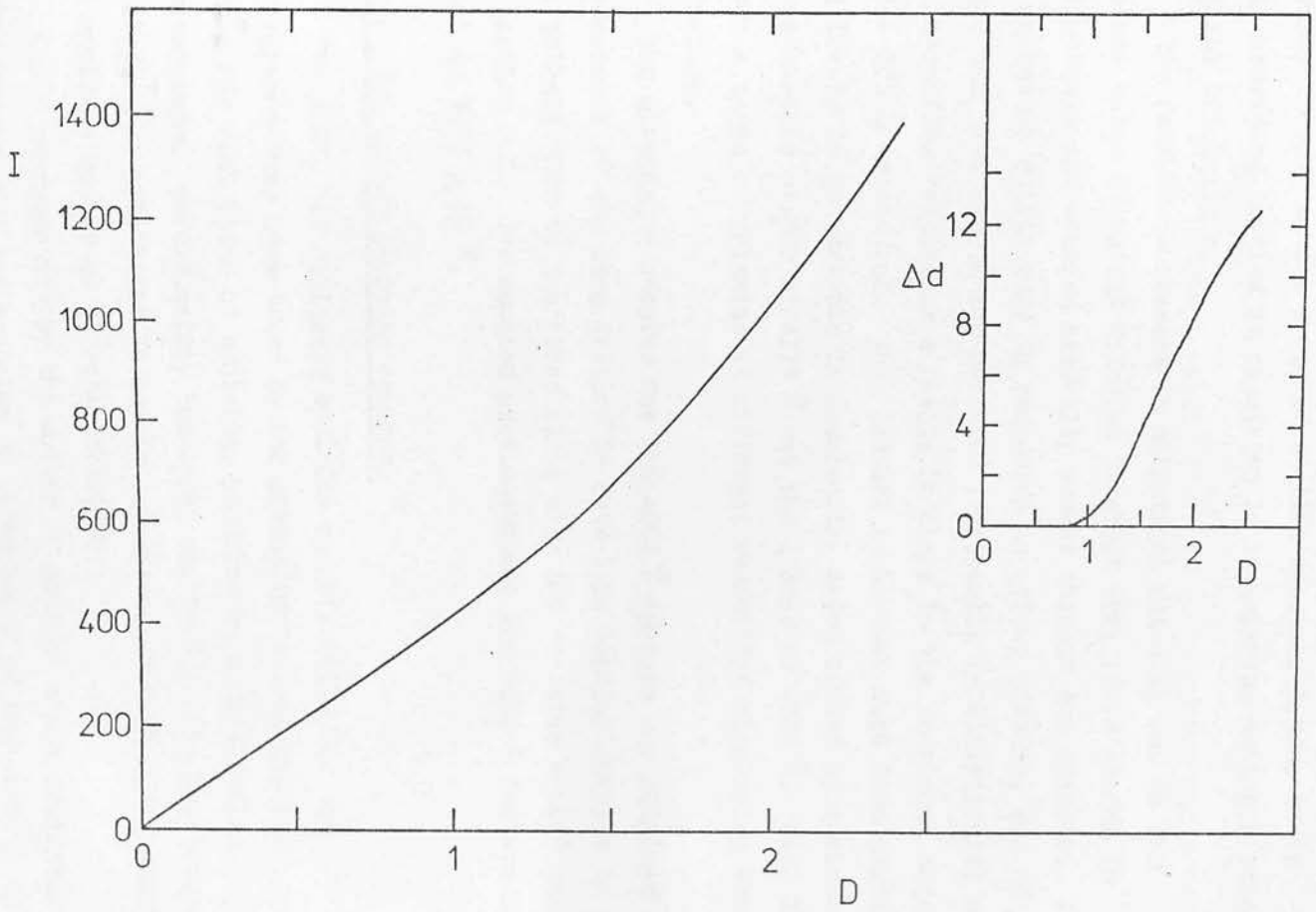

Fig. 3.3.3

The intensity - density plot from the east step wedge of plate UJ2461P. Intensity is in terms of the UKSTU step wedge values, density is above sky level. The inset shows the correction to the cutoff position, in microns, in terms of peak density of the cutoff above sky, for a cutoff

of Faÿ, Stein and Warren (1974); the feature shows very little variation with spectral type from G0 to early M, its position corresponding to the long wavelength side of the CaI H line. For wavelengths shortward of this line blends of metallic lines act to lower the effective continuum level, giving rise to the characteristic 'step' of the 4000 Å feature. Because of the presence of the feature in such a wide range of stellar spectral types, it is not surprising to find it consistently in galaxies having a range of stellar populations.

The feature is present in elliptical galaxies and in the nuclear bulge of spiral galaxies to about Sbc; it is strong in ellipticals and becomes gradually weaker through the spirals. It is generally fairly easy to recognise in galaxy spectra, due to its size, and also due to the presence (especially in ellipticals) of an absorption feature or a change in slope in the continuum some 200 - 300 Å to the red. This feature is however much less pronounced, and likely to be variable in wavelength, being caused by a mixture of metal-line blends at 4227 Å and the G band at 4300 Å. Fig. 3.3.4 shows a range of galaxies at different velocities displaying the 4000 Å feature.

The wavelength adopted for the 4000 Å feature was obtained by measurement of the same feature in late-type stellar spectra in our own galaxy; this is described along with the emulsion cutoff checks in section 3.5. The adopted wavelength for the 4000 Å feature mid point is 3990 $\pm$ 20 Å.

3.3.6 The IIIa-J emulsion response

The UKSTU has monitored emulsion sensitivities for the photographs they have taken by the production of calibration plates for each batch of emulsion, produced on a calibration spectrograph. Unfortunately the light source for this spectrograph is itself not calibrated in wavelength terms, so a response curve for the emulsion cannot be directly obtained.

Early measurements by the author of some of these calibration plates showed that the emulsion γ (the slope of the density vs exposure plot) varies significantly with wavelength, being steepest in the mid-range of wavelengths (4000 - 5000 Å) and

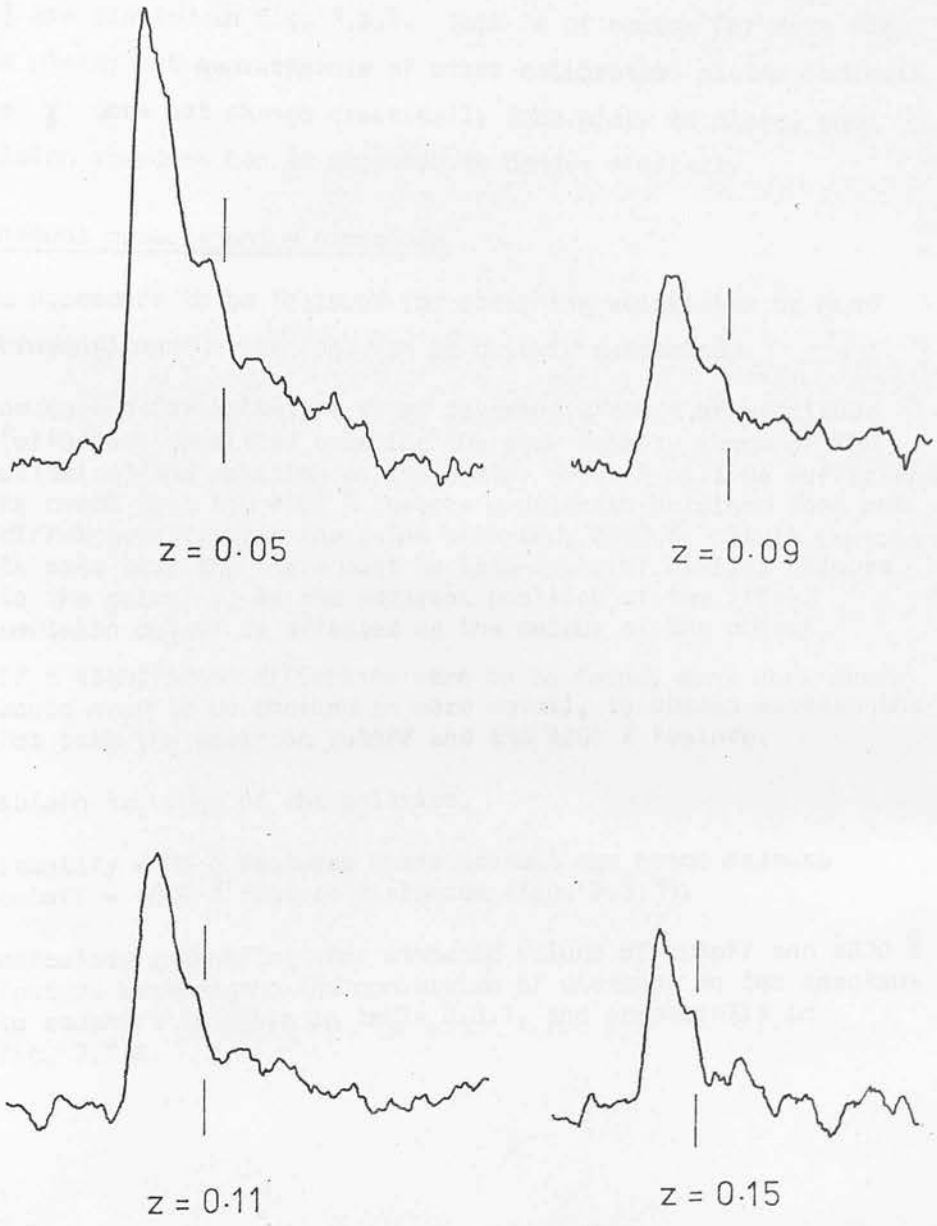

Fig. 3.3.4

Tracings of the spectra of galaxies at varying redshift, showing the 4000 Å feature (indicated). The ordinate is density.

decreasing towards the short wavelength range. More detailed measurements by Clowes et al (1980) show that γ rises near the cutoff wavelength. Clowes et al assumed a black body curve for the calibration spectrograph lamp to produce values for the emulsion grain response function; the resulting data (Clowes et al, Table 1) are plotted in fig. 3.3.5. This is of course for data from only one plate; but measurements of other calibration plates indicate that the γ does not change drastically from plate to plate, and the emulsion response can be expected to behave similarly.

3.3.7 Manual measurement - procedure

The procedure to be followed for obtaining velocities by hand from microdensitometer tracings can be quickly summarised.

(i) measure a few late-type stars covering a range of magnitude (with peak densities covering the peak density range of the galaxies) and position on the plate; about 5 will be sufficient to check that the 4000 Å feature wavelength obtained does not differ greatly from the value accepted, 3990 Å. It is important to note that the stars must be late-type, of similar colours to the galaxies, as the apparent position of the IIIa-J emulsion cutoff is affected by the colour of the object.

If a significant difference were to be found, many more stars would need to be checked in more detail, to obtain wavelengths for both the emulsion cutoff and the 4000 Å feature.

(ii) obtain tracings of the galaxies.

(iii) identify 4000 Å features where present and hence measure cutoff - 4000 Å feature distances (fig. 3.3.1).

(iv) calculate redshifts: for standard values of cutoff and 4000 Å feature wavelengths the conversion of distance on the spectrum to redshift is given in table 3.3.1, and graphically in fig. 3.3.6.

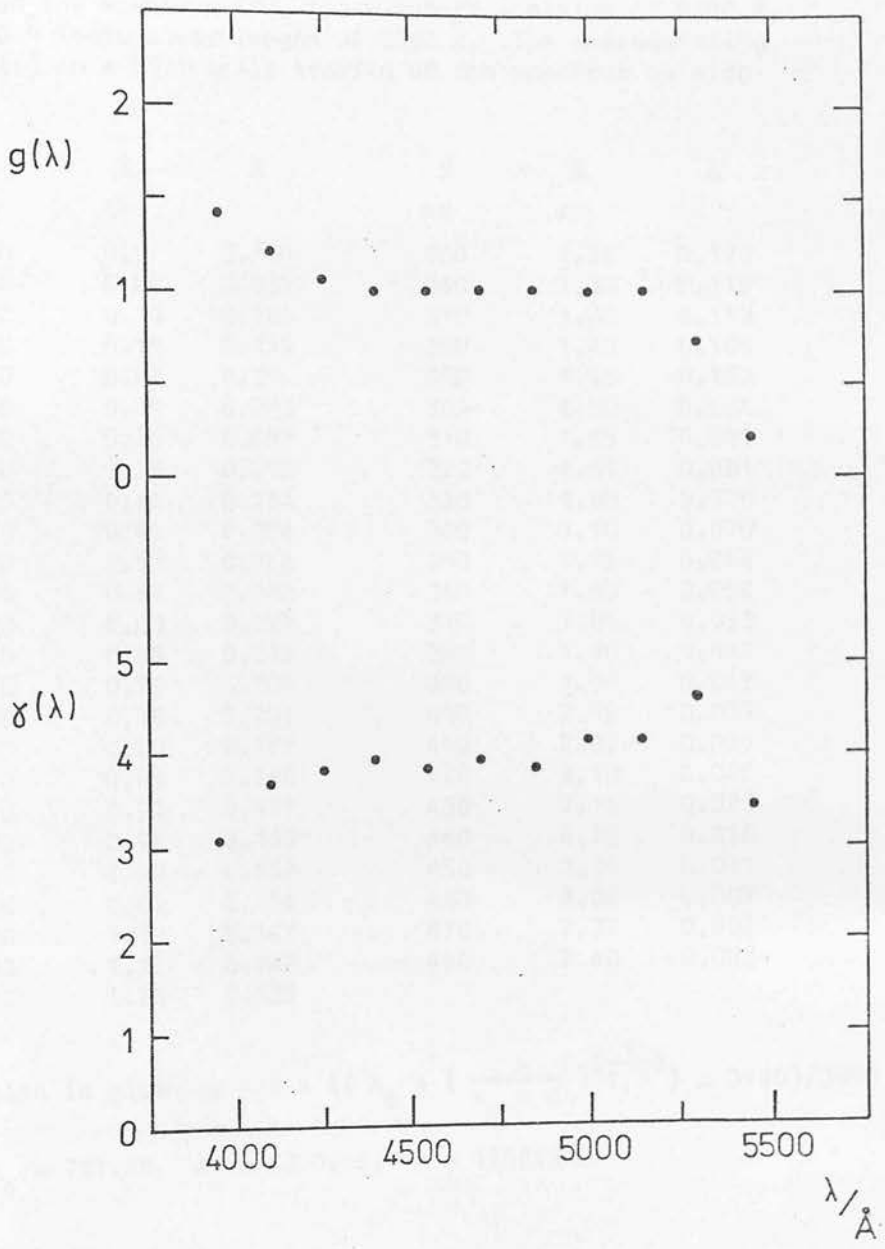

Fig. 3.3.5

The measured IIIa-J response and γ variation from Clowes et al (1980). No error estimate is given by Clowes et al.

Table 3.3.1

Redshift (z) in terms of emulsion cutoff to 4000 Å feature distance on the spectrum (d), for a cutoff position of 5380 Å, and a 4000 Å feature wavelength of 3990 Å. The corresponding distance (x) on a 50:1 scale tracing of the spectrum is also given.

d	x	z	d	x	z
μm	cm		μm	cm	
0	0.0	0.348	250	1.25	0.126
10	0.05	0.337	260	1.30	0.119
20	0.10	0.326	270	1.35	0.113
30	0.15	0.315	280	1.40	0.106
40	0.20	0.304	290	1.45	0.100
50	0.25	0.293	300	1.50	0.094
60	0.30	0.283	310	1.55	0.087
70	0.35	0.273	320	1.60	0.081
80	0.40	0.264	330	1.65	0.075
90	0.45	0.254	340	1.70	0.070
100	0.50	0.245	350	1.75	0.064
110	0.55	0.236	360	1.80	0.058
120	0.60	0.227	370	1.85	0.053
130	0.65	0.218	380	1.90	0.047
140	0.70	0.209	390	1.95	0.042
150	0.75	0.201	400	2.00	0.037
160	0.80	0.193	410	2.05	0.031
170	0.85	0.185	420	2.10	0.026
180	0.90	0.177	430	2.15	0.021
190	0.95	0.169	440	2.20	0.016
200	1.00	0.162	450	2.25	0.011
210	1.05	0.154	460	2.30	0.007
220	1.10	0.147	470	2.35	0.002
230	1.15	0.140	480	2.40	-0.003
240	1.20	0.133			

The relation is given by $z = ((\lambda_o + (\frac{a}{x_o + d})^{(\frac{1}{1.2})}) - 3990)/3990$

where $x_o = 727.48$, $\lambda_o = 1313.41$, $a = 15591900$

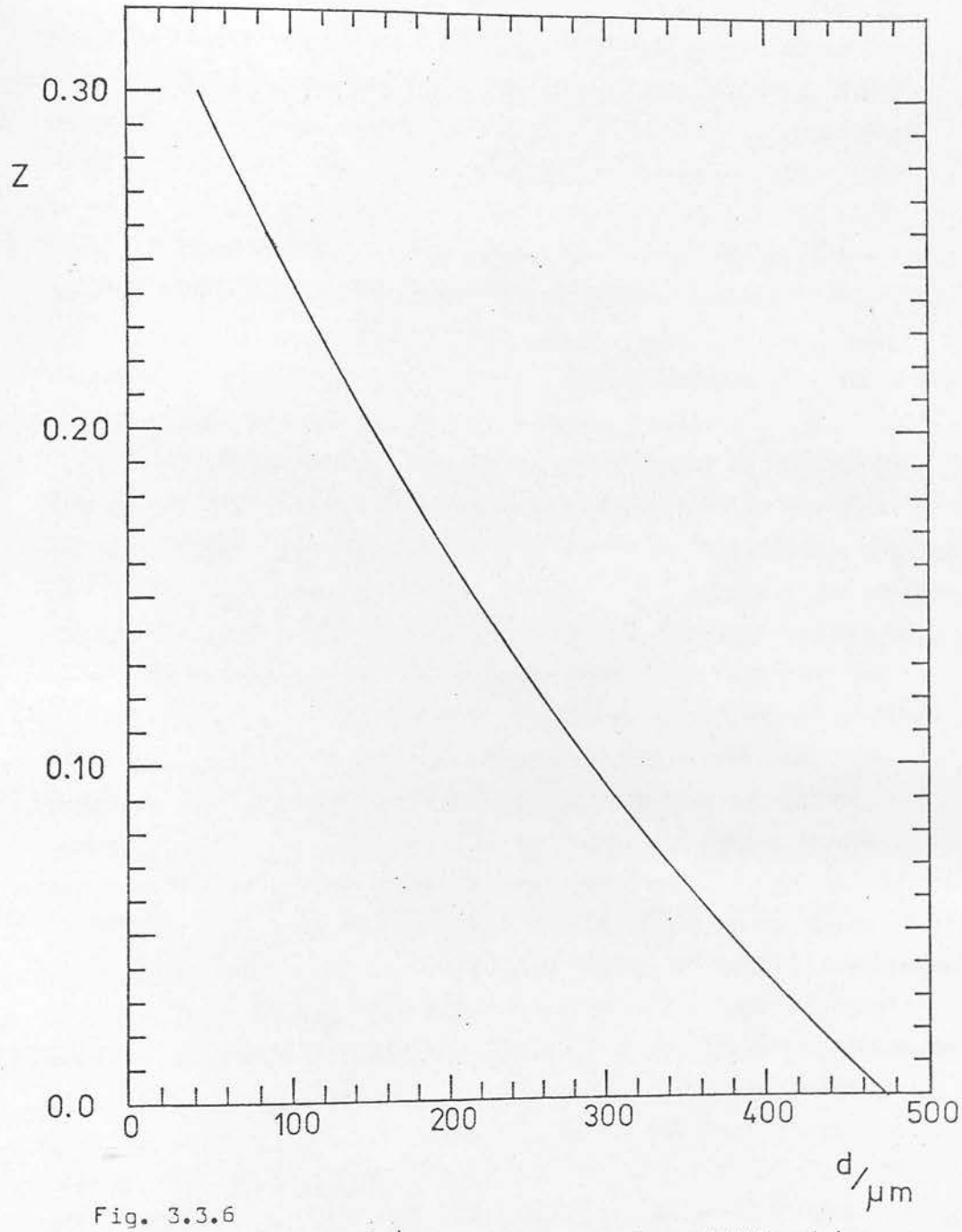

Fig. 3.3.6

Table 3.3.1 given in graphical form. Z is redshift, d is the emulsion cutoff to 4000 Å feature distance for IIIa-J.

3.4 Radial velocities - machine measurement

A simple technique for measuring the radial velocities of faint galaxies from tracings of their objective prism spectra has been described in section 3.3. There are large numbers of faint galaxies on objective prism photographs taken away from the galatic plane. Using data from Shane (1975), we could expect about 1000 galaxies on the photograph to an apparent magnitude of $m_{\beta} \sim 18$ (very roughly; there are large errors present in this estimate from uncertainties in the Zwicky and Lick counts; Shane (1975), table 3). This number increases by about a factor of three per magnitude. Fig. 3.4.1 shows estimated galaxy numbers from Brown (1974), as calculated by Emerson (private communication).

Such large numbers of objects cannot easily be handled by hand measurement, if several photographs are involved, and thus the photographs have been measured at the Royal Observatory, Edinburgh (ROE) using the COSMOS measuring machine. This involves the production of data which are most easily handled by computer techniques.

There are two main areas to the problem of analysing the data; firstly, the identification of galaxy, as opposed to stellar, spectra; secondly, the analysis of the spectra themselves. Two possible approaches immediately suggest themselves for galaxy identification: the galaxies could be identified from a direct plate of the region using the technique described by MacGillivray et al (1976a) then these identifications transferred to the prism plate; or, if only late-type spectra are considered, the stellar spectra could be separated from the galaxy spectra by redshift. MacGillivray's original technique involves the use of a plot of two COSMOS measurement parameters; a plot of T_{min} (the minimum COSMOS transmission value in an image) against log A (the log of the COSMOS area parameter). This plot is calibrated for a subset of the data on which the procedure is to be used, galaxies and stars in the subset being separated by visual inspection of the plate material. The procedure is then applied to the whole data set. This problem is discussed in more detail in section 4.2. In this section the principles of making redshift measurements automatically from COSMOS data are described, with a description of the algorithm used to obtain redshifts.

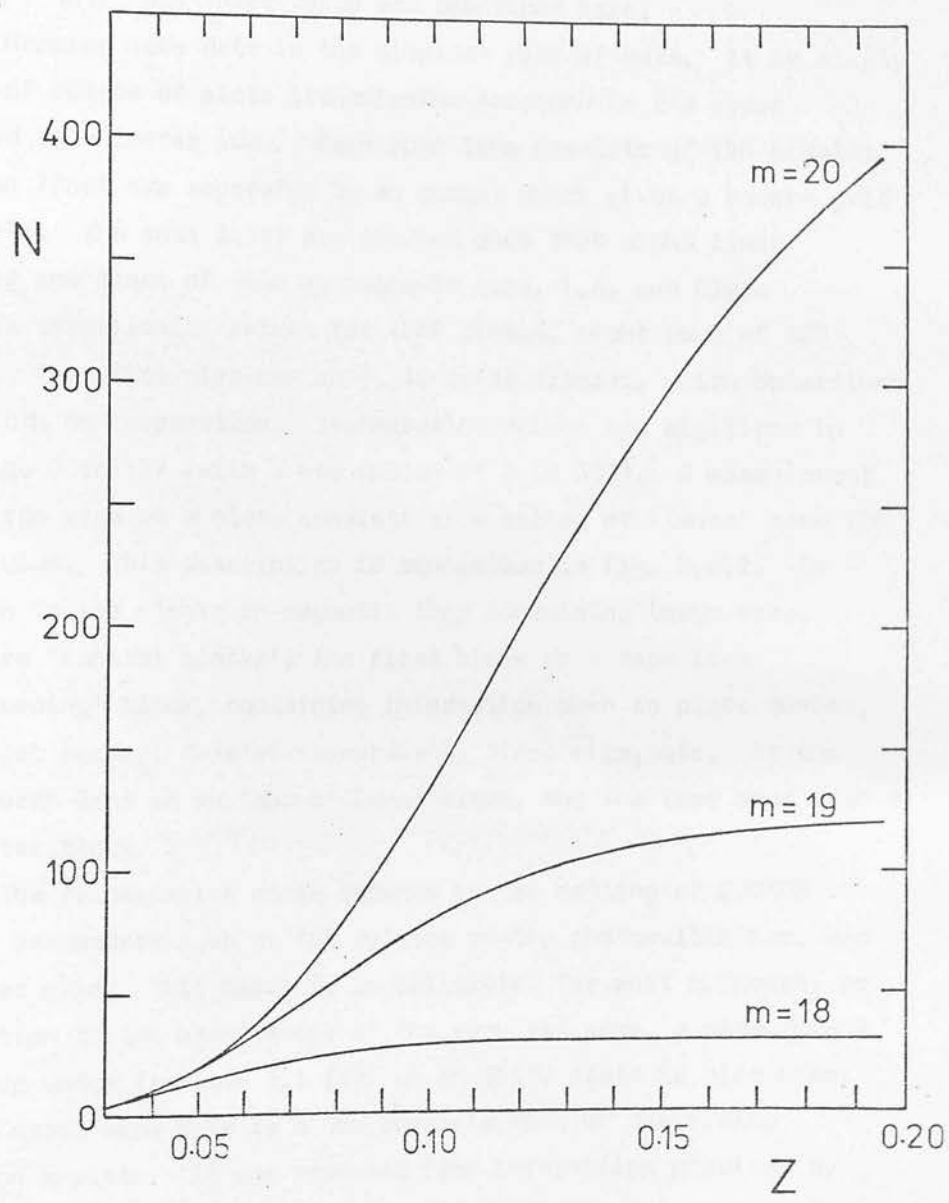

Fig. 3.4.1

Estimated galaxy numbers, given as integral counts out to a given redshift (z), to a limiting photographic magnitude m. Data from Brown(1974).
N is the number of galaxies per square degree.

3.4.1 Description of the data

The majority of the COSMOS data used is the type 'mapping mode' - MM. An early form of COSMOS data, 'coarse mode' - CM - has also been used; this is now superceded by a new form: 'image analysis mode', IAM (alternatively called 'threshold mapping', TM). All three types are described here.

Mapping mode data is the simplest form of data. It is simply a list of values of plate transmission arranged in the order provided by a raster scan. Each scan line consists of 128 pixels; the scan lines are separated by an amount which gives a square grid of pixels. The scan lines are grouped such that eight lines comprise one block of data on magnetic tape, i.e. one block contains transmission values for 1024 pixels, eight rows of 128 pixels. The pixel size can be 8, 16 or 32 microns, which determines line width and separation. Transmission values are digitised in the range 0 to 127 (with a new option of 0 to 255). A measurement of a large area on a plate consists of a series of 'lanes' each 128 pixels wide. This description is summarised in fig. 3.4.2. In addition to the blocks on magnetic tape containing image data, there are 'control blocks'; the first block on a tape is a 'housekeeping' block, containing information such as plate number, COSMOS job number, date of measurement, pixel size, etc. At the end of each lane is an 'end of lane' block, and the tape ends with a terminator block.

The transmission scale depends on the setting of COSMOS machine parameters such as EHT voltage on the photomultiplier, and amplifier gain. This needs to be calibrated for most purposes, so in addition to the measurement of the required area, a measurement of a step wedge (section 3.1 (d)) on an UKSTU plate is also made.

Coarse mode data is a now obsolete form of describing images on a plate. It was produced from information provided by a hardware pattern analysis system, and consists of a series of parameters for each image in the area measured, an image being defined as a set of connected pixels having transmission values less than some threshold value. The parameters are given in table 3.4.1; again these data can be produced for pixel sizes of 8, 16 or 32 μm.

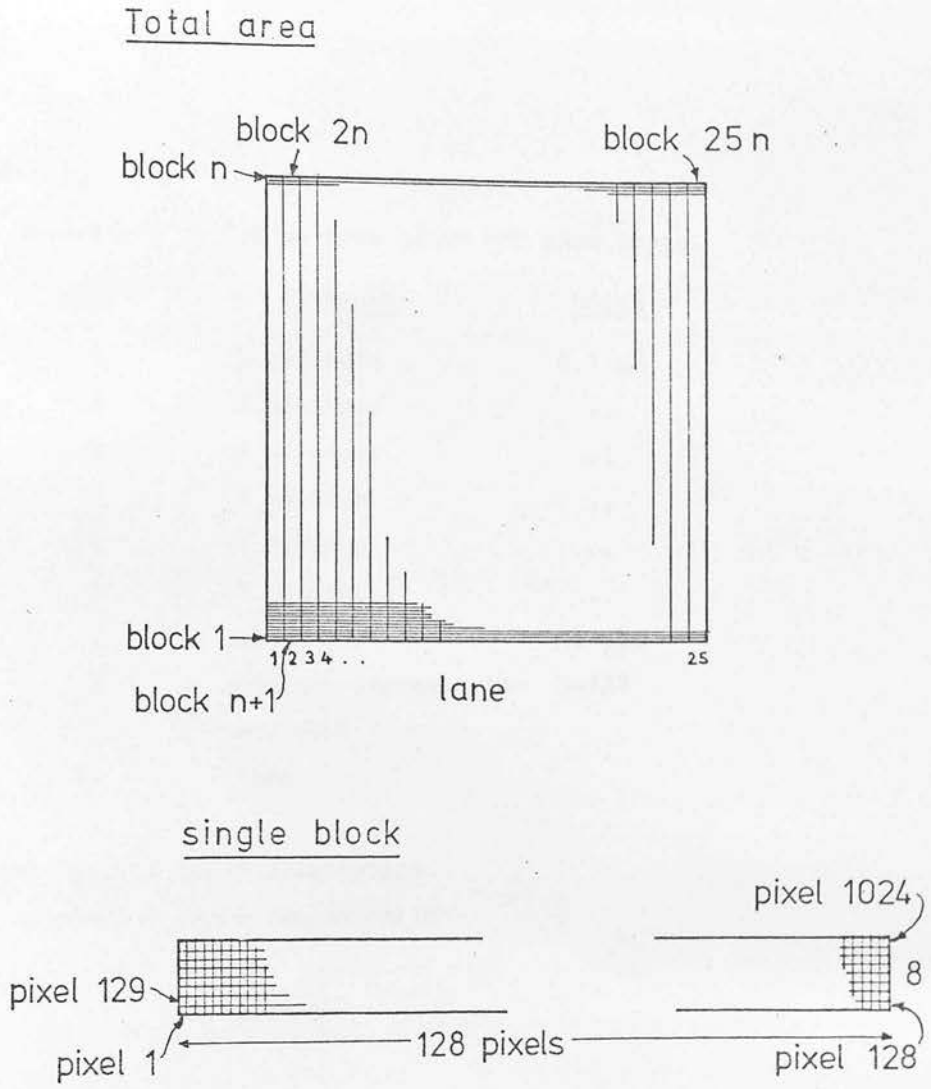

Fig. 3.4.2

The COSMOS MM data format. The 'total area' is contained on a single magnetic tape.

Table 3.4.1

COSMOS parameters in Coarse Mode given for each image.

Word	Contents	Units
1	X centroid	0.1 μm
2	Y centroid	..
3	X minimum	..
4	X maximum	..
5	Y minimum	..
6	Y maximum	..
7	area	pixels
8	minimum transmission	0-127
9	quadrant	
10	code	

'quadrant' gave a rough orientation

'code' related to image recombination

The data are blocked up to magnetic tape in the same size blocks as for MM data; with 10 parameters per image this means that there are 4 unused words in each block. 'Pseudo coarse mode' data has been produced by several users of COSMOS data, including the author, by processing MM data with a program which mimics the operation of the COSMOS pattern analyser. This processing is now done for IAM data.

Image analysis mode data has not been used directly for this work, but as it replaces CM data it is directly relevant to future work, and so a list of image analysis parameters (at present - June 1980) is given in table 3.4.2. Once again these can be obtained for the three pixel sizes, and are blocked up into standard COSMOS data blocks.

3.4.2 Data reduction software

A great deal of software has been written to handle COSMOS data from UKSTU objective prism plates, along with additional software to aid this processing. The relevant programs (no apologies are made for the spelling of this word) are described in the following sections to the extent needed to understand their operation. The listing of only one program is given in appendix A; but this is the central program to this thesis. Practically all of the programs are written in FORTRAN, with documentation within the source of the programs. The software has been fairly flexible; this was required both because of changes to the COSMOS data and because of improvements in techniques. The system as presented here, however, represents a working system.

The software falls into the following groups:

(a) production of magnetic tapes containing spectra in either MM or 'tracing' format (described in section 3.4.3.)

(b) the redshift program (section 3.4.4.)

(c) 'results analysis' programs (section 3.4.5.)

(d) support programs (e.g. co-ordinate transformation, line- and curve-fitting).

3.4.3 Production of tapes containing spectra

Initial COSMOS measurements of the prism plates at present

Table 3.4.2

COSMOS parameters in Image Analysis Mode given for each image.

Word	Contents	Units
1	X centroid } unweighted	0.1 μm
2	Y centroid } unweighted	"
3	X minimum	"
4	X maximum	"
5	Y minimum	"
6	Y maximum	"
7	area	pixels
8	minimum transmission	0-127
9	$-250 \log \left(\sum_i (I_i - I_{sky}) \right)$	
10	I_{sky} at centroid	
11	X centroid } intensity weighted	0.1 μm
12	Y centroid } intensity weighted	"
13	semi-major axis } intensity weighted	"
14	semi-minor axis } intensity weighted	"
15	orientation } intensity weighted	degrees
16	semi-major axis } intensity weighted	0.1 μm
17	semi-minor axis } intensity weighted	"
18	orientation } intensity weighted	degrees
19	blank	
20	error word	

consist of MM data of large areas. The first problem in examining spectra (of both galaxies and stars) is to extract the spectra from the MM data. There are now two approaches that can be taken. The first consists of a series of programs that were developed to extract all possible spectra from the MM data. After analysis of this type of data had shown that in many of the fainter objects the signal-to-noise ratio was very poor indeed, a second simpler approach was developed to extract quickly most of the objects from MM data, excluding the fainter objects; this approach uses a single computer program.

The original series of programs is best explained with the aid of a flowchart (Fig. 3.4.3). Both MM and CM data are obtained of an area on the plate. A co-ordinate transformation is established from the CM measurements to the MM measurements. Images are then selected (e.g. by a magnitude-related parameter) from the CM data and their co-ordinates in the MM frame found; this acts as a finding list for the MM data. A program then uses this list to find spectra in the MM data, and output them to magnetic tape. This tape contains spectra neatly aligned within COSMOS MM-type data blocks.

The core of this series of programs is the individual program 'SPEC2'. This extracts the spectra from positions in the MM data given by the finding list, and puts these spectra out to tape in a format similar to MM. This format consists of an information block for each spectrum (containing identification and co-ordinates) plus two other blocks (for 16 micron pixel size) containing the spectrum and adjacent plate background. The usual COSMOS housekeeping and terminator blocks are retained.

The program works by taking the finding list (in the co-ordinate frame of the MM data) and generating from this a list of the MM blocks containing segments of image; each image needing an area 3 blocks wide by 2 blocks high (16 micron pixel data) to be sure of containing the image (fig. 3.4.4 (a)). This list is then sorted into the order that the data blocks appear on the tape.

A single pass is then made through the tape; blocks containing image are stored as required to direct access backing store. In lane 3 some images become complete; as they are completed the relevant

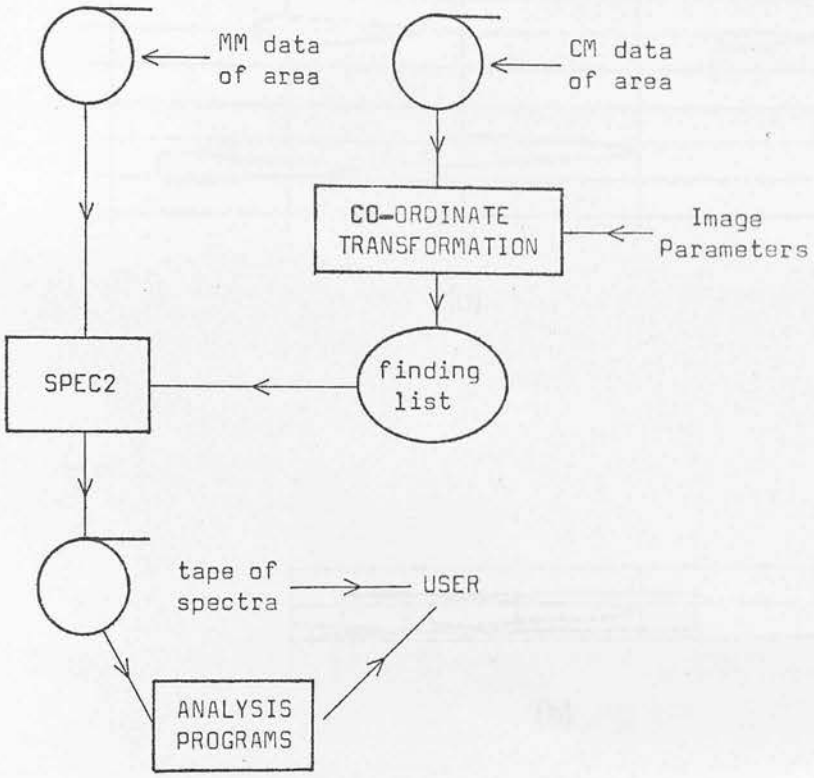

Fig. 3.4.3

Flowchart describing the production of tapes containing spectra from COSMOS MM data.

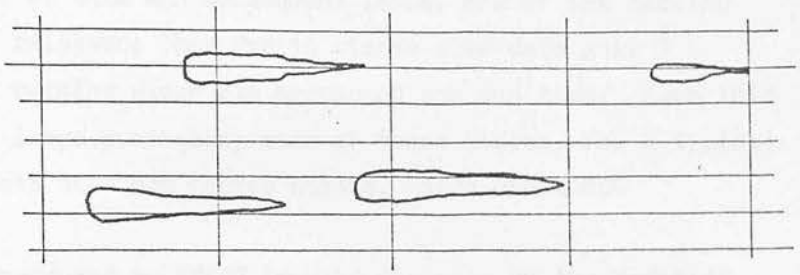

(a)

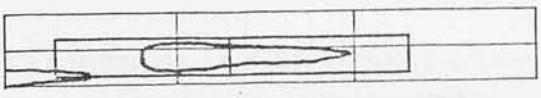

(b)

Fig. 3.4.4

(a) Each spectrum may be contained in an area 3 blocks wide by 2 blocks high.

(b) From this 3 x 2 area, 2 blocks may be extracted with the spectrum centrally aligned.

(not to scale)

blocks are retrieved from backing store and placed in an array in core. The exact location of the area containing the spectrum is known (from the finding list) and using this an area two blocks wide and one high is extracted from this array (fig. 3.4.4 (b)) and output to tape along with the information block.

At the end of this and subsequent lanes, one of the backing store files is released; thus for 16 micron step data only 3 lanes-worth of backing store are needed at any one time. Even this creates fairly large overheads; each of these stores, for a typical galatic cap plate area one degree square, needs about 800 kilobytes.

The data produced by SPEC2 is used directly by the redshift program; however it is also possible to run this data through another program, TRACE4, which, given smoothing parameters, intensity conversion, normalisation or not as required, can produce another tape containing spectra as linear arrays instead of 2-D arrays. This is really intended as a 'user-facility' for the suite of programs and has not been used very much for the present work.

A vital stage in this set of programs is clearly the production of the finding list. This is an area which unfortunately still involves a certain amount of manual work in the present system, but which can be drastically reduced in the future using new interactive programming facilities becoming available (section 3.2.2). The problem splits into three stages:

1) obtain CM or pseudo-CM data of the area on both direct and prism plates

2) match images and perform the co-ordinate transformation

3) use the transformation to produce a finding list.

For (1), pseudo-CM has mostly been used, due to the variable status of the COSMOS CM mode through this work. For direct plates, the MM data of a direct plate of the area were processed using MacGillivray's programs (privately communicated), which were forerunners of the present IAM; those of the prism plate were processed using COARSE2, written by the author. This is simply

another program written to produce psuedo-CM data from MM data, being in this case oriented to prism plate MM data.

Image matching requires some manual intervention: programs are used which produce graphical output of the images in small areas of the data, and lineprinter output of parameters of these images (fig. 3.4.5). This is done for both prism and direct plate data. The graphical output is then used to match images by eye, and the X, Y co-ordinates of these matched images obtained. The program is generally used to produce data of 25 areas in a grid arrangement (5 by 5) within the data; an average of about 3 images for each of these 25 areas is used to perform the co-ordinate transformation.

The transformation program itself works by obtaining a least squares fit to polynomial transformations from (x,y) to (u,v) such that

$$u = f(x) + g(y)$$
$$v = d(x) + e(y)$$

where d, e, f, and g are polynomials.

This fit requires the solution of a large number of simultaneous equations; this has been achieved by two methods:

(1) solution by 'brute force', solving determinants to obtain a first approximation to the transformation, then using the method of variation of parameters (appendix B) to obtain the least squares fit.

(2) Once the programs were transferred to the IBM 360/195's of the Rutherford Laboratories, a standard routine at RL for solving simultaneous equations was used, to save the time of updating the original program to work at the same accuracy.

The program generally gives rms errors in the transformations of the order of 10 microns, using the number of images given above. This accuracy is just sufficient to centre the spectra within the output data blocks.

Stage (3) is simple; the list of image co-ordinates obtained from the direct plate is processed using the transformation obtained in (2) to produce a list of the images in the co-ordinate frame of the prism plate data. In addition, offsets are applied in (u,v) to give the co-ordinates of the corner of the pair of blocks containing the spectrum, rather than using the co-ordinate of the 'head' end of the spectrum itself. This offset is chosen to

Direct plate image co-ordinates

	Centroid X	Y
1	3877520	935720
2	3887840	928200
3	3877920	924440
4	3870480	920520
5	3904560	908840

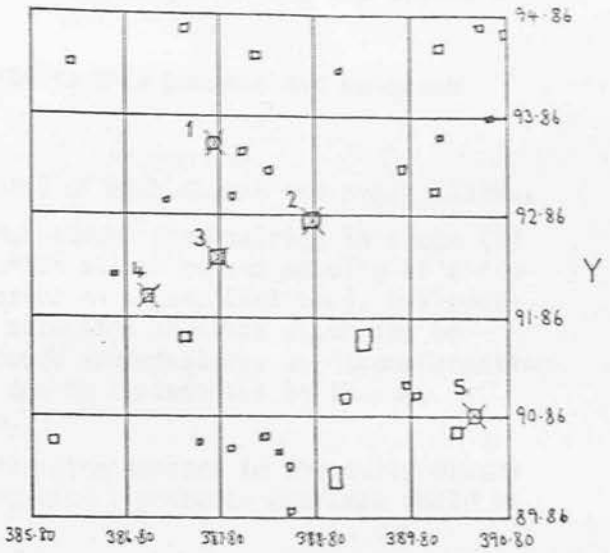

Area corner X= 385800 Y= 89860

Prism plate image co-ordinates

	Xmin	$\overline{Y}$
1	3851780	936860
2	3861700	929020
3	3852100	925660
4	3844900	921340
5	3878980	909660

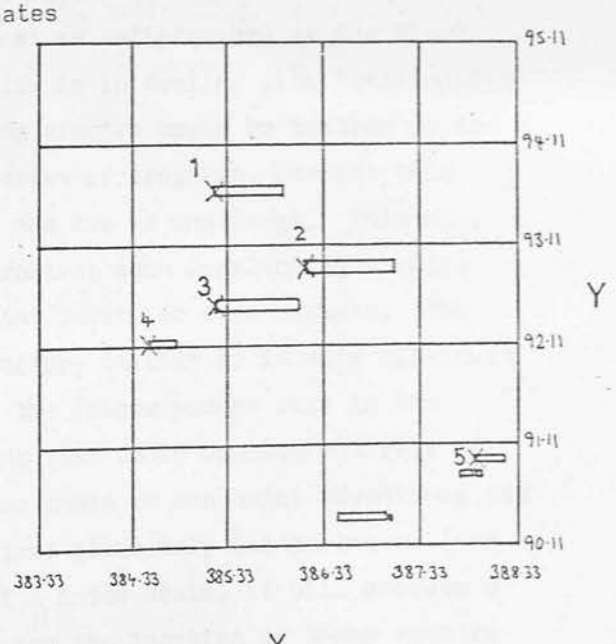

Area corner X= 383330 Y= 90110

Fig. 3.4.5

Graphical output, and relevant lineprinter output, used to provide data for the image co-ordinate transformation program. This area is one of (normally) 25 used to establish the transformation.

place the spectrum centrally along the length of the two blocks in u, and to centre it in v.

Future possible improvements to this process and programs include:

(1) better CM-type data (TM data) of both direct and prism plates.

(2) replacement of the laborious manual star-pairing in stage (2) by an interactive system which allows manual pairing of a few images (e.g. by using a cursor on a graphical VDU), followed by automatic pairing of a selection of stars which can be checked visually, and if found satisfactory, the transformation allowed to proceed. This can be implemented on the new computer systems available.

(3) detection of possible overlapping spectra in the early stages of generating the finding list : probable overlaps could be removed or marked.

The second approach for extracting spectra from MM data is rather simpler. It consists of a single program which operates to extract the spectra in a similar way to 'SPEC2', but instead of using a finding list to identify image positions, the program 'looks for' images as it passes through the data. This is done by examining the data for connected pixels above a threshold which is set as a variable in the program; the threshold level determines the faintest images that are picked out.

This approach is clearly not as satisfactory as the first method described. One difficulty is in dealing with 'overlapping' spectra; each of two overlapping spectra could be centred up in output blocks from the first series of programs, whereas this alternative program will count the two as one image. This may, in fact, not be considered a problem; such overlapping spectra are often either difficult to interpret, or even useless. The approach is also not as satisfactory in that it is more difficult to apply selection criteria to the images picked out; in the first approach, an image finding list could consist entirely of galaxies, for instance. However there is one major advantage; the program is a 'single pass' system; given only one parameter (the threshold level) and MM data of a prism plate, it will produce a tape of spectra and a plot showing the location of those spectra within the area. As such it is the quickest way of obtaining such a tape.

3.4.4 The redshift program.

Probably more time has been spent on developing this one piece of software than on any other program, and being central to this thesis it merits a special description, and an inclusion of the listing of the FORTRAN source code (appendix A).

The program specification is relatively simple; input data consists of a tape of spectra in the 'SPEC2' format. Additional parameters are used, giving information on prism dispersion, spectral features anticipated, parameters of the COSMOS data, etc. The spectra are then processed in turn to obtain a redshift, if possible, for each one. Finally a plot of the tracing through the spectrum is made (giving information on the features identified, to allow checking by eye) and information about the spectrum, including the redshift obtained, printed on a lineprinter.

The spectra themselves are of fairly low resolution due to the low dispersion used (2400 Å mm^{-1} at 4300 Å) and the smearing of the spectra due to the finite size of the galaxies. The method developed for machine measurement of redshifts is a development of that of Griffin (1967) who measured stellar radial velocities by matching the position of a mask of expected lines to the lines present in a spectrum. This basic technique has been applied by Sandage, Kristian and Westphal (1976) and Faber and Dressler (1977) and subsequent authors, who have correlated an expected galaxy spectrum at different redshifts with the observed spectrum, to obtain the redshift. If no intensity calibration is available for a photograph this method cannot easily be used as the observed continuum in density terms on the photograph would depend on the magnitude of the object. However the correlation method can be refined by removing the continuum of the observed spectrum using a convolution technique described by Thompson (1970); the same convolution is applied to a set of expected features, and the resulting function correlated at different redshifts to obtain the best correlation and hence the redshift. With a digitised spectrum $S(x_i)$ and a convolution $C(x_j)$ the convolved spectrum is

$$T(x_i) = \sum_j C(x_j - x_i)\, S(x_j)$$

Thompson used

$$C(x) = 1 \quad |x| < X$$
$$= -1 \quad X < |x| < 2X$$
$$= 0 \quad \text{otherwise}$$

where 4X was approximately the width of the features he was attempting to emphasise. A similar function is used in the technique described here.

This function acts to remove constant and first order terms from the function $S(x_i)$, and smooths the resulting function by an amount depending on its width (in Thompson's case, 4X). The amount of smoothing is thus beneficial if the noise present in the spectrum is at higher spatial frequencies than the features present. Whether or not this is the case, if the convolution 'gate' function $C(x)$ is matched in size to the features in the spectrum, they will be enhanced with respect to the continuum.

Once the function $T(x_i)$ is obtained, the correlation technique can be applied to obtain a redshift, by correlating $T(x_i)$ with a standard, stepping the standard in redshift. In wavelength (λ) terms, with an expected spectrum $P(\lambda)$, if the correlation function is

$$F(z_i) = \sum_j \left[T(\lambda_j) - P(\lambda_j(1+z_i))\right]^2$$

$F(z_i)$ should go through a minimum at $z_i = z_o$ where z_o is the redshift of the spectrum being measured, provided that the features match accurately enough.

The structure of the program is given in a flow diagram (Fig. 3.4.6). There is no complicated structure, and the program is ideal for batch processing of large amounts of data. The individual 'blocks' in the flow diagram can be described in detail:

Read external parameters

This section reads in data from a file. The data include parameters for COSMOS data format, smoothing of the spectrum, details of the features expected in the spectrum, and the redshift range over which the correlation is to be performed. Details of the intensity conversion are also needed. In addition, some parameters are used to reject spectra, for example those which are too bright.

Generate intensity look-up table

Before processing, the spectrum, written in COSMOS 'transmission'

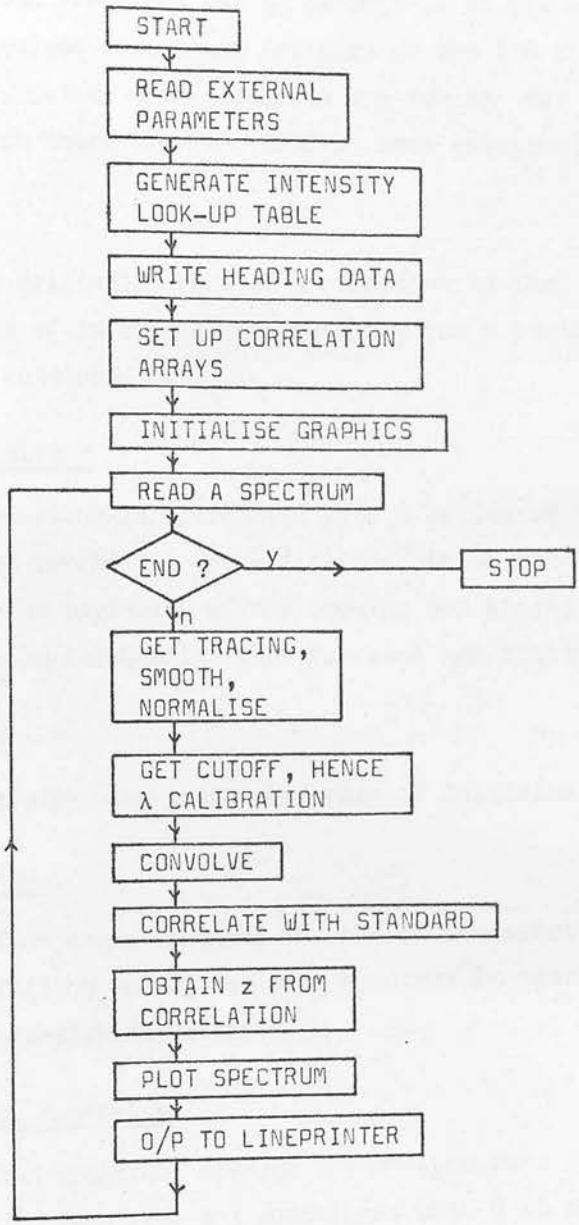

Fig. 3.4.6

Flow diagram of the redshift program (section 3.4.4, and appendix A).

terms, is converted to intensity terms. Each pixel needs to be converted, so the most efficient way to do this is to use a 'look-up table' of values calculated for each of the 128 COSMOS transmission levels, rather than calculate the result for every pixel (of which there are over 1000 in each spectrum).

Write heading data

The parameters originally read in are written to the lineprinter for ease of reference when checking how a particular set of results was obtained.

Set up correlation arrays

The observed spectrum is correlated with a series of standard spectra at different redshift. For efficiency, these are calculated once here at the beginning of the program and stored in arrays, rather than re-calculating them for each new spectrum.

Initialise graphics

Any graphics system used needs some form of initialisation.

Read a spectrum: end?

Data is read from magnetic tape; the end of the spectra can be detected here, failing which, the next spectrum is read in for processing, then intensity converted.

Get tracing, smooth, normalise

A 'tracing' (1-D spectrum) through the MM-type data is obtained, smoothed if required, and normalised with 0 at sky level and 1 at spectrum peak intensity.

Get cutoff, hence λ calibration

The position of the green cutoff of the IIIa-J emulsion is found by obtaining the half-height in intensity. With this position in the spectrum defined, the wavelength of each pixel in the spectrum can be obtained by using the prism dispersion relation.

Convolve

The spectrum is convolved with the 'gate' function to remove the continuum (above). This leaves a convolved spectrum with only sharp features.

Correlate with standard

The standard spectra, stepped in redshift, are retrieved one by one and correlated with the convolved observed spectrum. The value of the correlation for each redshift is stored. This value should pass through a minimum (representing maximum correlation) when the redshifts of standard spectrum and observed spectrum match.

Obtain z from correlation

The minimum in the correlation curve is found, and a parabola fitted through the few points around the minimum, to give the best approximation to the redshift.

Plot spectrum

A plot of the spectrum, with features identified, is made to facilitate checking of the working of the program. Examples are given in fig. 3.4.7.

O/P to lineprinter

Details of the spectrum identification, calculated redshift, and other parameters are output to the lineprinter. At present two important parameters are given, which give information on the strength of the correlation, and on the fit to the maximum correlation. Monochromatic magnitudes at several points in the spectrum are also given.

Output is also written to a data file.

The redshift-obtaining algorithm is described in words under the sections 'Convolve' to 'obtain z from correlation' above. It is useful to give more details in diagrammatic form. The process of convolution and correlation of the convolved spectrum

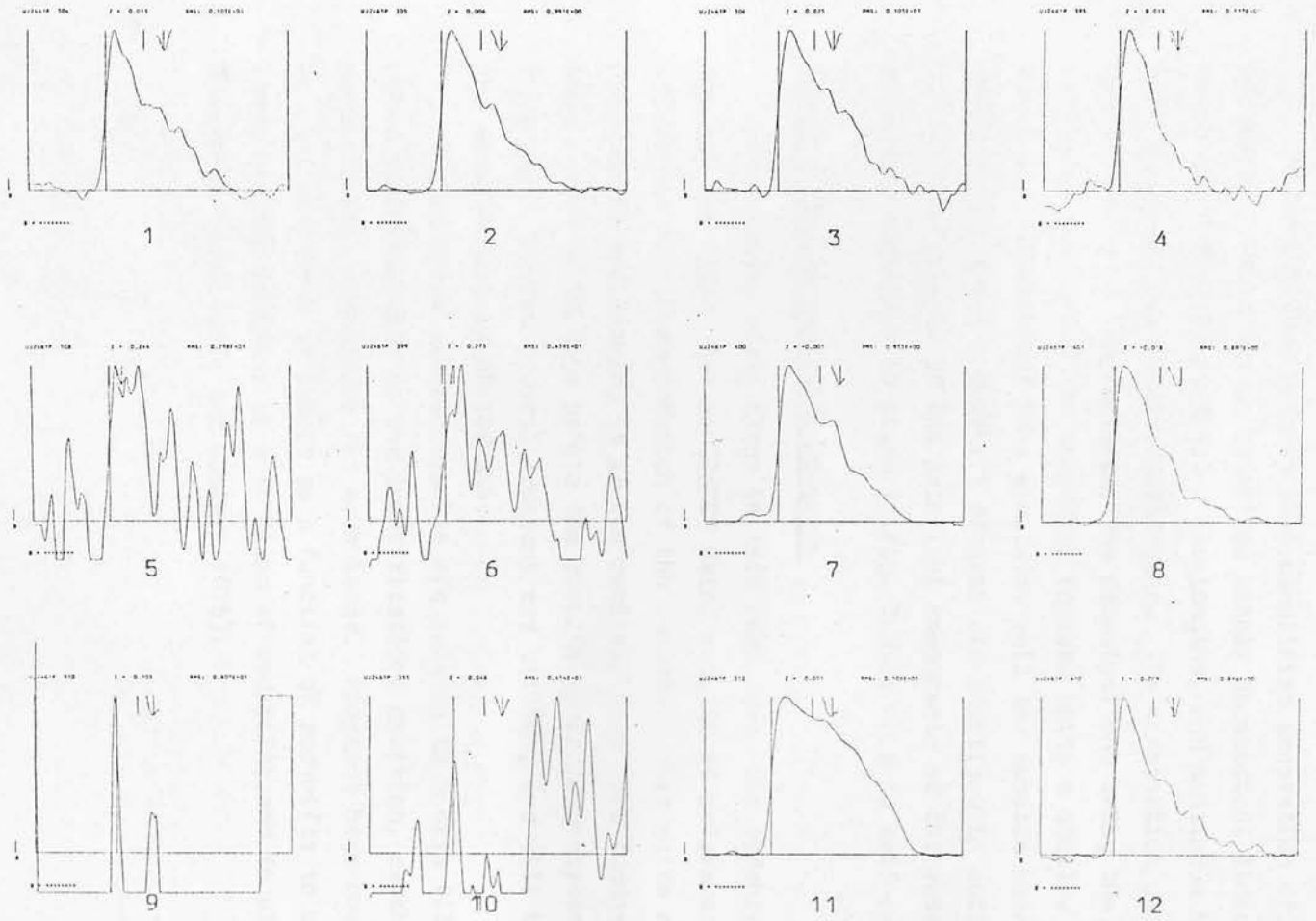

Fig. 3.4.7

An example of 'plot' output from the redshift program. This includes several late-type stars (2,7,8,12), a saturated image (11) and several images too noisy to measure (5,6,9,10).

is shown in fig. 3.4.8. The effect of the convolution is clearly seen from (a) to (b). The reason for the use of the convolution is given above; it is to remove the effects of objects being at different brightness and different colours. The correlation should be dependent only on the sharp features in the spectra.

The convolution process also simplifies generation of the standards. These can be specified simply as spectral lines (with depth and width) at particular wavelengths, and continuum breaks (with size given) at particular wavelengths. The combination used to date consists of just two features, the principal one being the 4000 Å continuum break, and the secondary feature being a shallow line at the G band wavelength; this simulates well the spectra observed. Tests on the machine redshift program are described in section 3.5.

A flow diagram of the principal components of the redshift-obtaining algorithm is given in fig. 3.4.9: this is self-explanatory.

3.4.5 'Results analysis' programs

At a fairly early stage in this work, when the redshift program was first used on COSMOS data, a suite of programs was written to aid interpretation of the results. This suite of programs is unfinished, as it was realised that more fundamental work needed to be done before the results could be analysed in this way. However several programs are written, and will be of use for future analysis of results.

The redshift program results are written to a data file. This contains information on the identification, position, redshift and monochromatic magnitudes for each image. Programs have been written to plot positions of images as a function of redshift; to plot colour-colour diagrams as a function of redshift; and to plot 'cone diagrams' (e.g. Tifft and Gregory 1976).

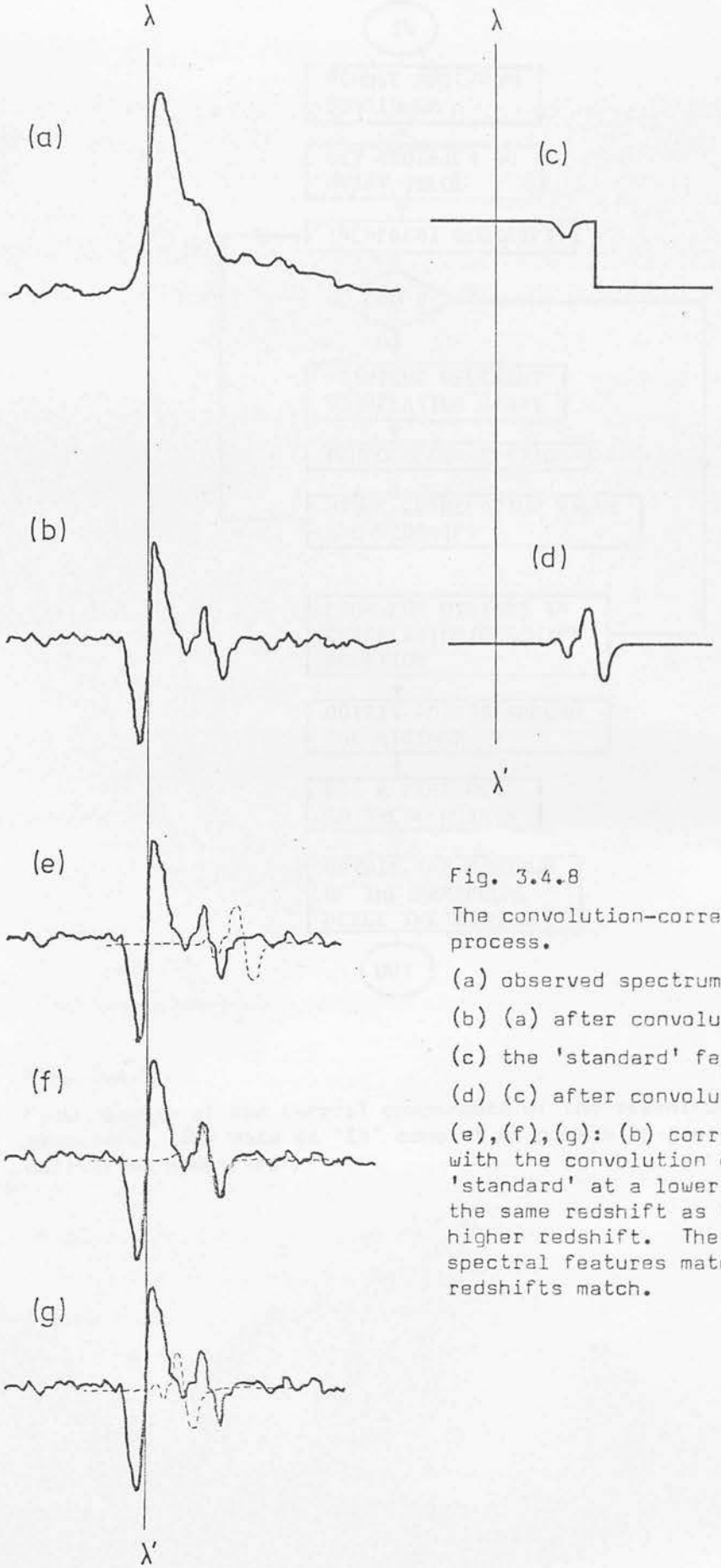

Fig. 3.4.8

The convolution-correlation process.

(a) observed spectrum

(b) (a) after convolution

(c) the 'standard' features

(d) (c) after convolution

(e),(f),(g): (b) correlated with the convolution of the 'standard' at a lower redshift, the same redshift as (b), and a higher redshift. The convolved spectral features match when the redshifts match.

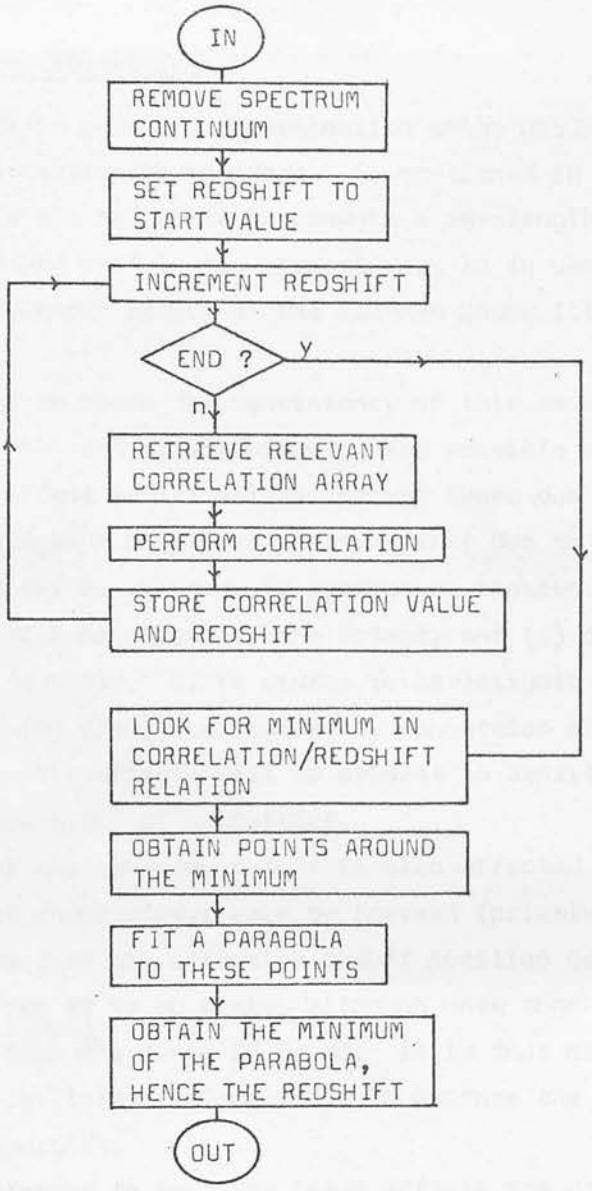

Fig. 3.4.9

Flow diagram of the central components of the redshift-obtaining algorithm. The data at 'IN' consist of pixels in a wavelength calibrated spectrum.

3.5 Checks and Calibration

3.5.1 Plate emulsion properties

A major element in redshift determination using UKSTU objective prism plates is the wavelength standard. As mentioned in section 3.3, several methods are available to produce a wavelength calibration; the method used in the present work is to use the very sharp long wavelength cutoff of the Eastman Kodak IIIa-J emulsion.

It is essential to check the consistency of this emulsion feature if it is to be used to any extent. The possible variations that are likely to affect radial velocities are those due to (a) position on the photographic plate; (b) any effect due to the emulsion characteristic curve, which could produce an apparent change in cutoff position with magnitude of the object, and (c) emulsion changes from plate to plate. It is useful to investigate these effects even though (b) should be removed by conversion of the image to intensity. The effects will be present in density tracings used for manual measurement of velocities.

The position of the emulsion cutoff is also affected by the colour of the object under study; work by Emerson (private communication) indicates that the effective cutoff position can change by up to $\sim$ 100 Å from B0 to M0 stars, although more than half of this change occurs over the range K0 to M0. It is thus necessary to use stars of a fairly limited colour range to perform the checks on the emulsion properties.

The checks performed to test for these effects are described below; they were made on plate material covering a common area, most of the photographs being centred on UKSTU survey area 345; details of the photographs are given in section 3.1.

(a) and (b); consistency with position and magnitude

Plate UJ2461P has been used most extensively for early work on redshift determination, and so this plate was chosen for the positional emulsion consistency checks.

For these checks, a set of 16 areas across the plate was

selected in a 4 by 4 grid, and in each of these areas a number of late-type stellar spectra were traced using a Joyce-Loebl microdensitometer. The stars were selected purely on the basis of brightness, to cover a suitable magnitude range. Very few had to be rejected due to being an unsuitable spectral type, as most of the faint stars on the deep photographs in the galatic cap appear to be in spectral classes G and K. In each area 6 to 8 stars were traced, with the exception of the area chosen for comparison from plate to plate; in this area 10 stars were traced.

The analysis of these data was as follows: the stars were first grouped into 4 magnitude ranges, to produce 4 sets of objects each of small magnitude range; any effects due to position were then looked for in each group. The method used to look for emulsion variations was to examine the separation between the cutoff position and the 4000 Å continuum break. Here we are of course assuming that the 4000 Å feature is itself unaffected by what we are trying to measure. The height of the break is in fact small relative to the height of the emulsion cutoff on any given tracing, so, with its sharpness comparable to that of the cutoff, its midpoint as determined on the tracing cannot vary much due to the emulsion characteristics. We do not expect any intrinsic variation in the 4000 Å feature (section 3.3.5).

The results of the analysis for positional variation are given in table 3.5.1. It is clear from this that there is no systematic variation within measurement error, for any magnitude range. This allows us to proceed with the tests for magnitude effects, by combining together the results for all areas. Fig. 3.5.1 is a plot of the cutoff position against object brightness (determined by peak density above sky). A correlation between brightness and cutoff position can be seen, and this is to be expected for measurements of cutoff position defined by the mid-point in density. In section 3.3 we noted that strictly the mid-point in intensity should be used. Applying a conversion from density to intensity (fig. 3.5.2 (a)) we can draw up a (calculated) correction for position of the cutoff, depending on object brightness (fig. 3.5.2 (b)). This correction has been applied to the raw data, grouped in small brightness ranges, and the results of the corrected measurements

Table 3.5.1

Results of analysis for position variation of the IIIa-J emulsion cutoff. Stars were divided into 4 brightness groups, with peak densities above sky as follows: a, 0-0.67; b, 0.67-1.34; c, 1.34-2.02; d, 2.02 upwards. Cutoff to 4000 Å feature distances are given for each of the 16 areas, arranged as on the plate. All four groups are combined in e, with the magnitude correction of fig. 3.5.2 applied as follows (in cm): a, 0; b, 0; c, -0.03; d, -0.05. The total number of stars used in each area is given in f.

a)

--	2.45	2.40	2.30
2.35	2.35	2.40	2.35
--	2.35	2.30	2.33
2.40	2.35	2.40	--

b)

2.40	2.45	2.37	2.35
2.40	2.35	2.43	2.45
2.40	2.40	2.40	2.40
2.40	2.38	2.38	2.38

c)

2.35	2.40	2.35	2.35
2.40	2.43	2.40	2.40
--	2.40	2.40	2.35
2.40	--	2.35	2.40

d)

2.40	2.40	2.50	2.35
2.40	--	2.40	2.45
2.45	2.40	2.50	--
2.50	2.40	2.35	2.38

e) Corrected mean

2.36	2.41	2.38	2.32
2.38	2.38	2.39	2.39
2.40	2.37	2.38	2.35
2.41	2.37	2.36	2.35

f) Number of stars

5	4	6	4
6	5	6	5
4	4	5	4
6	4	5	6

'--' indicates no stars in that density group in that area.

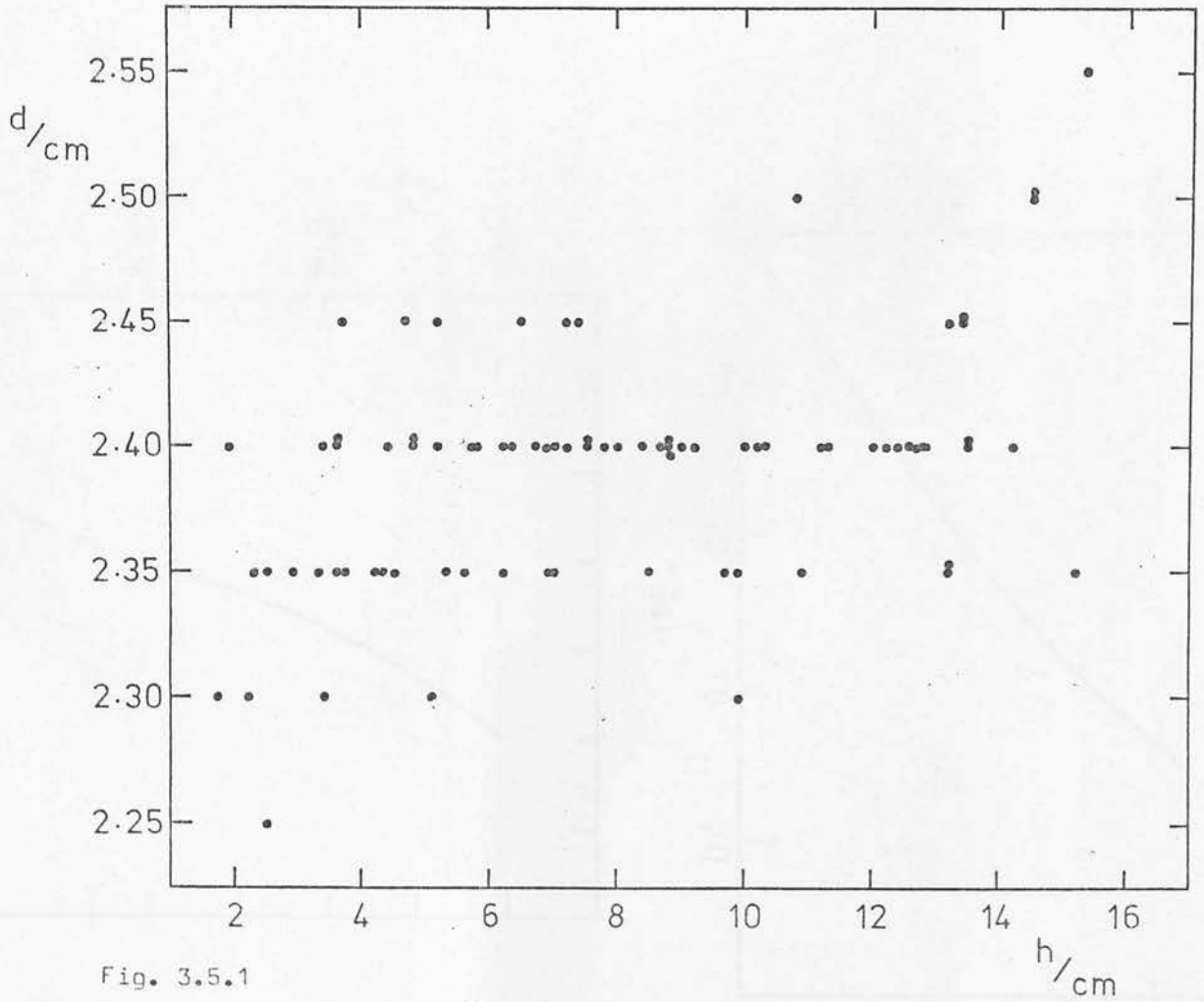

Fig. 3.5.1

Emulsion cutoff to 4000 Å feature distance (d) plotted against the maximum density of the spectrum, in terms of the height of the tracing(h). The conversion from height to density is given by D = 0.168h, where D is density above plate background.

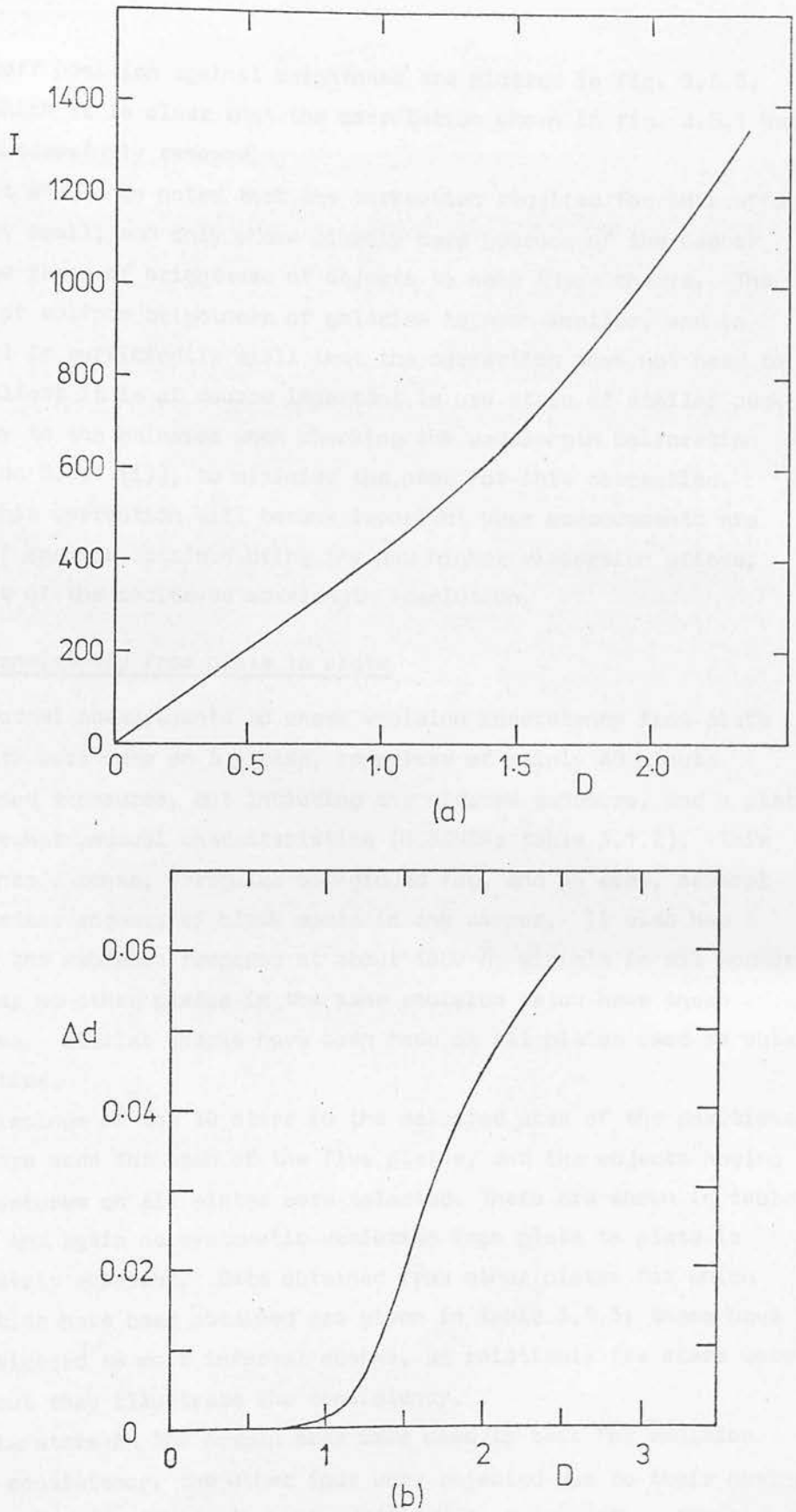

Fig. 3.5.2

The intensity - density relation (as fig. 3.3.3).
(b) gives the calculated correction to the cutoff position measured on a 50:1 scale tracing, in cm, in terms of the object peak density.

of cutoff position against brightness are plotted in fig. 3.5.3, from which it is clear that the correlation shown in fig. 3.5.1 has been successfully removed.

It should be noted that the correction required for this effect is very small, and only shows clearly here because of the use of a large range of brightness of objects to make these checks. The range of surface brightness of galaxies is much smaller, and in general is sufficiently small that the correction does not need to be applied; it is of course important to use stars of similar peak density to the galaxies when checking the wavelength calibration (section 3.3.7 (i)), to minimise the need for this correction.

This correction will become important when measurements are made of spectra obtained using the new higher dispersion prisms, because of the increased wavelength resolution.

(c): consistency from plate to plate

Formal measurements to check emulsion consistency from plate to plate were made on 5 plates, comprised of mainly 40 minute unwidened exposures, but including one widened exposure, and a plate of somewhat unusual characteristics (UJ3092P: table 3.1.2). This plate has a dense, irregular background fog, and an area, several centimetres across, of black spots in one corner. It also has a dip in the emulsion response at about 4800 Å, visible in all measured spectra; no other plates in the same emulsion batch have these features. Similar checks have been made on all plates used to obtain velocities.

Tracings of the 10 stars in the selected area of the positional test were made for each of the five plates, and the objects having good features on all plates were selected. These are shown in table 3.5.2, and again no systematic variation from plate to plate is immediately apparent. Data obtained from other plates for which velocities have been obtained are given in table 3.5.3; these have to be considered as more informal checks, as relatively few stars were used, but they illustrate the consistency.

Six stars in the common area were used to test for emulsion cutoff consistency; the other four were rejected due to their having either small (in density) or broad 4000 Å features. The effect

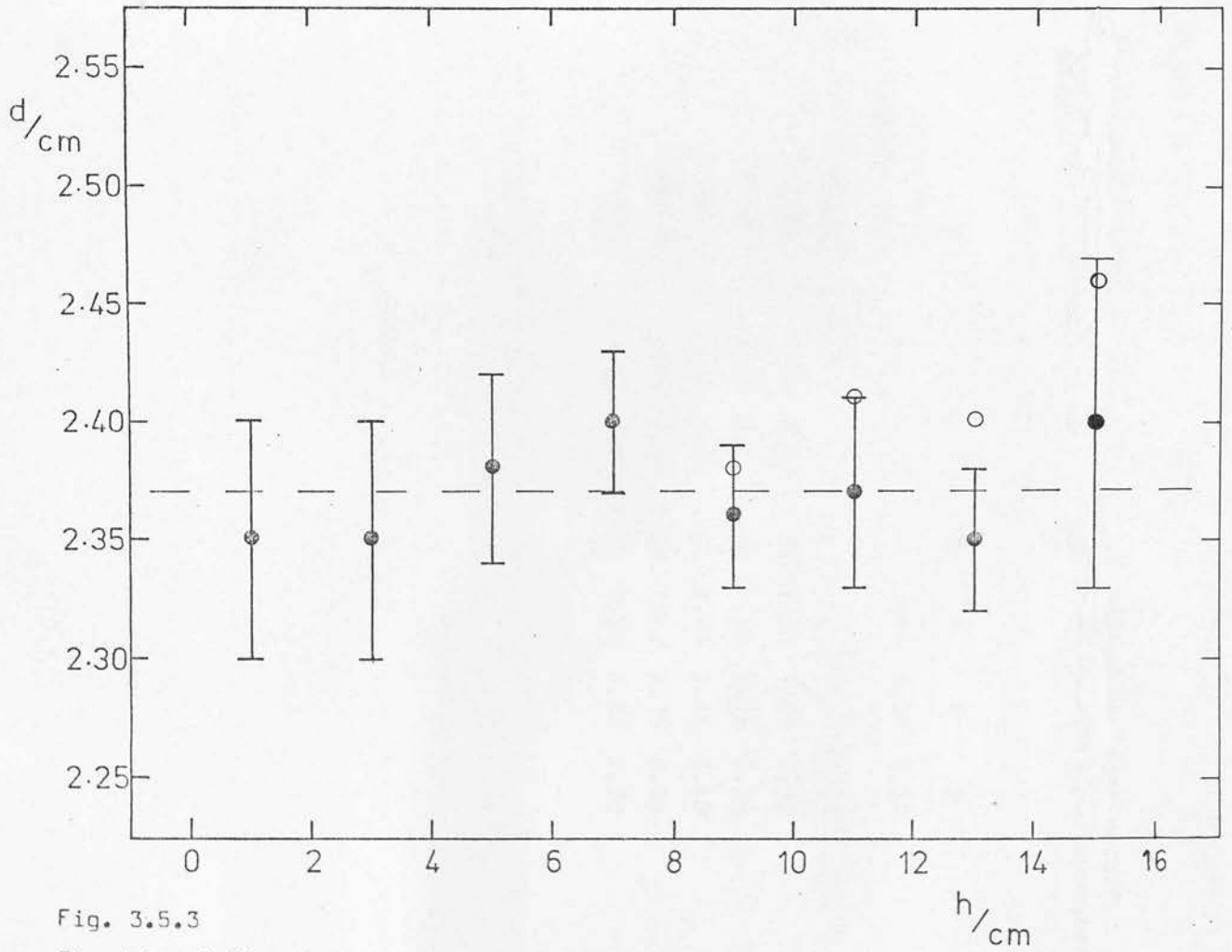

Fig. 3.5.3

The data of fig. 3.5.1 grouped, with the correction of fig. 3.5.2 applied. Uncorrected points for the groups are shown as open circles. Error bars show the calculated dispersion in the means for the groups. The adopted mean cutoff - 4000 Å feature separation is shown as a dotted line

Table 3.5.2

Analysis for position variation of the IIIa-J emulsion cutoff over five plates: cutoff to 4000 Å feature distances as measured, in cm.

Object:	1	4	6	7	8	9
Peak density above sky:	2.15	1.13	1.18	1.55	2.27	2.22
Plate						
UJ2461P	2.40	2.35	2.35	2.40	2.40	2.30
UJ3092P	2.25	2.30	2.25	2.35	2.35	2.35
UJ4539P	2.40	2.40	2.40	2.40	2.40	2.40
UJ4563P	2.40	2.35	2.35	2.40	2.35	2.30
UJ4530P	2.40	2.40	2.30	2.30	2.35	2.30

Table 3.5.3

IIIa-J emulsion cutoff to 4000 Å feature separations (d), measured on plates not included in the formal analysis. The values given are means from n tracings of stellar spectra.

Plate	mean d cm	n
UJ2451P	2.38	5
UJ2620P	2.37	3
UJ3682P	2.36	5
UJ4117P	2.35	2
UJ4543P	2.34	5
UJ4551P	2.43	3

observed with density ((b) above) was corrected for in the measurements, and the results are given in table 3.5.4. It can be seen that the agreement is good, and no significant difference between the plates is apparent, apart from the fact that the result for plate 3092 is low. This is not unexpected, being the 'rogue' plate mentioned above. A mean value (for the cutoff to 4000 Å feature separation on the tracings) obtained from the remaining plates, 2.34 ± 0.04 cm, is perfectly consistent with that obtained for many areas on a single plate, 2.37 ± 0.02 cm. The mean obtained from the single plate is adopted as standard (as it was determined from a larger sample); with a cutoff wavelength (obtained from density tracings of faint objects) of 5380 Å determined from the dispersion curve, this gives a wavelength for the 4000 Å feature as 3990 ± 20 Å.

3.5.2 The intensity calibration procedure

Intensity calibration is only used as a matter of course for digitised data. Chiefly this procedure has been used for data from the COSMOS machine, but a similar procedure has been used to convert to intensity data obtained digitally from a Joyce-Loebl microdensitometer (Kelly et al, 1980a). This procedure relies totally on the calibration of the step wedges provided by the UK Schmidt telescope unit.

The intensity calibration procedure is best explained with a specific example. Here data is taken from measurement of an area on plate UJ2461P, which is processed by a computer program and plotted as in fig. 3.5.4. Measurements are made using the COSMOS machine of the east step wedge (this having the best profile - fig. 3.1.3). The same machine gain is used for the step wedge measurement as for the measurement of the area of interest. Also given are measurements of COSMOS transmission for clear plate (T_c) and for 'black' plate (with a cap over the COSMOS detector), T_B. These parameters are then used in the expression

$$\log I = \gamma \log\left(\frac{T_c - T_B}{T - T_B} - 1\right) + C$$

Where γ and C are constants to be determined. The constant γ is related to the 'photographic' γ, the slope of the H-D curve.

Table 3.5.4

Results of the analysis for position variation of the IIIa-J emulsion cutoff over five plates. d is the mean cutoff to 4000 Å feature separation (with the corrections of fig. 3.5.2 applied using an appropriate offset for the different sky background densities of each plate); σ the standard deviation in this mean.

Plate	d cm	σ cm
UJ2461P	2.33	0.04
UJ3092P	2.27	0.05
UJ4539P	2.37	0.02
UJ4563P	2.33	0.05
UJ4530P	2.33	0.05

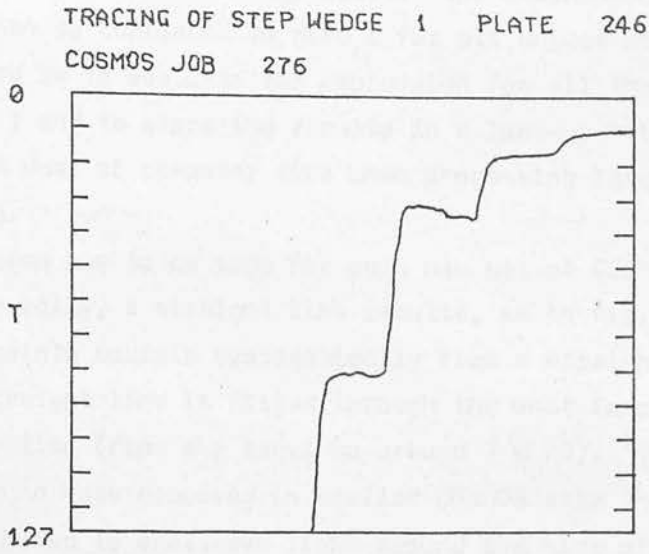

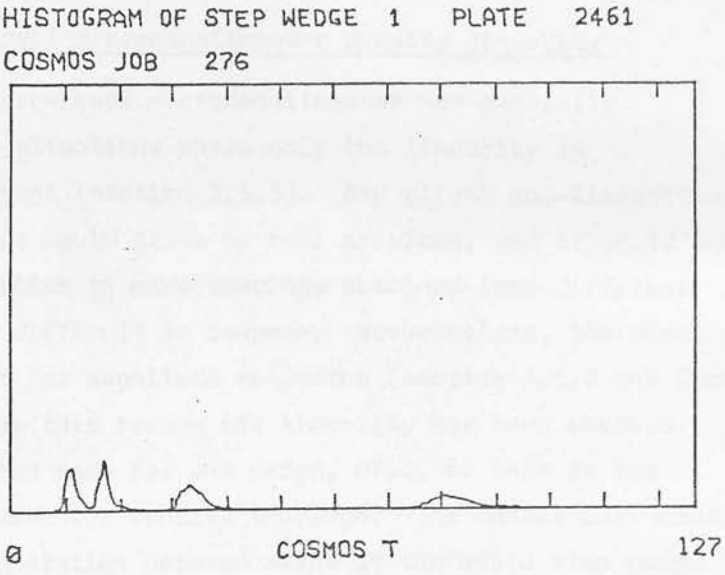

Fig. 3.5.4

Plots of COSMOS data from the step wedge used to obtain the intensity calibration.

A plot of log I against log $((T_c - T_B)/(T - T_B) - 1)$ is drawn and the constants γ, C determined from the straight line obtained. This is illustrated in fig. 3.5.5. The expression given above can then be evaluated to give I for all values of T. The usual procedure is to evaluate the expression for all the integer values of T and to store the results in a look-up table; this saves a great deal of computer time when processing large quantities of data.

This calibration has to be made for each new set of COSMOS measurements. Generally, a straight line results, as in fig. 3.5.5. Occasionally the points deviate systematically from a straight line; in such cases a straight line is fitted through the most important part of the calibration (from sky level to around T = 20). This problem seems only to have appeared in earlier COSMOS data though and could be attributed to scattered light around the side of the step wedge. The scattered light problem should now have been mostly alleviated(section 3.5.7).

3.5.3 The Joyce-Loebl microdensitometer density linearity

Use of the Joyce-Loebl microdensitometer has generally been restricted to situations where only the linearity in position was important (section 3.5.5). Any slight non-linearities in the density scale would cause no real problems; and it would need serious non-linearities to make tracings obtained from different parts of the wedge difficult to compare. Nevertheless, the density scale has been used for magnitude estimates (section 3.5.9 and Cooke et al, 1977) and for this reason its linearity has been checked.

Checks have been made for one wedge, D760, as this is the wedge most widely used for density tracings. The checks were made by comparing the separation between steps of the UKSTU step wedge when measured at different points on the microdensitometer wedge; this was done by using the density offset wedge on the microdensitometer. Wedge D760 was initially chosen for measurements because, of course, of its suitable density range (0.080 cm^{-1}) but also because the manufacturer's calibration curve for this wedge is flat, indicating that no density corrections are needed. This is borne out by the checks made; repeat measurements indicate that the wedge constant

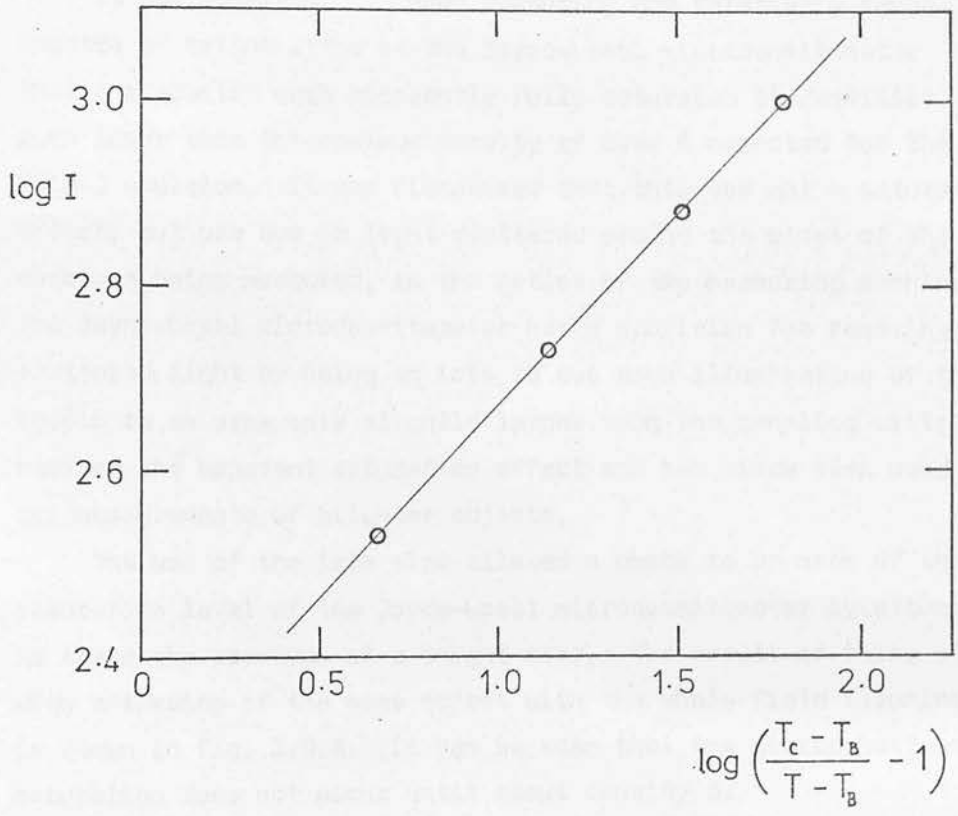

Fig. 3.5.5

The intensity calibration for the step wedge of fig. 3.5.4. For these measurements, $T_B = 4$, $T_C = 433$; from this straight line values of γ and C of 0.42 and 2.26 respectively are obtained.

is ∿1% less near the 'dense' end of the wedge than it is at the 'clear' end. This is certainly adequately linear.

3.5.4 Microdensitometer density limit

A problem to be considered with all density or transmission measuring machines is the problem of saturation; this is discussed for COSMOS in section 3.5.6.

It was observed when measuring the relatively dense spectra of bright stars on the Joyce-Loebl microdensitometer that the spectra were apparently fully saturated at densities much lower than the maximum density of over 4 expected for the IIIa-J emulsion. It was discovered that this was not a saturation effect, but was due to light scattered around the sides of the spectrum being measured, in the optics of the measuring machine. The Joyce-Loebl microdensitometer has a provision for removing such scattered light by using an iris to cut down illumination of the sample to an area only slightly larger than the sampling slit; this removed the apparant saturation effect and has since been used for all measurements of brighter objects.

The use of the iris also allowed a check to be made of the density saturation level of the Joyce-Loebl microdensitometer by attempting to trace the spectrum of a bright star. The result of this, along with a tracing of the same object with the whole field illuminated, is shown in fig. 3.5.6. It can be seen that the microdensitometer saturation does not occur until about density 5.

3.5.5 Microdensitometer ratio arm linearity

Since redshift measurements are made from the tracings produced via the microdensitometer ratio arm, it is important to check that this ratio is constant along the length of the tracing. In an early series of measurements making use of a 300:1 ratio arm, non-linearities obvious to the eye were noted. The only other ratio arm available at the time gave a 50:1 ratio; this was tested and used.

The ratio was tested by making a density tracing of part of a Moiré grating having approximately 20 lines per mm. The line separation over ten line periods was measured across the tracing. As an additional check, to be sure of the intrinsic uniformity of

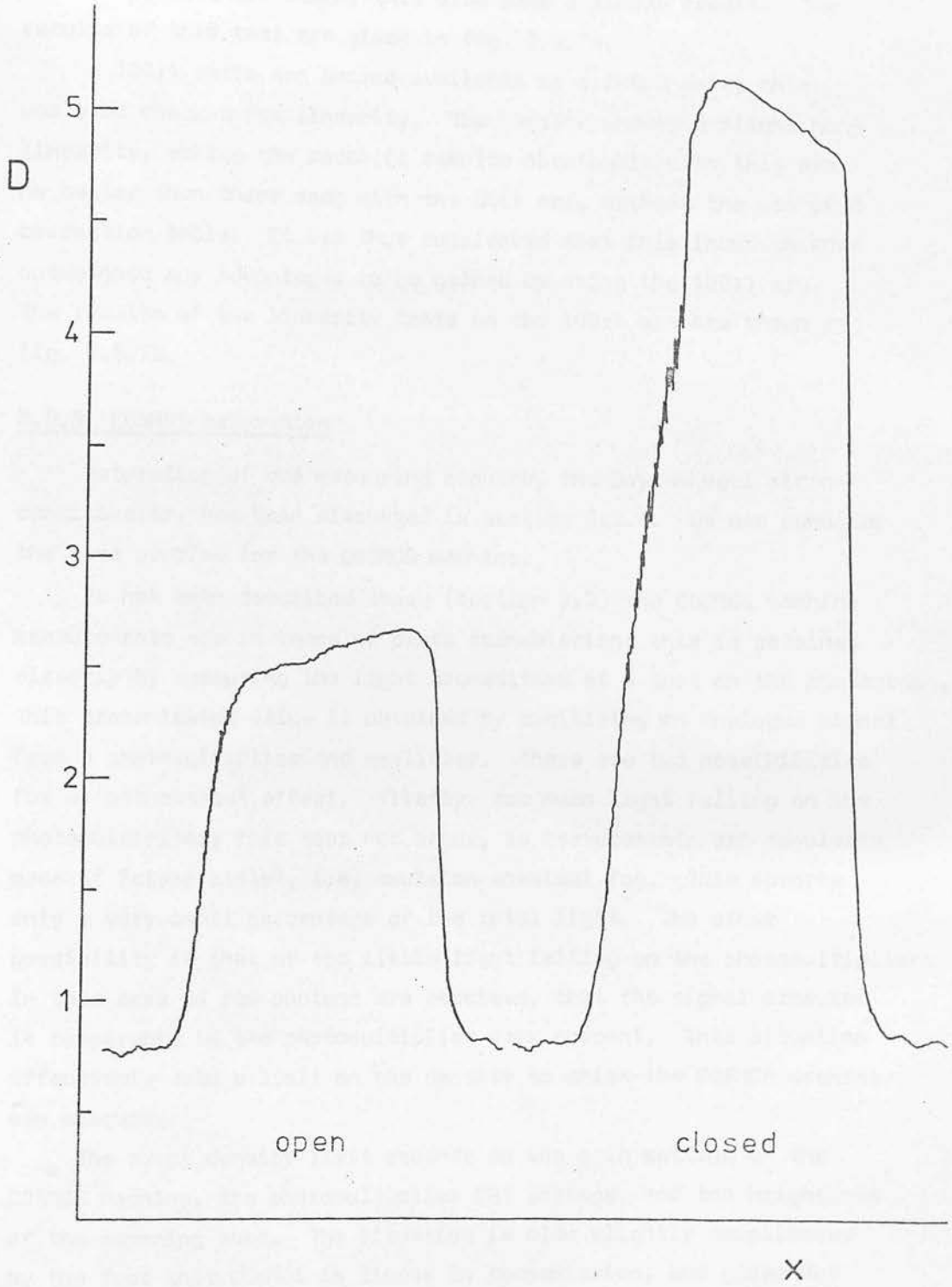

Fig. 3.5.6

Illustrating the density saturation of the Joyce-Loebl microdensitometer. Saturation with the iris open (scattered light present) and closed (limiting scattered light) are shown. The ordinate is density; the tracings are of a very bright star, probably saturated itself on the emulsion.

the Moiré grating, another part of the same grating was measured in the opposite direction; this also gave a linear result. The results of this test are given in fig. 3.5.7a.

A 100:1 ratio arm became available at a later date; this was also checked for linearity. The results showed a slight non-linearity, making the redshift results obtainable with this arm no better than those made with the 50:1 arm, without the use of a correction table. It was thus considered that this inconvenience outweighed any advantages to be gained by using the 100:1 arm. The results of the linearity tests on the 100:1 arm are shown in fig. 3.5.7b.

3.5.6 COSMOS saturation

Saturation of one measuring machine, the Joyce-Loebl micro-densitometer, has been discussed in section 3.5.4. We now consider the same problem for the COSMOS machine.

As has been described above (section 3.2) the COSMOS machine measurements are in terms of plate transmission; this is obtained directly by measuring the light transmitted at a spot on the photograph. This transmission value is obtained by digitising an analogue signal from a photomultiplier and amplifier. There are two possibilities for a 'saturation' effect. Firstly, too much light falling on the photomultiplier; this does not occur, as measurements are regularly made of "clear plate", i.e. emulsion chemical fog. This absorbs only a very small percentage of the total light. The other possibility is that of too little light falling on the photomultiplier; in this case so few photons are received, that the signal produced is comparable to the photomultiplier dark current. This situation effectively sets a limit on the density to which the COSMOS machine can measure.

The exact density limit depends on the gain setting of the COSMOS machine, the photomultiplier EHT voltage, and the brightness of the scanning spot. The situation is also slightly complicated by the fact that COSMOS is linear in transmission, and gives out integer T values; as T approaches T_{black}, a single step in T is equivalent to a large density step; thus in addition to the machine not being able to measure densities greater than a certain value,

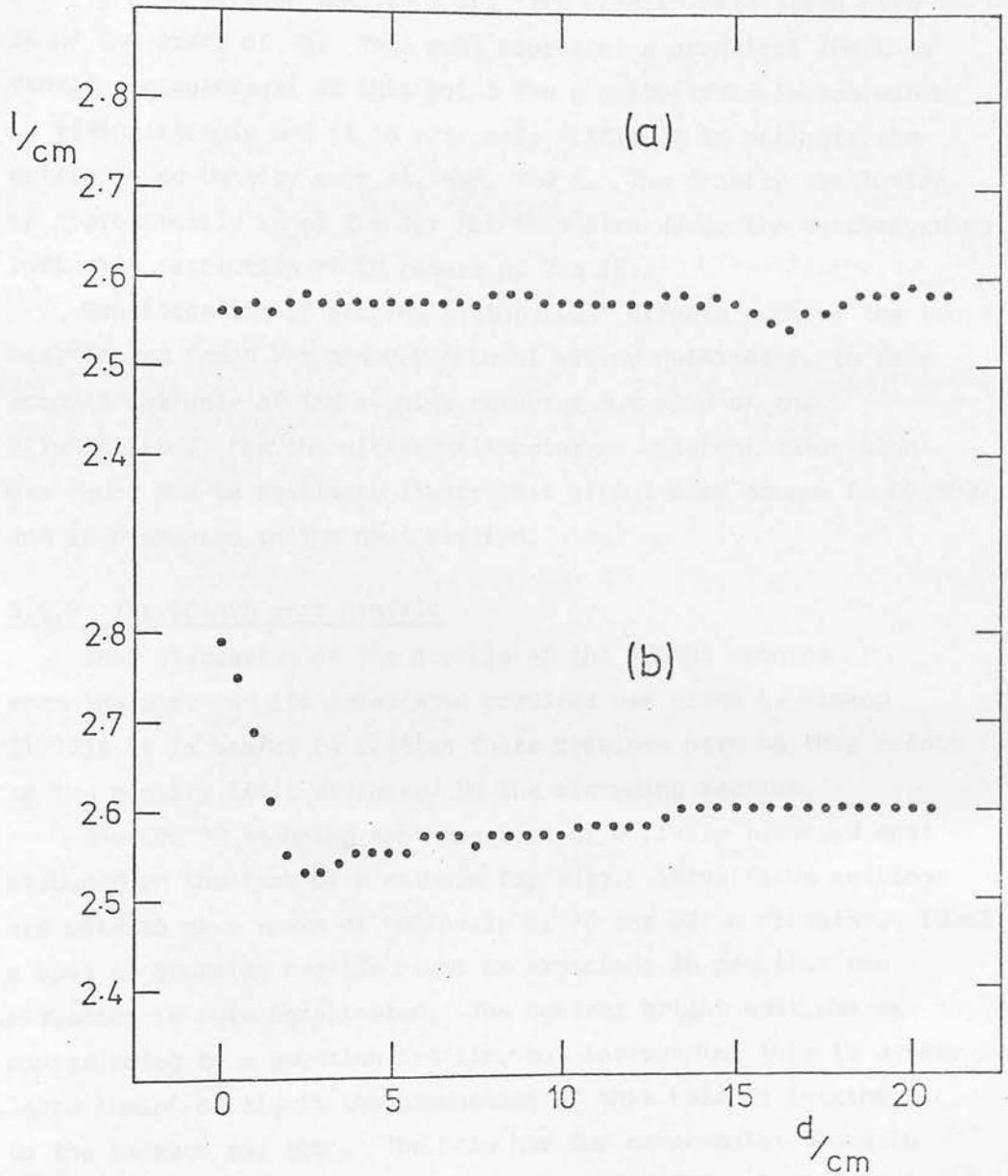

Fig. 3.5.7

The linearity tests for the 50:1 (a) and 100:1 (b) ratio arms of the Joyce-Loebl microdensitometer. l is the length of 10 line periods of the grating for (a), and of 5 periods for (b). d is the distance along the tracing. Errors are estimated to be of the order 0.01 cm.

the density resolution becomes very poor as T approaches this value. This condition is illustrated in table 3.5.5, taking data from the step wedge in fig. 3.5.4. The value of T_{black} given by COSMOS is 4; the most dense step of the step wedge lies at T = 11, with diffuse density 2.33. The density resolution here is of the order of 4%. This must represent a practical limit to density measurement; at this point the density/transmission curve is rising steeply and it is extremely difficult to estimate the extrapolated density even at, say, T = 6. The density resolution is approximately 2% at T = 32; for this step wedge the corresponding intensity resolution of 2% occurs at T = 26.

Consideration of machine 'saturation' effects such as the above, has, as was found for the Joyce-Loebl microdensitometer, to take account not only of the machine detector but also of the illumination. For the microdensitometer an apparent saturation was found due to scattered light; this effect also occurs in COSMOS, and is discussed in the next section.

3.5.7 The COSMOS spot profile

Some discussion of the profile of the COSMOS machine scanning spot and its associated problems was given by Pickup (1979); it is useful to mention these problems here as they relate to the density limit discussed in the preceding section.

The COSMOS scanning spot consists of a finely focussed spot produced on the face of a cathode ray tube. Three focus settings are used to give spots of nominally 8, 16 and 32 m diameter. Ideally a spot of gaussian profile might be expected; in practice the situation is more complicated. The central bright spot can be approximated by a gaussian profile, but surrounding this is a very large 'halo' of light; the production of this halo is intrinsic to the cathode ray tube. The halo has two components: the main component is 6 cm across on the tube (corresponding to 1cm projected on to the plate) which contains 1% of the total tube light; a secondary component 6 mm across on the tube contains 0.5% of the total tube light. Most of this is now removed, however, using a mask on the cathode ray tube face; as the spot is scanned in only one direction a mask with a narrow slot corresponding to the scan

Table 3.5.5

Computed values of density (D) and intensity (I) from the step wedge data of fig. 3.5.4, for values of COSMOS T. Values for I > 1000 are extrapolated from an assumed linear D vs logI relation for IIIa-J at these densities and thus should be used with caution; the table does, however, show the loss of resolution in density for low values of T. Values of logI are computed from the relation in section 3.5.2.

T	log I	I	D
5	3.37	2318	3.50
6	3.24	1731	3.07
7	3.16	1459	2.82
8	3.11	1291	2.65
9	3.07	1175	2.53
10	3.04	1087	2.43
11	3.01	1018	2.33
12	2.98	961	2.23
13	2.96	914	2.16
14	2.94	874	2.10
15	2.92	839	2.03
16	2.91	808	2.00
17	2.89	780	1.94
18	2.88	755	1.90
19	2.87	733	1.87
20	2.85	713	1.81

can be used to remove all of the halo with the exception of the part remaining in the slot.

The effect of the halo is similar to an effect due to light scattered around the spot being measured; the measured value of transmission appears to be greater than the true value. Unfortunately this cannot be taken out by the intensity conversion; the intensity calibration is obtained from a step wedge consisting of areas of approximately uniform density; the halo effect here is greatly reduced when compared to a measurement of a small, dense, spectrum surrounded by photographic plate at sky fog level. The net effect on the appearance of an intensity-converted tracing of a spectrum is to reduce the intensity at the intensity peak. Thus, when normalised, such spectra have features further above sky fog level than should be. This effect is noticeable in fig. 1 of Kelly et al (1980a).

Once again, this is not an effect which has any bearing on the obtaining of radial velocities of faint galaxies.

3.5.8 Overlapping Spectra.

A problem with all photographs of fields of objects is that the images of some objects overlap due to the proximity of these objects in the photograph. This effect is worsened in objective prism work, as the image of each object is elongated by the dispersion, thus increasing the likelihood of overlapping images.

The basic problem of overlapping images is simply that some objects, because their spectra are overlapped, are excluded from detailed study; it becomes impossible to obtain a clear spectrum. With two partially overlapped images, where there was some uncontaminated element of each image for every spectral resolution element, it might be possible, by careful processing of machine measurements of the area, to deconvolve the two images. This process would have to be very carefully applied to avoid introducing artefacts into the spectra, and in most cases is probably not worth applying. It may be considered worthwhile in a situation where one of the objects posesses an unusual spectrum.

A more subtle side to the problem of overlapping images is the case where the objects having overlapped spectra lie exactly in the direction of dispersion. An 'unusual' spectrum, with features possibly resembling emission lines, can result. Some of these cases can be excluded directly from the prism photograph, by reason of their impossibly long length, having spectra apparently extending well beyond the ultraviolet end of the emulsion and atmospheric cutoff. To be sure of a correct interpretation of other spectra, though, it is necessary to examine a direct photograph as well as the objective prism photograph. This is the procedure adopted when performing searches of the photographs.

Counts have been made to determine the numbers of overlapping spectra in fields of interest on UKSTU objective prism photographs. In field 345, at galactic latitude of approximately 60^{o}, a total of about 5% of images are overlapped (83 out of 1616 images, counting to the plate limit in a total area of one square degree).

3.5.9 Estimates of magnitudes.

A question frequently asked of the technique is: to what

magnitude can velocities be obtained? There are at present no galaxies having velocities obtained by the technique and independently determined magnitudes from either photographic or photoelectric photometry. Thus to answer this question at all we are reduced to making estimates by some means.

The most accurate estimates are probably those of Corwin (private communication) who, by using a photographic step-scale of 'standard' galaxies for sky limited IIIa J direct photographs, estimated that the fainter of the galaxies for which redshifts could be obtained are at about 18th to 19th magnitude in the blue. Corwin's step-scale magnitudes were calibrated initially from photoelectric aperture photometry of the galaxies.

Some additional support for these estimates comes from a photoelectric stellar sequence. In August 1979 B, V photometry was obtained of 39 stars in UKSTU area 345 (see section 3.5.12) covering a magnitude range from B = 14.4 to 17.9, using a 'people's' photometer on the 1m telescope at the South African Astronomical Observatory. This allowed a rough calibration to be made of the appearance of stellar spectra on the objective prism photograph UJ2461P; the scale was extrapolated a little to give a calibration from B = 14 to B = 19.

It was considered that the dispersed spectra of faint galaxies and faint stars are easily compared by eye to obtain brightness estimates; this comparison is much easier than a comparison of the images on direct photographs, as there is less saturation on the prism photographs. The comparison is clearly of the nuclear regions of the galaxies rather than of the whole of the galaxies with the stars; it is likely that the total galaxy magnitudes are up to a magnitude brighter than the values obtained from this comparison.

Using this comparison method, estimates were made of the (nuclear) magnitudes of galaxies in a cluster in area 345, ranging from about B = 14 to B = 19.

Microdensitometer tracings were made of these galaxies, and an attempt made to correlate the measured peak density of the spectra above sky with the estimated magnitudes. This correlation is shown in fig 3.5.8. There is clearly a reasonable

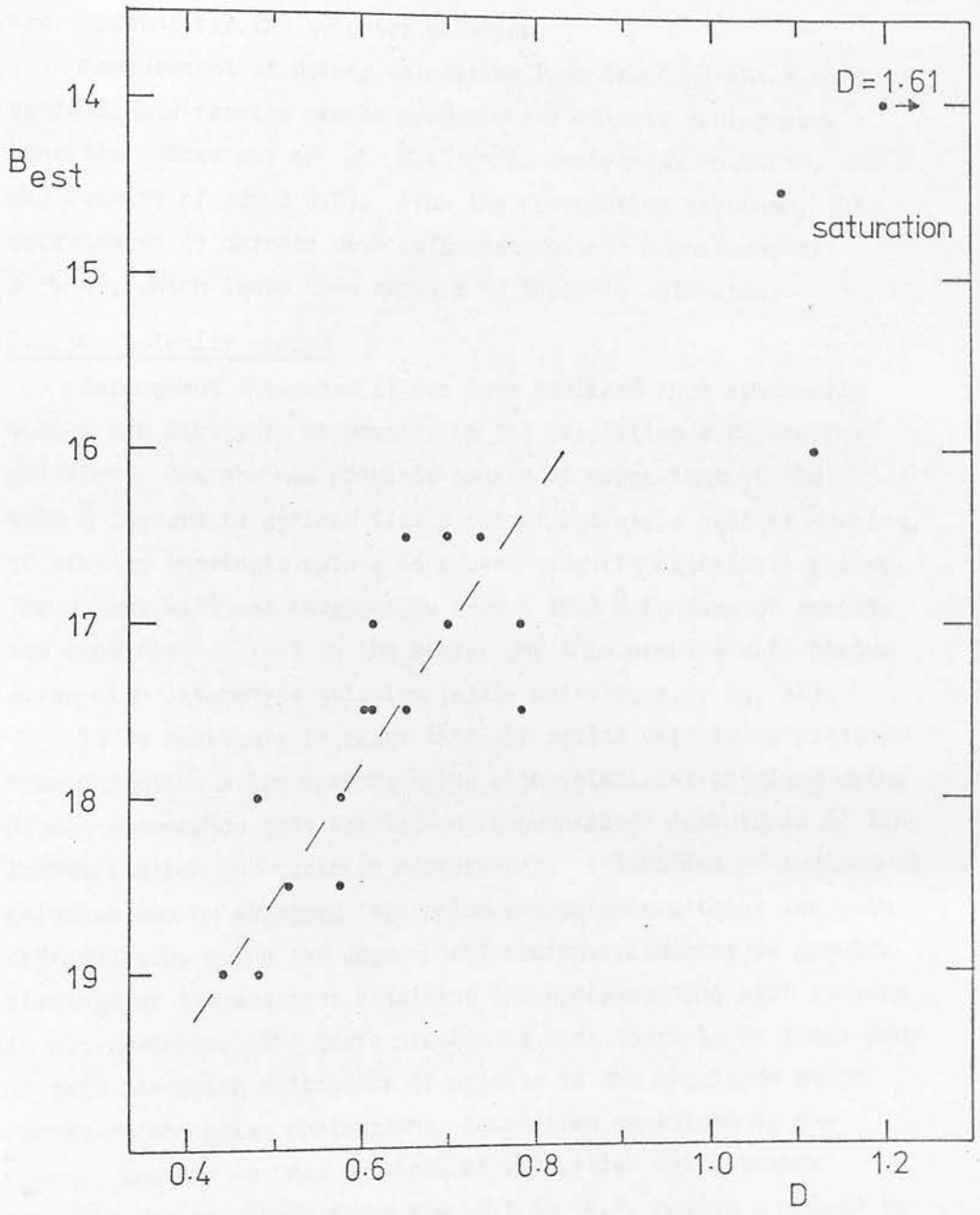

Fig. 3.5.8

Magnitude estimates (B_{est}) of galaxies plotted against peak density (D). 'saturation' indicates the area of probable photographic saturation of the images. The dotted line is a linear regression line through the points below 16th magnitude.

correlation over the fainter magnitude range, with a dispersion of about 0.5 magnitude. A linear regression line through the points below 16th magnitude is shown; non-linear saturation effects are apparent for the brighter galaxies.

Measurement of galaxy velocities from tracings shows that satisfactory results can be produced for objects having peak densities above sky of $\gtrsim$ 0.45 (this photograph, UJ2461P, has a sky density of about 0.7). From the correlation obtained, this corresponds to objects with estimated nuclear magnitudes of B $\sim$ 19, which lends some support to Corwin's estimates.

3.5.10 Velocity checks

Throughout this work it has been realised that systematic errors are likely to be present in the velocities obtained for galaxies. One obvious possible source of error is that the 4000 Å feature is defined from a set of late-type stellar spectra, of similar intrinsic colour to a zero redshift elliptical galaxy. The galaxy will not necessarily have a 4000 Å feature of exactly the same form as that in the stars; and this problem will become worse with later-type galaxies (early spirals, e.g. Sa, Sb).

It is necessary to check that the radial velocities obtained from objective prism spectra agree with velocities obtained using higher dispersion slit spectra and conventional techniques of line identification and position measurement. Velocities of individual galaxies can be obtained from prism photographs without too much difficulty by using the Joyce-Loebl microdensitometer to provide tracings of the spectra; obtaining the corresponding slit spectra is not so simple. The basic problem is that there is no large body of data providing velocities of objects in the magnitude range usable on the prism photographs, in an area contained by one plate. Ideally we need a sample of velocities for galaxies covering the magnitude range B = 15.5 to 18.5, having z = 0.05 to z = 0.1, on one southern high galactic latitude UKSTU survey field. In addition the galaxies should cover a range of galaxy types. Data available is mainly restricted to single galaxies at random locations (e.g. catalogues noted in section 2.3) or, in some fortunate cases, to clusters of galaxies (e.g. Oemler 1973). Thus telescope time has been sought throughout this project to obtain velocities of faint galaxies

in the areas of available objective prism photographs. In this section these velocities, and the published velocities for Abell 2670 (Oemler 1973) are compared with the objective prism velocities.

We have used three allocations of UK telescope time for velocity work on telescopes as listed in table 3.5.6.

The spectra obtained at SAAO in August 1976 were taken using the EMI tube in the f/1.4 image tube spectrograph at the Cassegrain (f/18) focus of the 1.9m telescope. The spectra were unwidened, and exposures of $\sim$1 hour were used for the fainter objects. The spectrograph slit was of width $\sim$ 1.2 arcsec and length $\sim$ 4.3 arcsec, and was orientated in right ascension. Calibration was by a copper-argon lamp. The spectra were recorded on unbaked Eastman Kodak IIaO plates. The dispersion used was 210 $\mathring{A}$ mm^{-1}.

Only grey time was offered for this observing run; it was accepted in the absence of any information on the performance of the spectrograph for galaxy work under various conditions. The spectra obtained were seriously affected by the presence of the moon, especially with the addition of thin cloud. In reduction, in addition to measuring the lines of the objects observed, night sky lines, and occasionally the moon H and K lines were measured as a check on zero error. The lines measured include: 3727 (OII), 3934 CaII K, 3969 CaII H, 4959 (OIII), 5007 (OIII), 5184 MgI, 5270 FeI (blend), 6563 Hα, 6584 (NII). Night sky lines present include 5577 (OI), 5890-56 NaI, 6300 (OI). The measurements were made using a travelling microscope, with repeat measurements to give an estimate of the measurement error.

The velocities obtained, and comparisons with Martin's (1976) velocities for the standards, are given in table 3.5.7. A correction of -101 kms^{-1} has been applied to the measured velocities, this being the mean correction derived from measurements of moon absorption and night sky emission lines. The mean internal standard error in the velocities is $\sim$180 kms^{-1}, and the estimated total error is about $\pm$ 200 kms^{-1}.

In addition to the 5 programme galaxies and 3 standard galaxies shown in the table, spectra of 10 other programme galaxies

Table 3.5.6

Use of telescope time allocated for velocity work.

Date	Nights D	G	B	Telescope	Observers	Total clear	Useful spectra P	S	others
August 1976	-	3	3	SAAO 1.9m	CEH	$4\frac{1}{2}$	6	3	2
March 1977	3	2	-	INT	CE	$1\frac{1}{2}$	3	2	2
October 1979	7	-	-	SAAO 1.9m	CEK	4	10	4	4

D, G, B: dark, grey, bright time

Observers: C, the author; E, D.Emerson; H, M.R.S.Hawkins; K, B.D.Kelly

P: programme objects; S: standards

Table 3.5.7

Velocities of galaxies obtained from slit spectra (v_s), for comparison with objective prism velocities (v_p). Velocities of standards (v_o) are also given. 'Anonymous' galaxies are identified by IAU format co-ordinates. All velocities are in kms^{-1}.

Object	Observers	v_s	v_o	$v_s - v_o$	v_p	$v_s - v_p$
22313-3842	CkEH	9,446			4,800	+4,646
22383-4006	..	19,044			17,400	+1,644
22403-4021	..	17,315			17,400	-85
22410-4019	..	38,023			42,000	-3,977
22410-4029	..	9,881			12,600	-2,719
NGC 6770	..	4,032	3,910	+122		
NGC 6771	..	4,406	4,290	+116		
NGC 7496	..	1,609	1,540	+69		
12397-0550	CnE	6,533			2,400	+4,133
22240-3825	CkEK	26,450			24,300	+2,150
22211-3814	..	41,463			39,900	+1,563
22219-3793	..	49,969			48,600	+1,369
22208-3831	..	32,040			35,700	-3,660
00462-2951	..	31,376			28,200	+3,176
00491-2867	..	34,390			28,200	+6,190
NGC 1537	..	1,378	1,378	(0)		
NGC 1726	..	3,777	4,072	-295		
NGC 1546	..	1,227	1,190	+37		
NGC 1587	..	3,429	3,890	-461		
A2670 no.1	O	23,200			22,800	+400
4	..	21,260			24,600	-3,340
6	..	21,430			22,800	-1,370
7	..	22,900			22,800	+100
8	..	23,400			21,000	+2,400
9	..	22,350			24,600	-2,250
10	..	22,700			22,800	-100

Observers: Ck, the author; Cn, H.G.Corwin,Jr.; E, D.Emerson; H, M.R.S.Hawkins; K, B.D.Kelly; O, Oemler (1973).

Velocities are given only for those programme objects having objective prism velocities.

$$\sigma_{v_s - v_p} = \sqrt{\frac{\sum (v_s - v_p)^2}{n - 1}} = 2,975 \text{ kms}^{-1}$$

$$\frac{\sum (v_s - v_p)}{n} = +541 \text{ kms}^{-1}$$

were obtained. However these were too contaminated by moonlight for spectral features to be reliably identified. This indicated the necessity for dark time for observations of this type, even for the brighter (B $\sim$ 15) objects.

The second allocation of time was on the Isaac Newton Telescope in March 1977. Dark time was allocated, but most of the time available in the 6 nights was lost due to bad weather. The instrumentation used was almost identical to that used at SAAO (except that baked Eastman Kodak IIIa J plates were available) but poor sky conditions, low altitude of the field and the Pevensey Bay street lights rendered the few spectra taken unusable.

The most recent allocation of time for galaxy velocity work was again on the 1.9m telescope at SAAO, in October 1979. The spectrograph was essentially the same as for the first run (though modifications now allow remote operation), but the detector used was the Boksenberg Image Photon Counting System (IPCS) (e.g. Boksenberg 1972). This system allows simultaneous observations of programme object and sky; the sky spectrum can then be subtracted from the spectrum of (object + sky). Dark time was again available for this observing run.

The spectrograph slit used was of width $\sim$ 2.4 arcsec, and had a length of $\sim$ 36 arcsec recorded in 8 data 'increments'. The 'data area' used on the image tube was 2000 'lines' by 8 'increments', with a resolution of 2.6 Å per line. The dispersion used was again 210 Å mm^{-1}. Calibration was by a copper-argon lamp, with a liquid copper sulphate filter to reduce the intensity of four strong lines in the red, to protect the image tube. Integration times up to 2 hours total were used, and even then counts of only 50 photons per 'line' were recorded in the continuum for the programme galaxies. These integrations were split up into runs of 1000 seconds, interspersed with calibration arc spectra, to check for any mechanical or electrical drift in the positioning of the 'data area'. All the data were recorded on computer magnetic tape.

Final reduction of the data was performed by Dr. B.D. Kelly, who wrote the software needed for the reduction process. The procedure was as follows. First, sky subtraction was performed

for each 1000 second run. With no drift of the data area apparent from the arc spectra, all the runs for a given object were then added. A calibration was obtained from the relevant arcs, and the programme object counts rebinned into an array linear in wavelength. This reduced spectrum could then be plotted for inspection, and stored for later processing. This procedure was applied to all the programme and standard galaxies.

Velocities were then obtained by a correlation technique similar to that used by the author for objective prism spectra measured by machine. In Kelly's system, the continuum is removed, and the spectrum again rebinned into an array where distance along the array, x, is given by $x = k \log\lambda + c$ where k and c are constants. This relation means that redshifted spectral features will all be shifted by the same amount in x, i.e. by the same distance along the array, which simplifies correlation of two spectra at different redshifts. The velocities given in table 3.5.7 were obtained by correlating the spectrum of NGC 1537 (the standard having the best signal-to-noise ratio) with each of the others. Velocities are given for all objects observed. Velocities of standard galaxies are taken from Sandage (1978) and Gisler and Friel (1979). No corrections have been applied to these velocities; in the present form they are intended purely for comparison with the objective prism velocities. As yet no estimate of the internal error of the correlation process has been made. However comparison with the standards indicates that the total error, after corrections have been applied, might be of the order of $\pm$ 300 kms^{-1}.

The observing runs have shown clearly the difficulties of observing faint galaxies. The galaxies to be observed generally have no emission lines in their spectra, hence a good signal to noise ratio in the continuum is needed to detect absorption lines . This requires large amounts of observing time to secure good spectra. The spectra obtained with the IPCS are still far from satisfactory; integration times of approximately 5 - 10 hours would be needed to obtain good signal to noise ratio spectra (with counts of about 300 in the continuum) for most of the objective prism photograph galaxies having prism velocities. The magnitude range of interest is such that ideally the 3.8m Anglo-

Australian telescope should be used, but to the present no time has been allocated on that telescope.

In addition to the observations above, the velocities given by Oemler (1973) for Abell 2670 have been used; an UKSTU objective prism photograh was taken centred on the cluster. The velocities for Abell 2670 are described in section 4.1.2, and are given in table 4.1.1. The velocities obtained from the prism photograph compared with those given by Oemler give a value for σ of 2000 kms^{-1}.

One further velocity for the comparison was obtained by Emerson and Corwin (private communication) at SAAO using the image tube spectrograph. This is also given in table 3.5.7.

From all these sources, we have velocity comparisons between prism and slit spectra for 19 objects, which are plotted in fig. 3.5.9. There appear to be no gross systematic trends, though with so few objects it is difficult to be certain. The value of σ for the agreement is calculated to be 2975 kms^{-1}, on average. In fact we expect the higher velocities to be less accurate, because of the dispersion curve and the measurement method. Calculating errors for each galaxy separately in terms of the effective distance on the photographic plate, we find that the measurements have a σ of about 18 microns on the plate. This is approximately what would be expected from the measurement method used; with a measurement accuracy of 0.5mm on the tracing (corresponding to 10 microns on the plate), and uncertainties in the absolute wavelengths of the emulsion cutoff and the 4000 Å feature (corresponding to 6 microns and 11 microns respectively) we would expect a combined error of this size.

3.5.11 Tests of the redshift program.

The problems of obtaining large numbers of velocities using the redshift program described in section 3.4 are discussed in section 4.2. Because of these problems additional means of testing the working of the program were required. When the program was first being developed, it was tested on synthetic spectra generated to resemble objective prism spectra; however it was felt that a better test was needed using real data.

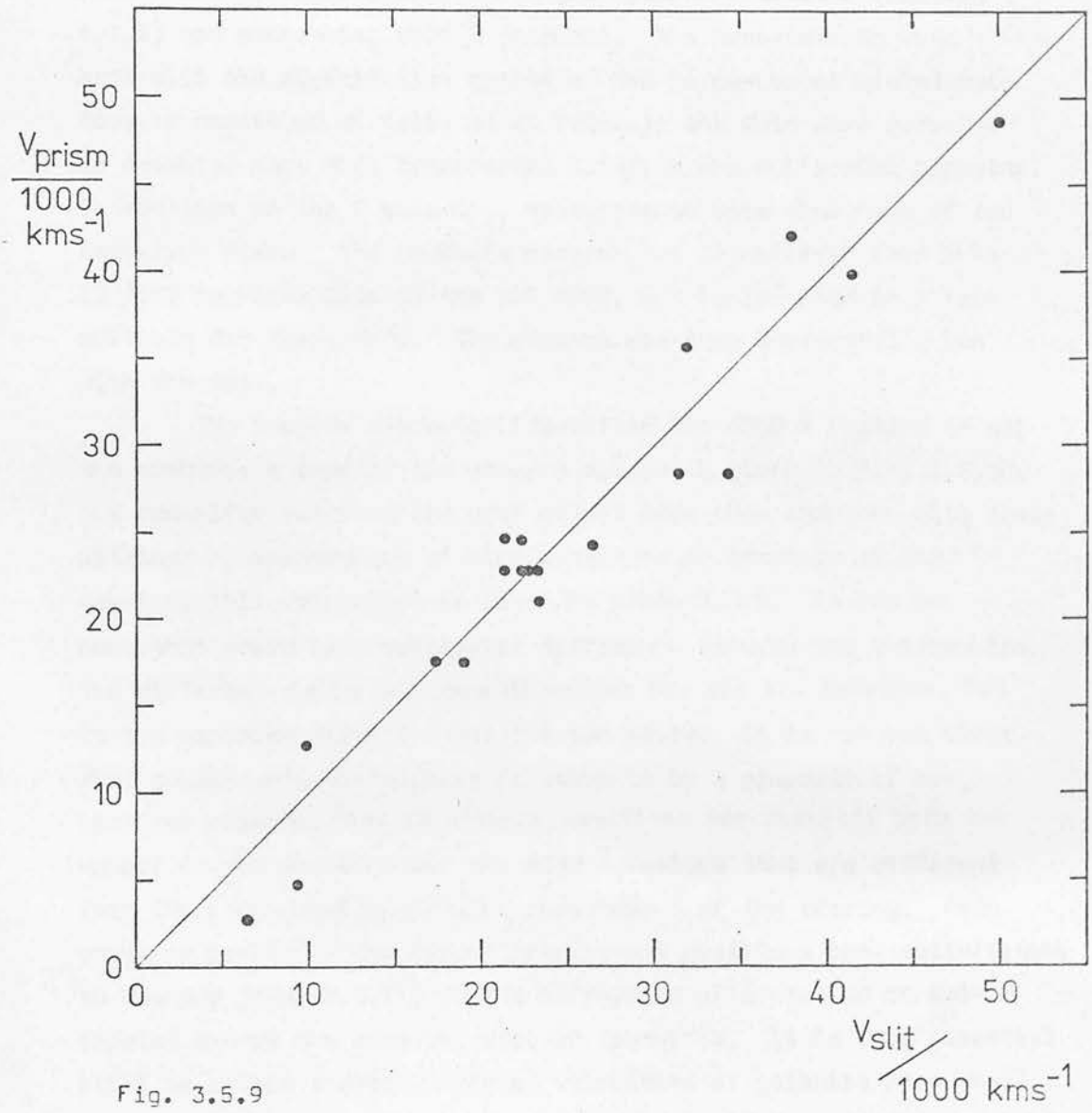

Fig. 3.5.9

Comparison of radial velocities of 19 objects obtained from both prism and slit spectra.

To this end measurements were made of 5 galaxies in cluster Abell 133 from plate UJ4543P; the galaxies were selected from those previously traced using a microdensitometer (section 4.1.3) and possessing 4000 Å features. The measurements were made with the digitisation system on the Joyce-Loebel microdensitometer described by Kelly et al (1980a); the data were recorded on cassette tape then transferred later to the ROE's 4082 computer. In addition to the 5 galaxies, measurements were also made of two late-type stars. The redshift program was transferred from RL's 360/195 machines also to the ROE 4082, and implemented in a form suitable for these data. The program was then successfully run with the data.

The program correctly identified the 4000 Å feature in all the spectra; a copy of the program output is given in fig. 3.5.10. The redshifts obtained for each object were then compared with those obtained by measurement of microdensitometer tracings of the spectra; this comparison is given in table 3.5.8. It can be seen that there is a systematic difference between the two results. The difference is in the same direction for all the galaxies, but in the opposite direction for the two stars. It is not yet clear what causes this difference; it seems to be a property of the computer program, that it obtains positions for possibly both the cutoff of the emulsion and the 4000 Å feature that are different from those obtained by direct measurement of the tracing. Both computer positions and direct measurement positions look satisfactory to the eye (fig. 3.5.11) so the difference will have to be calibrated out of the computer-derived redshifts. It is thus essential still to obtain a good sample of velocities of galaxies in a small area from slit spectra, covering a wide velocity range.

3.5.12 Spectral classification.

Although not a direct part of the work on velocities of galaxies, the classification of spectra on objective prism plates forms an important part of the project as a whole, and is of relevance here especially with regard to the classification of galaxy spectra. The starting point for classification on objective prism photographs, however, is the classification of

```
REDSHIFT PROGRAM
----------------

DATA :

SPECTRUM OFFSET :          60
SPECTRUM LENGTH :         170
STEP SIZE :                16
VER. AV. :                  8
HOR. AV. :                  8
BACKGROUND PEAK :          15
RANGE FACTOR :            4.0
IMAX ALLOWED :           2000
CONV. GATE SIZE :           5
LOW Z LIMIT :          -0.020
HIGH Z LIMIT :          0.300
HARTMANN PARAMETERS :
   X0 :     0.727528E+00
   W0 :     0.131341E+04
    A :     0.155919E+05
INTENSITY CONVERSION :
   I0     : 435.0
   IB     :   4.0
   GAMMA  :  0.42
   CONST  :  2.26

FEATURES:
     WAV          DEP          WID

  3970.000      -0.150        0.000
  4300.000      -0.100       20.000

IDENTIFICATION      Z          RMS          PARAB        M4425    MPEAK    M4900    M4200    M3600

             7   0.048   0.101E+01   0.651E+03   18.12   17.13   17.28   18.31   19.62
            11   0.050   0.138E+01   0.805E+03   18.63   17.55   17.87   19.34   20.48
            14   0.039   0.109E+01   0.544E+03   18.25   16.93   17.13   18.46   19.17
            18   0.043   0.101E+01   0.612E+03   17.96   16.70   16.96   18.21   19.51
            19   0.045   0.112E+01   0.647E+03   18.36   17.26   17.58   18.60   19.48
             2   0.018   0.962E+00   0.601E+03   17.23   16.38   16.59   17.35   18.60
             3   0.016   0.101E+01   0.806E+03   18.58   17.64   17.81   18.64   19.97
```

Fig. 3.5.10

Redshift program lineprinter output for the test objects of table 3.5.8.

Table 3.5.8

Comparison of redshifts obtained from measurement of micro-densitometer tracings (z_t) and from the computer correlation technique on COSMOS data (z). The corresponding emulsion cutoff to 4000 Å feature distances (x_t and x) are also given, x_t as measured, x as calculated from the computer redshift. Galaxy (G) and star (S) identifications are as in plate 4.1.2.

Object	z	z_t	x	x_t	$z_t - z$
G4	0.048	0.053	1.89	1.85	0.005
G8	0.050	0.058	1.88	1.80	0.008
G11	0.039	0.053	1.98	1.85	0.014
G13	0.043	0.053	1.94	1.85	0.010
G14	0.045	0.047	1.92	1.90	0.002
S1	0.018	0.007	2.18	2.30	-0.011
S2	0.016	0.002	2.20	2.35	-0.014

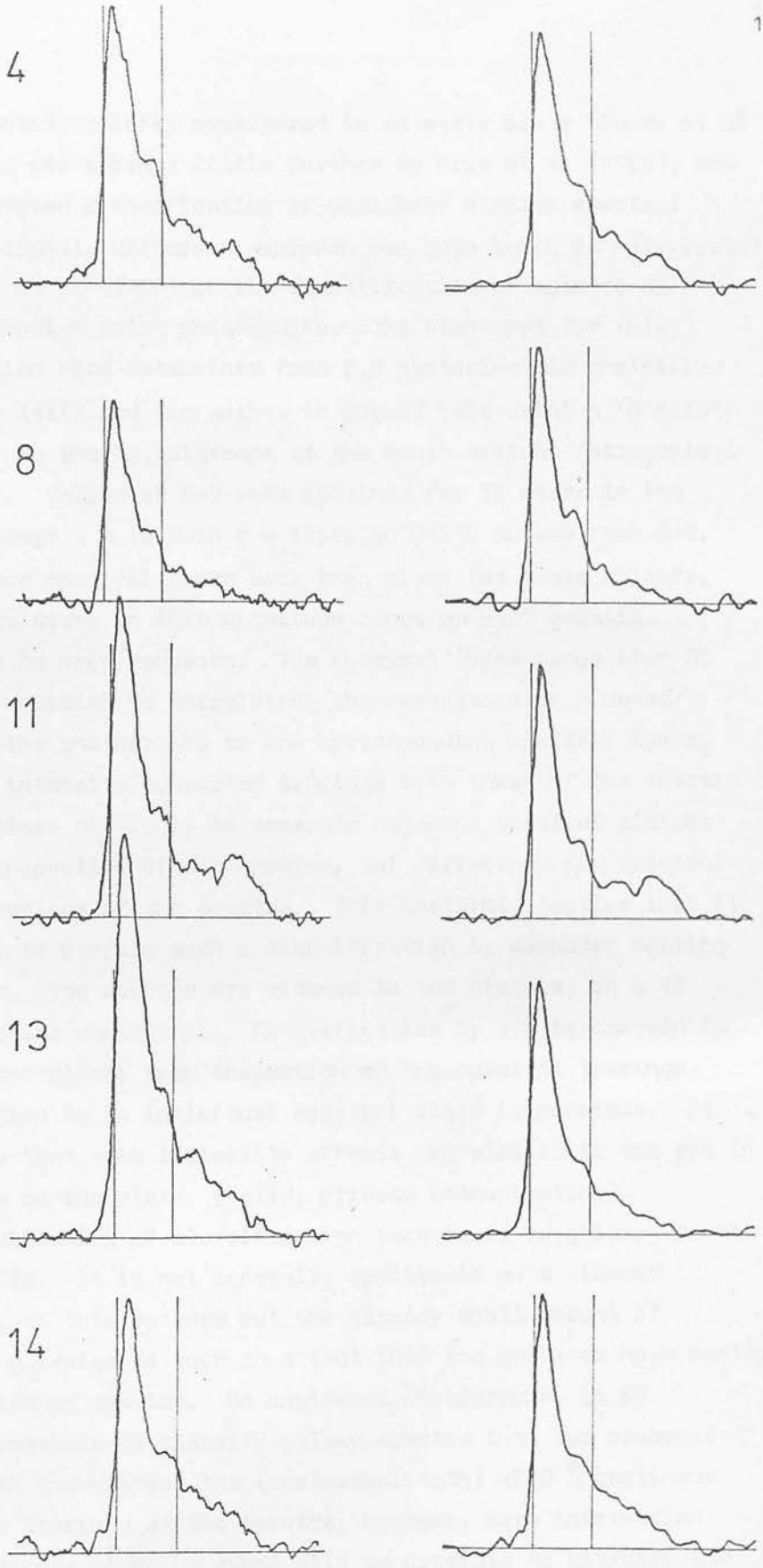

Fig. 3.5.11

A comparison of the direct measurement (left) and computer derived (right) positions of the cutoff and 4000 Å feature for the galaxies in table 3.5.8. The tracings are (left) in density and (right) in intensity and normalised.

Note that the horizontal scales are similar but not identical.

stellar spectra, briefly considered in an early paper (Nandy et al 1977). This was taken a little further by Krug et al (1980), who again considered classification of unwidened stellar spectra.

A slightly different approach has been taken in more recent work (Kelly et al 1980b) on the classification of spectra on widened objective prism photographs. The standards for this classification were determined from B,V photoelectric photometry obtained by Kelly and the author in August 1979 using a 'people's photometer' on the 1m telescope at the South African Astronomical Observatory. Values of B-V were obtained for 39 stars in the magnitude range V = 13.5 to V = 17.1, in UKSTU survey area 345. Main sequence spectral types were then given for these colours, assuming the stars in this magnitude range at -60° galatic latitude to be main sequence. The spectral types range from B2 to M0. In addition to correlating the appearance of widened spectra on the photographs to the corresponding spectral types, normalised intensity converted tracings were taken of the spectra. It is sometimes difficult to separate adjacent spectral classes by visual inspection of the spectra, but differences are apparent from the tracings of the spectra. This certainly implies that it is possible to perform such a classification by computer sorting of the data. The spectra are widened to 100 microns, on a 40 minute exposure photograph. Classification by eye is certain to half a letter class; from inspection of the spectral tracings classification to an individual spectral class is possible. It is possible that some luminosity effects are visible to the eye in the spectra on the plate. (Kelly, private communication).

Application of classification techniques to galaxy spectra is not simple. It is not generally applicable on a widened photograph, as this spreads out the already small amount of light from galaxies to such an extent that few galaxies have easily examined widened spectra. On unwidened photographs, it is generally possible to classify galaxy spectra into two classes: spectra with and without the (rest-wavelength) 4000 $\mathring{A}$ continuum drop. From tracings of the spectra, however, more information can be obtained; it might eventually be possible to classify the spectra by the strength of the 4000 $\mathring{A}$ feature.

There are, of course, still further complications to this picture; some galaxies possess emission lines in their nuclear spectra, and in scanning plates for other purposes, galaxies with, apparently, a Balmer jump in their spectra have been noted. Clearly there is much scope for further work in this area, with both the present prism, and also when the increased resolution provided by the new higher dispersion prism becomes available.

4. Aplications and conclusions

4.1 Clusters of galaxies.

Initial attempts to obtain radial velocities from objective prism photographs were restricted to fields for which plates became available near the start of this project. Early work was generally on spectra of galaxies in the field, rather than specifically cluster galaxies; the plate selected for much of the early work (UJ2461P, UKSTU survey area 345) has no rich clusters of galaxies in the magnitude range suitable for redshift measurement. This area was one of several selected by the UKSTU for test plates taken with QSO searches in mind; subsequent work has shown (Clowes, thesis in preparation, 1980) that this area does have a rather patchy QSO distribution. There are unfortunately no galaxy counts for this area; neither the Shane and Wirtanen (1967) nor the Zwicky et al (1961 - 1968) catalogues cover this area. Some early work showed the value of the redshift technique in the study of clusters; this and subsequent work on clusters of galaxies is described in this section, 4.1.

The application of the techniques for obtaining galaxy velocities in clusters is the easiest application. It is a fairly simple matter to obtain microdensitometer tracings of galaxies in a cluster. There are also other attractions. To begin with, a cluster of galaxies is an attractive test of the accuracy of the redshift determination. The internal velocity dispersions of most clusters lie in the range $\sim$ 100 to $\sim$ 2000 kms^{-1} (Yahil and Vidal, 1977); this is smaller than the error expected for a single prism spectrum, so a cluster of galaxies represents a group that might be considered to lie at the same velocity, as far as the redshift technique is concerned. A preponderence of elliptical galaxies is also generally noted in clusters, which is an additional advantage; as noted in section 3.3, elliptical galaxies are the objects possessing most clearly the features needed for redshift determination.

4.1.1 Cluster associations.

Measurements of cluster galaxies were first made as a test

of the application of the redshift technique in collaboration with MacGillivray of ROE, who had examined three clusters (numbers 1, 2 and 3 of MacGillivray et al (1976b)) located within a few degrees of each other. A prism plate (UJ2620P) was taken of this area, centred on the clusters.

Four areas were initially selected near the centre of the plate, three on each of the clusters, and one close to the others but not containing any obvious cluster (fig. 4.1.1). In each area the brighter galaxies were traced and redshifts obtained for those with suitable features. The results of these measurements appear as the first four histograms on fig 4.1.2, showing the distribution in velocity for each area. The peaks due to the clusters show up well, and slightly better to the eye in the 'smoothed' histograms (smoothed to take out artefacts due to measurement accuracy). The distribution in the area not containing a cluster is almost as peaked; thus the distributions for rather more general areas on the plate were obtained (5 and 6 in fig. 4.1.1) by applying identical measurement procedures. The results are plotted as the last two histograms in fig. 4.1.2.

From the histograms for the three clusters, field galaxies with $z > 0.02$ from the cluster means were excluded from the sample. Mean velocities were obtained for the remaining galaxies in each cluster.

The conclusion of this work is that the three clusters, although close together in the sky, are separated by quite large distances in depth. The velocities obtained for the means of the three clusters are 39,300, 44,400 and 33,900 kms^{-1}, giving distances of 786, 888, and 678 Mpc assuming a value for H_o of 50 kms^{-1} Mpc^{-1} (e.g. Sandage and Tammann (1975b) give H_o = 57 kms^{-1} Mpc^{-1}). At these distances, the separations on the sky ($\sim$ 1 degree) correspond to distances of $\sim$ 15 Mpc. The three clusters are thus well separated in depth.

4.1.2 Velocity accuracy.

The second set of measurements of velocities from a cluster was made as a check on accuracy. The cluster concerned is Abell 2670, which has ten velocities determined by Oemler (1973)

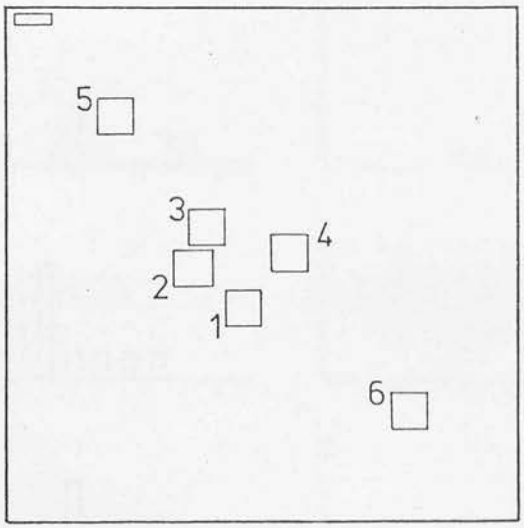

Fig. 4.1.1

Selected areas on plate UJ2620P.
1,2,3 containing clusters of galaxies
4 the initial control area
5,6 additional distant control areas

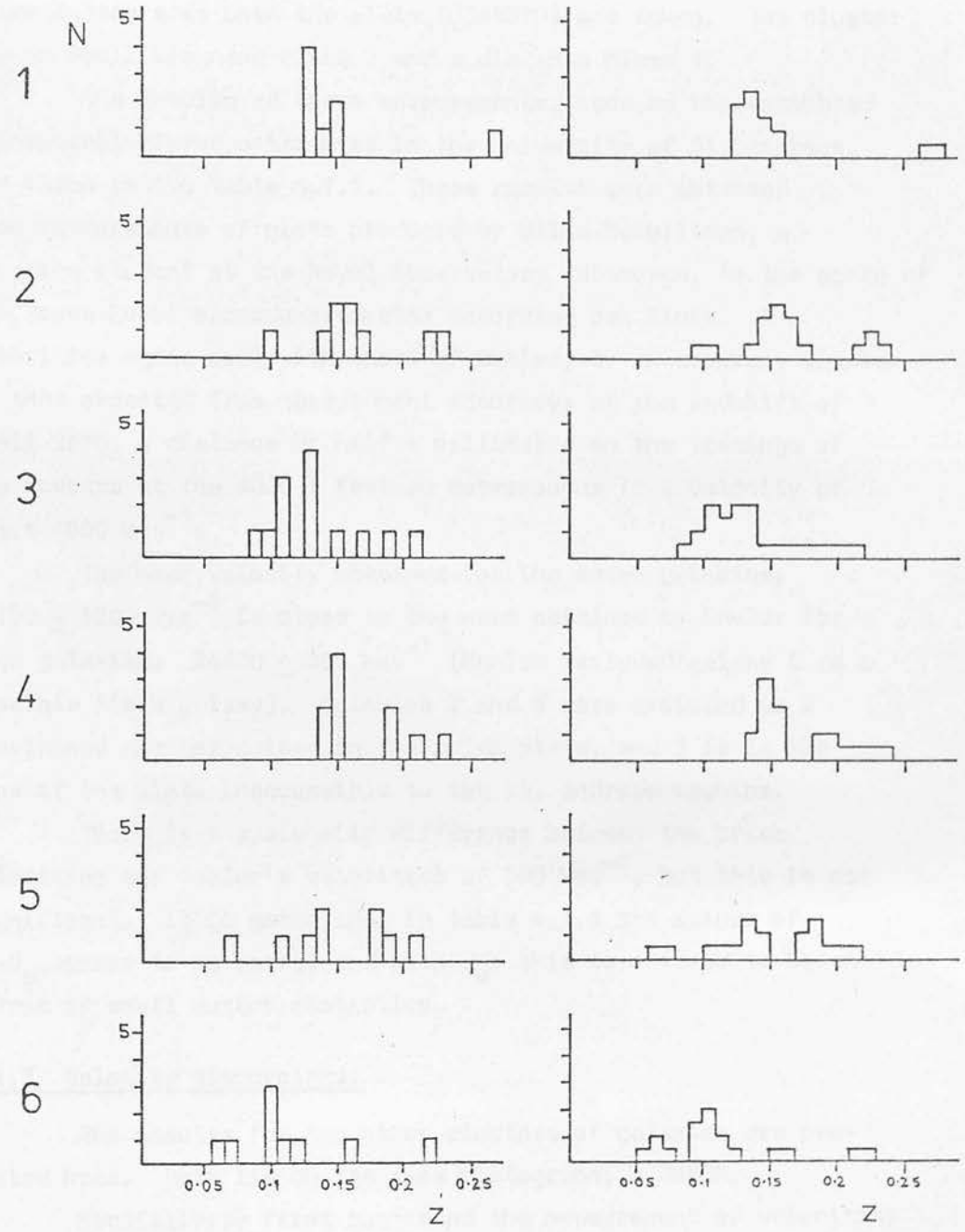

Fig. 4.1.2

Velocity histograms for the 6 areas shown in fig. 4.1.1. Z is the redshift. The histograms on the right are from the data on the left, smoothed over two redshift bins

and as such represented the largest collection of velocities greater than 10,000 kms^{-1} available on a single southern hemisphere survey area when the plate (UJ4551P) was taken. The cluster has an Abell richness class 3 and a distance class 4.

The results of these measurements, made on the automated Joyce-Loebl microdensitometer in the University of St. Andrews, are shown in the table 4.1.1. These results were obtained from measurements of plots produced by Wilma McKellican, a vacation student at the Royal Observatory, Edinburgh, to the scale of the Joyce-Loebl microdensitometer recording pen plots. The velocities agree well with those of Oemler, to an accuracy similar to that expected from measurement accuracy; at the redshift of Abell 2670, a distance of half a millimetre on the tracings of the spectra at the 4000 Å feature corresponds to a velocity of about 1800 kms^{-1}.

The mean velocity obtained for the seven galaxies, 23100 $\pm$ 1200 kms^{-1} is close to the mean obtained by Oemler for nine galaxies: 26600 $\pm$ 300 kms^{-1} (Oemler excluded galaxy 5 as a possible field galaxy). Galaxies 2 and 3 were excluded as 2 overlapped another galaxy on the prism plate, and 3 is in the area of the plate inaccessible to the St. Andrews machine.

There is a systematic difference between the prism velocities and Oemler's velocities of 590 kms^{-1}, but this is not significant. It is noted that in table 4.1.1 the values of $V_p - V_o$ appear to be correlated with V_o; this is assumed to be an effect of small number statistics.

4.1.3 Velocity dispersions.

The results for two other clusters of galaxies are presented here. Both lie on the same photograph, UJ3453P.

MacGillivray first suggested the measurement of velocities in cluster Abell 140 on this photograph as the cluster appears to have two main centres of concentration on the direct photograph (plate 4.1.1(a)). It was anticipated that possibly velocities would resolve the cluster into two components. This work has been submitted for publication along with the work described in 4.1.2 (Cooke et al, 1980). Abell 140 has an Abell richness class 3 and

Table 4.1.1

Radial velocities in Abell 2670.

Galaxy (Oemler no.)	Velocities (kms^{-1}) prism v_p	Oemler v_o	$v_p - v_o$
1	22,800	23,200	-400
4	24,600	21,260	+3,340
6	22,800	21,430	+1,370
7	22,800	22,900	-100
8	21,000	23,400	-2,400
9	24,600	22,350	+2,250
10	22,800	22,700	+100

$$\overline{v_p} = 23{,}057 \text{ kms}^{-1}$$

$$\sigma_{v_p - v_o} = \sqrt{\frac{\sum (v_p - v_o)^2}{n - 1}} = 2{,}000 \text{ kms}^{-1}$$

$$\frac{\sum (v_p - v_o)}{n} = 590 \pm 760 \text{ kms}^{-1}$$

(n is the number of galaxies)

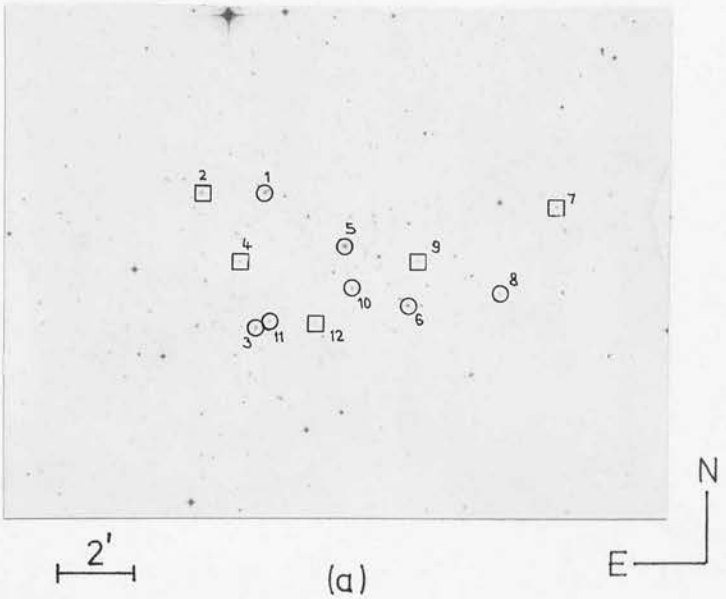

(a)

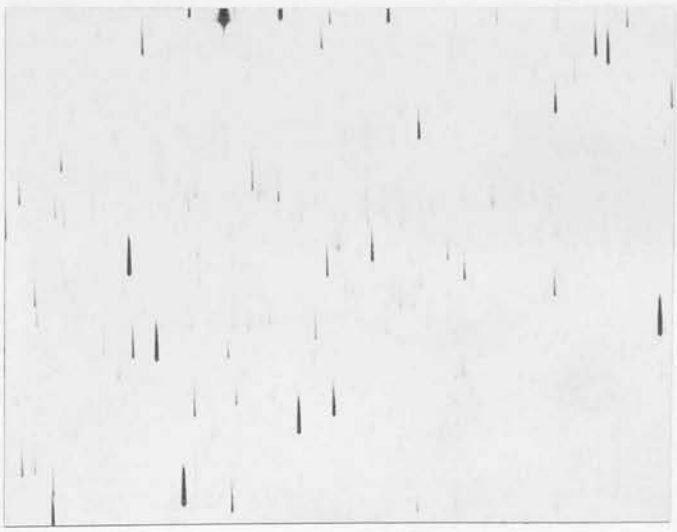

(b)

Plate 4.1.1

Abell 140: (a) direct (b) prism plate

distance class 6.

The results of measurements in this cluster are shown in table 4.1.2, and the cluster itself shown in plate 4.1.1. Galaxies with velocities less than the mean of the distribution are marked with circles, and those with velocities greater than the mean marked with squares. There is no apparent spatial correlation of velocity with position. This is not particularly remarkable, although it was surprising. What is more remarkable is the dispersion in velocity observed. We have already seen from Abell 2670 that the measurement accuracy introduces a dispersion, for Abell 140 corresponding to 2200 kms^{-1}. The measured dispersion is 3800 kms^{-1}; even deconvolving 2200 kms^{-1} from this leaves a dispersion of 3100 kms^{-1}, which is very large for a single cluster of galaxies (e.g. Yahil and Vidal 1977). This large dispersion is not due to one or two galaxies with large differences from the mean; fig. 4.1.3 (a) is a histogram of the measured positions of the 4000 Å feature, at 0.5 mm intervals (the measurements are made to 0.5 mm); it can be seen that the distribution is flat, as compared to that for A 2670 (fig 4.1.3 (b)) or A 133 (fig. 4.1.3 (c), described below.) If all the galaxies measured in Abell 140 are in a single cluster, then its velocity dispersion is the highest known (e.g. Yahil and Vidal, 1977). Speculation as to the consequences of clusters with such distributions are left to the submitted paper.

The second cluster, Abell 133, lying on the same photograph, is much closer (Abell distance class 4, richness class 0) but in spite of its low richness it provides many velocities partly because of the brightness of the galaxies in it. Partly also, because there seems to be a large concentration of elliptical galaxies, particularly in one part of the cluster.
In all, 50 of the brightest galaxies in the area of the cluster were measured; 26 of these give good velocities. In addition, 6 others provide velocities from somewhat uncertain 4000 Å features. The velocity distribution of this cluster is much more like a 'normal' cluster than A 140: the 4000 Å feature position histogram (fig 4.1.3 (c)) shows a markedly peaked distribution, with most galaxies falling into 3 bins, as for A 2670. If Yahil and Vidal's (1977)

Table 4.1.2

Radial velocities in Abell 140.

Galaxy	Velocity (kms^{-1})	
	v_p	$v_p - \overline{v}_p$
1	44,000	-550
2	46,400	+1,850
3	38,000	-6,850
4	48,500	+3,950
5	44,000	-550
6	44,000	-550
7	48,500	+3,950
8	40,100	-4,450
9	46,400	+1,850
10	40,100	-4,450
11	44,000	-550
12	50,600	+6,050

$$\overline{v_p} = 44{,}550 \text{ kms}^{-1}$$

$$\sigma_{v_p} = \sqrt{\frac{\sum (v_p - \overline{v_p})^2}{n - 1}} = 3{,}800 \text{ kms}^{-1}$$

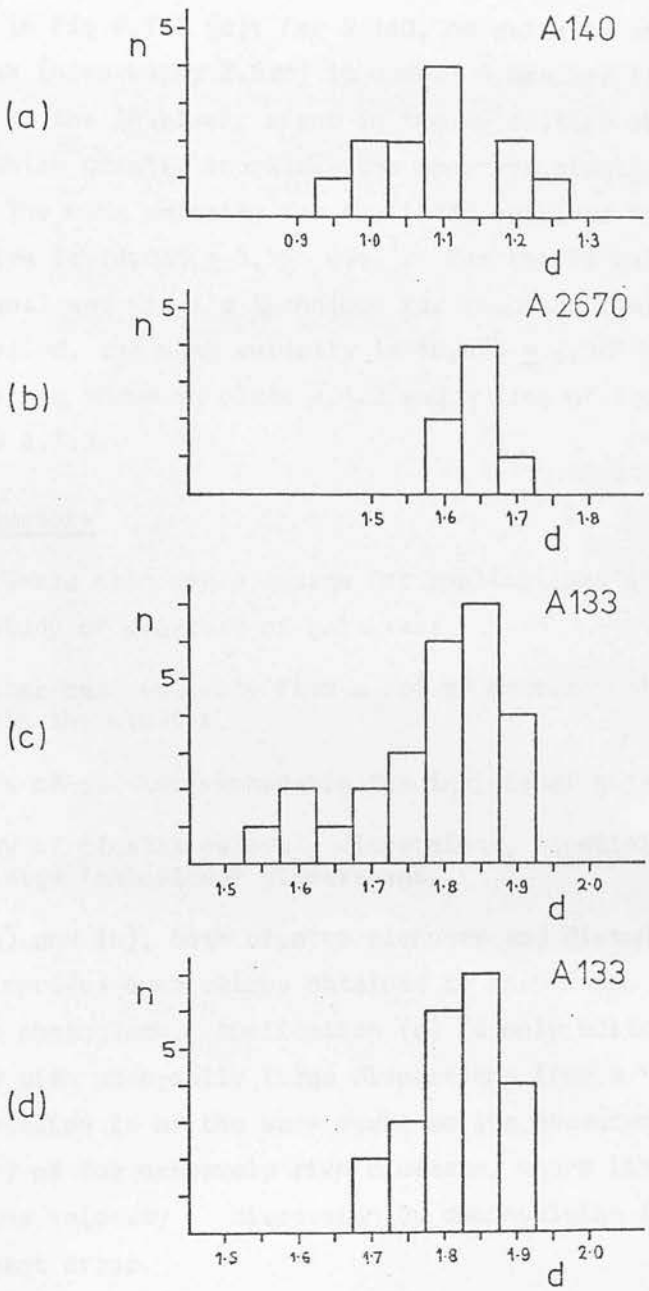

Fig. 4.1.3

Velocity histograms for Abell clusters measured (section 4.1.3). The abscissa is given in terms of the cutoff to 4000 Å feature separation, in cm,'d', to avoid problems of rebinning into redshift.

technique (using a limit of 2.5σ rather than the 3σ Yahil and Vidal used) for removing field galaxies is applied, the distribution changes to that in fig 4.1.3 (d); for A 140, no galaxies are removed if this technique (also using 2.5σ) is used. A smaller limit is required because of the intrinsic error in the velocities obtained using the prism, which greatly increases the apparent cluster dispersion.

The mean velocity for Abell 133 obtained from all 26 'good' velocities is 18,035 $\pm$ 3,355 kms^{-1}. For the 22 galaxies left after Yahil and Vidal's technique for removing field galaxies has been applied, the mean velocity is 16,895 $\pm$ 2,063 kms^{-1}. The galaxies are shown in plate 4.1.2 and a list of the velocities given in table 4.1.3.

4.1.4 Summary

Three main areas emerge for applications of the redshift method to the study of clusters of galaxies:

(a) cluster mean velocity from a set of measurements of galaxies within the cluster.

(b) tests of cluster membership for individual galaxies.

(c) study of cluster velocity dispersions, especially with regard to large 'anomalous' dispersions.

Using (a) and (b), both cluster richness and distance estimates can be improved over values obtained by inspection or counting on a direct photograph. Application (c) is only suitable for clusters with abnormally large dispersions (for a 'normal' cluster the dispersion is of the same order as the measurement technique accuracy) or for extremely rich clusters, where limits could be set on the velocity dispersion by deconvolving the known measurement error.

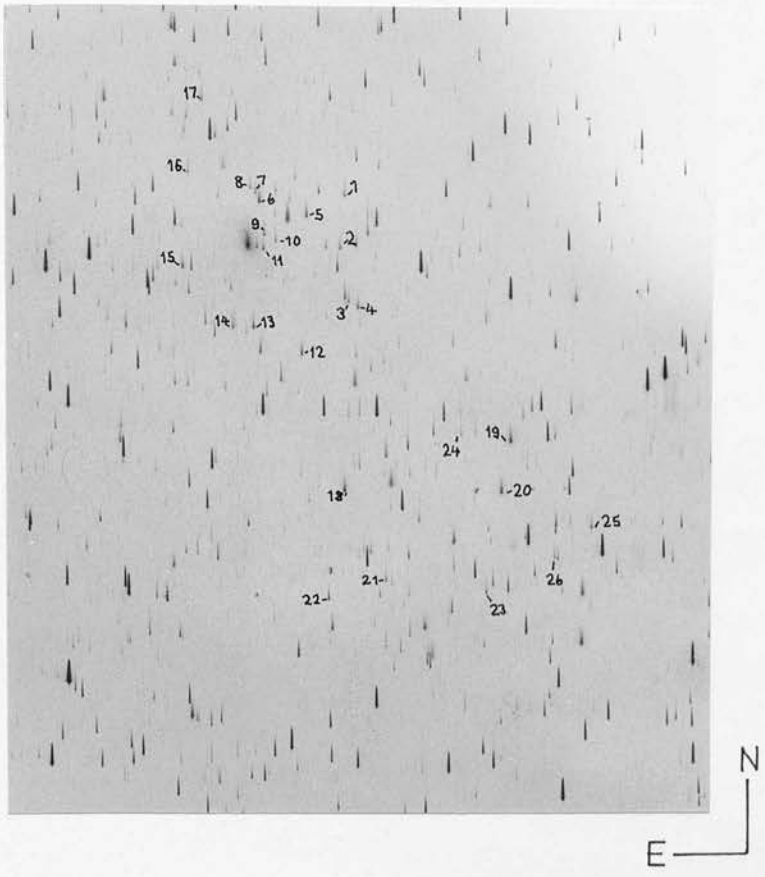

Plate 4.1.2

Galaxies in the area of Abell 133
(Stars S1, S2 also shown)

Table 4.1.3

Radial velocities of galaxies in the field of Abell 133. Galaxies removed by the application of a technique similar to that of Yahil and Vidal (1977) are marked '*'. Identifications are given in plate 4.1.2.

Galaxy	v / kms^{-1}	
1	19,200	
2	21,000	
3	15,900	
4	15,900	
5	15,900	
6	14,100	
7	17,400	
8	17,400	
9	17,400	
10	14,100	
11	15,900	
12	15,900	
13	15,900	
14	14,100	
15	14,100	
16	24,300	*
17	17,400	
18	17,400	
19	21,000	
20	19,200	
21	19,200	
22	15,900	
23	22,500	*
24	26,100	*
25	17,400	
26	24,300	*

4.2 The general field

The application of the method for obtaining radial velocities of faint galaxies to a general fieldon an objective prism photograph is a rather different undertaking to the cluster application. In the case of the general field, the need is to determine velocities of all possible objects in a given area of the photograph. This poses more problems than in the cluster case; it is true that we could choose to measure all objects in an area containing a cluster, but generally, for clusters, we would select a limited number of objects for measurement.

In this section we first briefly look at the contents of the 'general field': the galaxy distribution and types. Secondly we look at the methods of measuring velocities in such a general field, and discuss the problems involved.

4.2.1 Galaxies in the general field

A sky limited UKSTU direct plate contains information on galaxies covering a magnitude range of, say, from B $\sim$ 10 to B $\sim$ 23 on a typical plate. At the bright end of this scale, the galaxies are large (several millimetres across on the plate) and their morphology can readily be observed. At the opposite end of the scale, galaxy images are very small ($\sim$ 20 microns across) and barely distinguishable from stellar images; indeed, some are indistinguishable.

When working with objective prism photographs the magnitude range is reduced. At the bright end, galaxies become so large at a magnitude of B $\sim$ 15 or 16 that spectral information is seriously smeared out. At the faint end, the signal to noise ratio becomes very poor for galaxies fainter than about B $\sim$ 18.

The exact distribution of galaxy types in a general field is hard to ascertain, as a morphological classification of faint galaxies is fairly difficult. There is information on the distribution of galaxy types in clusters (e.g. Dawe, Dickens and Peterson 1977) and in a large sample of low redshift objects (RSGC, de Vaucouleurs et al 1976). The preliminary study of an area on a CTIO plate (Cooke et al 1977) gave the most relevant information

on galaxy types, in terms of the spectral features present. In that area, 1.4 degrees square, 120 non-stellar objects were identified by eye. Of these, 60 were considered too faint to show clearly any spectral features. Of the remaining 60 galaxies, velocities were obtained for 29 having 4000 Å features. It was therefore expected that approximately 50 per cent of galaxies in a field chosen at random could be expected to have 4000 Å features strong enough to allow velocities to be obtained.

The distribution in type affects the percentage of galaxies able to have velocities obtained by the method described in this work. For these galaxies, it is possible to investigate the spatial distribution. On the photograph the 2-D distribution is obtained; the distribution in the radial direction is obtained from the velocity by assuming a uniform Hubble flow. The redshift technique has not yet been applied on this large scale; but its development means that studies of the spatial distribution of galaxies in the general field can be performed over much larger volumes of space than was hitherto possible using individually obtained slit spectra (e.g. Chincarini and Rood 1980).

4.2.2 Velocities in the general field

Ideally an area of a photograph could be examined, the galaxies located, then the velocity of each galaxy obtained from its objective prism spectrum. Practically the situation is rather more complex than this.

Firstly there are practical measurement limits. The bright and faint magnitude limits have been mentioned above. There is also a redshift limit; at a redshift of about 0.35 the 4000 Å feature is coincident with the emulsion cutoff of IIIa J. In practice the limit occurs before this happens; objects with the highest redshift yet measured using this technique (two galaxies in cluster Abell 141) have redshifts of $\sim$ 0.26, with some uncertainty in the identification of the 4000 Å feature. These limits all restrict the range of galaxies for which velocities can be obtained.

Additionally, at present only galaxies with the 4000 Å feature can have their velocities determined. Eventually it may be possible, from galaxy spectral classification, to look for

features other than the 4000 Å feature, but this has not yet been investigated. At present it would seem to be extremely difficult to assign velocities to the class of spiral galaxies having an objective prism spectrum resembling an exponential curve.

The number of galaxies in a general field for which we can obtain velocities is, therefore, limited. If machine measurements of all the spectra in a given field are made, and we can identify the galaxies in this sample, it should be possible to apply selection criteria to the sample of galaxies to reject objects with unsuitable spectra for obtaining redshifts. A magnitude criterion is easy to apply; but at present it is found necessary to apply the redshift program to all remaining objects, and then reject unsuitable objects on the basis of parameters produced by the program. This is illustrated in the following example.

4.2.3 Trial results for the general field.

An illustration of the correct working of the redshift program has been given in section 3.5.11. Here the same program has been applied to a small sample of COSMOS data covering an area of one square degree.

For a completely automatic program, as originally envisaged, the computer program would have to decide when the 4000 Å feature had been correctly identified. To this end, tests were run on this area of "general field" in which galaxies, stars, and potentially overlapping images had previously been identified by eye. Data for this field was available from COSMOS measurements of three different plates, for comparison purposes. The plates used were UJ2461P, UJ3092P and UJ2620P, with the field examined in the overlap of the three plates. There are no rich clusters of galaxies in this field. A plot of the objects in the field is given in fig. 4.2.1; these objects were identified by eye using both direct and prism photographs of the area.

The spectra of objects in this area (stars and galaxies) were run through the redshift program to test its performance on such a general field. The resulting plotted output from the program for about the first 200 objects was examined for correctness of fitting to possible 4000 Å features. Incorrect and correct identifications

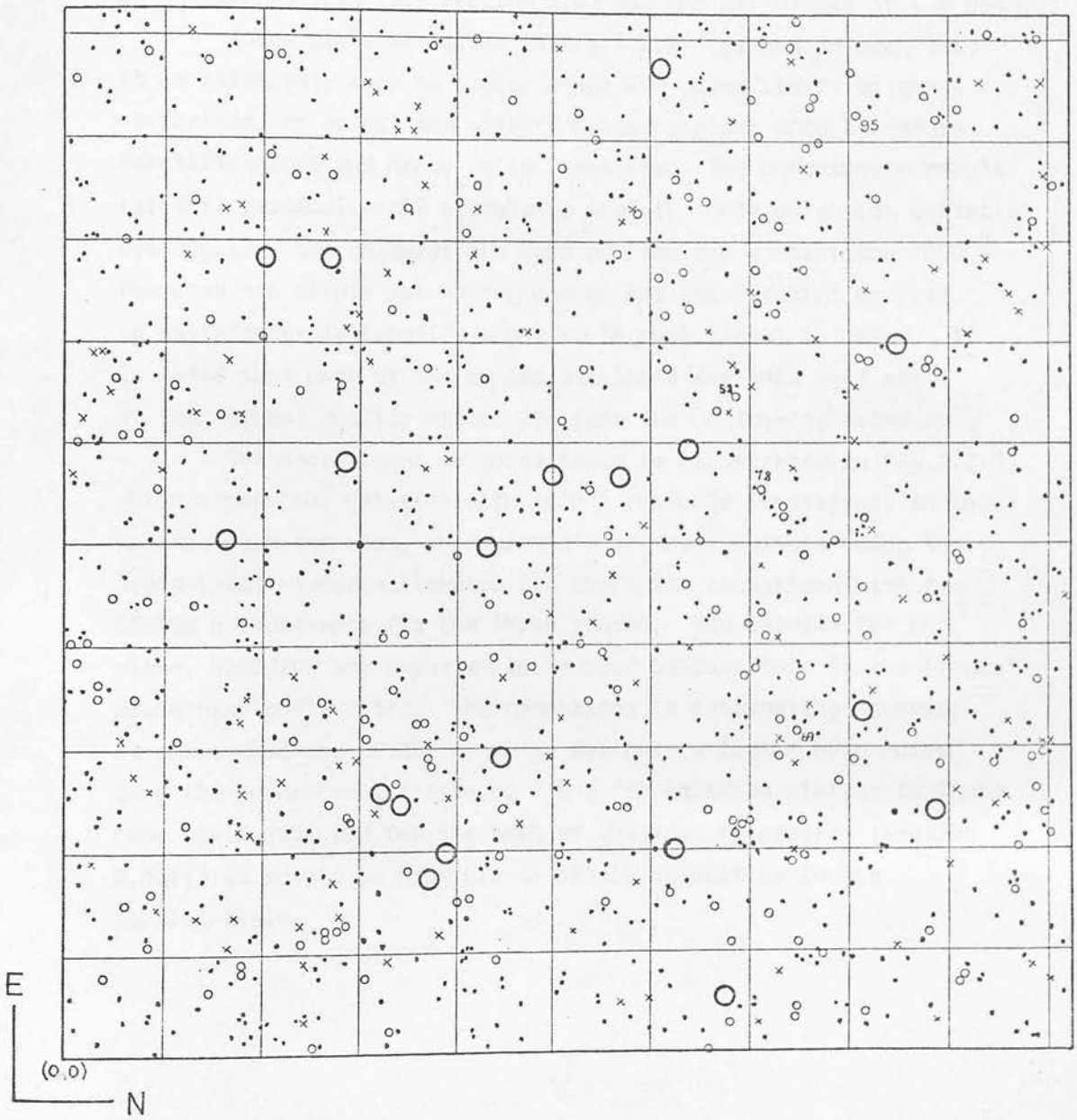

Fig. 4.2.1

Objects identified by eye in the test field.
Open circles: galaxies
Dots: stars
Crosses: objects with overlapped spectra
The area was not searched to the plate limit.
(0,0) is at X= 298mm, Y= 235mm on UJ2461P.

Large open circles indicate bright objects not recorded in the COSMOS data.

were then plotted for the corresponding values of 'RMS' and 'MPEAK' obtained by the program; these parameters describe the strength of the correlation (see section 3.4) and the brightness of the object.

These plots are given in fig 4.2.2. It can be seen that it is relatively easy to assign upper and lower limits to these parameters, to select the objects having correct 4000 Å feature identifications and hence valid redshifts. The unfortunate result for this particular set of data is that if these selection criteria are applied, the galaxies are removed from the sample; the 4000 Å features are simply not strong enough for the redshift program to satisfactorily identify them, due to poor signal to noise. It is noted that none of the plates available for this test are of the highest quality obtainable from the UK Schmidt telescope.

The poor signal to noise ratio is illustrated in fig 4.2.3, which shows four galaxies with 4000 Å features (indicated) in their spectra from the area. Measurements of these objects using the Joyce-Loebl microdensitometer are shown for comparison with the COSMOS measurements for the three plates. The results for one plate, UJ3092P, are expected to be poor because this is the 'rogue' plate previously noted. The comparison is interesting however; it shows that the COSMOS tracings are only a little more noisy than the Joyce-Loebl tracings. Thus for galaxies similar to those from Abell 133 used for the test of the redshift program (section 3.5.11) it should be possible to obtain velocities in the general field.

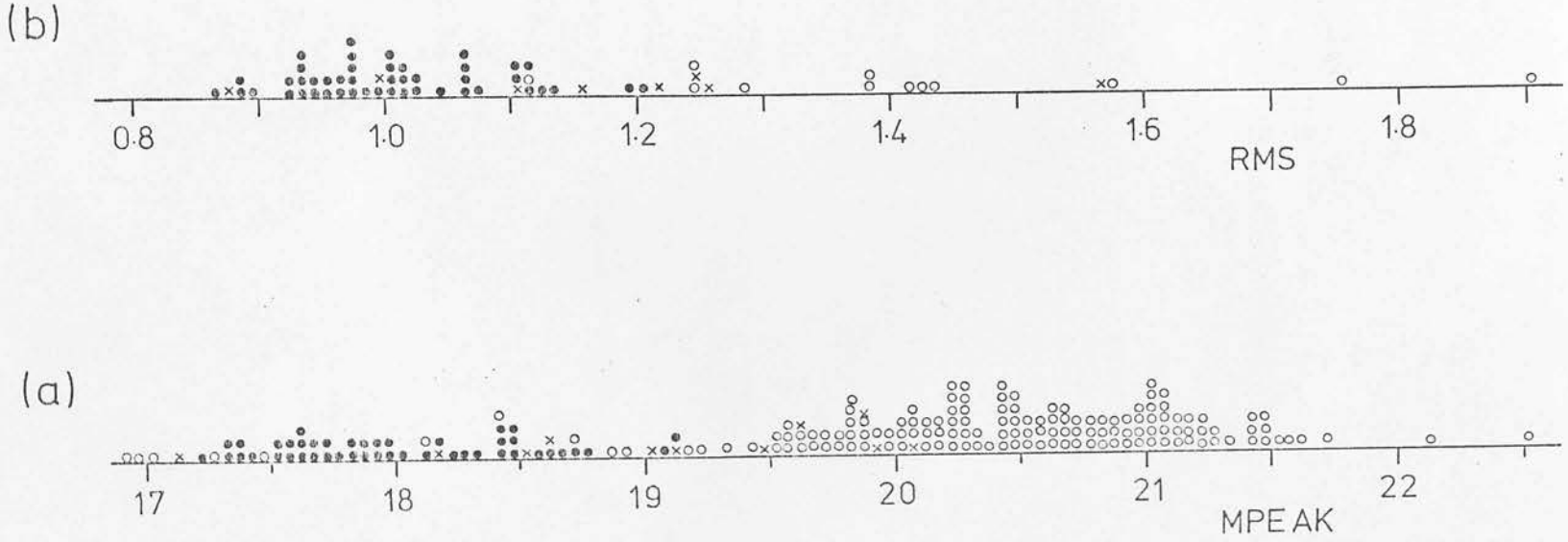

Fig. 4.2.2

Values for parameters MPEAK and RMS produced by the redshift program, for 200 objects in the test area. Filled circles indicate objects where the program has correctly identified the 4000 Å feature; open circles indicate objects with incorrectly identified features; crosses denote uncertain cases. The lower diagram (a) contains all objects; (b) contains all objects with MPEAK in the range 17 to 19.5, except for those having a negative value for the parameter PARAB, indicating an anti-correlation in redshift.

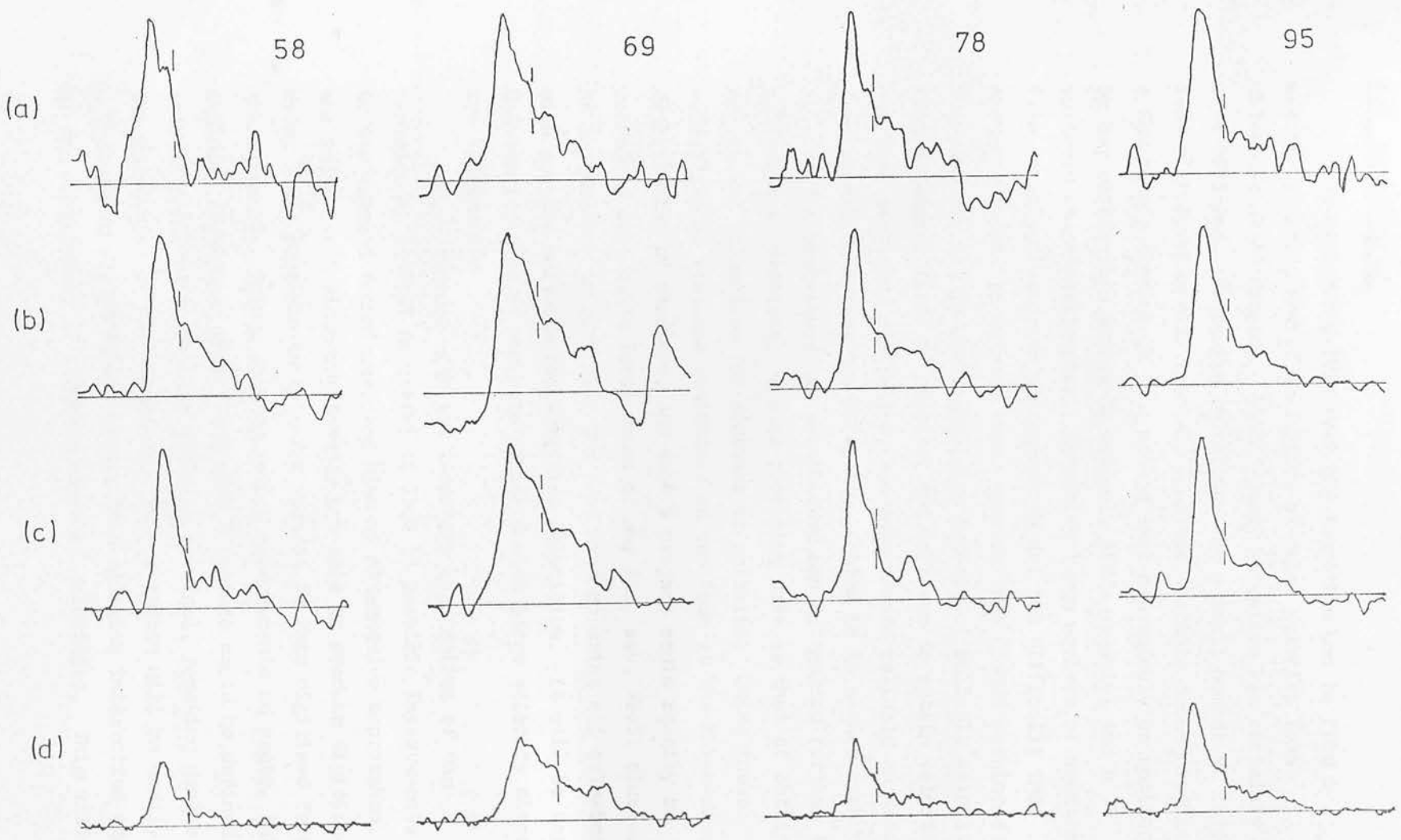

Fig. 4.2.3

A comparison of COSMOS measurements (in intensity and normalised) from plates UJ3092P (a), UJ2620P (b), and UJ2461P (c), and Joyce-Loebl measurements (in density) from plate UJ2461P, for galaxies in the test field. These galaxies have values for MPEAK of 19.5 (58), 19.2 (69), 19.4 (78) and 18.9 (95). The galaxies were selected from the microdensitometer tracings to have 4000 Å features; the expected positions of the feature in the COSMOS data are also shown. The horizontal lines indicate a distance of 2mm.

4.3 Conclusions.

On commencing this work the intention was to find a way of obtaining radial velocities of faint galaxies from objective prism spectra. This primary objective has certainly been achieved. Obtaining velocities for a small number of objects from microdensitometer tracings involves a simple procedure with a few simple checks; it is a method that can quickly be applied by any worker with access to suitable plate material and a suitable microdensitometer. Obtaining large numbers of spectra from an objective prism photograph is not too difficult; the software exists to extract these spectra from COSMOS machine data. The problems lie in producing large numbers of reliable velocities from a general field of objects; the software to obtain velocities has been developed and tested, but only proved reliable on data of good signal to noise; the remaining problem is to secure such data.

The techniques now established can be applied further to astronomical problems. A most promising area is that of obtaining radial velocities for clusters of galaxies. Using these velocities as distance indicators we can look at the three-dimensional distribution of clusters, and such a project could readily be performed over quite large areas of sky for, say, Abell clusters, as a precursor to work over the same area covering all galaxies with spectra suitable for obtaining velocities. It will be very interesting also if any more clusters with large velocity dispersions are discovered.

Simultaneous with the immediate application of the techniques, it will be useful to look at possible improvements to the present techniques, and also at alternative approaches. With the Joyce-Loebl microdensitometer now able to produce digitised data, it is possible to transfer spectra in this digitised form into the computer. Rather than by making measurements on paper, the emulsion wavelength cutoff and 4000 Å feature could be defined interactively at a computer graphics terminal, removing part of the inaccuracy of the technique. Such a system will be easily adaptable to COSMOS measurements, thus allowing interactive control of the measurement of larger numbers of velocities. This will allow

much more experience to be gained in the measurement of galaxy spectra, and may possibly suggest further improvements to the automatic redshift program.

One interesting test yet to be performed is a trial of the Stock and Osborne technique (section 2.1) applied to galaxy spectra on the UKSTU photographs. Two photographs have been taken for such a trial, but special measurements using the COSMOS machine will be needed to test the method fully. It is a method that could provide increased accuracy for velocities where required, but is unlikely to replace the method described in this thesis as it is a much more complicated technique to apply.

An important development on the UK Schmidt telescope will be the availability of the new higher dispersion prism. Two main applications are relevant to the techniques developed. Firstly, using the IIIa-J emulsion, higher spectral resolution is available over the present wavelength range, which will enable more accurate velocities to be obtained, although only for the brighter objects. Secondly, using a suitable red-sensitive emulsion, spectra can be examined in the red where the dispersion will be similar to that now obtained in the blue; we might expect to be able to obtain velocities for higher redshift objects by following the 4000 $\mathring{A}$ feature into the red. The new prism will also give additional information for spectral classification.

The application of the techniques described in this thesis to study the large-scale structure of the universe is a fairly long-term project. The technique has the capability of examining much larger volumes of space than has hitherto been possible; certainly out to Hubble velocities of 50,000 kms^{-1}. Correspondingly, large areas of sky need to be covered; it will be essential to combine data from several adjacent UKSTU survey fields. It will also be important to study different directions in space, to look for any possible anisotropy. Both these requirements mean that a moderate number of UKSTU objective prism plates will have to be taken; with the fairly short prism runs as at present, this could take several years to complete.

List of Abbreviations

BGC	Bright galaxy catalogue: de Vaucouleurs et al (1964)
CM	Coarse mode (COSMOS)
COSMOS	Co-Ordinates, Sizes, Magnitudes, Orientations and Shapes
CRT	Cathode ray tube
CTIO	Cerro Tololo Interamerican Observatory
HMS	Humason, Mayall and Sandage (1956)
IAM	Image analysis mode (COSMOS); also TM
IPCS	Image photon counting system
MM	Mapping mode (COSMOS)
RBGC	Revised bright galaxy catalogue: de Vaucouleurs et al (1976)
ROE	Royal Observatory, Edinburgh
RL	Rutherford Laboratories
SAAO	South African Astronomical Observatory
SRC	Science Research Council
T	Transmission: COSMOS parameter
TM	Threshold mapping (COSMOS); also IAM
UKST	United Kingdom Schmidt Telescope
UKSTU	United Kingdom Schmidt Telescope Unit
VDU	Visual display unit

References

Abt, H.A., Smith, G.H. 1969 PASP 81, 332

Barbier, M., Fehrenbach, C. 1955 J. des Obs. 38, 180

Baum, W.A. 1957 AJ 62,6

Baum, W.A. 1958 PASP 70, 450

Baum, W.A. 1962 IAU symposium no. 15, p390, MacMillan

Bidelman, W.P. 1964 Vistas Astr. 8, 53

Bidelman, W.P. 1972 Conference proceedings 'The Role of the Schmidt Telescope in Astronomy', p53 ed. Haug, ESO/SRC

Blanco, V.M. 1974 PASP 86, 841

Bok, B.J., McCuskey, S.W. 1937 Ann. Harv. Coll. Obs. 105, 327

Boksenberg, A. 1972 Proceedings of conference on auxiliary instrumentation for large telescopes, p295 eds. Lausten, S., Reiz, A. ESO/CERN, Geneva

Bolton, J.G. 1977 IAU symposium no. 74, p85, D. Reidel

Brown, G. 1974 PhD thesis, University of Texas at Austin

Burbidge, E.M., Burbidge, G.R., Prendergast, K.H. 1965 ApJ 142, 641

Burbidge, E.M., Burbidge, G.R. 1975 'The Masses of Galaxies'; 'Stars and Stellar Systems', 9, 81 eds. Sandage, A, Sandage, M., Kristian, J. Chicago.

Cherry, B. 1937 Ann. Harv. Coll. Obs. 105, 355

Chincarini, G., Rood, H.J. 1980 Sky and Telescope 59, 364

Clowes, R.G. 1980 PhD thesis in preparation, University of Edinburgh

Clowes, R.G., Emerson, D., Smith, M.G., Wallace, P.T., Cannon, R.D., Savage, A., Boksenberg, A. 1980 MNRAS in press

Code, A.D. 1959 PASP 71, 118

Comstock, G.C. 1906 ApJ 23, 148

Cooke, J.A., Emerson, D., Nandy, K., Reddish, V.C., Smith, M.G. 1977 MNRAS 178, 687 (Appendix C)

Cooke, J.A., Emerson, D., Kelly, B.D., MacGillivray, H.T., Dodd, R.J. 1980 preprint (Appendix C)

Davenhall, A.C., Bunclark, P.S., Fraser, C.W., MacLean, B.J., Stapleton, J.R., Stewart, G.C. 1979 Proc. of the third BIS computers and space technology conference.

Dawe, J.A., Dickens, R.J., Peterson, B.A. 1977 MNRAS 178, 675

de Vaucouleurs, G. 1948 Comptes Rendus Acad. Sci. 227, 466

de Vaucouleurs, G. 1961 ApJ Supp. 5, 233

de Vaucouleurs, G. 1972 Mem. RAS 77,1

de Vaucouleurs, G. 1976 ApJ 205, 13

de Vaucouleurs, G. 1977 unpublished preprint, material appearing in ApJ 223, 351 (1978), ApJ 224, 14 (1978), ApJ 227, 380 (1979)

de Vaucouleurs, G., de Vaucouleurs, A. 1964 'Reference Catalogue of Bright Galaxies', Texas (BGC)

de Vaucouleurs, G., de Vaucouleurs, A., Corwin, H.G., Jr.. 1976 'Second Reference Catalogue of Bright Galaxies', Texas (RBGC)

de Vaucouleurs, G., Bollinger, G. 1979 ApJ 233, 433

Doroshkevich, A.G., Shandarin, S.F. 1978 Astron. Zh. 55, 1144 translated in Sov. Astron. 22, 653

Duflot, M., Fehrenbach, C. 1955a J. des Obs. 38, 172

Duflot, M., Fehrenbach, C. 1955b J. des Obs. 38, 176

Eastman Kodak Company 1973 Publication P-315, 'Kodak plates and films for scientific photography'

Eastmond, T.S., Abell, G.O. 1978 PASP 90, 367

Emerson, D. 1979 internal report, Dept. of Astronomy, University of Edinburgh

Faber, S.M., Dressler, A. 1977 AJ 82, 187

Farnell, G.C. 1966 'The Relationship Between Density and Exposure' in 'The theory of the photographic process', eds. Mees, C.E.K., James, T.H., MacMillan, New York

Fay, T.D., Stein, W.L., Warren, W.H. 1974 PASP 86, 772

Fehrenbach, C. 1944 Comptes Rendus Acad. Sci. 219, 201

Fehrenbach, C. 1947a Ann. d'Astrophys. 10, 257

Fehrenbach, C. 1947b Ann. d'Astrophys. 10, 306

Fehrenbach, C. 1948 Ann. d'Astrophys. 11, 35

Fehrenbach, C. 1955a J. des Obs. 38, 165

Fehrenbach, C. 1955b J. des Obs. 38, 167

Fehrenbach, C. 1966 Advances in Astronomy and Astrophysics 4,1

Fredrick, L.W., Gutsch, W.A. 1974 Pub. Leander McCormick Obs. 15, 39

Gisler, G.R. Friel, E.D. 1979 Index of Galaxy Spectra, Pachart, Tucson

Griffin, R.F. 1967 ApJ 148, 465

Gunn, J.E., Oke, J.B. 1975 ApJ 195, 255

Hawkins, M.R.S., Martin, R. 1977 Nature 265, 711

Henry Draper Catalogue

(1918-24) Cannon, A.J., Pickering, E.C. Ann. Harv. Coll. Obs. 91 to 99
(1925-36) Cannon, A.J. Ann. Harv. Coll. Obs. 100

Hoag, A.A. 1976 PASP 88, 860

Hoag, A.A., Smith, M.G. 1977 ApJ 217, 362

Holmberg, E. 1961 AJ 66, 620

Holmberg, E. 1975 'Galaxies and the Universe'; 'Stars and Stellar Systems', 9, 125 eds. Sandage, A., Sandage, M., Kristian, J. Chicago

Houk, N., Cowley, A.P. 1975 University of Michigan Catalogue of Two-dimensional Spectral Types for the HD Stars, 1 Michigan

Hubble, E. 1929 Proc. Nat. Acad. Sci. 15, 168

Hubble, E., Humason, M.L. 1931 ApJ 74, 43

Humason, M.L., Mayall, N.U., Sandage, A. 1956 AJ 61, 97 (HMS)

Johnson, H.M. 1979 ApJ 230, L137

Kelly, B.D., Cooke, J.A., Emerson, D. 1980a Observatory 100, 76 (Appendix C)

Kelly, B.D., Cooke, J.A., Emerson, D. 1980b preprint (Appendix C)

Kelton, P.W. 1980 AJ 85, 89

Kirshner, R.P., Oemler, A., Jr., Schechter, P.L. 1978 AJ 83, 1549

Kirshner, R.P., Oemler, A., Jr., Schechter, P.L. 1979 AJ 84, 951

Kristian, J., Minkowski, R. 1975 'Optical identifications of 3CR Sources'; 'Stars and Stellar Systems', 9, 199 eds. Sandage,A., Sandage, M., Kristian, J. Chicago

Kristian, J., Sandage, A., Westphal, J.A. 1978 ApJ 221, 383

Kron, R.G., Spinrad, H., King, I.R. 1977 ApJ 217, 951

Krug, P.A.,Morton, D.C., Tritton, K.P. 1980 MNRAS 190, 237

Lindblad,B. 1922 ApJ 55, 85

Lindblad, B., Stenquist, E. 1934 Pub. Stockholm Obs. 11 no. 12

MacGillivray, H.T., Martin, R., Pratt, N.M., Reddish, V.C., Seddon, H., Alexander, L.W.G., Walker, G.S., Williams, P.R. 1976a MNRAS 176, 265

MacGillivray, H.T., Martin, R., Pratt, N.M., Reddish, V.C., Seddon, H., Alexander, L.W.G., Walker, G.S., Williams, P.R. 1976b MNRAS 176,649

Markaryan, B.E. 1967 Astrofizika 3,55 (English translation p24)

Markaryan, B.E. 1969a Astrofizica 5, 443 (E 206)

Markaryan, B.E. 1969b Astrofizica 5, 581 (E 286)

Markaryan, B.E., Lipovetskii, V.A. 1971 Astrofizica 7, 511 (E 299)

Markaryan, B.E., Lipovetskii, V.A. 1972 Astrofizica 8, 155 (E 89)

Markaryan, B.E., Lipovetskii, V.A. 1973 Astrofizica 9, 487 (E 283)

Martin, W.L. 1976 MNRAS 175, 633

McCarthy, M.F. 1960 Specola Astr. Vaticana Ric. Astr. 6, 301

Millman, P.M. 1931 J. Roy. Astr. Soc. Canada 25, 281

Minkowski, R. 1946 PASP 58, 305

Minkowski, R. 1960 ApJ 132, 908

Morgan, W.W., Meinel, A.B., Johnson, H.M. 1954 ApJ 120, 506

Morton, D.C., Spinrad, H., Bruzual, G.A., Kurucz, R.L. 1977 ApJ 212, 438

Nandy, K. 1964 Pub. ROE 3, 142

Nandy, K. 1965 Pub. ROE 5, 13

Nandy, K. 1966 Pub. ROE 5, 233

Nandy, K. 1967 Pub. ROE 6, 25

Nandy, K. 1968 Pub. ROE 6, 169

Nandy, K., Smriglio, F. 1970 Pub. ROE 7,1

Nandy, K., Smriglio, F. 1971 Pub. ROE 7,73

Nandy, K., Smriglio, F. 1976 Pub. ROE 9, 117

Nandy, K., Reddish, V.C., Tritton, K.P., Cooke, J.A., Emerson, D. 1977 MNRAS 178, 63P (Appendix C)

Nassau, J.J. 1945 ApJ 101, 275

Nassau, J.J., Morgan, W.W. 1950 ApJ 113, 141

Nassau, J.J., Blanco, V.M. 1954a ApJ 120, 129

Nassau, J.J., Blanco, V.M. 1954b ApJ 120, 464

Oemler, A., Jr. 1973 ApJ 180, 11

Oke, J.B. 1962 IAU symposium no. 15, p. 34 MacMillan

Oke, J.B. 1964 ApJ 140, 689

Oke, J.B. 1969 PASP 81, 11

Oke, J.B. 1971 ApJ 170, 193

Oke, J.B., Sandage, A. 1968 ApJ 154, 21

Oke, J.B., Schild, R.E. 1970 ApJ 161, 1015

Oke, J.B., Schwarzchild, M. 1975 ApJ 198, 63

Pence, W. 1976 ApJ 203, 39

Philip, A.G.D. 1970 PASP 82, 69

Philip, A.G.D., Sanduleak, N. 1966 PASP 78, 30

Philip, A.G.D., Sanduleak, N. 1970 PASP 82, 53

Pickering, E.C. 1891a Ann. Harv. Coll. Obs. 26, xx

Pickering, E.C. 1891b Ann. Harv. Coll. Obs. 26, xiv

Pickup, G.E. 1979 PhD thesis, University of Edinburgh

Pratt, N.M. 1977 Vistas Astr. 21, 1

Pratt, N.M., Martin, R., Alexander, L.W.G., Walker, G.S., Williams, P.R. 1975 'Image processing techniques in astronomy' p217 eds. de Jager, C., Nieuivenhuijzen, H. D. Reidel

Robinson, L.B., Wampler, E.J. 1972 PASP 84, 161

Rubin, V.C., Ford, W.K., Thonnard, N., Roberts, M.S., Graham, J.A. 1976a AJ 81, 687

Rubin, V.C., Thonnard, N., Ford, W.K., Roberts, M.S. 1976b AJ 81, 719

Samson, W.B. 1969 Pub. ROE 6, 225

Sandage, A. 1958 ApJ 127, 513

Sandage, A. 1961, ApJ 133, 355

Sandage, A. 1972a ApJ 173, 485

Sandage, A. 1972b ApJ 178, 1

Sandage, A. 1972c ApJ 178, 25

Sandage, A. 1973a ApJ 180, 687

Sandage, A. 1973b ApJ 183, 711

Sandage, A. 1973c ApJ 183, 731

Sandage, A. 1973d ApJ 183, 743

Sandage, A. 1975a 'The Redshift'; 'Stars and Stellar Systems' 9, 761 eds. Sandage, A., Sandage, M., Kristian, J. Chicago

Sandage, A. 1975b ApJ 202, 563

Sandage, A. 1978 AJ 83, 904

Sandage, A., Kristian, J., Westphal, J.A. 1976 ApJ 205, 688

Sandage, A., Tammann, G.A. 1974a ApJ 190, 525

Sandage, A., Tammann, G.A. 1974b ApJ 191, 603

Sandage, A., Tammann, G.A. 1974c ApJ 194, 223

Sandage, A., Tammann, G.A. 1974d ApJ 194, 559

Sandage, A., Tammann, G.A. 1975a ApJ 196, 313

Sandage, A., Tammann, G.A. 1975b ApJ 197, 265

Sandage, A., Tammann, G.A. 1976 ApJ 210, 7

Sandage, A., Tammann, G.A., Hardy, E. 1972 ApJ 172, 253

Sandage, A., Tammann, G.A., Yahil, A. 1979 ApJ 232, 352

Savage, A. 1978 D. Phil thesis, University of Sussex

Schalen, C. 1952 Uppsala Astr. Obs. Ann. 2 no 4

Schalén, C. 1954 Arkiv för Astron 1, 545

Schild, R.E. 1972 ApJ 178, 617

Schild, R.E., Oke, J.B. 1971 ApJ 169, 209

Schulte, D.H. 1956 ApJ 123, 250

Schwarzchild, M. 1954 AJ 59, 273

Seares, F.H. 1916 Proc. Nat. Acad. Sci. 2, 553

Secchi, A. 1869 Astr. Nachr. 73, 129

Seitter, W.C. 1970 Bonner Spektral-Atlas I Bonn

Seitter, W.C. 1973 IAU symposium no. 50, p80, D. Reidel

Seitter, W.C. 1975 Bonner Spektral-Atlas II Bonn

Shane, C.D. 1975 'Distribution of Galaxies'; 'Stars and Stellar Systems' 9, 647 eds. Sandage, A., Sandage, M., Kristian, J. Chicago

Shane, C.D., Wirtanen, C.A. 1967 Pub. Lick Obs. 22 part 1

Shapley, H. 1929 Proc. Nat. Acad. Sci. 15, 565

Sim, M.E. 1977 A.A.S. Photo-bulletin 14, 9

Sim, M.E., Hawarden, T.G., Cannon, R.D. 1976 A.A.S. Photo-bulletin 11, 3

Slipher, V.M. 1914 Lowell Obs. Bull. 2, 56

Smith, M.G. 1975 ApJ 202, 591

Smith, M.G. 1978 Vistas Astr. 22, 321

Solinger, A.B., Tucker, W.H. 1972 ApJ 175, L107

Spinrad, H. 1976 PASP 88, 565

Spinrad, H., Taylor, B.J. 1971 ApJ Supp. 22, 445

Spinrad, H., Smith, H.E., Hunstead, R., Ryle, M. 1975 ApJ 198, 7

Spinrad, Smith, H.E., 1976 ApJ 206, 355

Stebbins, J., Whitford, A.E. 1937 ApJ 86, 247

Stebbins, J., Whitford, A.E. 1948 ApJ 108, 413

Stebbins, J., Whitford, A.E. 1952 ApJ 115, 284

Stephenson, C.B. 1966 Vistas Astro. 7, 59

Stobie, R.S., Smith, G.M., Lutz, R.K., Martin, R. 1979 Proceedings of the International Workshop on Image Processing in Astronomy, Trieste

Stock,J. 1956 ApJ 123, 253

Stock, J., Osborn, W. 1972 Conference proceedings 'The Role of the Schmidt Telescope in Astronomy', p63, ed. Haug ESO/SRC

Stock, J., Osborn, W. 1973 IAU symposium no. 50, p290, D. Reidel

Strömberg, G. 1925 ApJ 61, 353

Tammann, G.A., Yahil, A., Sandage, A. ApJ 234, 775

Tammann, G.A., Sandage, A., Yahil, A. 1980 Physica Scripta 21, 630

Tarenghi, M., Tifft, W.G., Chincarini, G., Rood, H.J., Thompson, L.A. 1979 ApJ 234, 793

Thompson, G.I. 1970 Pub. ROE 7, 19

Tifft, W.G. 1961 AJ 66, 390

Tifft, W.G. 1963 AJ 68, 302

Tifft, W.G. 1969 AJ 74, 354

Tifft, W.G., Gregory, S.A. 1976 ApJ 205, 696

Treanor, P.J. 1948 MNRAS 108, 189

Treanor, P.J. 1969 Vistas Astr. 11, 147

van den Bergh, S., Henry, R.C. 1962 D.D.O. Publ. 2, 281

Vanderkerkhove, E. 1963 Comm. Obs. Roy. Belgique 9 no. 216

Vanderkerkhove, E. 1965 Comm. Obs. Roy. Belgique 10 no. 239

Van Houten, C.J. 1961 Bull. Astr. Inst. Netherlands 16, 1

Vogel, H.C. 1883 Publ. Astrophys. Obs. Potsdam 3, 127

Wells, D. 1973 Ph D thesis, University of Texas at Austin

Whitford, A.E. 1936 ApJ 83, 424

Whitford, A.E. 1962 IAU symposium no. 15, p40, MacMillan

Whitford, A.E. 1971 ApJ 169, 215

Whitford, A.E. 1975 'Galaxies and the Universe'; 'Stars and Stellar Systems' 9, 159 eds. Sandage, A., Sandage, M., Kristian, J. Chicago

Wood, D.B. 1966 ApJ 145, 36

Yahil, A., Vidal, N.V. 1977 ApJ 214, 347

Zwicky, F., Herzog, E., Wild, P., Karpowicz, M.,Kowal, C.T. 1961 - 1968 Catalogue of Galaxies and Clusters of Galaxies, Vols I to VI California Institute of Technology

Appendix A

The redshift program (version JCZED6).

A listing of the FORTRAN source code for the redshift program. This version runs on the RL 360/195 computer, using the SMOG graphics system and RL routines UZERO and UMOVE for fast array clearing and moving. The program is described in section 3.4.

```
C     JCZED6
C     ------
C
C     SPECTRA ARE READ FROM THE MTDAMT OUTPUT TAPE,
C     NORMALISED AND CALIBRATED FROM THE CUTOFF POSITION.
C     THE FILTERED SPECTRUM IS THEN CORRELATED WITH THE STANDARD
C     FOR A BEST-FIT REDSHIFT.
C
C
C
C
C
C
C                                        JOHN COOKE   NOVEMBER 1978
C
      INTEGER B(1024),A(1024),SPEC(512,8),ITOT(8),
     -  VAV,HAV,BCKCON,GTSIZ,STSZ,OFS,ROFS,TMIN,IDIN(3),
     -  INTCON(126)
      REAL WAV(20),DEP(20),WID(20),SPECT(512),SPECN(512),
     -  VERFIT(21),POSFIT(21),FITCOE(21),PSPEC(512),CONSPC(512),
     -  WSPEC(512),STORE(100,2),C(21),SWAV(20),CORR(512),
     -  XPLOT(15),YPLOT(15),ZSTO(80),MISSTO(80),MASSTO(80),
     -  SUBCOR(100,80),CMUL(512)
      COMMON /IDEN/ID2,JLEN2
      COMMON /HART/HX0,HW0,HA
      COMMON /MAGN/SPECT,POSN2,BACK
      COMMON /PLOT/SPECN,XZED,XRMS,POSN,ID,XPLOT,YPLOT,
     -  WAV,NFEAT,BSTP,BVAL,JLEN
      DATA CORR/512*0./,IDOFS/-1/
      DATA CMUL/57*0.,0.01,0.02,0.05,0.08,0.13,0.19,0.25,
     -  0.32,0.42,0.52,0.63,0.75,0.87,0.94,0.97,0.99,
     -  439*1./
      JLEN=256
      JLEN2=JLEN
C
C     READ BUMPH BLOCK
C
C     READ(8)B
C
C     READ ALL THE CARD DATA
C
C
C     SPECTRUM OFFSET, LENGTH (IN STEPS: 512 STEPS = 4MM)
C
      READ(5,*)IOFS
```

```
      READ(5,*)LEN
      OFS=IOFS-8
      ROFS=IOFS+LEN
C
C     STEP SIZE
C
      READ(5,*)STSZ
C
C     AVERAGING WINDOWS
C
      READ(5,*)VAV
      READ(5,*)HAV
      IF(VAV.NE.1.AND.VAV.NE.2.AND.VAV.NE.3.AND.VAV.NE.8)GOTO900
C
C     EXPECTED BACKGROUND SCATTER
C
      READ(5,*)BCKCON
      BKPEAK=FLOAT(BCKCON)
C
C     NOISE RANGE FACTOR
C
      READ(5,*)TRANG
C
C     TMIN ALLOWED
C
      READ(5,*)TMIN
C
C     GATE SIZE FOR CONTINUUM REMOVAL
C
      READ(5,*)GTSIZ
      TST=FLOAT(GTSIZ)/2.-FLOAT(GTSIZ/2)
      IF(TST.EQ.0.)GOTO901
C
C     REDSHIFT LIMITS
C
      READ(5,*)ZLO,ZUP
      IF(ZLO.GT.ZUP)GOTO902
C
C     NUMBER OF EXPECTED FEATURES
C
      READ(5,*)NFEAT
C
C     DETAILS OF FEATURES
C     WAVELENGTH,DEPTH,WIDTH
C     (WID IS ZERO FOR STEPS)
C
      DO20I=1,NFEAT
 20   READ(5,*)WAV(I),DEP(I),WID(I)
```

```
C
C     GET MIN AND MAX WAVELENGTHS
C
      WMIN=10000.
      WMAX=0.
      DO17I=1,NFEAT
      IF(WAV(I).GT.WMIN)GOTO18
      WMIN=WAV(I)
      WIDMIN=WID(I)
      GOTO17
 18   IF(WAV(I).LT.WMAX)GOTO17
      WMAX=WAV(I)
      WIDMAX=WID(I)
 17   CONTINUE
      WMIN=WMIN-WIDMIN*5.
      WMAX=WMAX+WIDMAX*5.
C
C     DETAILS OF HARTMANN FIT FOR DISPERSION
C
      READ(5,*)HX0,HW0,HA
C
C     INTENSITY CONVERSION PARAMETERS
C
      READ(5,*)TZERO,TBASE,GAMMA,CALCON
C
C     SET UP INTENSITY CONVERSION LOOKUP TABLE
C
      ILOW=TBASE+1.
      ISTART=ILOW+1
      DO610I=ISTART,128
      SI=I-1
      BDENS=ALOG10((TZERO/(SI-TBASE))-1.)
 610  INTCON(I)=10.**(GAMMA*BDENS+CALCON)
      DO620I=1,ILOW
 620  INTCON(I)=INTCON(ISTART)
      WRITE(6,630)INTCON
 630  FORMAT(1H //1X,'INTCON:'/(1X,8I10))
C
C     WRITE OUT DATA
C
      WRITE(6,14)IOFS,LEN,STSZ,VAV,HAV,BCKCON,TRANG,TMIN,GTSIZ,ZLO,
     -  ZUP,HX0,HW0,HA,TZERO,TBASE,GAMMA,CALCON
 14   FORMAT(1H1/////1X,'REDSHIFT PROGRAM'/1X,
     -                  '---------------'///1X,'DATA :'//1X,
     -  'SPECTRUM OFFSET :  ',I5/1X,
     -  'SPECTRUM LENGTH :  ',I5/1X,
     -  'STEP SIZE :        ',I5/1X,
     -  'VER. AV. :         ',I5/1X,
```

```
     -  'HOR. AV. :          ',I5/1X,
     -  'BACKGROUND PEAK :   ',I5/1X,
     -  'RANGE FACTOR :      ',F5.1/1X,
     -  'IMAX  ALLOWED :     ',I5/1X,
     -  'CONV. GATE SIZE :   ',I5/1X,
     -  'LOW  Z LIMIT :      ',F6.3/1X,
     -  'HIGH Z LIMIT :     ',F6.3/1X,
     -  'HARTMANN PARAMETERS :'/1X,
     -  '   X0 :',E16.6/1X,'   W0 :',E16.6/1X,'    A :',E16.6/1X,
     -  'INTENSITY CONVERSION :'/1X,
     -  '  TO    :',F6.1/1X,'  TB    :',F6.1/1X,'  GAMMA :',F6.2/1X,
     -  '  CONST :',F6.2//)
      WRITE(6,514)
 514  FORMAT(' FEATURES:'/6X,'WAV',8X,'DEP',7X,'WID'/)
      DO15I=1,NFEAT
 15   WRITE(6,16)WAV(I),DEP(I),WID(I)
 16   FORMAT(1H ,3F10.3)
      WRITE(6,515)
 515  FORMAT(1H ///' IDENTIFICATION',8X,'Z',8X,'RMS',9X,'PARAB',7X,
     -  'M4425    MPEAK    M4900    M4200    M3600'/)
C
C     SET UP POSNS OF CORR DATA POINTS
C
      DO4505I=1,JLEN
 4505 PSPEC(I)=(FLOAT(64-I))*0.008
C
C     SET UP THE CORRELATION ARRAYS IN SUBCOR
C
      INZED=(ZUP-ZLO)/0.005+1.
      Z=ZLO
      DO4502IZED=1,INZED
      Z=Z+0.005
      ZSTO(IZED)=Z
      ZP1=Z+1.
C
C     CORRECT THE WAVELENGTHS
C
      DO215I=1,NFEAT
 215  SWAV(I)=WAV(I)*ZP1
C
C     GET MIN AND MAX WAVELENGTHS
C
      SWMIN=WMIN*ZP1
      SWMAX=WMAX*ZP1
C
C     WAVELENGTH TO X (MM)
C
      SXMIN=HX0-HA/(SWMIN-HW0)**1.2
```

```
      SXMAX=HX0-HA/(SWMAX-HW0)**1.2
C
C     X (MM) TO STEP - NOTE: MINSTP IS > MAXSTP
C
      MINSTP=64-INT((SXMIN*1000.)/8.)+2
      MAXSTP=64-INT((SXMAX*1000.)/8.)-2
C
C     ALLOW FOR CONV GATE
C
      MINSTP=MINSTP+GTSIZ*2
      MAXSTP=MAXSTP-GTSIZ*2
C
C     NOW WE HAVE CORRECTED LINE POSITIONS
C
C
C     NOW OBTAIN WAVELENGTHS OF ALL THE POINTS
C     IN THE SPECTRUM
C
      DO103I=MAXSTP,MINSTP
  103 WSPEC(I)=HW0+(HA/(HX0-PSPEC(I)))**(1./1.2)
C
C     FILL IN CORRELATING ARRAY, DECREASING IN WAVELENGTH
C
      DO217I=MAXSTP,MINSTP
      WSPECI=WSPEC(I)
C
C     LOOP FOR ALL LINES
C
      DO218K=1,NFEAT
      WIDKJ=WID(K)
      DEPKJ=DEP(K)
      SWAVKJ=SWAV(K)
      IF(WIDKJ)1041,104,1041
 1041 YY=ABS(WSPECI-SWAVKJ)/WIDKJ
      IF(YY-5.)2181,2181,218
 2181 SS=DEPKJ/EXP(YY)
      GOTO105
  104 IF(WSPECI-SWAVKJ)1042,1042,1043
 1042 SS=DEPKJ
      GOTO105
 1043 SS=0.
  105 CORR(I)=CORR(I)+SS
  218 CONTINUE
  217 CONTINUE
      MISSTO(IZED)=MINSTP
      MASSTO(IZED)=MAXSTP
      ITCOR=(MINSTP-MAXSTP)+1
      IF(ITCOR.GT.100)GOTO903
```

```
C
C     CONVOLVE THE CORRELATING FUNCTION
C
      CALL CORCON(CORR,GTSIZ,MAXSTP,MINSTP,JLEN)
      DO4503ICORS=MAXSTP,MINSTP
      JCORS=(ICORS-MAXSTP)+1
 4503 SUBCOR(JCORS,IZED)=CORR(ICORS)*CMUL(ICORS)
C
C     ZERO CORRELATING FUNCTION
C     (ALLOW FOR GATE SIZE CONVOLUTION)
C
      MINCL=MAXSTP-GTSIZ*2
      IF(MINCL.LE.0)MINCL=1
      MAXCL=MINSTP+GTSIZ*2
      IF(MAXCL.GT.JLEN)MAXCL=JLEN
      INUM=MAXCL-MINCL+1
      IPLUS=MINCL+1
      CORR(MINCL)=0.
      CALL UMOVE(CORR(MINCL),CORR(IPLUS),INUM)
 4502 CONTINUE
C
C     INITIALISE GRAPHICS SYSTEM
C
      CALL FRHCS
      CALL APER
      CALL LIMITV(0.,0.,600.,600.)
      CALL CHSIZE(10.)
      GOTO30
C     GOTO2732
C
C
C
C     ERRORS IN DATA
C
  900 WRITE(6,1000)VAV
 1000 FORMAT(1H //1X,'IMPERMISSIBLE VERTICAL AVERAGE : ',I3/////)
      STOP
  901 WRITE(6,1001)GTSIZ
 1001 FORMAT(1H //1X,'GATE SIZE : ',I3,' MUST BE ODD'/////)
      STOP
  902 WRITE(6,1002)
 1002 FORMAT(1H //1X,'REDSHIFT LIMITS INCORRECT'/////)
      STOP
  903 WRITE(6,1003)
 1003 FORMAT(1H //1X,'TOO MANY STEPS FOR SUBCOR'/////)
      STOP
C
C
```

```
C
C
C     ENTRY POINT FOR READING A NEW SPECTRUM
C
 30   READ(8)A
      IF(A(1024).EQ.-9999)GOTO90
C
C***  ID FROM NEW FORMAT
C
      ID=A(1)
      ID2=ID
      IXSPOS=A(2)
      IYSPOS=A(3)
      A(1)=A(129)
      A(2)=A(130)
      A(3)=A(131)
      GOTO32
 31   IF(A(1024).NE.-5555)GOTO1190
      WRITE(6,60)
 60   FORMAT(1H /////1X,'END OF AREA'/////)
      GOTO30
C
C     DATA BLOCKS NOW
C
 32   IF(STSZ.EQ.16)GOTO33
      IF(STSZ.EQ.8)GOTO34
      GOTO1192
C
C     8 MICRON STEP
C
 34   DO37I=1,4
      READ(8)A
      DO37J=1,8
      DO37K=1,128
      L=(I-1)*128+K
      M=(J-1)*128+K
      ITVAL=A(M)+1
      IF(ITVAL.LT.1.OR.ITVAL.GT.128)WRITE(6,651)ID,ITVAL
 651  FORMAT(1H /1X,I12,' - DATA ERROR - ',I12)
 37   SPEC(L,J)=INTCON(ITVAL)
      GOTO70
C
C     16 MICRON STEP
C     MODIFIED TO WORK ON LH BLOCK ONLY (FOR JLEN=256)
C
 33   CONTINUE
C     READ(8)A
      DO35J=1,8
```

```
      DO35K=1,128
      L=K*2
      M=(J-1)*128+K
      ITVAL=A(M)+1
      IF(ITVAL.LT.1.OR.ITVAL.GT.128)WRITE(6,651)ID,ITVAL
      INEW=INTCON(ITVAL)
      SPEC(L,J)=INEW
      IF(K.EQ.1)GOTO631
      SPEC(L-1,J)=(IOLD+INEW)/2
      IOLD=INEW
      GOTO35
  631 IOLD=INEW
      SPEC(1,J)=INEW
   35 CONTINUE
C     READ(8)A
C
C     TEST FOR COMPLETE AVERAGING
C
      IF(VAV.EQ.8)GOTO655
C
C
C
C     FIND THE ROW CONTAINING THE MOST DENSE
C     PART OF THE SPECTRUM
C
   70 DO36I=1,8
   36 ITOT(I)=0
      DO38I=1,8
      DO38J=1,JLEN
   38 ITOT(I)=ITOT(I)+SPEC(J,I)
C
C     GET ROW WITH MAXIMUM TOTAL
C
      MAX=0
      DO39I=1,8
      IF(ITOT(I).LT.MAX)GOTO39
      MIN=ITOT(I)
      J=I
   39 CONTINUE
C
C     IF J IS AT THE EDGE THE WRONG SPECTRUM HAS BEEN
C     FOUND - GO TO THE CENTRE
C
      IF(J.NE.1.AND.J.NE.8)GOTO43
      IF(J.EQ.8)J=5
      IF(J.EQ.1)J=4
      ID=IDOFS
C
```

```
C     ROW J CONTAINS THE MAXIMUM TOTAL
C
 43   IF(VAV.EQ.1.OR.VAV.EQ.3)GOTO41
C
C     FOR EVEN VAV FIND THE NEXT MAX TOTAL
C
      IUP=ITOT(J+1)
      ILO=ITOT(J-1)
      IF(IUP.LT.ILO)GOTO44
      K=J+1
      GOTO45
 44   K=J-1
C
C     GET THE 2-WIDE SPECTRUM
C
 45   DO46I=1,JLEN
 46   SPECT(I)=FLOAT(SPEC(I,J)+SPEC(I,K))/2.
      GOTO50
C
C     ODD VAV
C
 41   IF(VAV.EQ.3)GOTO47
C
C     GET THE 1-WIDE SPECTRUM
C
      DO48I=1,JLEN
 48   SPECT(I)=SPEC(I,J)
      GOTO50
C
C     GET THE 3-WIDE SPECTRUM
C
 47   DO49I=1,JLEN
 49   SPECT(I)=FLOAT(SPEC(I,J-1)+SPEC(I,J)+SPEC(I,J+1))/3.
      GOTO50
C
C     8-WIDE SPECTRUM
C
 655  DO656I=1,JLEN
      JSUM=0
      DO657J=1,8
 657  JSUM=JSUM+SPEC(I,J)
 656  SPECT(I)=FLOAT(JSUM)/8.
C
C     GET MOVING AVERAGE
C
 50   CALL MOVAV(SPECT,HAV,JLEN)
C
C     SPECTRUM IS NOW IN INTENSITY AND SMOOTHED
```

```
C
C
C
C     REJECT SPECTRUM IF TOO BRIGHT
C
      TRMAX=0.
      DO1023I=1,JLEN
      IF(SPECT(I).GT.TRMAX)TRMAX=SPECT(I)
 1023 CONTINUE
      IF(TRMAX.LT.FLOAT(TMIN))GOTO1021
C
C     REJECTED SPECTRUM - TOO BRIGHT
C
      WRITE(6,61)ID,TRMAX
 61   FORMAT(1H /1X,I12,' REJECTED - IMAX IS ',F8.1)
      GOTO30
C
C     NOW GET THE FIRST APPROXIMATION TO THE BACKGROUND
C
C     GET MIN INTENSITY
C
 1021 RIMIN=100000.
      DO51I=1,JLEN
      IF(SPECT(I).LT.RIMIN)RIMIN=SPECT(I)
 51   CONTINUE
C
C     OFFSET BY BCKCON
C
      APPX=RIMIN+BKPEAK
C
C     CHECK TOTAL RANGE (INTENSITY) OUTSIDE SPECTRUM
C
      RLO=100000.
      RHI=0.
      DO52I=1,JLEN
      IF(I.GT.OFS.AND.I.LT.ROFS)GOTO52
      IF(SPECT(I).GT.RHI)RHI=SPECT(I)
      IF(SPECT(I).LT.RLO)RLO=SPECT(I)
 52   CONTINUE
      RANG=RHI-RLO
      TLIM=TRANG*2.*BKPEAK
      IF(RANG.GT.TLIM)GOTO53
C
C     NO BIGGER SPECTRA IN THE FIELD - GET BACKGROUND
C     BY AVERAGEING
C
      NSUM=0
      TOT=0.
```

```
      RIMIN=100000.
      DO54I=1,JLEN
      IF(I.GT.OFS.AND.I.LT.ROFS)GOTO54
      NSUM=NSUM+1
      TOT=TOT+SPECT(I)
      IF(SPECT(I).LT.RIMIN)RIMIN=SPECT(I)
 54   CONTINUE
      BACK=TOT/FLOAT(NSUM)
C
C     UPDATE THE BACKGROUND PEAK APPROXIMATION
C
      BKPEAK=(BKPEAK+BACK-RIMIN)/2.
      GOTO55
C
C     OTHER SPECTRA IN THE FIELD - REPLACE BY A CONSTANT BACKGROUND
C
 53   DO56I=1,JLEN
      IF(I.GT.OFS.AND.I.LT.ROFS)GOTO56
      SPECT(I)=APPX
 56   CONTINUE
      BACK=APPX
C
C     GET IMAX AROUND THE SPECTRUM
C
 55   SPMAX=0.
      DO57I=OFS,ROFS
      IF(SPECT(I).GT.SPMAX)SPMAX=SPECT(I)
 57   CONTINUE
C
C     SPECTRUM OK - NOW NORMALISE IT
C     SPECN HAS 0 AT PLATE, 1 AT MAX
C
      HITE=SPMAX-BACK
C     REJECT IF HITE -VE
      IF(HITE.GT.0)GOTO755
      WRITE(6,756)ID,HITE
 756  FORMAT(1H /1X,I12,' REJECTED - HITE IS ',E10.3)
      GOTO30
755   DO59I=1,JLEN
 59   SPECN(I)=(SPECT(I)-BACK)/HITE
C
C
C
C
C     NORMALISED SPECTRUM NOW CONTAINED IN SPECN
C
C
C
```

```
C
C
C     GO ALONG THE SPECTRUM, LOOKING FOR THE CUTOFF
C
      DO251I=OFS,JLEN
      IF(SPECN(I).LE.0.5)GOTO251
      ICUT=I
      GOTO252
 251  CONTINUE
      GOTO1194
C
C     GET THE 21 POINTS AROUND THE CUTOFF
C
 252  DO101I=1,21
      J=ICUT-11+I
      POSFIT(I)=J
 101  VERFIT(I)=SPECN(J)
C
C     FIT A 3-ORDER POLYNOMIAL WITH POSITION AS Y
C
      CALL NEWPOL(1,3,21,VERFIT,POSFIT,IORD,FITDEV,FITCOE)
C
C     GET THE POSITION OF HALF-MAX INTENSITY
C
 3233 CALL POLVAL(3,FITCOE,0.5,POSN)
      IPOSN=INT(POSN)
      IF(IPOSN.GT.0.AND.IPOSN.LT.JLEN)GOTO350
      WRITE(6,3235)ID,POSN
 3235 FORMAT(1H /1X,I12,' REJECTED - POSN IS ',E16.7)
      GOTO30
 350  CONTINUE
      IF(IPOSN.GT.40.AND.IPOSN.LT.88)GOTO351
      WRITE(6,3241)ID,IPOSN
 3241 FORMAT(1H /1X,I12,' REJECTED - IPOSN IS ',I4)
      GOTO30
 351  CONTINUE
C
C     GET THE POSITIONS OF ALL THE DATA POINTS, RELATIVE TO THE CUTOF
C     IN MM
C
      LOWPOS=INT(POSN)
      SHIFT=POSN-FLOAT(LOWPOS)
      DO102I=1,JLEN
 102  PSPEC(I)=(FLOAT(LOWPOS-I)+SHIFT)*0.008
C
C     NOW REMOVE THE CONTINUUM
C
      CALL REMCON(SPECN,CONSPC,GTSIZ,JLEN)
```

```
C
C
C
C
C     WE NOW ENTER THE REDSHIFT-MATCHING SEQUENCE
C
C
C     REDSHIFT LOOP
C
      DO216IZED=1,INZED
      Z=ZSTO(IZED)
      MINSTP=MISSTO(IZED)+LOWPOS-64
      MAXSTP=MASSTO(IZED)+LOWPOS-64
      IF(MINSTP.GT.JLEN)MINSTP=JLEN
      IF(MAXSTP.LE.0)MAXSTP=1
C
C     RETRIEVE THE RELEVANT PORTION OF CORR
C
      DO4501I=MAXSTP,MINSTP
      K=(I-MAXSTP)+1
 4501 CORR(I)=SUBCOR(K,IZED)
C
C     AND CORRELATE IT WITH THE SPECTRUM CONVOLUTION
C
      SIGSQD=0.
      DO219I=MAXSTP,MINSTP
 219  SIGSQD=SIGSQD+(CORR(I)-CONSPC(I))**2
      STORE(IZED,1)=Z
      STORE(IZED,2)=SQRT(SIGSQD)
C
C     ZERO CORRELATING FUNCTION
C     (ALLOW FOR GATE SIZE CONVOLUTION)
C
      MINCL=MAXSTP-GTSIZ*2
      IF(MINCL.LE.0)MINCL=1
      MAXCL=MINSTP+GTSIZ*2
      IF(MAXCL.GT.JLEN)MAXCL=JLEN
      INUM=MAXCL-MINCL+1
      IPLUS=MINCL+1
      CORR(MINCL)=0.
      CALL UMOVE(CORR(MINCL),CORR(IPLUS),INUM)
 216  CONTINUE
C
C     NOW WE HAVE THE CORRELATION/REDSHIFT PLOT (STORE).
C     WE LOOK FOR THE MINIMUM IN THIS, FIT A PARABOLA
C     TO IT, LOCATING THE BEST-FIT REDSHIFT
C
 222  TEST=1.E+10
```

```
      DO223I=1,INZED
      IF(STORE(I,2).GE.TEST)GOTO223
      TEST=STORE(I,2)
      IPOS=I
  223 CONTINUE
      DO224I=1,15
      JP=IPOS+I-8
      IF(JP.LT.1)JP=1
      IF(JP.GT.INZED)JP=INZED
      XPLOT(I)=STORE(JP,1)
  224 YPLOT(I)=STORE(JP,2)
C
C     FIT THE PARABOLA
C
      CALL NEWPOL(1,2,15,XPLOT,YPLOT,ORD,RDV,C)
C
C     GET THE MINIMUM
C
      XZED=-C(2)/(2.*C(3))
      IF(XZED.LT.ZLO.OR.XZED.GT.ZUP)GOTO845
      GOTO846
  845 WRITE(6,847)ID,XZED
  847 FORMAT(1H /1X,I12,' REJECTED - Z OUT OF RANGE: ',F6.3)
      GOTO30
  846 PARAB=C(3)
C
C
C     REDSHIFT NOW OBTAINED FOR THAT SPECTRUM
C
      XRMS=C(1)+C(2)*XZED+C(3)*XZED*XZED
C
C     GET I AT MAGNITUDE POSNS
C     (AT REST WAVELENGTHS)
C
      POSN2=POSN
      B4425=RMAGN(4425.)
      B4900=RMAGN(4900.)
      B4200=RMAGN(4200.)
      B3600=RMAGN(3600.)
      BPEAK=23.5-2.5*ALOG10(HITE)
C
C     PLOT ALL SPECTRA
C
  275 CALL ZEDPLT
C
C     AND WRITE TO LINEPRINTER
C
      WRITE(6,106)ID,XZED,XRMS,PARAB,B4425,BPEAK,B4900,B4200,B3600
```

```
 106  FORMAT(1H ,I12,7X,F6.3,3X,E10.3,3X,E10.3,5(3X,F6.2))
C
C     AND TO O/P FILE
C
      WRITE(17,770)ID,IXSPOS,IYSPOS,XZED,B4425,BPEAK,B4900,B4200,
     -  B3600,XRMS,PARAB
 770  FORMAT(I12,2I8,F6.3,5F6.2,F8.2,F8.0)
C
C     RETURN TO NEW SPECTRUM
C
      GOTO30
C
C
C
C     END OF TAPE
C
  90  WRITE(6,13)
  13  FORMAT(1H /////1X,'END OF TAPE'/////)
      ITER=-9999
      Z=0.
C     WRITE(17,771)ITER,ITER,Z,Z,Z,Z
 771  FORMAT(12X,2I8,F6.3,F6.1,2E10.3)
      CALL ENDSPR
      STOP
C
C     ERRORS IN PROGRAM
C
 1190 WRITE(6,1191)
 1191 FORMAT(1H //1X,'BLOCK ORDER ERROR'/////)
      STOP
 1192 WRITE(6,1193)
 1193 FORMAT(1H //1X,'INCORRECT STEP SIZE'/////)
      STOP
 1194 WRITE(6,1195)
 1195 FORMAT(1H //1X,'NORMALISATION FAULT'/////)
      STOP
      END
C
C  RMAGN:  CALCULATES MAGNITUDE ABOVE PLATE AT WAV
C
      FUNCTION RMAGN(WAV)
      REAL SPECT(512)
      COMMON /IDEN/ID,JLEN
      COMMON /HART/HX0,HW0,HA
      COMMON /MAGN/SPECT,POSN,BACK
      IR=JLEN-1
      XWAV=HX0-HA/(WAV-HW0)**1.2
      STP=POSN-XWAV*125.
```

```
      ISTP=INT(STP)
      IF(ISTP.LT.2.OR.ISTP.GT.IR)GOTO12
      S1=SPECT(ISTP-1)
      S2=SPECT(ISTP)
      S3=SPECT(ISTP+1)
      SINT=(S1+S2+S3)/3.
      IF(SINT.LE.BACK)SINT=BACK+1.
      RMAGN=23.5-2.5*ALOG10(SINT-BACK)
      RETURN
 12   WRITE(6,13)ID,POSN
 13   FORMAT(1H /1X,I12,' REJECTED - STEP ERROR IN RMAGN - POSN IS ',
     -  E16.7)
      RETURN
      END
C
C  NEWPOL:  POLYFIT MK II, USING TCHEBYCHEFFS
C           MAXIMUM 100 POINTS
C
      SUBROUTINE NEWPOL(II,K,N,X,Y,L,RDEV,A)
C  II: 0: POLYFIT, 1: ENDFIT
C  K: MAX ORDER
C  N: NO. POINTS
C  X: ARRAY
C  Y: ARRAY
C  L: BEST ORDER
C  RDEV: RMS DEV.
C  A: COEFF ARRAY (21)
      DIMENSION X(N),Y(N),A(21),P(21,22),PV(21,600),T(21),DA(21)
      KL=K+1
      KJ=K+2
C  ZERO COEFF ARRAY
      DO36I=1,21
36    A(I)=0.
C  ZERO P,PV
      DO31I=1,KL
      DO32J=1,KJ
32    P(I,J)=0.
      DO31J=1,N
31    PV(I,J)=0.
C  SET & CALCULATE P0,P1,PV0,PV1,T0,T1
      SX=0.
      SY=0.
      DO33I=1,N
      SY=SY+Y(I)
33    SX=SX+X(I)
      T(1)=SY/N
      P(1,2)=1.
      P(2,2)=-(SX/N)
```

```
      P(2,3)=1.
      DO34I=1,N
      PV(1,I)=1.
34    PV(2,I)=X(I)-(SX/N)
      YPS=0
      XPS=0
      PS=0
      DO35I=1,N
      YPS=YPS+Y(I)*PV(2,I)
      XPS=XPS+X(I)*PV(2,I)*PV(2,I)
35    PS=PS+PV(2,I)*PV(2,I)
      AA=XPS/PS
      BB=PS/N
      T(2)=YPS/PS
      A(1)=T(1)*P(1,2)+T(2)*P(2,2)
      A(2)=T(2)*P(2,3)
C  ENTER LOOP, SEEKING P2 (CORRESP. P(L=3))
C  SET POLY ORDER
      L=1
C  LOOP
20    L=L+1
C  TEST FOR END
      IF(L-K)21,21,51
21    LIM=L+2
C  EQUATE COEFFS IN GEN FN
      DO10J=2,LIM
10    P(L+1,J)=P(L,J-1)-AA*P(L,J)-BB*P(L-1,J)
C  GET POLY VALUE
      DO11M=1,N
11    PV(L+1,M)=(X(M)-AA)*PV(L,M)-BB*PV(L-1,M)
C  GET NUM,DEN FOR AA,BB,T
      PMS=PS
      XPS=0
      PS=0
      YPS=0
      DO12I=1,N
      XPS=XPS+X(I)*PV(L+1,I)*PV(L+1,I)
      PS=PS+PV(L+1,I)*PV(L+1,I)
12    YPS=YPS+Y(I)*PV(L+1,I)
C  GET AA,BB
      AA=XPS/PS
      BB=PS/PMS
C  GET FOURIER COEFFS
      T(L+1)=YPS/PS
C  ADD NEW TERMS TO COEFF ARRAY
      DO41I=1,LIM
C  REMEMBER OLD ARRAY
      OA(I)=A(I)
```

```
41    A(I)=A(I)+T(L+1)*P(L+1,I+1)
C  GET SIGMASQD
      SUM=0.
      DO42I=1,N
      CALL POLVAL(L,A,X(I),YY)
      YIMYY=Y(I)-YY
42    SUM=SUM+YIMYY*YIMYY
C  GET RMS DEV
      RDEV=SQRT(SUM/(N))
      IF(II.EQ.1)GOTO43
      IF(L-2)43,43,44
44    IF(RDEV-STR)43,43,50
43    STR=RDEV
      GOTO20
C  WRITE OUTPUT
 50   CONTINUE
C     CALL OUT(STR,L-1,OA,N,1)
      L=L-1
      RDEV=STR
      DO52I=1,21
52    A(I)=OA(I)
      RETURN
 51   CONTINUE
C     CALL OUT(RDEV,L-1,A,N,2)
      L=L-1
      RETURN
      END
C  OUT:  NEWPOL'S OUTPUT ROUTINE
      SUBROUTINE OUT(RMS,L,A,N,IFL)
      DIMENSION A(21)
      LN=L+1
      WRITE(9,61)L,N,RMS
61    FORMAT(1H ,5X,'POLYNOMIAL FIT TO DATA POINTS'///10X,
     -  'ORDER OF POLYNOMIAL : ',I2//10X,'NUMBER OF POINTS :',
     -  I3//10X,'RMS DEVIATION :',E14.6//)
      GOTO(62,63),IFL
62    WRITE(9,64)
64    FORMAT(1H ,9X,'MINIMUM ERROR REACHED'//)
      GOTO65
63    WRITE(9,66)
66    FORMAT(1H ,9X,'MAXIMUM SIZE REACHED'//)
65    DO67I=1,LN
67    WRITE(9,68)I,A(I)
68    FORMAT(1H ,15X,I2,2X,E13.6)
      WRITE(9,69)
69    FORMAT(1H /////)
      RETURN
      END
```

```
C
C  POLVAL:  GIVEN X, OF NPOLY'TH ORDER
C        POLYNOMIAL, GETS Y
C
      SUBROUTINE POLVAL(NPOLY,COEFF,X,Y)
      DIMENSION COEFF(21)
      N=NPOLY+1
      Y=COEFF(1)
      DO 1 I=2,N
1     Y=Y+COEFF(I)*X**(I-1)
      RETURN
      END
C
C  REMCON:  REMOVES CONTINUUM BY G.I. THOMPSON CONVOLUTION
C
      SUBROUTINE REMCON(S,C,IW,JLEN)
      REAL S(512),C(512)
C  TEST FOR IW EVEN
      TEST=FLOAT(IW)/2.-FLOAT(IW/2)
      IF(TEST.EQ.0.)GOTO69
C  SET L,R LIMITS
      IGM=IW/2
      IGS=IW+IGM
      ILL=IW*2
      IRL=JLEN-ILL
C  ZERO OUTPUT ARRAY
      CALL UZERO(C,JLEN)
C  CONVOLVE
      DO61I=ILL,IRL
      DO63K=1,IW
      C(I)=C(I)-0.5*S(I-IGS+K-1)
      C(I)=C(I)+S(I-IGM+K-1)
63    C(I)=C(I)-0.5*S(I+IGM+K)
61    CONTINUE
      RETURN
69    WRITE(6,70)
70    FORMAT(1H //1X,'WIDTH PARAMETER FOR REMCON MUST BE ODD'//)
      STOP
      END
C
C     CORCON: CONVOLVES CORRELATING FUNCTION
C
      SUBROUTINE CORCON(C,IW,ILO,IHI,JLEN)
      REAL C(512),D(512)
      DATA D/512*0./
C     TEST FOR IW EVEN
      TEST=FLOAT(IW)/2.-FLOAT(IW/2)
      IF(TEST.EQ.0.)GOTO69
```

```
C     SET L,R LIMITS
      IGM=IW/2
      IGS=IW+IGM
      ILX=IW*2
      IRX=JLEN-ILX
      ILL=ILO-IGS
      IF(ILL.LT.ILX)ILL=ILX
      IRL=IHI+IGS
      IF(IRL.GT.IRX)IRL=IRX
C     CONVOLVE..
      DO61I=ILL,IRL
      DO63K=1,IW
      D(I)=D(I)-0.5*(C(I-IGS+K-1))
      D(I)=D(I)+(C(I-IGM+K-1))
 63   D(I)=D(I)-0.5*(C(I+IGM+K))
 61   CONTINUE
      NMOV=IRL-ILL+1
      CALL UMOVE(D(ILL),C(ILL),NMOV)
      NCLE=NMOV-1
      ITO=ILL+1
      D(ILL)=0.
      CALL UMOVE(D(ILL),D(ITO),NCLE)
      RETURN
 69   WRITE(6,70)
 70   FORMAT(1H //1X,'WIDTH PARAMETER FOR CORCON MUST BE ODD'//)
      STOP
      END
C
C     ZEDPLT: PLOTS SPECTRUM, IDENTIFYING 4000 FEATURE
C
      SUBROUTINE ZEDPLT
      COMMON /HART/XO,WO,A
      COMMON /PLOT/SPECN,XZED,XRMS,POSN,ID,XPLOT,YPLOT,
     -  WAV,NFEAT,BSTP,BVAL,JLEN
      REAL SPECN(512),XPLOT(15),YPLOT(15),WAV(20)
      CALL SETXY(552.,500.)
      CALL TOXY(552.,100.)
      CALL TOXY(40.,100.)
      CALL TOXY(40.,500.)
      Y=SPECN(1)*400.+100.
      CALL SETXY(41.,Y)
      CONST=512./FLOAT(JLEN)
      DO12I=2,JLEN
      X=40.+FLOAT(I)*CONST
      Y=SPECN(I)*400.+100.
      IF(Y.LT.0.)Y=0.
      IF(Y.GT.500.)Y=500.
 12   CALL TOXY(X,Y)
```

```
C
C     PLOT CUTOFF POSITION
C
      CUTPOS=POSN*CONST+40.
      CALL SETXY(CUTPOS,500.)
      CALL TOXY(CUTPOS,100.)
C
C     TAG ALL FEATURES
C
      ZP=1.+XZED
      DO15I=1,NFEAT
      WSH=WAV(I)*ZP
      XSH=X0-A/(WSH-W0)**1.2
      XPOS=POSN-XSH*125.
      XPOS=XPOS*CONST+40.
      CALL SETXY(XPOS,500.)
 15   CALL TOXY(XPOS,450.)
C
C     TAG B WAVELENGTH
C
      BPOS=BSTP*CONST+40.
      CALL SETXY(BPOS,100.)
      CALL TOXY(BPOS,130.)
      CALL SETXY(BPOS,80.)
      CALL HPLOTS('B')
C
C     PLOT CORRN AROUND FEATURE 1
C
      CMIN=1.E20
      CMAX=0.
      DO19I=1,15
      IF(YPLOT(I).LT.CMIN)CMIN=YPLOT(I)
      IF(YPLOT(I).GT.CMAX)CMAX=YPLOT(I)
 19   CONTINUE
      CRAN=CMAX-CMIN
      CMUL=50./CRAN
      ZP=1.+XPLOT(1)
      WSH=WAV(1)*ZP
      XSH=X0-A/(WSH-W0)**1.2
      XPOS=POSN-XSH*125.
      XPOS=XPOS*CONST+40.
      YPLT=500.-CMUL*(CMAX-YPLOT(1))
      CALL SETXY(XPOS,YPLT)
      DO20I=2,15
      ZP=1.+XPLOT(I)
      WSH=WAV(1)*ZP
      XSH=X0-A/(WSH-W0)**1.2
      XPOS=POSN-XSH*125.
```

```
      XPOS=XPOS*CONST+40.
      YPLT=500.-CMUL*(CMAX-YPLOT(I))
 20   CALL TOXY(XPOS,YPLT)
C
C     DETAILS AROUND THE PICTURE
C
      CALL SETXY(30.,540.)
      CALL JTYPEN(ID,11)
      CALL SETXY(200.,540.)
      CALL HTEXT(4,'Z = ')
      CALL TYPNMB(XZED,1.,3.)
      CALL SETXY(350.,540.)
      CALL HTEXT(5,'RMS: ')
      CALL TYPNMB(XRMS,0.,3.)
      CALL SETXY(30.,10.)
      CALL HTEXT(4,'B = ')
      CALL TYPNMB(BVAL,5.,1.)
      CALL ADVFLM
      RETURN
      END
C
C  MOVAV:  GETS MOVING AVERAGE OF A SPECTRUM, SLIT N STEPS WIDE
C
      SUBROUTINE MOVAV(SPECT,N,JLEN)
      REAL SPECT(512),SPEC(512)
      TOT=0.
      DO10I=1,N
 10   TOT=TOT+SPECT(I)
      TS=TOT/FLOAT(N)
      DO11I=1,N
 11   SPEC(I)=TS
      M=N+1
      DO20I=M,JLEN
      TOT=TOT-SPECT(I-N)
     -  +SPECT(I)
 20   SPEC(I)=TOT/FLOAT(N)
      CALL UMOVE(SPEC(1),SPECT(1),JLEN)
      RETURN
      END
```

Appendix B

Method of variation of parameters

The following technique has been found to be very useful for curve fitting to sets of data points which should lie on a curve given by a known function. It can provide a better fit than a polynomial fit, and can sometimes even produce a fit where a polynomial fit breaks down.

To apply this method we need:

(i) a function the data are supposed to fit

(ii) a first approximation to the variable parameters of the function

(iii) the data points

We use enough data points to obtain the parameters giving the best fit to the data, by minimising the mean square deviation between the values calculated and the values in the data.

The technique has been applied to fit the dispersion curve of the UKSTU thin prism, using the Hartmann formula, and has also been used to calculate the best-fit parameters for a polynomial transformation. To describe the technique, we take this as an example.

We consider only one co-ordinate; the procedure for the other is identical.

The assumed transformation is

$$u = f(x) + g(y)$$

where f and g are polynomials; we assume second order here. These are then given by

$$f(x) = a + bx + cx^2$$

$$g(y) = d + ey + fy^2$$

We wish to determine a, b, c, d, e, f from the data, and so first need an approximation (we can put a: = a + d)

$$u \approx a' + b'x + c'x^2 + e'y + f'y^2$$

These parameters for the first approximation are calculated by simply solving five linear equations from five data points.

We then assume errors in a', b', etc. such that

$$a = a' + \Delta a$$
$$b = b' + \Delta b \quad \text{etc.}$$

Where a, b, ... are values for the 'best fit'.

For the best fit solution we then have

$$u = (a' + \Delta a) + (b + \Delta b)x + (c + \Delta c)x^2 + (e + \Delta e)y + (f + \Delta f)y^2$$

and for data point (u_i, x_i, y_i) the deviation from this solution is

$$S_i = (a' + \Delta a) + (b' + \Delta b)x_i + (c' + \Delta c)x_i^2 + (e' + \Delta e)y_i + (f' + \Delta f)y_i^2 - u_i ;$$

the mean square deviation for all data points is then

$$S = \frac{1}{i} \sum_i (S_i)^2 \qquad (1)$$

and we wish to minimise this w.r.t. Δa, Δb, ...

i.e. $\frac{\partial S}{\partial \Delta a} = 0$, $\frac{\partial S}{\partial \Delta b} = 0$, ...

Now S_i can be written

$$S_i = \Delta a + \Delta b x_i + \Delta c x_i^2 + \Delta e y_i + \Delta f y_i^2 + (a' + b'x_i + c'x_i^2 + e'y_i + f'y_i^2 - u_i) \qquad (2)$$

and differentiating (1) we get

$$\frac{\partial S}{\partial \Delta a} = \frac{1}{i} \sum 2(S_i) = 0$$
$$\frac{\partial S}{\partial \Delta b} = \frac{1}{i} \sum 2(S_i)(x_i) = 0$$
$$\frac{\partial S}{\partial \Delta c} = \frac{1}{i} \sum 2(S_i)(x_i^2) = 0$$
$$\frac{\partial S}{\partial \Delta e} = \frac{1}{i} \sum 2(S_i)(y_i) = 0$$
$$\frac{\partial S}{\partial \Delta f} = \frac{1}{i} \sum 2(S_i)(y_i^2) = 0$$

Omitting the constant terms, and writing the expression parentheses in (2) above as C_i, we have

$$\Delta a \sum_i 1 + \Delta b \sum_i x_i + \Delta c \sum_i x_i^2 + \Delta e \sum_i y_i + \Delta f \sum_i y_i^2 + \sum_i C_i = 0$$
$$\Delta a \sum_i x_i + \Delta b \sum_i x_i^2 + \Delta c \sum_i x_i^3 + \Delta e \sum_i x_i y_i + \Delta f \sum_i x_i y_i^2 + \sum_i C_i x_i = 0$$
$$\Delta a \sum_i x_i^2 + \Delta b \sum_i x_i^3 + \Delta c \sum_i x_i^4 + \Delta e \sum_i x_i^2 y_i + \Delta f \sum_i x_i^2 y_i^2 + \sum_i C_i x_i^2 = 0$$

$$\Delta a \sum_i y_i + \Delta b \sum_i x_i y_i + \Delta c \sum_i x_i^2 y_i + \Delta e \sum_i y_i^2 + \Delta f \sum_i y_i^3 + \sum_i C_i y_i = 0$$

$$\Delta a \sum_i y_i^2 + \Delta b \sum_i x_i y_i^2 + \Delta c \sum_i x_i^2 y_i^2 + \Delta e \sum_i y_i^3 + \Delta f \sum_i y_i^4 + \sum_i C_i y_i^2 = 0$$

which is a set of linear equations that can be solved for Δa, Δb, Δc, Δe, and Δf. These variations are then applied to the first approximations to obtain a, b, c, e, and f.

It is to be noted that many of the coefficients in the linear equations appear more than once, which reduces the amount of calculation required.

Appendix C

Papers published or in preprint form.

1 J.A. Cooke, D. Emerson, K. Nandy, V.C. Reddish, M.G. Smith (1977) MNRAS 178,687

2 K. Nandy, V.C. Reddish, K.P. Tritton, J.A. Cooke, D. Emerson (1977) MNRAS 178,63P

3 B.D. Kelly, J.A. Cooke, D. Emerson (1980a) Observatory 100,76

4 B.D. Kelly, J.A. Cooke, D. Emerson (1980b) preprint

5 J.A. Cooke, D. Emerson, B.D. Kelly, H.T. MacGillivray, R.J. Dodd (1980) preprint

Mon. Not. R. astr. Soc. (1977) 178, 687–691

Radial velocities of faint galaxies from objective prism plates

J. A. Cooke and D. Emerson *Department of Astronomy, University of Edinburgh, Blackford Hill, Edinburgh EH9 3HJ*

K. Nandy and V. C. Reddish *Royal Observatory, Blackford Hill, Edinburgh EH9 3HJ*

M. G. Smith *Cerro Tololo Inter-American Observatory, La Serena, Chile*

Received 1976 June 28

Summary. A method of obtaining radial velocities of faint galaxies from low-dispersion objective prism spectra is described, and preliminary results are presented. The highest radial velocity measured corresponds to $z \sim 0.15$.

1 Introduction

The object of this note is to investigate the possibility of obtaining the redshifts of faint galaxies from low-dispersion objective prism spectra. Direct and objective prism plates were taken with the Curtis Schmidt telescope of the Cerro Tololo Inter-American Observatory. The prism has a dispersion of 1400 Å/mm at Hγ (Blanco 1974). Smith (1975) has pointed out that on these plates galaxies can readily be distinguished from stars. An area 5 cm (1.4 degrees) square on a plate centred at $12^h\ 40^m$, $-4°$ was searched down to the plate limit, both on the direct and prism plates, for galaxies. About 120 non-stellar objects were found on the prism plate and their spectra traced with a microdensitometer. All spectra with peak densities less than about 0.2 above the sky density level were then rejected from the sample, being too faint to show clearly spectral features. This left about 60 objects, and redshifts were obtained for 29 of them having identifiable absorption features. Redshifts were also obtained for five objects from the catalogue of Zwicky, Herzog & Wild (1961) in the northern half of the plate.

2 Method of obtaining redshifts

Redshifts were obtained by using the green cut-off of the IIIaJ emulsion as a wavelength standard, and the observable features in the galaxy spectra. The emulsion cut-off (λ_c) for the area under study was found by fitting a dispersion curve to five stars with well defined lines or blends, and to the published dispersion curve for the Curtis Schmidt prism (Blanco 1974). The value obtained is $\lambda_c = 5360 \pm 30$ Å.

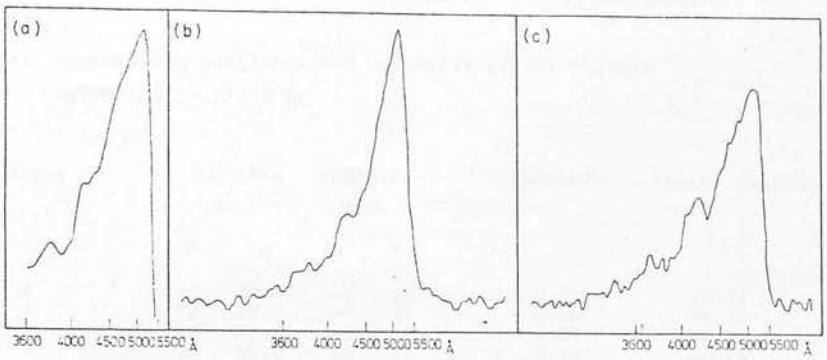

Figure 1. (a) Mean E-S0 energy distribution modified to correspond to the dispersion of the Curtis Schmidt prism. (b) Low-dispersion spectrum of galaxy No. 1 in Table 1, from the prism plate. (c) Low-dispersion stellar spectrum from the prism plate.

Pence (1976) has given energy distributions for galaxies of different types; Fig. 1(a) shows Pence's spectrum for a galaxy of type E-S0 modified to correspond to the varying dispersion of the prism. One feature stands out in the distribution for E-S0 galaxies; a sharp drop in intensity at about 4000 Å. This feature is sufficiently large to show up in our low-dispersion spectra; an example is given in Fig. 1(b). The same feature shows up well in low-resolution spectral scans of late-type stars (Fay, Stein & Warren 1974); an example of a stellar spectrum from our plate is given in Fig. 1(c). The consistency in position of the λ 4000 feature relative to λ_c over the area under study, and for a range of magnitudes, was checked using about 30 late-type stars. No systematic effect with magnitude or position on the plate was found. The wavelength of the λ 4000 feature was calculated from the above value of λ_c; assuming zero error in λ_c, $\lambda_0 4000 = 4010 \pm 30$ Å. An additional feature, a small dip in intensity at about 4200 Å appears in many of the late-type stars – *cf.* Fig. 1(c) – and in most of the 29 galaxies measured. This feature was treated in the same way for a sample of about 20 stars, giving $\lambda_0 4200 = 4280 \pm 40$ Å.

The positions of the green cut-off and the λ 4000 feature were defined by the mid-points in density on the tracings; strictly the mid-points in intensity should be used to avoid any effects due to the image size on the plate. The error introduced by using density instead of intensity is small due to the steep plate cut-off and the much smaller height of the λ 4000 feature, as compared to other errors in the positions of the features.

Redshifts were obtained by measurement from the densitometer tracings of the cut-off and the λ 4000 feature. The position of the λ 4200 feature which corresponds to the position of the *G* band in stellar spectra was also measured, and using the redshift obtained from the λ 4000 feature, the rest wavelength, λ_0, of the λ 4200 feature was calculated, as a check on systematic error. For redshifts less than $\log cz = 4.4$ no correlation in $\lambda_0 4200$ with $\log cz$ was found, but for $\log cz$ greater than 4.4 the values of $\lambda_0 4200$ were consistently low. This is probably caused by the λ 4000 feature becoming very low in density and thus the definition of the position of λ 4000 becoming uncertain, whereas the λ 4200 feature, as a dip, has its position well defined although the actual scatter in its rest wavelength is larger than that of the λ 4000 feature. Thus for $\log cz$ greater than 4.4 the redshift given is that obtained using the λ 4200 feature only, with error in z estimated to be ± 0.02. For $\log cz$ less than 4.4 the mean of values obtained from both features is used, with a smaller error in z, apart from two exceptions where the λ 4000 feature is poorly defined. The value of the rest wavelength of the λ 4200 feature obtained for the galaxies is $\lambda_0 4200 = 4220 \pm 60$ Å, as compared to the value, mentioned above, of 4280 ± 40 Å for the stars.

Table 1.

(a) Approximate positions and redshifts of the objects appearing in plate I.

Galaxy	Position (1950.0) RA h	m	DEC °	′	Redshift	Baker density
1	12	39.7	-5	30	0.02 *	+0.21
2	12	39.7	-5	31	0.00 *	+0.50
3	12	39.6	-5	25	0.05 *	-0.43
4	12	38.6	-5	27	0.14	-0.65
5	12	38.3	-5	31	0.11	-0.61
6	12	38.3	-5	32	0.04 *	-0.33
7	12	38.8	-5	23	0.04 *	-0.35
8	12	38.4	-5	10	0.07 *	-0.69
9	12	37.7	-5	03	0.13	-0.43
10	12	39.5	-4	52	0.08 *	-0.57
11	12	38.6	-4	55	0.13	-0.83
12	12	38.1	-4	49	0.11	-0.80
13	12	38.0	-4	52	0.00 *	+0.80
14	12	38.0	-4	55	0.10	-0.50
15	12	35.8	-4	52	0.14	-0.90
16	12	39.4	-4	36	0.08 *	-0.63
17	12	39.0	-4	32	0.06	-0.35
18	12	39.0	-4	35	0.14	-1.02
19	12	38.7	-4	44	0.01	+0.78
20	12	37.5	-4	42	0.11	-0.72
21	12	37.0	-4	40	0.07 *	-0.38
22	12	36.8	-4	36	0.03 *	-0.11
23	12	36.9	-4	25	0.10	-0.86
24	12	36.3	-4	21	0.09	-0.83
25	12	36.0	-4	18	0.11	-0.53
26	12	35.7	-4	30	0.07 *	-0.08
27	12	35.1	-4	27	0.15	-0.74
28	12	34.9	-4	29	0.07	-0.30
29	12	34.7	-4	17	0.11	-0.42

(b) Objects from Zwicky et al (1961) with measured redshifts.

Position (1950.0) RA h	m	DEC °	′	Redshift	Baker density
12	43.3	-1	24	0.03 *	+0.01
12	45.3	-1	22	0.00 *	+0.80
12	32.9	-2	03	0.02 *	+0.10
12	33.3	-2	07	0.01 *	+0.17
12	40.6	-1	09	0.03 *	-0.05

* obtained using both the 4000 Å and 4200 Å features.

3 Results

A list of the objects for which redshifts have been obtained is given in Table 1; the area studied is shown in Plate 1 with the objects identified.

Baker (1949) found a function of transmission on a photographic plate that is approximately linear with magnitude; it is defined as $B = \log(1/T - 1)$, where T is the transmission. This is found to be fairly well correlated with magnitude over a limited range, for objects from Zwicky *et al.* (1961), but there are no accurate magnitudes of faint objects to extend the relation between Baker density and magnitude. It seems meaningless to extrapolate the

relation linearly, as the brighter objects are only being partially sampled by the densitometer slit, and the fainter objects will be over sampled in comparison with the Zwicky objects. As no accurate magnitude calibration is available, Baker density instead of magnitude is plotted as the abscissa in Fig. 2. Three of the objects in Table 1 do not appear, their redshifts being too small. The rms scatter in Fig. 2 is $\sim \pm 0.03$ in z.

The mean magnitude and redshift for the four Zwicky objects appearing in Fig. 2 are $\bar{m}_{Zw} = 15.4$ and $\bar{z} = 0.023$ ($\log c\bar{z} = 3.83$). The magnitude of the galaxies with the largest redshifts can be assessed in the following way: if these are for very distant giant ellipticals with $M_B = -23$, then for $\log cz = 4.65$, $m_B = 17.5$ is obtained from values given in Sandage & Tammann (1975). Smith (1975) quotes the limiting blue magnitude for thin prism plates on the Curtis Schmidt as 18.

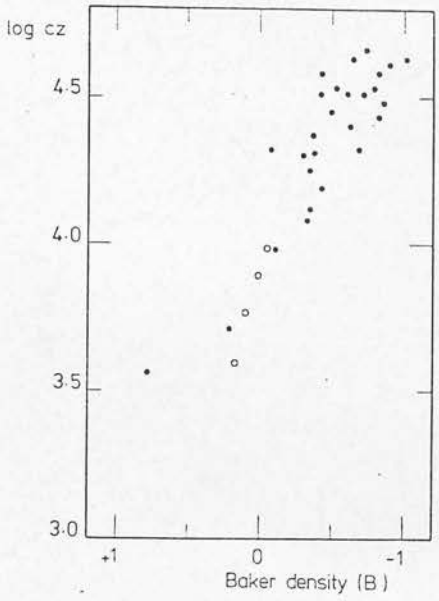

Figure 2. Redshift plotted against Baker density at $\lambda = 4400$ Å. Circles indicate objects from Zwicky *et al.* (1961).

4 Discussion

One difficulty with the method is apparent: the λ 4000 feature on its own is not completely unambiguous for faint objects. It would be possible, for example, to confuse it with a similar feature occurring at a different wavelength in a spectrum of a faint star, and it is, therefore, essential to ascertain that only galaxies are being measured.

The angular size of the galaxy, together with the seeing, determines the effective resolving power of the prism; thus no redshifts can be obtained for large nearby galaxies. For large redshifts the method is limited by the movement of the features used beyond the plate cut-off, and more fundamentally by the low dispersion of the prism in the red.

The 4000 Å feature is present in ellipticals and in the nuclear bulge of spiral galaxies. The possibility of detecting this feature in spirals depends on the ratio of the nuclear bulge to the disc, but the integrated spectra of Wells (1972) suggest that it should be detectable in spirals as late as Sb. Very late type galaxies, however, show strong emission lines which can be used to determine redshifts; several galaxies with emission features are present in our sample, but

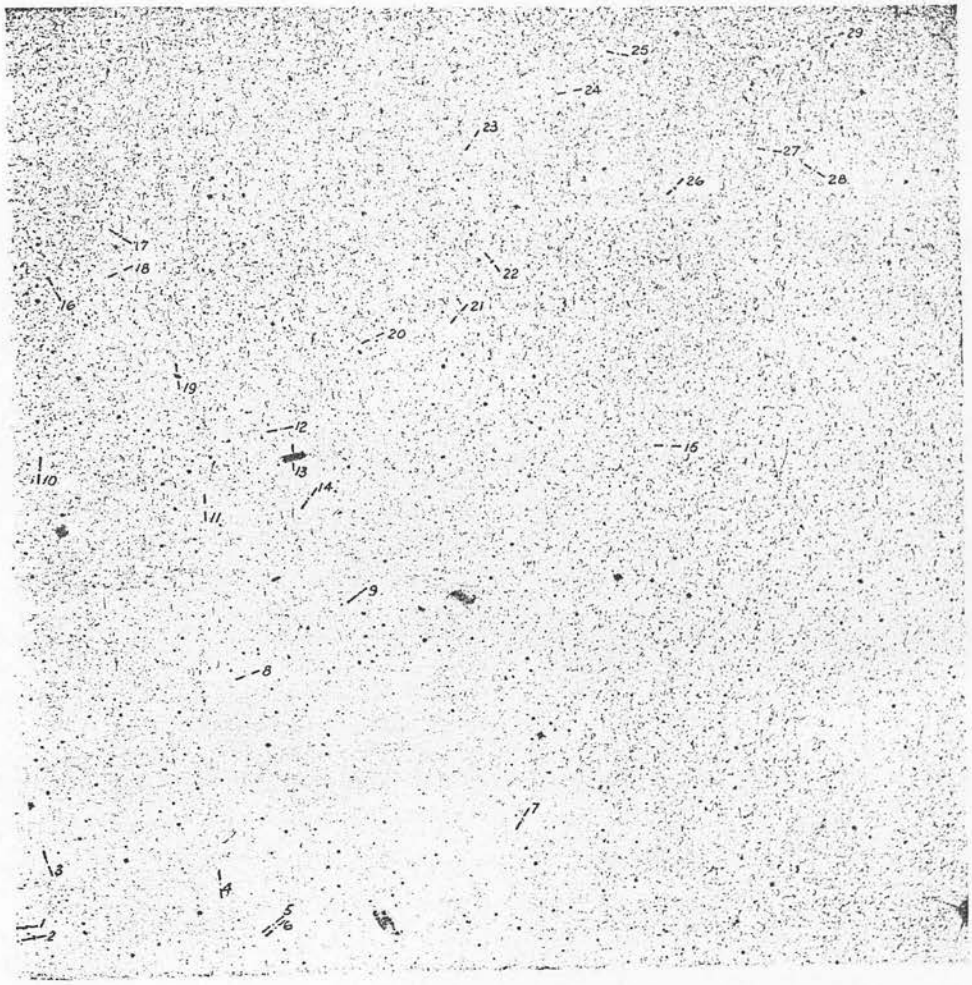

Plate 1.

[*facing page* 690]

for the present paper we have confined ourselves to measuring redshifts from absorption features. Many of the remaining relatively bright galaxies which show no definite 4000 Å feature are probably Sbc and Sc type galaxies.

Acknowledgments

One of the authors (JAC) wishes to thank the SRC for a research studentship.

References

Baker, E. A., 1949. *Publ. R. Obs. Edinburgh*, 1, 15.
Blanco, V. M., 1974. *Publ. astr. Soc. Pacific*, 86, 841.
Fay, T. D., Stein, W. L. & Warren, W. H., 1974. *Publ. astr. Soc. Pacific*, 86, 772.
Pence, W., 1976. *Astrophys. J.*, 203, 39.
Sandage, A. & Tammann, G. A., 1975. *Astrophys. J.*, 197, 265.
Smith, M. G., 1975. *Astrophys. J.*, 202, 591.
Wells, D. C., 1972. *PhD thesis*, University of Texas.
Zwicky, F., Herzog, E. & Wild, P., 1961. *Catalogue of galaxies and of clusters of galaxies*, California Institute of Technology.

Mon. Not. R. astr. Soc. (1977) 178, *Short Communication*, 63P–66P

Low-dispersion objective prism spectra from the UK 1.2-m Schmidt telescope

K. Nandy, V. C. Reddish, K. P. Tritton *Royal Observatory, Blackford Hill, Edinburgh EH9 3HJ*

J. A. Cooke and D. Emerson *Department of Astronomy, University of Edinburgh, Blackford Hill, Edinburgh EH9 3HJ*

Received 1976 December 20

Summary. The new thin objective prism for the UK 1.2-m Schmidt telescope has a dispersion of 2480 Å/mm at Hγ and 3515 Å/mm at Hβ. The dispersion curve is given; several features in the spectra of late-type stars are resolved and a method of spectral classification is described.

Introduction

The new thin prism, specified by one of us (VCR) and manufactured by Sir Howard Grubb-Parsons & Co. Ltd in the UK, has a diameter of 1.26 m, with an apex angle of [redacted]; it is made of Schott BK7 glass and has a high ultraviolet transmission. The first trial plates with this prism on the UK Schmidt telescope at Siding Spring were taken in 1976 July. Bolton *et al.* (1976) have reported that the unwidened spectra of stars having photoelectrically determined *B* magnitudes of 19.5 mag are readily visible on 30- and 60-min exposure IIIaJ (hypersensitized) plates, and they estimated that 60-min unwidened exposures reach beyond 20 mag. In this letter, we present results concerning the dispersion curve and the resolution of the prism. Spectral classification using this prism is also discussed.

* 44′

Observational material

Tracings taken with a Joyce Loebl microdensitometer have been obtained from UJ 2461P, an unwidened, 60-min exposure, centred on $22^h\,32^m$, $-40°$, and from UJ 2451P, a 2-min exposure widened to 0.4 mm centred on 19^h, $-60°$. Both plates have the Eastman Kodak IIIaJ emulsion; UJ 2461P was hypersensitized. Fig. 1 illustrates some sample tracings of stars in the spectral range A to M, from UJ 2451P; and the tracings of two galaxies from UJ 2461P. These galaxies are identified on the prism plate by their diffuse appearance. At the galactic latitude of plate UJ 2451P ($b \sim -25°$) the nearby B stars are overexposed. Fig. 1 shows that the hydrogen lines are resolved in A stars, and a number of features appear in the spectra of F, G and K stars. These features are in general the blends of several atomic and molecular lines, and they have been identified using the list of lines detected in the low-

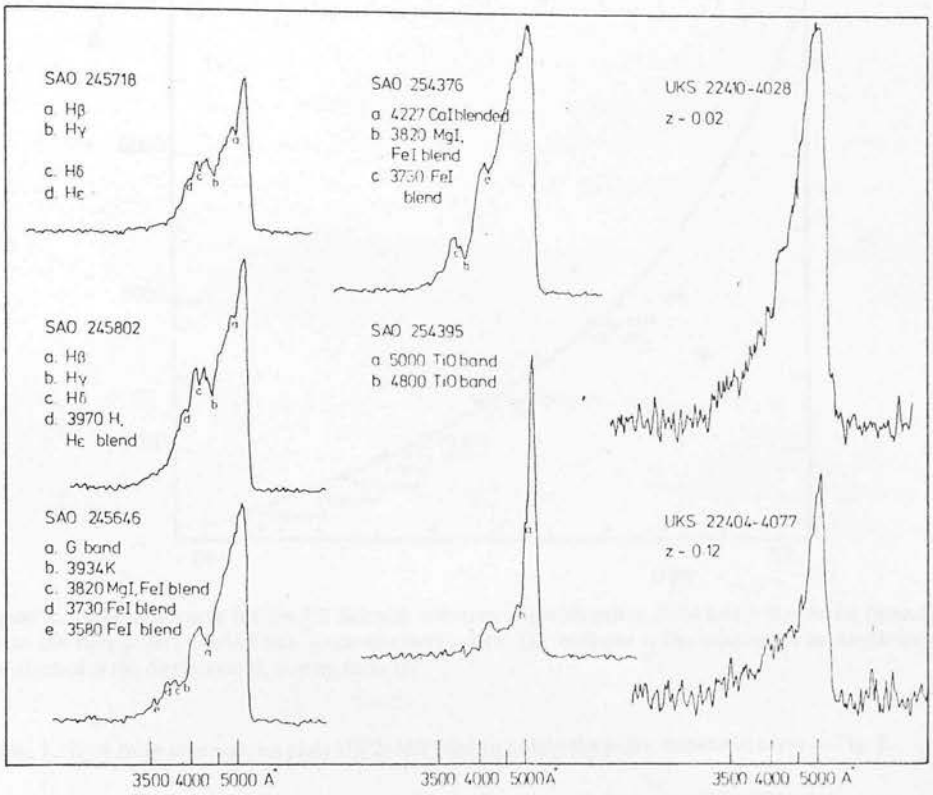

Figure 1. Examples of stellar spectra traced from plate UJ 2451 P, and two galaxies from plate UJ 2461 P. Spectral types from SAO catalogue: 245718, A2. 245802, F3; 245646, G6; 254376, K0; 254395, M2. The ordinate is density, but the scale is not constant. The redshifts of the galaxies have been determined from the position of the discontinuity at 4000 Å (Cooke *et al.* 1976).

resolution spectral scans of Fay, Stein & Warren (1974). The mean wavelength has been used for blends. The identifications of the features observed in the objective prism spectra are also given in Fig. 1.

The dispersion curve of the prism

Measurements of 35 individual lines from a total of nine stars were used to obtain the dispersion curve given in Fig. 2. The sets of lines for the stars were superimposed by eye to give the best fit to a smooth curve; all the points were used to fit a Hartmann dispersion formula by a least-squares method. The reduced data is given in Table 1; column 3 gives the mean position for each line (shown as a filled circle in Fig. 2) and column 4 shows the number of measurements of each line. Over the range of measurements the fitted curve agrees very well with the manufacturer's predicted curve, the deviation being less than the rms scatter (± 14 Å). Outside the measured range, to the red, the manufacturer's curve is given, shown by the dashed line in Fig. 2. Spectral response tails off into the ultraviolet, the spectrum having almost disappeared at 3200 Å.

Using the tracings of 19 stars, a value has also been obtained for the plate cutoff of the IIIaJ emulsion, defined as the half-maximum density point. The error in this value is derived from the scatter of this point in position, when all the sets of lines are fitted to a smooth

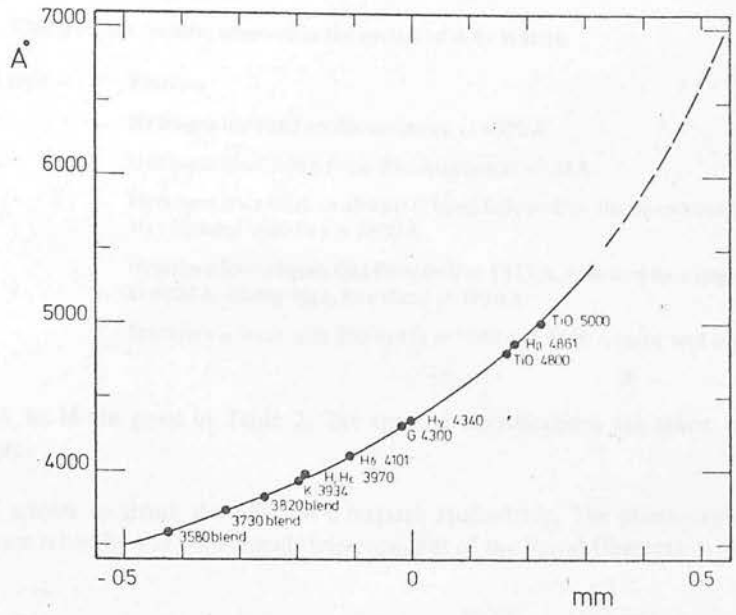

Figure 2. Dispersion curve for the UK Schmidt telescope objective prism. Solid line – Hartmann formula fit to the data points. Dashed line – manufacturer's data. The ordinate is the wavelength in Ångströms, the abscissa is the displacement, in mm, from Hγ.

Table 1. Data from nine stars on plate UK 2451 P used to obtain the prism dispersion curve in Fig. 2.

Feature	λ (Å)	x (mm)	n
TiO	5000	+0.228	1
Hβ	4861	+0.180	4
TiO	4800	+0.168	1
Hγ	4340	0.0	5
G	4300	−0.016	3
Hδ	4101	−0.106	5
H, Hε	3970	−0.184	2
K	3934	−0.196	5
Mg I, Fe I blend	3820	−0.254	4
Fe I, H_{11-14} blend	3730	−0.322	3
Fe I blend	3580	−0.422	2

λ – wavelength in Å; x – distance in mm from Hγ; n – number of measurements, from different stars.

curve. The value of the cutoff is 5380 ± 30 Å. From the measurements of the hydrogen lines observed in the spectrum of the star SAO 245718 (*cf.* Fig. 1) the spectral resolution is found to be ~ 70 Å at Hβ and ~ 40 Å at Hδ.

Spectral classification

The lines and features observed in the widened objective prism spectra enable a spectral classification of the stars to half a spectral class to be obtained by visual inspection of the tracings. The characteristic features seen in these spectra for stars in the range of spectral

Table 2. Characteristic features observed in the spectra of A to M stars.

Spectral type	Features
A	Hydrogen lines and no discontinuity at 4000 Å
F	Hydrogen lines, and a small discontinuity at 4000 Å
G	Hydrogen lines weak or absent; *G* band followed by the discontinuity at 4000 Å; Mg I blended with Fe I at 3820 Å
K	Hydrogen lines absent, Ca I (blended) at 4227 Å, followed by a large discontinuity at 4000 Å. Strong Mg I, Fe I blend at 3820 Å
M	Spectrum is short with TiO bands at 5000 and 4800 Å being well separated

types A to M are given in Table 2. The spectral classifications are taken from the SAO catalogue.

JAC wishes to thank the SRC for a research studentship. The photographs used in this work were taken by the UK Schmidt telescope unit of the Royal Observatory, Edinburgh.

References

Bolton, J. G., Cannon, R. D., Savage, A., Smith, M. G. & Tritton, K. P., 1976. IAU Symp. 74, *Radio astronomy and cosmology*, Cambridge, August 1976, in press.

Cooke, J. A., Emerson, D., Nandy, K., Reddish, V. C. & Smith, M. G., 1977. *Mon. Not. R. astr. Soc.*, 178, 687 (this issue).

Fay, T. D., Stein, W. L. & Warren, W. H., 1974. *Publ. astr. Soc. Pacific*, 86, 841.

Reprinted from *The Observatory*, Vol. 100, No. 1036, pp. 76–77
1980 June

NOTES FROM OBSERVATORIES

Simple Computer Control of a Joyce–Loebl Microdensitometer for the Measurement of Objective-Prism Spectra

By B. D. Kelly, J. A. Cooke and D. Emerson
Department of Astronomy, University of Edinburgh

Introduction. As part of a continuing programme to study faint galaxies using UK Schmidt objective-prism plates, we have a requirement for measuring individual spectra. These are[1] at a dispersion of 2480 Å/mm at *Hγ*, and are approximately 1 mm long when Eastman Kodak IIIa–J emulsion is used. Large areas of these plates have been measured with the COSMOS machine at the Royal Observatory, Edinburgh[2], and individual spectra can be extracted from these data[3]; but to trace the spectra of individual objects, as required, we have used a Joyce–Loebl microdensitometer. The application of an intensity calibration to the microdensitometer measurements is intrinsically desirable, and also allows us to compare the data with results produced by COSMOS. This implies that digitization of the tracing is necessary, and so the system described here has been developed.

Equipment and Operation. The microdensitometer is a Joyce–Loebl model Mk III CS with a lead-screw fitted to the table for x-motion, the drive being applied through a gearbox by a stepping motor. The density reading is sensed by a potentiometer operated by the system which originally moved the recording pen. The system is operated through a Commodore PET 2001 mini-computer and controlled by the user through interactive programmes. There are two modes of operation, MANUAL and SCAN. In MANUAL mode, the PET responds to the user's command to take individual steps in a specified direction, and displays the current measurement on the screen. This mode is for use when measuring a step-wedge image or when setting up and removing backlash prior to scanning a spectrum. SCAN mode drives the carriage 2 mm in a user-specified direction while storing densities in the PET memory. At the end of the scan the spectrum is displayed on the PET VDU, either on the density scale or, if required, after conversion to relative intensity. This enables the user to check the validity of the data and also to determine the wavelengths of features of interest. The original data can then be recorded on cassette tape or sent to a teletype as required.

Limitations. The measurement parameters are limited by the microdensitometer. The step size along the scan is in multiples of 6·25 microns, which corresponds to one step of the stepping motor. Density range, sample-slit size, and other microdensitometer adjustments are set as for normal use.

The system is, of course, very slow, taking typically one minute to scan one spectrum. In addition, the specimen table is currently driven only in the x-direction, so setting up on each image has to be done manually.

Measurements. Data obtained from our system and from COSMOS measurements of the same images are shown in Fig. 1. The measurements have been converted to intensity using a Baker density fit to the step-wedge, and are normalized to the same height. This comparison is interesting given that COSMOS is a slitless flying-spot machine, as opposed to the Joyce–Loebl density measurements. It can be seen that there is a progressive difference from the fainter to the brighter object, which is in the sense of COSMOS

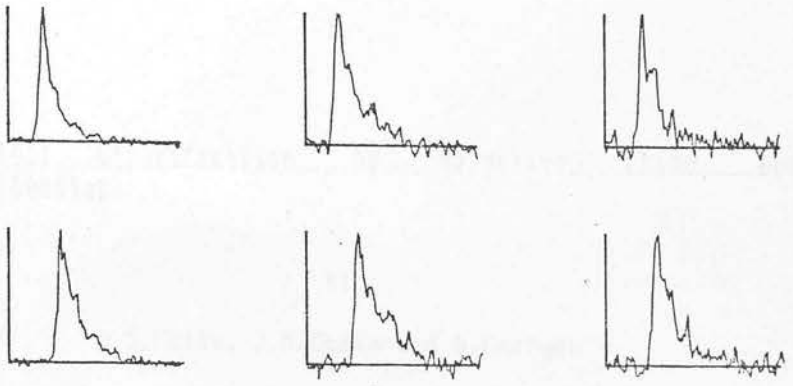

FIG. 1

Comparison of microdensitometer (upper) and COSMOS (lower) measurements of three spectra on a UKSTU objective-prism plate. The objects have peak densities above sky of 1·20 (left), 0·62 (centre) and 0·40 (right).

measurements underestimating the higher intensities. This is to be expected from the known properties of the COSMOS scanning spot[4].

The noise amplitude within each spectrum can be estimated from inspection of the adjoining sky background signal. The right-hand spectrum corresponds, in our opinion, to the faintest usable image.

Conclusion. Objective-prism spectra can be measured automatically using COSMOS, or can be scanned rather more slowly using the PDS microdensitometer at the Royal Greenwich Observatory, or the fully computerized Joyce–Loebl isodensitracer at the University Observatory, St Andrews. Our machine is designed to be a low-cost alternative to the latter two machines, and is available to us in Edinburgh.

The system has shown itself to be well suited to our needs for measurements of individual spectra, and it is particularly helpful to be able to perform the intensity conversion immediately, on-line. The system would be further improved by the addition of a stepping motor drive in the y direction, and this would probably necessitate an expansion of the PET's memory capacity (currently 8 K), to accommodate additional control software. As it stands, it is an easily constructed system, requiring little more than plugging together the various components and writing the programmes, and was assembled, excluding the microdensitometer and teletype, for under £3000.

Acknowledgements. We wish to thank the UK Schmidt Telescope Unit for its continuing perseverance in taking plates for us, the Image and Data Processing Unit of the Royal Observatory, Edinburgh, for COSMOS measurements, and the Science Research Council for a grant which enabled our system to be put together.

References

(1) K. Nandy *et al.*, *M.N.*, 178, 63P, 1977.
(2) R. S. Stobie *et al.*, *Proceedings of the International Workshop on Image Processing in Astronomy*, Trieste, 1979.
(3) J. A. Cooke, thesis, in preparation.
(4) G. E. Pickup, unpublished Ph.D. thesis, University of Edinburgh, 1979.

Printed by Sumfield & Day Ltd., Eastbourne, East Sussex, BN21 4RQ

Spectral Classification by Objective Prism and Microdensitometer

BY

B.D.Kelly, J.A.Cooke and D.Emerson

Department of Astronomy
University of Edinburgh
Blackford Hill
Edinburgh EH9 3HJ

(Received 1980)

Proofs and correspondence to Mr. H.Seddon
Royal Observatory
Blackford Hill
Edinburgh EH9 3HJ

Abstract

Microdensitometer scans of 40 stellar spectra within a one square degree area of a widened UK Schmidt objective prism plate have been compared with (B,V) photoelectric photometry of the same objects. The results imply that microdensitometry can enable spectral classification with an accuracy of one or two spectral sub-types to be carried out on these plates.

Introduction

The UK Schmidt telescope used in conjunction with the thin objective prism produces spectra with dispersion 2480 A/mm at nγ (Nandy et al., 1977). This extremely low dispersion combined with the optical qualities of the telescope and the properties of Eastman Kodak IIIaJ emulsion enables faint limiting magnitudes to be achieved whilst retaining resolution of prominent spectral features (eg. Clowes et al., 1979). The low dispersion also minimizes the problems of overlapping spectra, and so enables fainter limiting magnitudes to be reached in crowded stellar fields (Kilkenny and Kelly, in preparation). The question of using these objective prism plates for general stellar spectral classification was raised by Nandy et al., and applied by Krug et al. (1980) to a one-quarter square degree field. This latter work used an unwidened prism plate and succeeded in achieving an accuracy of one letter class down to the plate limit (B~19.5).

The present work is intended to achieve a much higher classification accuracy at the expense of a considerable loss in limiting magnitude.

Plate Material

The plate used was UJ4530P, a 40-minute exposure on hypersensitized IIIaJ, widened to 100 microns. The plate is coincident with UK Schmidt survey area 345 (22h30,-40). The seeing is estimated to be 3 arcsec.

Candidate objects were selected from a one degree square area centred at 22h23,-38 (plate 1) by using COSMOS measurements of a direct plate of area 345 (J2599) to define a practicable magnitude range, and allocating approximate spectral types to all objects within this range by visual inspection of the prism plate.

Photometry

Photoelectric (B,V) photometry of 38 of the candidate objects was carried out at SAAO during August 1979, using a 'Peoples' photometer on the 1m. telescope. Standard S-13 photomultiplier and (B,V) filters were used.(EMI 6256, 1mm. BG12

+ 4mm. GG385, 2mm. OMAG302) Colour equation and zero points were determined using E-region standards (Cousins,1973 augmented by more recent data available at SAAO).

Fig.1 shows the residuals in V and (B-V) after corrections for:

(1) a dependence of V zero-point upon Hour-angle due to instrumental problems

(2) drift in V zero point during the night

(3) colour corrections such that

$$V = v - 0.011(b-v)$$

$$(b-v)' = 0.970(b-v)$$

$$(B-V) = (b-v)' + m + c(b-v)'$$

where

$$m = -0.005,\ c = 0.019;\ (b-v)' < 0.6$$

$$m = 0.006,\ c = 0.0;\ 0.6 < (b-v)' < 0.9$$

$$m = 0.027,\ c = -0.024;\ (b-v)' > 0.9$$

Clearly, systematic errors have been held to well below 0.01.

The observed stars (plate 1) were selected from the list of candidates by using the approximate spectral types to ensure coverage of the colour range. The photometric results (table 1) show that the observed sample covers the range $13.8<V<17$, $-0.8<B-V<1.2$.

Two or more integrations were obtained for all except one of the stars; however, only nine of them were observed on two separate nights. The standard errors in an individual observation, as indicated by the repeatability of the measurements, are the same in V and (B-V) and are 0.015 ($V<15.5$,

27 stars) and 0.04 (V>15.5, 10 stars). Star no. 27 is suspect because of the following external discrepancies:

(a) The objective prism spectrum matches with spectral type F0, but the photometry indicates F5.

(b) Iris diaphragm microphotometry of a UK Schmidt direct plate measured by H.Hartl reveals no. 27 lying well away from the sequence defined by the rest of our sample.

(c) COSMOS measurements analysed by H.T.MacGillivray agree with (b).

Star 27 apart, our data should provide a useful calibration sequence for photographic photometry in this high galactic latitude field.

Star 201 lies just outside our one square degree area, but it supplies a valuable extension of our sequence towards earlier spectral types. UBV photometry of this star was kindly obtained for us by I.M.Coulson (SAAO) during November 1979.

Microdensitometry

The spectra of all the stars with photoelectric measurements were scanned using the University of Edinburgh Joyce-Loebl microdensitometer, which is controlled in digitized mode by a PET computer (Kelly et al., 1980). The measurements were recorded on magnetic cassette, and subsequently converted into relative intensities using the UK Schmidt step wedge calibration. The spectra were then scaled and plotted on a PET controlled digital plotter.

Results

The area 345 lies at galactic latitude -60. We have assumed a reddening of E(B-V)=0.06 (deVaucouleurs et al., 1976). Plate 2 lists the de-reddened (B-V) values and the corresponding main sequence spectral types listed by Johnson (1966) for an example of each spectral type in our sample. Plate 2 also shows the corresponding intensity converted, scaled microdensitometer scans, and photographs of the examples.

Plate 2 shows a clear sequence of changes in the appearance of the scans, with small but detectable differences between objects adjacent in spectral type. The classification criteria to use are, as expected, the continuum slope and the strengths of the Balmer discontinuity, 4000A discontinuity and the G-band. The photographs of the original spectra show these same properties, but interpretation of relative strengths of features tends to depend on the density of the individual image, and so much lower accuracy is attainable by direct inspection of the images, although classification by that method is much faster.

Internal Sources of Error

The intensity conversion applied to the microdensitometer measurements is clearly of central importance, given that one is classifying on the basis of the 'shape' of the resulting picture. If the intensity conversion is inadequate, the 'shape' will be a function of magnitude. We fitted the step-wedge data by a Baker density function, and had to extrapolate it considerably for the brighter objects. Fortunately we had examples of objects of similar (B-V) but differing in V by two magnitudes. No distortion was apparent when the scans of these objects were compared. However, this is obviously a problem which has to be approached with caution when spectral typing uncalibrated fields.

Discussion

The work described here deviates systematically from standard MK spectral classification in two ways. Firstly, our 'standards' are obtained from (B,V) photometry. Secondly, our criteria for spectral typing are completely different from the MK criteria. The first deviation could be corrected in future if necessary, but the second deviation is intrinsic to the nature of the very low dispersion used. The lines used for standard MK classification are not visible at this dispersion. Essentially, we are compensating for this loss of information by making use of the sensitivity of the UK Schmidt to wavelengths shorter than 4000A, and also by using the continuum slope information.

Summary

We have demonstrated a method for spectral classification at very low dispersion, and provided a set of examples which can

serve as standards. This work shows the information which can be extracted from UK Schmidt objective prism plates either at relatively faint magnitudes (14<B<17) or at brighter magnitudes in crowded fields. The technique should be valuable for statistical (number count) work and also for the detection of peculiar spectra lacking strong emission lines.

Acknowledgements

We are grateful to PATT for the allocation of observing time, to Mrs.R.M.Banfield (SAAO) who carried out the initial reductions of the photometry, and to I.M.Coulson (SAAO) for the photometry of star 201.

We wish to thank the UK Schmidt Unit for taking the photographic plates, and the COSMOS group for their measurements.

We also wish to thank the ROE photographic department for producing plates 1 and 2.

References

Clowes, R.G., Smith, M.G., Savage, A., Cannon, R.D., Boksenberg, A., & Wall, J.V. 1979. M.N.R.A.S. 189, 175.

Cousins, A.W.J. 1973. Mem.R.A.S. 77 , 223.

de Vaucouleurs,G., de Vaucouleurs,A., and Corwin,H.G. 1976. Second Reference Catalogue of Bright Galaxies.

Johnson, H.L. 1966. Ann.Rev. 4, 193.

Kelly, B.D., Cooke, J.A., & Emerson, D. 1980. Observatory. 100, 76.

Kilkenny, D., & Kelly, B.D. 1980. in preparation.

Krug, P.A., Morton, D.C., and Tritton, K.P. 1980. M.N.R.A.S. 190, 237.

Nandy, K., Reddish, V.C., Tritton, K.P., Cooke, J.A., & Emerson, D. 1977. M.N.R.A.S. 178, 63P.

Table 1. Photometry of stars indicated in plate 1. Star 201 has U-B = -1.0. Star 27 is suspect (see text).

Star	V	B-V	Star	V	B-V
2	15.12	0.67	68	15.24	0.62
3	14.60	0.86	70	15.38	1.04
12	14.57	1.34	71	16.41	0.42
19	14.72	0.53	73	14.28	1.33
20	14.73	0.40	87	14.61	0.35
27	(15.31)	(0.54)	88	14.98	0.53
42	13.47	0.92	91	14.55	1.18
44	14.62	0.65	92	14.46	0.11
45	13.62	0.96	101	17.07	0.78
46	15.50	0.57	102	16.21	1.50
47	14.95	0.65	103	16.73	0.99
48	15.00	0.64	104	16.89	0.69
53	14.70	0.66	105	15.74	0.88
54	14.02	1.10	106	15.99	0.66
55	14.20	0.87	107	16.64	0.92
56	14.85	0.77	108	16.94	0.42
57	14.48	0.72	109	16.05	0.76
58	14.19	1.15	110	15.35	1.12
66	13.91	0.82	201	14.88	-0.22 *
67	14.91	0.67			

Figure captions

Fig. 1 Residuals in (B-V) and V for the E region standards used. Each point represents an individual observation. The residuals are in the sense (Cousins) minus (present work).

Plate captions

Plate 1 Finding chart for the stars in table 1.

Plate 2 The sequence of spectral type standards. Features indicated are: a - $H\beta$; b - $H\gamma$; c - H_∞ ; d - G band; e - 4000Å discontinuity; f - CaI 4227Å (blended).

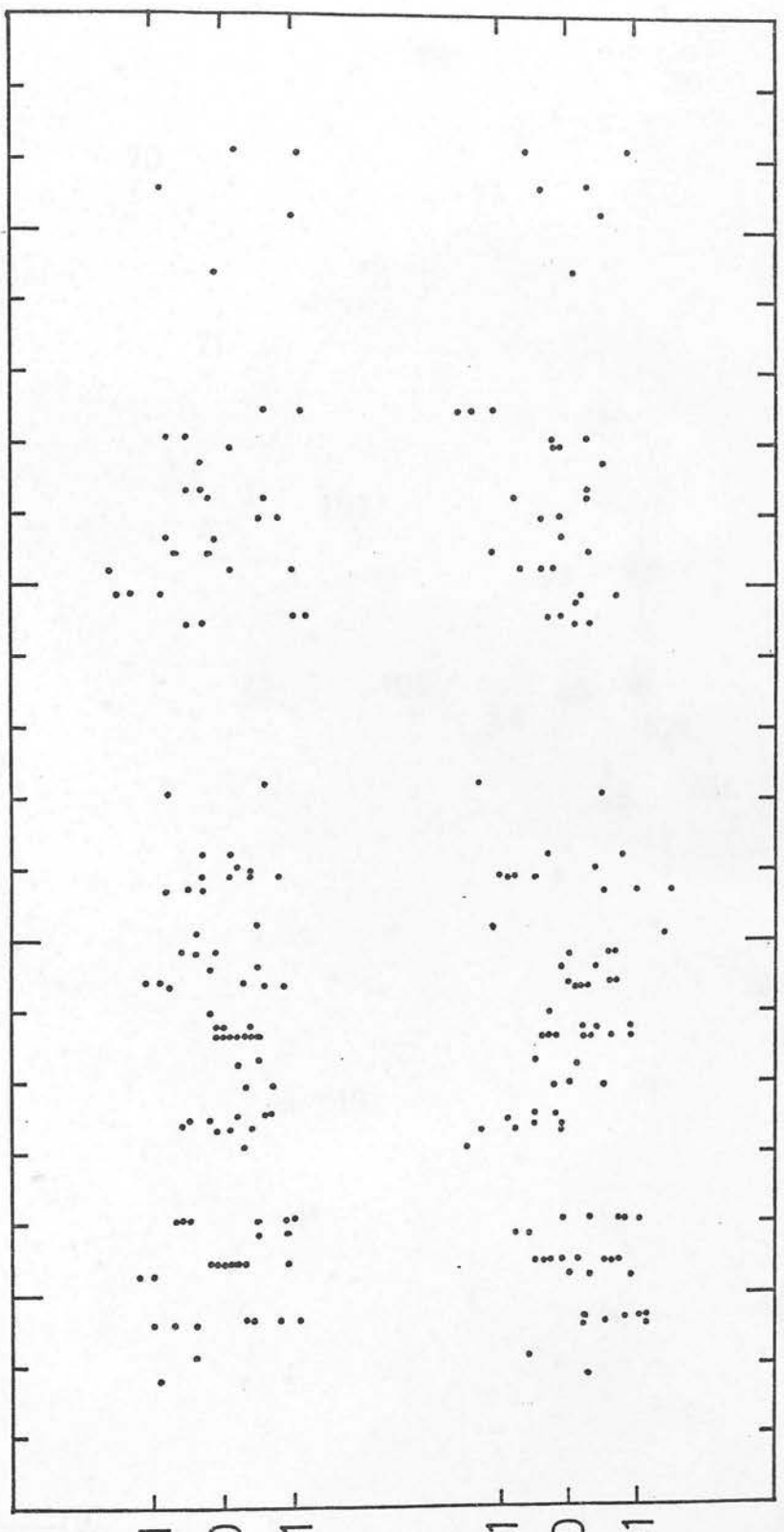

fig. 1

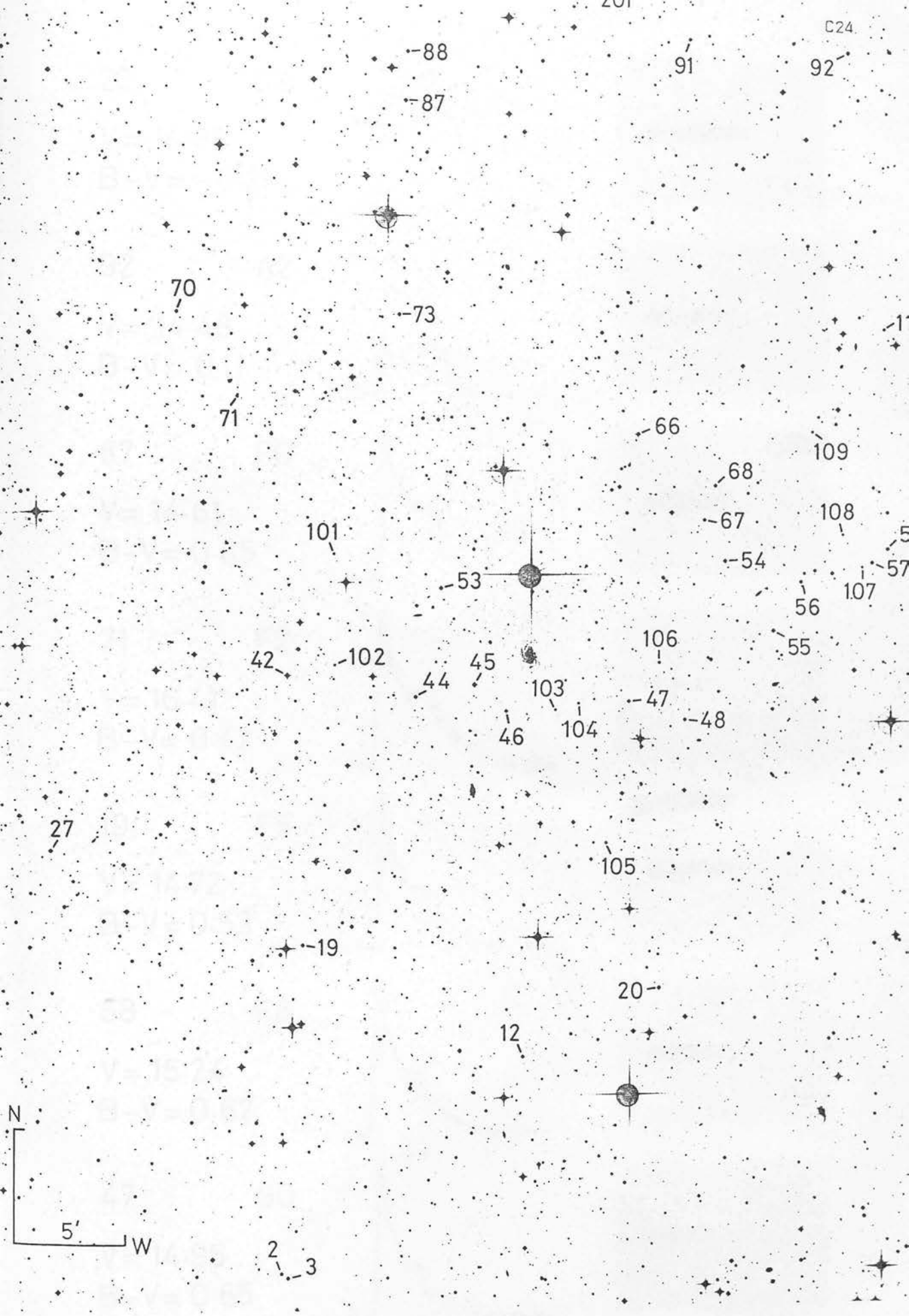
C24
88
87
91
92
70
73
71
66
109
68
67
108
101
54
53
57
107
56
55
106
42
102
45
44
103
47
48
46
104
27
105
19
20
12
N
5'
W
2
3

Plate 1

201 B2

V = 14·88
B–V = –0·22

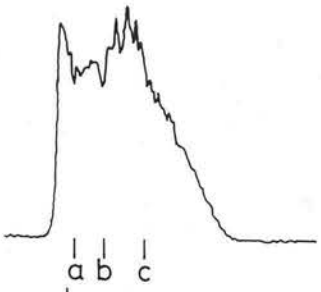

92 A2

V = 14·46
B–V = 0·11

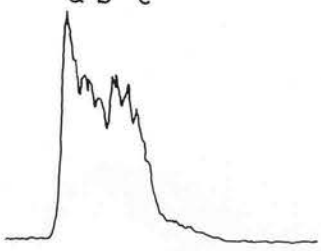

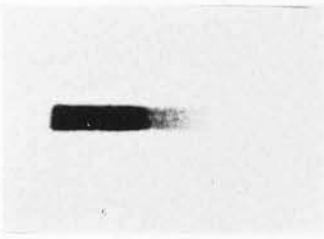

87 F0

V = 14·61
B–V = 0·35

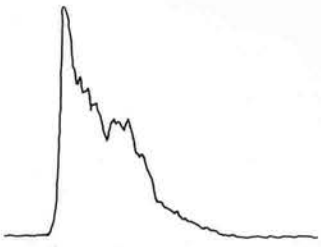

71 F2

V = 16·41
B–V = 0·42

19 F5

V = 14·72
B–V = 0·53

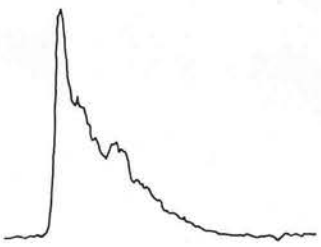

68 F8

V = 15·24
B–V = 0·62

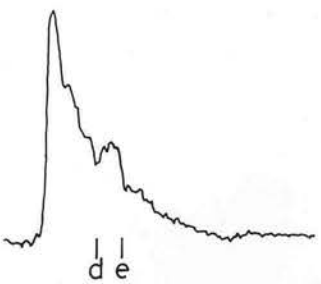

47 G0

V = 14·95
B–V = 0·65

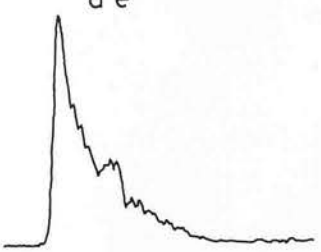

104 G2

V = 16·89
B–V = 0·69

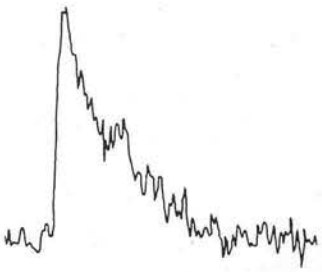

56 G8

V = 14·85
B–V = 0·77

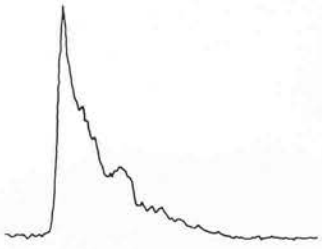

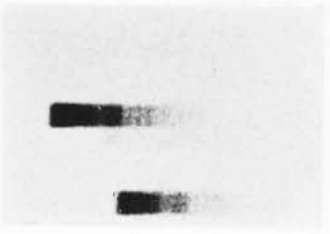

57 K0

V = 14·48
B–V = 0·92

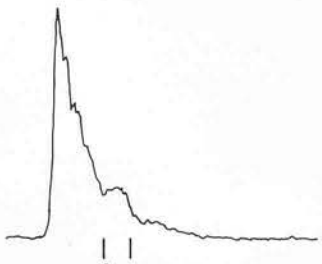

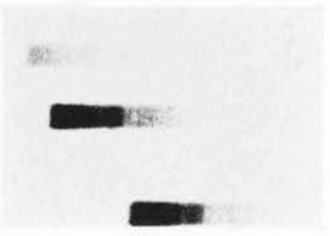

70 K2

V = 15·38
B–V = 1·04

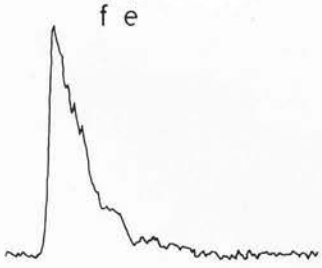

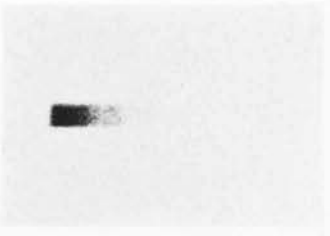

54 K5

V = 14·02
B–V = 1·10

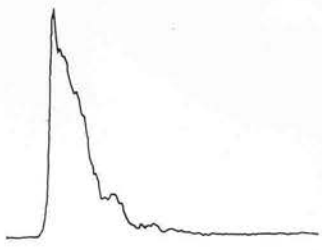

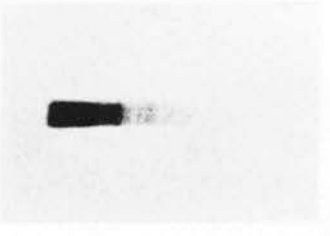

73 K7

V = 14·28
B–V = 1·33

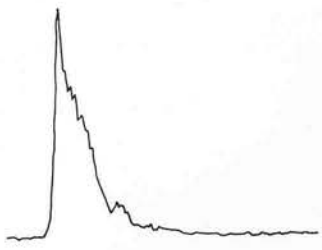

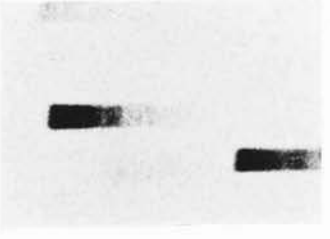

102 M0

V = 16·21
B–V = 1·50

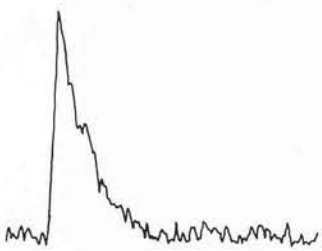

Objective prism radial velocities of cluster galaxies from UK Schmidt Telescope plates

by

J. A. Cooke, D. Emerson and B. D. Kelly
Department of Astronomy, University of Edinburgh, Blackford Hill, Edinburgh, EH9 3HJ.

H. T. MacGillivray and R. J. Dodd
Royal Observatory, Blackford Hill, Edinburgh, EH9 3HJ.

(Received 1980)

Proofs and correspondence to

Mr. H. Seddon,
Royal Observatory,
Blackford Hill,
Edinburgh,
EH9 3HJ.

Abstract

Radial velocities for galaxies in the cluster Abell 2670 have been measured on an objective prism plate and compared with previously published velocities from slit spectra. These indicate that the prism velocities are accurate to $\sim 1800\,km\,s^{-1}$. Similar velocities have been measured for the cluster of galaxies Abell 140, the results indicating a wider dispersion in velocities than would be expected for a single cluster. We conclude that the technique is useful for determining the radial velocities of clusters, for testing cluster membership and for resolving superimposed clusters or locating apparent clusters with anomalously high velocity dispersions.

Introduction

A method has previously been described (Cooke et al., 1977) for obtaining radial velocities of faint galaxies from objective prism spectra. This method has been adapted (Cooke, 1980, in preparation) for use with UK Schmidt telescope plates taken with the low dispersion objective prism, as part of a continuing programme to study the spectra of faint galaxies. The method uses the cutoff of the IIIaJ emulsion as a wavelength standard, and a strong feature at about 3970 Å occurring in the spectra of early-type galaxies. In this paper we firstly establish the accuracy of the method using previously published velocities we then apply it to study the radial velocities in a cluster of galaxies. The unexpected results illustrate the usefulness of the technique; further application to other clusters could provide important new information on cluster velocity dispersions.

The problem of calibration

The spectral resolution of stellar objective prism spectra is limited by the size of the seeing disc during the exposure. The resolution of galaxy spectra is obviously additionally limited by the effective angular size of the galaxy. At the low dispersion used here ($2400\,Å\,mm^{-1}$ at Hγ) the spectra become excessively smeared out for normal galaxies brighter than $B \sim 16$ m. In order to check the

validity of radial velocities of galaxies determined from objective prism plates, it is therefore necessary to have a reasonable sample of faint galaxies, preferably lying within the field of a single UK Schmidt plate, having independently determined velocities. The best sample available is that represented by the cluster Abell 2670, within which 10 radial velocities have been determined by Oemler (1973), using slit spectra at a dispersion of 190 Å mm^{-1}. Oemler determined the standard deviation for the velocity of an individual galaxy to be 120 $km\,s^{-1}$; this is much smaller than the measurement errors in the prism technique and will thus be ignored.

Plate material

The objective prism plates used for this work were both taken with the UK Schmidt telescope. UJ4551P is an unwidened 60-minute exposure centred approximately on cluster Abell 2670. UJ4543P has unintentional non-uniform widening, and is also a 60-minute exposure; it is taken on the UKSTU survey field 475, and Abell 140 is some distance from the centre of the plate, although still in the unvignetted region. Both plates were taken using the low dispersion prism.

Tests of the method: Abell 2670

Galaxies in cluster Abell 2670 were measured using the University of St. Andrews automated Joyce-Loebl microdensitometer. The measurements obtained were processed by computer to produce tracings identical in scale (1 mm on the tracing = 20 μm on the plate) to those normally produced using the Edinburgh microdensitometers. The tracings were then measured by hand to obtain radial velocities by a simple procedure, which was described by Cooke et al. (1977). Firstly, a wavelength standard is defined using the cutoff of the IIIaJ emulsion (at approximately 5380 Å; the wavelength of the cutoff is checked on each plate area using stellar spectra). Then a spectral feature occurring at about 3970 Å is identified (we refer to this feature as the 4000 Å feature) and the separation between this and the cutoff measured to 0.5 mm on the tracing (= 10 μm on the plate). From this distance the wavelength of the feature as observed is calculated using the prism dispersion curve (Nandy et al., 1977) and from this the radial velocity obtained. The wavelength of the 4000 Å feature has been

found to be constant to within measuring error on objective prism spectra of F, G and K stars; it also appears to be constant to within ± 10 Å in published low dispersion spectrophotometry of stars and galaxies.

Strictly we should define the features by their half-intensity points. We are, however, working with fairly faint objects and for these the difference between the half-maximum position in density and intensity is negligibly small compared with the measurement error. The size of this magnitude dependent correction was determined from a sample of stellar spectra covering a range of density on the plate, and for our measurement accuracy can be considered to be zero up to a density of 1.3 above the sky background, and only 0.2 mm from density 1.3 to 1.7 above sky. The cutoff definition depends also on the colour of the object; but similar objects were used to define the cutoff position initially (i.e. late-type stars, as compared to elliptical galaxies), so again this effect can be ignored here.

A series of tests have been carried out (Cooke, 1980, in preparation) to check the consistency of the wavelength scale. These tests involved producing tracings of late-type stars of differing magnitudes chosen to cover the full area of a Schmidt plate, and additional tests were made on different plates. This data was then used to check for systematic trends in the wavelength calibration. The only one found was the expected magnitude dependence mentioned above. Apart from this the wavelength scale showed no trends. For the stars used, a standard deviation of 0.44 mm was obtained for the cutoff to 4000 Å feature separation as defined for galaxy velocity measures. Taking the stars in brightness groups, there were no large changes in this value from the fainter to the brighter stars. It is concluded that the wavelength scale does not vary with position on a single plate, nor from plate to plate, and that the measurement errors over the magnitude range concerned are similarly independent of positional and magnitude effects.

The velocities obtained for the galaxies in Abell 2670 are given in table I. The dispersion in $(V - V_0)$ is determined from the residuals between the prism velocities and the Oemler velocities; this quantity is a guide to the accuracy of the velocities, and is close to what we would expect, since ± 0.5 mm at this redshift corresponds to ± 1800 km s^{-1}. The mean velocity obtained for the seven galaxies, 23100 ± 1200 km s^{-1} is close to the mean obtained by Oemler for nine galaxies: 22600 ± 300 km s^{-1} (galaxy 5 was excluded as a possible field galaxy).

There is a systematic difference between the prism velocities and Oemler's velocities of 590 $km\,s^{-1}$, but this is not significant. It is noted that in table I the values of $V - V_0$ appear to be correlated with V_0; we assume that this is an effect of small number statistics. Note that we are not using the prism velocities to obtain a dispersion for cluster Abell 2670.

Velocities in Abell 140

We next applied the method to another cluster: Abell 140 on plate UJ4543P. This is a more distant cluster: both this and Abell 2670 have richness class 3, but A140 has a distance class 6 whereas A2670 has a distance class 4. Abell 140 was initially selected because on the direct plate it was suspected of being a combination of two clusters from its galaxy distribution.

The measurements for this cluster were made using a pen-recording Joyce-Loebl microdensitometer at Edinburgh. The 27 brightest galaxies in the area of the cluster were measured, but only 12 showed the 4000 Å feature well enough for redshift determination. Repeat measurements were made to be sure of the position of the 4000 Å feature, as the galaxies in this cluster are rather faint. The velocities obtained for Abell 140 are given in table II. The mean velocity of the galaxies in the region is approximately 45000 $km\,s^{-1}$, and at this velocity ± 0.5 mm corresponds to ± 2200 $km\,s^{-1}$. If all the galaxies were cluster members, we would expect the dispersion in V to be comparable with other cluster dispersions, i.e. velocities up to about 1500 $km\,s^{-1}$ (e.g. Yahil and Vidal, 1977; Faber and Dressler, 1977). In fact the apparent dispersion is rather larger than this, being 3100 $km\,s^{-1}$ after removing the contribution due to measurement error by assuming gaussian distributions for both the underlying cluster dispersion and the measurement error.

As noted by Faber and Dressler (1977) the cz velocity dispersions obtained here are not strictly correct, overestimating the true velocity dispersion by a factor (1 + z). Applying this correction the velocity dispersion is reduced to 2700 $km\,s^{-1}$.

Discussion

It is noted that three possible sources of systematic error could give rise to the differences in our two sets of measurements. Firstly, Abell 140 is considerably more distant than Abell 2670, and so its galaxies are at fainter apparent magnitudes. Secondly, the two clusters are on separate photographs, and are at different distances from the plate centre. Finally, the two sets of measurements were made using different microdensitometers, the St. Andrews machine being driven by stepping motors and lead-screws, whereas the Edinburgh machine was driven using the normal ratio arm.

All three of these possibilities are eliminated by the wavelength scale consistency tests described above carried out using the Edinburgh microdensitometer, and by measurements of a few late-type stellar spectra on the plate measured using the University of St. Andrews automated microdensitometer. We conclude that the large velocity dispersion shown by Abell 140 is real, and requires explanation.

Plate I shows the area of Abell 140, the numbers corresponding to the identifications in table II. We have superimposed squares on those galaxies with velocities greater than the mean, and circles on those with velocities less than the mean. This division does not show the correlation with position which would be expected if Abell 140 was in fact a combination of two clusters. However, this explanation cannot be ruled out given that an exact line-of-sight superposition is possible, and that our sample of 12 galaxies is not sufficient to enable the nature of the velocity distribution to be determined.

If all the galaxies measured in Abell 140 are in a single cluster, then its velocity dispersion is the highest known (e.g. Yahil and Vidal, 1977). However this does not render the single cluster hypothesis invalid. Relatively few clusters have as many as 12 determined radial velocities for their members, and well-determined dispersions for moderately faint clusters are very rare. If the upper bound for observed cluster dispersions does in fact require modifying, then this could have an important impact on the interpretation of groups of quasars with redshifts differing by several thousands of kilometers per second (e.g. Hazard et al., 1979), since these would no longer be so incompatible with the notion that extremely distant clusters of quasars are being observed.

Conclusion

We have established the accuracy of a method to determine radial velocities of cluster galaxies from objective prism plates, and have used this method to examine the velocity distribution in cluster Abell 140. This serves as an illustration of the use of the method for resolving superimposed clusters at different redshifts or making checks of cluster membership, although this particular cluster is either an exact superposition of two clusters or has an anomalously high velocity dispersion. The technique cannot be applied to all individual galaxies since redshifts cannot be obtained for most spirals (Cooke et al., 1977), but is very suitable in connection with groups or clusters. An application that readily comes to mind is the determination of cluster Bautz-Morgan type (Bautz and Morgan, 1970) which is vulnerable to contamination by foreground or background galaxies.

Acknowledgements

We are grateful to the UK Schmidt Telescope Unit for the use of plate material, and to the University of St. Andrews Department of Astronomy for allowing us to use their Joyce-Loebl microdensitometer.

Wilma McKellican performed the preliminary reduction of the St. Andrews microdensitometer data whilst working as a vacation student at the Royal Observatory, Edinburgh.

References

G. O. Abell (1958), Ap. J. Suppl., 3, 211.

L. P. Bautz & W. W. Morgan (1970), Ap. J., 162, L149.

J. A. Cooke, D. Emerson, K. Nandy, V. C. Reddish & M. G. Smith (1977), Mon. Not. R. astr. Soc., 178, 687.

J. A. Cooke (1980), thesis in preparation.

S. M. Faber & A. Dressler (1977), Astr. J., 82, 187.

C. Hazard, H. C. Arp & D. C. Morton (1979), Nature, 282, 271.

K. Nandy, V. C. Reddish, K. P. Tritton, J. A. Cooke & D. Emerson (1977), Mon. Not. R. astr. Soc., 178, 63P.

A. Oemler, Jr. (1973), Ap. J., 180, 11.

A. Yahil & N. V. Vidal (1977), Ap. J., 214, 347.

TABLE I

Radial velocities in Abell 2670

Galaxy (Oemler no.)	Velocities ($km\,s^{-1}$) Prism V	Oemler V_0	$V - V_0$
1	22,800	23,200	- 400
4	24,600	21,260	+3,340
6	22,800	21,430	+1,370
7	22,800	22,900	- 100
8	21,000	23,400	-2,400
9	24,600	22,350	+2,250
10	22,800	22,700	+ 100

$$\overline{V} = 23{,}057 \text{ km s}^{-1}$$

$$\sigma_{V-V_0} = \sqrt{\frac{\Sigma(V - V_0)^2}{n - 1}} = 2{,}000 \text{ km s}^{-1}$$

$$\frac{\Sigma(V - V_0)}{n} = 590 \pm 760 \text{ km s}^{-1}$$

TABLE II

Radial velocities in Abell 140

Galaxy	Velocity ($km\,s^{-1}$) (prism)	
	V	$V - V_{mean}$
1	44,000	- 550
2	46,400	+1,850
3	38,000	-6,850
4	48,500	+3,950
5	44,000	- 550
6	44,000	- 550
7	48,500	+3,950
8	40,100	-4,450
9	46,400	+1,850
10	40,100	-4,450
11	44,000	- 550
12	50,600	+6,050

$$V = 44{,}550 \text{ km s}^{-1}$$

$$\sigma_V = \sqrt{\frac{\Sigma (V - V_{mean})^2}{n - 1}} = 3{,}800 \text{ km s}^{-1}$$

Figure caption

Plate I (a) direct plate (b) prism plate
field containing cluster Abell 140.

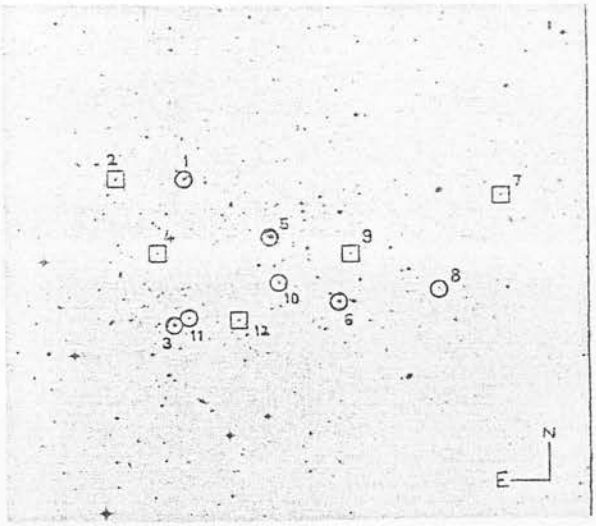
1
2
3
4
5
6
7
8
9
10
11
12
N
E